

Chondrolabral damage in the Natural Hip Joint

Mudit Dubey

(MEng, Hons)

Submitted in accordance with the requirements for the degree of
Doctor of Philosophy

The University of Leeds

Institute of Medical and Biological Engineering

School of Mechanical Engineering

September 2023

The candidate confirms that the work submitted is his/her own, except where work which has formed part of jointly-authored publications has been included. The contribution of the candidate and the other authors to this work has been explicitly indicated below. The candidate confirms that appropriate credit has been given within the thesis where reference has been made to the work of others.

Jointly-authored work from the paper Jimenez-Cruz D, Dubey M, Board T, Williams S. An in vitro methodology for experimental simulation on the natural hip joint. PLoS One. 2022 Aug 18;17(8):e0272264. doi: 10.1371/journal.pone.0272264. PMID: 35980907; PMCID: PMC9387788.] related to Chapter 3 and 4.

Dr. David Jimenez-Cruz collaborated in gathering data and protocols to develop the in vitro natural hip methodology. The results featured in the publication are from a series of experimental conditions where the tissue was overloaded in three different loads. The testing of porcine tissue was shared between us in Pilot Study 1 featured in Chapter 4. The paper was drafted by David and summarised our final methodology which is described in my thesis, and includes some images in the results to show various damage which will feature in the thesis. I was involved in editing and reviewing the paper before publication.

In addition, Chapters 5 and 6 feature work which was conducted in collaboration with the Biophysics group at the University of Exeter. My own contributions are fully and explicitly indicated in the thesis. The work of collaborators included Dr. Jessica Mansfield for the operation of the multiphoton microscope system and helping in data gathering of my porcine labral samples using multi-modal multiphoton imaging; Dr. Ellen Green for the operation of the microscope system used for single spectra coherent Raman spectroscopy; Dr. Ben Sherlock for assisting with data gathering in the polarised multiphoton system.

This copy has been supplied on the understanding that it is copyright material and that no quotation from the thesis may be published without proper acknowledgement.

The right of Mudit Dubey to be identified as author of this work has been asserted by him in accordance with the Copyright, Designs and Patents Act 1988.

Acknowledgements

I am immensely grateful to my project supervisor Prof. Sophie Williams for all her advice and support over the years; I cannot express enough gratitude for her help during the toughest of moments and for creating an enriching atmosphere during the research project. I would also like to thank my entire supervision team, including Dr. Alison Jones, Dr. Hazel Fermor, Dr. Lin Wang and HTCA advisors Dr. Tim Board and Dr. Graham Isaac. Thank you for sharing your expertise with me and taking the time to direct me to consider the importance of my work and how it can benefit others.

I would like to thank my collaborators and mentors, David Jimenez-Cruz and Dawn Groves, for helping me progress natural joint research with them. Thanks for your training and assistance in different aspects of my project. I am especially grateful for David who supported me in developing the natural hip simulation methodology and for being a dependable friend throughout my project. I want to thank Dr. Claire Brockett for her help as CDT director and for solving difficult situations. I want to thank Debra Baldwin, Geraldine Macdonald and Michelle Byrne without whom my travel to Exeter would not have been possible.

I am hugely grateful to the Biophysics lab at Exeter. Working with the Dr. Jessica Mansfield, Dr. Ellen Green, Dr. Ben Sherlock and Professor Peter Winlove was an invaluable experience, and I hope to continue the brilliant collaboration in the future.

I would like to thank iMBE technicians for their ongoing support and lab manager Phil Wood for providing support when equipment would eventually breakdown. Special thanks to Nicola Conway who shared her years of expertise in histology helping me learn the method. I would like to extend my gratitude to the EPSRC and DePuy Synthes for funding of this research for supplying me with resources and funding for travel for the collaboration with the University of Exeter.

Finally, thanks to all my CDT peers, especially Taiyibah Afzal, Phil Straw, Patrick Lawson, Ahranee Camden, and Oluwasegun Kayode for their moral support. I hope we all stay in touch for years to come. Thank to my friends Saniya Patki, Minhaj Uddin and David Widdowson for constantly cheering me on.

Finally, I would like to thank my parents and grandpa for making all this possible, and for their constant guidance no matter the task. I am eternally grateful for their love and support.

Abstract

Previously, the labrum was considered the non-functional rim of the acetabulum of the hip joint and was resected when damaged or causing pain. However, there is increasing evidence suggesting the labrum plays a vital role in the healthy functioning of the hip. Contact stresses in acetabular articular cartilage can increase by 92% when the labrum has been removed. Underlying structural abnormalities such as femoroacetabular impingement (FAI) increase the risk of labral tearing. Labral tearing can lead to loss in mobility, joint degeneration and is often found in degenerative conditions like osteoarthritis. Although there has been some success in managing symptoms caused by labral tears, the long-term outcomes are poorly understood and there is little underpinning evidence of the best surgical strategy. There is a growing need for understanding the structure and function of the labrum and how it can become damaged in relation to structural abnormalities. In this thesis, an electromechanical hip simulator was used to simulate physiological joint loads and motions to simulate chondrolabral damage in porcine natural hip joints in an effort to better understand the damage mechanisms. Unloaded and loaded porcine acetabulae were investigated by altering the mechanical loading environment in terms of the axial load, the orientation of joint components, test duration, alignment, and motion. By first running some preliminary tests, it was identified how the simulation model could be applied to induce labral tearing and chondral delamination primarily through increased axial loading and a torsional motion applied on the joint to damage the articular cartilage. The tissues were subsequently characterised macroscopically and microscopically using histological examination and novel non-linear imaging methods to analyse changes to the structure in particular with collagen fibres present in the tissue to determine the effects of damage on the structure. The simulation model was developed with the potential for assessing early interventions, to aid in the management of labral tearing and associated chondral injuries. Multimodal multiphoton revealed preliminary insight into the mechanical disruption of collagen fibres through applied loading. It was noted that collagen fibres align with the direction of the tear and these fibres could be visualised and traced through the application of polarised-second harmonic imaging. In the future, this work can contribute to the understanding of chondrolabral damage and how surgeons may consider the fibre arrangement to restore mechanical function to the labrum.

Table of Contents

Acknowledgements	3
Abstract	4
Table of Contents	5
List of Abbreviations	9
List of Tables	10
List of Figures	12
Chapter 1 Introduction	24
1.1 Introduction	24
Literature Review	29
1.2 Hip Anatomy and Biomechanics	30
1.2.1 The hip joint	30
1.2.1.1 Acetabulum	31
1.2.1.2 Joint capsule	32
1.2.1.3 Ligaments of the hip joint	33
1.2.1.4 Femoral head	35
1.3 Hip Joint Biomechanics	36
1.3.1 Kinematics	36
1.3.3 Kinetics	40
1.4 Tissue structures of the Hip Joint	43
1.4.1 Types of cartilage	43
1.4.2 Articular Cartilage	45
1.4.3 Acetabular Labrum	47
1.4.3.1 Structure of the labrum	47
1.4.3.2 Vascularity of the labrum	49
1.4.3.3 Nerve supply of the labrum	50
1.5 ECM mechanics	52
1.5.1 Synovial fluid	52
1.5.2 Lamina Splendens (Superficial Layer of Articular cartilage)	53
1.5.3 Collagen	54
1.6 Labral tearing, Cartilage degeneration and Bony abnormalities	55
1.6.1 Femoroacetabular impingement	56
1.6.1.1 Cam type deformities	58
1.6.1.2 Pincer type deformities	58
1.6.2 Labral damage	59

1.7 Visualisation of labral damage	60
1.8 Classification of labral tearing and damage	62
1.9 Surgical management of labral tearing	62
1.10 Experimental and computational approaches for investigating the natural hip joint	64
1.10.1 Mechanical Hip Simulation	66
1.10.2 Characterisation of the chondrolabral junction using histology.....	74
1.10.3 Non-linear imaging methods for advanced investigation of chondrolabral tissue	83
1.11 Summary of Literature and Aim of the thesis	84
Chapter 2 Histological Characterisation of Porcine Labrum, Articular Cartilage and Chondrolabral Junction.....	87
2.1 Introduction.....	87
2.1.1 Chapter aim	88
2.1.2 Objectives.....	88
2.2 Preparation of tissue for histological examination	89
2.2.1 Selection and acquisition of porcine tissue.....	89
2.2.2 Dissection.....	90
2.2.3 Extraction of porcine labrum samples.....	93
2.3 General materials and methods for histological examination	96
2.3.1 Fixation of labral sections.....	96
2.3.2 Reagents for histology	97
2.3.2.1 Safranin O & Fast Green	97
2.3.2.2 Sirius red/Miller's elastin	98
2.3.2.3 Haemotoylin and eosin	100
2.4 Methodology for Histological Characterisation.....	100
2.4.1 Dewaxing	101
2.4.2 Rehydration.....	101
2.4.3 Dehydration.....	101
2.4.4 Staining.....	102
2.4.4.1 Haematoxylin and eosin.....	102
2.4.4.2 Sirius red and Miller's elastin	102
2.4.4.3 Safranin-O and fast green.....	103
2.4.5 Mounting.....	103
2.5 Results.....	103
2.5.1 Gross examination of the labrum of the acetabulum ...	103

2.5.2 General tissue architecture using H&E staining.....	105
2.5.3 Distribution of proteoglycans using Safranin-O & Fast green staining	110
2.5.4 Distribution of collagen fibres using Sirius red & Miller's elastin staining.....	113
2.5.5 Investigation of collagen fibre alignment using Polarised light	116
2.6 Discussion.....	119
2.7 Conclusion	124
Chapter 3 Developments in <i>In Vitro</i> Cyclic Whole Hip Joint Testing	126
3.1 Introduction.....	126
3.1.1 Motivation	126
3.1.2 Chapter aim	127
3.1.3 Background to Whole Natural Hip Joint Simulation.....	128
3.2 Materials	131
3.2.1 Materials and equipment required for cementing.....	131
3.2.2 Solutions and Media	131
3.2.3 Photogrammetry equipment.....	133
3.2.4 Simulation equipment	135
3.3 Methods	135
3.3.1 Joint dissection(Pallan, 2016).....	135
3.3.2 Potting and Alignment.....	136
3.3.3 Cementing	140
3.3.4 Choice of peak loading for use with porcine hip joint.....	141
3.4 Preliminary studies for method development.....	141
3.4 Experimental Study: Assessment of the Natural Hip Simulation Methodology	147
3.4.1 Study Design	147
3.4.2 Method	147
3.4.3 Results	153
3.4.5 Discussion.....	155
Chapter 4 Generating Chondrolabral Damage using Natural Hip Simulation	160
4.1 Introduction.....	160
4.1.1 Chapter aim and research objectives	160
4.2 Pilot Study 1: Generating labral tearing through overloading.....	161

4.2.1 Introduction	161
4.2.2 Methods	162
4.2.3 Results	164
4.2.3 Discussion.....	169
4.3 Pilot Study 2: Compressive torsional loading for inducing chondral delamination.....	175
4.3.1 Introduction	175
4.3.2 Method	176
4.3.3 Results	179
4.3.4 Discussion.....	184
Chapter 5 Developments in Non-linear Microscopy for Imaging the Chondrolabral Junction	188
5.1 Introduction.....	188
5.2 Working principles	190
5.3 Sources of contrast in non-linear microscopy	192
5.4 Microscope Systems used for Multi-Photon Imaging	192
5.5 Materials and Methods	193
5.6 Results.....	196
5.6.1 Multiphoton-imaging of the porcine acetabular labrum	196
5.6.1 Analysis of Multiphoton imaging of the porcine acetabular labrum	207
5.7 Discussion	208
Chapter 6 Investigation of Chondrolabral Damage using Non-linear Imaging Methods	213
6.1 Introduction.....	213
6.2 Chapter aims	214
6.3 Methods	215
6.4 Results.....	220
6.4.5 Specific example of tearing (chondrolabral separation)	257
6.5 Discussion.....	259
Chapter 7 Overall Discussion.....	264
7.1 General discussion.....	264
Appendix	272
Details of the hip simulator.....	272
Details of Photogrammetry	272
References	275

List of Abbreviations

- 2D** – Two dimensional
- 3D** – Three dimensional
- AA** – Abduction-adduction
- AP** – Anterior-posterior
- BMI** – Body mass index
- BW** – Body weight
- CoCr** – Cobalt chrome
- CoR** – Centre of rotation
- ECM** – Extracellular matrix
- EDTA** – Ethylenediaminetetraacetic acid
- FAI** – Femoroacetabular impingement
- FE** – Flexion Extension
- FNE** – Free nerve endings
- GAG** – Gycosaminoglycan
- H&E** – Haemotoxylin and eosion
- IE** – Internal and external rotation
- ISO** – International Organisation for Standardisation
- ML** – Medial lateral
- MMPs** – Matrix metalloproteinases
- MRI** – Magnetic resonance imaging
- NEO** – Nerve end organs
- OA** – Osteoarthritis
- PBS** – Phosphate buffered Saline
- PMMA** – Polymethylmethacrylate
- TAL** – Transverse acetabular ligament

List of Tables

Table 1.1 Average range of motion of the human hip joint. Adapted from (Paul, 1967; Burstein, 2001; Netter, 2006; Torricelli <i>et al.</i> , 2016).	37
Table 1.2 - Muscles of the hip joint and their axis of motion. Adapted from (Anderson, Strickland and Warren, 2001; Ramage and Varacallo, 2022).	39
Table 1.3 – Main characteristics of collagen types I and II. Adapted from (Ricard-Blum, 2011).	55
Table 1.4 : Intra and extra articular pathologies of the hip joint resulting in groin pain (Suarez <i>et al.</i> , 2013).	55
Table 1.5 - Comparison of studies conducting mechanical simulation.	67
Table 1.6 - Comparison of studies reporting histological or immunohistological examination of acetabulum labral tissue. (Continued overleaf)	75
Table 2.1 Chemicals and Reagents required for preparing Safranin-O and fast green stains	97
Table 2.2 Chemicals and Reagents required for preparing Sirius red/Miller's elastin	99
Table 2.3 Chemicals and Reagents required for preparing Haemotoylin and eosin	100
Table 3.1 Table of the cementing equipment, consumables, and simulator components	131
Table 3.2 Table of the photogrammetry equipment, consumables, and simulator components	133
Table 3.3 Table of the simulation equipment, consumables and simulator components required for mounting and running an experimental hip simulation.	135
Table 3.4 Table of the issues which were addressed through experimentation.	143
Table 3.5 Table of the main considerations found through testing	146
Table 3.6 Grading system for visual characterisation of chondro-labral damage.	152
Table 3.7 Visual assessment of chondro-labral damage in simulated samples.	153
Table 4.1 Visual assessment of chondro-labral damage in simulated samples.	164
Table 4.2 – Surface Photogrammetry of porcine samples	179

Table 6.1: Macroscopic observations of tissue after 14400 cycles (four 217 hours) of simulation.

Table 6.2: Key findings and tissue observations after 14400 simulation 259 cycles (four hours).

List of Figures

- Figure 1.1** – Bones from the Pelvis to the Knee. Drawing adapted from McGraw Hill. 30
- Figure 1.2** – Lateral view of the dislocated right hip joint. Drawing adapted from McGraw Hill. 31
- Figure 1.3** - Dissected human acetabulum (right hip). Lateral view showing the major muscle attachments, ligaments and surfaces that form the acetabular portion of the hip joint. Image adapted from Anatomy.tv, 2019, Primal Pictures, 2019. 31
- Figure 1.4** - Joint Capsule and Ligamentous support. A – Iliofemoral and Ischiofemoral ligaments with the weak spot highlighted in red. B – The major ligaments of the hip joint contributing to the overall stability of the joint. C – The joint capsule which is a combination of the synovial and fibrous membranes. Image adapted from (Melluso and Mansi, 2017). 33
- Figure 1.5** – Hip joint model with overlays of the proximal and distal osseous attachments of the articular capsule and capsular ligaments of the hip, respectively, in the acetabular rim and anterior portion of the proximal femoral epiphysis. Key: CLH capsular ligaments of the hip, IBILFL inferior band of the iliofemoral ligament, ILFL iliofemoral ligament, PFL pubofemoral ligament, SBILFL superior band of the iliofemoral ligament, ZO zona orbicularis (Wagner *et al.*, 2012). 34
- Figure 1.6** – Cross section of the hip joint showing the femoral neck axis and anatomical axis of the femur. 35
- Figure 1.7** – Human walking gait cycle based on three different profiles measuring the joint reaction force on the hip and its relation to the stance and swing phases. Adapted from (L. Gao *et al.*, 2022). 38
- Figure 1.8** – Free body diagram for calculation of the hip joint force while walking. **W** body weight. Moment arm **a** (the distance from the femur to the centre of gravity). Muscles **M** (abductor muscles which resist the movement). Moment arm **b** (caused by the force of the abductors from the centre of the femoral head). **R** joint reaction force. 41
- Figure 1.9** – Types of cartilage featuring histological differences typically observed with H&E staining. Hyaline cartilage contains rounded chondrocytes in columns known as lacunae, collagen fibres are not visibly stained in the matrix. Fibrocartilage contains thick, collagen bundles layered on top of one another with rows of chondrocytes intertwined 43

between the fibres. Elastic cartilage contains darkly stained elastic fibres in the matrix. Adapted from (Hu and Nukavarapu, 2019).

Figure 1.10 – Schematic diagram of the articular cartilage collagen and proteoglycans (aggrecan). The proteoglycan monomer consists of a protein core with covalently bonded glycosaminoglycan side chains consisting of keratan sulphate and chondroitin sulphate. The proteoglycan monomers are non-covalently attached to the hyaluronic acid backbone stabilised by the link proteins. The negatively charged GAG side chains attract water molecules with associated cations. Adapted from (Gahunia and Pritzker, 2020). 44

Figure 1.11– Cellular composition and arrangement of the articular cartilage. Taken from (Gahunia and Pritzker, 2020). 46

Figure 1.12 – Arrangement of Type II collagen in articular cartilage. The characteristics of the collagen orientation are provided for the superficial, transitional and radial zones. Taken from (Gahunia *et al.*, 2020). 47

Figure 1.13 – Structure of the human acetabular labrum as defined by (Lewis & Sahrmann, 2006). **A** Cross-section of the posterior labrum, showing the boundaries between different zones of subchondral bone, articular cartilage, and labrum. **B** Definitions of the width and thickness of the labrum where the labrum was found to be wider and thinner in the posterior region through arthroscopic examination (Lewis and Sahrmann, 2006). 48

Figure 1.14 – Schematic of the articular cartilage, showing the arrangement of collagen fibres within the different regions. Notice the superficial layer arranged with fibres parallel to the surface known as the lamina splendens. This would suggest this layer is particularly important for shear resistance. Taken from (Huyse and Verstraete, 2021). 54

Figure 1.15 – **A** – Bony prominence found centred on the anterolateral femoral head-neck junction (cam lesion). **B** Cam impingement is when the aspherical cam lesion glides under the labrum during flexion, making contact with the edge of the articular cartilage, resulting in progressive delamination. **C** Bony overcoverage of the anterior labrum results in pincer impingement. **D** The anterior labrum gets crushed by the pincer lesion against the neck of the femur. Adapted from (Byrd, 2014). 57

Figure 1.16 - Hip Acetabular Labral Repair. **A** - the entry portals chosen during hip arthroscopy. **B** - the two-portal technique. **C** - the use of a shaver to debride the torn labrum. **D** shows the drill and suturing procedure. **E** 63

shows the completed sutured labrum. Adapted from (Matsuda, Hurst and Biomet, 2016).

Figure 1.17 - Evaluation of range of motion restriction within the hip joint. 65

This graph shows the range of motion benchmark recorded and the associated impingement zones. Osseous impingement was most likely with flexion and flexion-adduction. Soft tissue impingement was most likely with abduction and flexion-abduction, and flexion-adduction. Image adapted from (Turley *et al.*, 2013).

Figure 2.1 – Schematic drawing of the porcine hip joint in a neutral 90 position.

Figure 2.2: Dissection of a right hind pig leg. **A** Skin, musculature and soft 91 tissues were removed after identifying the location of the hip joint until the joint capsule was exposed. **B-C** Surrounding soft tissue, ligaments and joint capsule were removed preserving the articular surfaces. The joint capsule was carefully excised following the attachment points close to the base of the femoral head avoiding any cartilage, releasing the synovial fluid, and destabilising the femoral head. **D** The femur and acetabulum were disarticulated by separating the ligamentum teres and remaining capsular connective tissue.

Figure 2.3 - Schematic drawing showing the difference between the 92 geometry of the human and porcine hip joints. The greater trochanter protrudes further in the porcine femur with an aspherical femoral head.

Figure 2.4 – Reduction of the greater trochanter. **A** – Red lines indicating 93 where on the porcine femur cuts were made using a bone saw. **B** – Schematic of a resected femur. **C** – Natural porcine femur with large greater trochanter. **D** – Resected Porcine femur.

Figure 2.5: **A** Quadrants of the acetabulum as defined in this project, the 94 schematic shows the clockface model used by surgeons as well as the definition of the peripheral and central zones of the acetabulum **B** Schematic drawings of extracted labral sample and acetabular labrum cross-section viewed from a transverse plane.

Figure 2.6: **B** Dissected porcine acetabulum with the joint capsule 94 resected. Note the morphological differences between the posterior and anterior regions. The posterior labral rim at 9° clock is deformed and extends beyond the bony margin. This was a common feature observed in some **B** extraction of porcine labral sections.

Figure 2.7 labral sections extracted for use in histology. The triangular-shaped sections measured approximately 2-7mm in depth. 95

Figure 2.8: Gross examination of labral sections extracted from porcine acetabulum. 104

Figure 2.9: Gross examination of labral sections extracted from porcine acetabulum from anterior, superior, and posterior regions. Black square: cartilage, plus-sign: dense fibrous connective tissue in external labrum, Black circle: subchondral bone, red dotted line: interface between internal and external labrum, red arrow: large fibres visible in the fibrous portion towards the capsular side. Black arrow: margin separating more fibrous and fibrocartilaginous regions. 104

Figure 2.10 – H&E-stained anterior porcine labrum with labels showing the various regions found in the cross-section. The acetabular labrum was found to be continuous with the articular cartilage and capsule hence had the presence of fibrocartilage internally. At the same time, there was more dense irregular connective tissue and fibrous connective tissue found towards the capsule. 106

Figure 2.11 – A representative set of H&E stained anterior porcine labrum. A – a magnified view of the external labrum. B – the subchondral bone structure. C – The cartilaginous region of the labrum and articular cartilage. Red arrow – artefact. Black arrow – the presence of holes or features resembling blood vessels. 107

Figure 2.12 – A representative set of H&E stained native porcine labrum from anterior, superior, and posterior regions. 108

Figure 2.13 – An image table comparing the key regions from Figure 2.11 of H&E-stained native porcine labrum from anterior, superior, and posterior regions. The black dashed line represents the transition between the fibrous and cartilaginous regions. The orange arrow represents the general direction of collagen fibres found in the anterior labrum in the fibrocartilage. BV represents the blood vessels found. 109

Figure 2.14 – A representative set of Safranin-O & Fast green stained porcine labrum from anterior, superior, and posterior regions. 111

Figure 2.15 – An image table comparing the key regions from Figure 2.14 of Safranin-O & Fast green stained porcine labrum from anterior, superior, and posterior regions. The black dashed line represents the transition between the fibrous and cartilaginous regions. The orange arrow 112

represents the general direction of collagen fibres. BV represents the blood vessels found.

Figure 2.16 – A representative set of Sirius red and Millers’ elastin-stained porcine labrum from anterior, superior, and posterior regions. Black circles represent bubbles created during the fixation process when applying a coverslip. A tissue artefact was present in the cartilage on the bottom right of C in the posterior labrum, where some subchondral bone appeared on top of the cartilage, which may have occurred during processing. 114

Figure 2.17 – An image table comparing the key regions from Figure 2.16 of Sirius red and Millers’ elastin-stained porcine labrum from anterior, superior, and posterior regions. The black dashed line represents the transition between the fibrous and cartilaginous regions. The orange arrow represents the general direction of collagen fibres. BV represents the blood vessels found. 115

Figure 2.18 – A representative set of Sirius red and Millers’ elastin-stained native porcine labrum viewed under polarised light from anterior, superior, and posterior regions. 117

Figure 2.19 – An image table comparing the key regions from Figure 2.18 of Sirius red and Millers’ elastin-stained porcine labrum from anterior, superior, and posterior regions. The yellow dashed line represents the transition between the fibrous and cartilaginous regions. The blue arrow represents the general direction of collagen fibres. 118

Figure 3.1 Schematics of pendulum friction simulator (Groves, Fisher and Williams, 2017) 128

Figure 3.2 Mounted whole natural porcine hip joint components in the pendulum friction simulator limited to flexion extension (FE) motion(Groves, Fisher and Williams, 2017) 129

Figure 3.3: Hip Simulator used in this project and by Pallan (2016). **A** - Schematic of Prosim 1-Station Deep Flexion Hip Simulator (Simulator Solutions, Stockport, UK). **B** – Photograph of the working environment and three degrees of freedom labelled within the hip simulator with a dummy femoral head and cup. 130

Figure 3.4 – Photogrammetry Set-up: a light tent used with acetate templates to position acetabular and femoral components. Wide and macro lenses were used with a digital camera to capture surface details of porcine acetabulum and femoral head at different stages of simulation. 134

Figure 3.5 Cuts made to reduce features around the acetabulum to fit the acetabular pot. The acetabulum was separated by making four cuts along the pubis and ischium bones of the pelvis. The yellow and blue lines represent cuts along the ischium while the green line represents the cut made along the pubis. The purple line was made along the base of the acetabulum and coincident with where the abattoir cuts the limb. This feature was reduced to allow more control when positioning the acetabulum during cementing. 137

Figure 3.6 – Left - Cuts made on porcine femur to remove the attached growth plate. The length of the femur was also shortened. This allowed the femoral head to fit the femoral head pot required to fit the dimensions of the simulator to prevent impingement 138

Figure 3.7 Schematic showing how the femur was placed in sizing template (top). The femur was placed into different diameter holes in the template to get a good match with the spherical diameter the simulator was designed to be used with. The epiphyseal line of the femoral head and the tear drop shaped marker (bottom) found above the lesser trochanter were used to align the head parallel with the template. This tear drop shaped marker was found in nearly all porcine femurs and was coincident with the centre of the TAL of the acetabulum which made it useful for setting appropriate alignment of the natural joint. 139

Figure 3.8 Flow chart showing the mechanical changes required to achieve damage associated with pincer and cam type impingement. 142

Figure 3.9 Issues with the previous pot used by Pallan (2016). The pot had a large flange which would impinge with the femoral pot due to its vertical height. Additionally, the deep pot would result in uneven cement pouring with some reaching the labrum and producing tiny cement debris which would impact the tests. 144

Figure 3.10 Updated acetabular pot had a lower lessened flange (top left) and a reduced vertical height (top right) to prevent contact with the femoral component. Additionally new threaded holes were included to allow polymer wires to be used to hold the acetabulum in place (bottom left) ensuring more even and consistent pouring (bottom right) preventing spillage onto the acetabular labrum. 145

Figure 3.11 Single station hip simulator showing mounted natural porcine hip. The simulator uses a 6-axis load cell which can be used to apply ISO standard walking cycles or custom profiles. The walking cycle is applied 149

using a demand wave cycle and can be monitored using a feedback wave cycle. The acetabular cup is mounted under the load cell while the femoral head is set on a cradle capable of moving in the simulator's three degrees of motion (FE, AA and IE).

Figure 3.12 Simulator loading and motion input profiles used to simulate a standard walking cycle based on average human gait as per the ISO 14242-2 standard for wear testing and tribology of THR. Axial load was scaled down by 70% to match the typical load undertaken by a porcine hip joint during a walking cycle. The total load was increased to a maximum of 1200N for an equivalent representation of loading experienced by an overweight porcine hip. In both testing scenarios, human motion inputs were used for flexion-extension, abduction-adduction and internal-external rotation as the porcine geometry was used to represent human range of motion. 150

Figure 3.13 Photogrammetry of control samples which were simulated under standard loading (peak axial loading of 900N), with motion set to human walking cycle from ISO 14242 standard with Ringer's solution as lubricant. The telephoto image of the acetabulum (left), the whole acetabular pot (center) and the wide image of the femoral head surface (right) prior to testing, after 2 hours, and after 4 hours. 154

Figure 4.1: Single station hip simulator showing mounted natural porcine hip. The simulator uses a 6-axis load cell which can be used to apply ISO standard walking cycles or custom profiles. The walking cycle is applied using a demand wave cycle and can be monitored using a feedback wave cycle. The acetabular cup was mounted under the load cell while the femoral head was set on a cradle capable of moving in the simulator's three degrees of motion (FE, AA and IE). 162

Figure 4.2: Simulator loading, and motion input profiles used to simulate a standard walking cycle based on a simplified human gait as per the ISO 14242-2 standard for wear testing and tribology of THR. 163

Figure 4.3: The telephoto images of the acetabulum showing the details of the articular surfaces and the acetabular labrum, fine details and tears can be identified as well as changes in surface topography. 165

Figure 4.4: Photogrammetry of sample 4 which was simulated under increased loading (peak axial loading of 1200N), with motion set to human walking cycle from ISO 14242 standard with Ringer's solution as lubricant. The telephoto image of the acetabulum (left), the whole acetabular pot (center) and the wide image of the femoral head surface (right) prior to testing, after 7200 and 14400 cycles. 166

Figure 4.5: Photogrammetry of sample 6 which was simulated under increased loading (peak axial loading of 1200N), with motion set to human walking cycle from ISO 14242 standard with Ringer's solution as lubricant. The telephoto image of the acetabulum (left), the whole acetabular pot (center) and the wide image of the femoral head surface (right) prior to testing, after 7200 and 14400 cycles. 168

Figure 4.6: Dents and fine scratches observed on the femoral head which would align anteriorly near the transverse acetabulum ligament in sample 6, as seen with macroscopic lens with 1x magnification. 169

Figure 4.7: Fine scratches observed on sample 6 on the surface of the acetabulum labrum extending to the chondro-labral margin and acetabular labrum. As seen with the macroscopic lens with 1x magnification. Initial scratch found before simulation near the anterior portion of the labrum (left), and after four hours of simulation under increased loading. 169

Figure 4.8 – Schematic of testing set-up, axial load was applied through the cup while the femoral head drove the motion. Input profile is shown by the graph representing the loads and motion profile used to generate compressive twisting (torsional) loading. The profile followed a simplified representation of human internal-external rotation and axial loading occurring during walking with the omission of abduction-adduction and flexion-extension. 178

Figure 4.9 – Photogrammetry showing surface changes on the femoral head and acetabulum observed when comparing porcine hips unloaded to increasing levels of torsional loading. Images represent changes associated with the different axial loads where indentation, blushing, blistering, and peripheral labral tears were observed, with the severity increasing with load. 180

Figure 4.10 – Photogrammetry showing surface changes on the femoral head and acetabulum. At 900N peak load, the tissue had a mild increase in blushing. 181

Figure 4.11 – Photogrammetry showing surface changes on the femoral head and acetabulum. At 1300N peak load, the tissue had a significant increase in blushing and the uneven wrinkled structure appeared like blistering on the articular cartilage surface. 181

Figure 4.12 – Photogrammetry showing surface changes on the femoral head and acetabulum. At 2250N there was significant changes to the appearance of the femoral head and acetabulum. Delamination of the articular cartilage from the subchondral bone had occurred on the femoral head and cartilage. Fine tears and scratches were observed as well as significant blushing and blistered texture on the cartilage surface. 182

Figure 4.13 – Photogrammetry showing the uneven surface changes and appearance of bubble-like texture on the acetabulum observed at the end of testing. In some samples, chondrolabral tearing was observed at the anterior-superior rim. 182

Figure 4.14 – **A** Photogrammetry showing an example of the uneven surface changes and appearance of bubble-like blistered texture on the acetabulum observed after 8 hours of testing under torsional overloading. **B** The blistered texture was observed even when there was a fine scratch running through the articular surface (black arrow). Chondrolabral separation was also present in the sample (red arrow). **C** The labral tear at the anterior-superior rim was lifted but had to change in the bubble like structure. **D** Removal of the labrum at the site of anterior-superior tear rim had no impact on the appearance of the bubble like structure. 183

Figure 4.15 – **A** Photogrammetry showing an example of the uneven surface changes and appearance of bubble-like blistered texture on the acetabulum observed after 4 hours of testing under torsional overloading. **B** A 3x magnified image of the bubble which had been scored with a scalpel blade and had no change to the appearance of the blister-like surface. 184

Figure 5.1 – A labral cross section was placed onto a metal chuck and frozen at -25°C using cryogel (left). A cryomicrotome was used to cryosection labral samples (centre). Samples were sliced using the cryomicrotome with 6-7µm sections (right). 195

- Figure 5.2** – After the frozen embedded labral samples were sectioned, they could frozen sections could be placed directly onto glass slide, hydrated with a PBS and covered with a glass coverslip 195
- Figure 5.3** – Structure of the anterior acetabular labrum in porcine tissue. Large collagen type I fibres were observed in the external labrum which integrated with thinner fibres at the chondrolabral interface. 197
- Figure 5.4** – Large map of the posterior acetabular labrum in porcine tissue spanning from the superficial external labrum to the chondrolabral junction and cartilage. A large tear in the form of a processing artefact was observed through the structure, which span across the specimen. 198
- Figure 5.5** – Structure of the posterior acetabular labrum in porcine tissue. At the superficial labrum, large collagen fibres were seen in wave-like patterns. In the middle zone, there was the alignment of large type I collagen fibre bundles. In the deep transition zone, large fibres integrated into the cartilage in a layered arrangement with fibres entangled on each other. Cartilage showed the presence of thin type II fibres in the cartilage matrix. 199
- Figure 5.6** – Structure of the superior acetabular labrum in porcine tissue. Large collagen fibres were observed integrating with the cartilage at the interface. A higher signal intensity was observed in the external labrum, with fibres appearing much brighter in this region. 200
- Figure 5.7** – Structure of the anterior acetabular labrum at the external-internal labrum interface. Small holes were observed throughout the structure at the periphery surrounded by collagen fibres. The collagen fibres were arranged in a wave-like pattern across this region. 201
- Figure 5.8** – Full area map of the anterior acetabular labrum in porcine tissue. Banding was observed in the image due to the image capturing process. 202
- Figure 5.9** – Structure of the anterior labrum at the external-internal interface, small holes were observed in the external fibrous portion. There was a distinct boundary between the cartilage and the external labrum. 203
- Figure 5.10** – Structure of the fibrous external labrum at the superior side. The external labrum had collagen fibre-like structures of various sizes arranged haphazardly. 204
- Figure 5.11** – Structure of the internal labrum at the superior side. There was more order and alignment of fibres in this region with fibres assuming 205

a wave-like structure and most fibres being arranged parallel to one another, there were thicker fibres interspersed (bottom right).

Figure 5.12 – Structure of the internal-external labrum interface at the superior side. The interface had a variety of different-sized collagen fibres arranged non-homogenously. A large, ruptured structure was present at the top left corner surrounded by smaller fibrous tissue structures. 206

Figure 6.1 - The source file was a tif file containing a stack of TPF, SHG and SRS which were obtained from detectors from three separate channels of the microscopy system. Multichannel multiphoton image strip of anterior porcine labrum under scaled loading. Scale bar: 348.48 μm . 219

Figure 6.2 – Colour composite images which were created in Image J by combining the multiple channels from TPF, SHG and SRS into green, red, and blue channels respectively. Multichannel multiphoton image strip of anterior porcine labrum under scaled loading. Scale bar: 348.48 μm . 219

Figure 6.3 - Composite image of the anterior chondrolabral junction area strip from an unloaded, native porcine hip joint. Scale bar: 1042.22 μm 222

Figure 6.4 – Composite image of the posterior chondrolabral junction area strip from an unloaded, native porcine hip joint. Scale bar: 380 μm 223

Figure 6.5 – Composite image of the superior chondrolabral junction area strip from an unloaded, native porcine hip joint. Scale bar: 426.28 μm 225

Figure 6.6 – Composite image of the unloaded inferior transverse acetabular ligament from a native porcine hip joint. Scale bar: 507.12 μm . 226

Figure 6.7 – Composite image of the anterior-superior chondrolabral junction area strip from a simulated scaled loaded (peak 900N) porcine hip joint. Scale bar: 348.48 μm . 227

Figure 6.8 – Composite image of the posterior-superior chondrolabral junction area strip from a simulated scaled loaded (peak 900N) porcine hip joint. Scale bar: 293.42 μm . 228

Figure 6.9 – Composite image of the superior chondrolabral junction area strip from a simulated scaled loaded (peak 900N) porcine hip joint. Scale bar: 272.56 μm . 230

Figure 6.10 – Composite image of the anterior-superior chondrolabral junction area strip from a simulated overloaded (peak 1130N) porcine hip joint. Scale bar: 507.12 μm . 231

Figure 6.11 – Composite image of the posterior-superior chondrolabral junction area strip from an overloaded (peak 1130N) porcine hip joint. Scale bar: 854.70 μm . 233

Figure 6.12 – Composite area strip of the superior fibrous region of the acetabular labrum from an overloaded (peak 1130N) porcine hip joint. 234

Scale bar: 222.74 μm .

Figure 6.13 – Composite image of the anterior-superior chondrolabral junction area strip from a simulated (peak 1130N) loaded porcine hip joint. 236

Scale bar: 538.72 μm .

Figure 6.14 – Composite image of the posterior-superior chondrolabral junction area strip from an overloaded (peak 1340N) porcine hip joint. 237

Scale bar: 380.73 μm .

Figure 6.15 – Composite image of the superior chondrolabral junction area strip from a simulated overloaded (peak 1340N) porcine hip joint. 239

Scale bar: 696.71 μm .

Figure 6.16 – Composite image of the anterior-superior chondrolabral junction area strip from a simulated overloaded (peak 1340N) porcine hip joint. 240

Scale bar: 601.92 μm .

Chapter 1 Introduction

1.1 Introduction

The hip joint is a ball and socket synovial joint located at the pelvis. The joint is composed of the femoral head (ball) of the femur which articulates in the acetabulum (socket). The hip joint often resists loads several times that of the body weight in activities such as running or jumping (Bergmann, Graichen and Rohlmann, 1993), providing stability during load bearing and movement. Furthermore, the joint can undergo motions that exceed the natural range of motion such as in trauma-related injuries or from extended mobility required in sports such as tennis or ballet.

The acetabular labrum is a commonly triangular-shaped lip that lines the rim of the acetabulum. Dislocation of the femoral head is limited by the labrum which deepens the cavity and prevents excessive translation of the femoral head. The labrum is increasingly recognised as an important structure involved in the joint stability (Lertwanich *et al.*, 2016), load transmission (Henak *et al.*, 2011), the regulation of synovial fluid hydrodynamic properties and, providing a negative pressure fluid seal (Ferguson *et al.*, 2003; Cadet *et al.*, 2012; Philippon *et al.*, 2014).

Hip or groin pain compromises the quality of life for patients as pain is often felt during basic activities such as sitting or standing. Hip or groin pain in young and active people commonly develops through cartilage injuries or torn labrum (Banerjee and Mclean, 2011), often in patients having bony abnormalities of the acetabulum or femoral head (Wenger *et al.*, 2004; Su, Chen and Yang, 2019; Makovitch, Mills and Eng, 2020) Changes to the natural bony morphology or abnormal articulating structures of the hip can result in loss of congruency (Weiss *et al.*, 2013), causing instability (Boykin *et al.*, 2011; Kraeutler *et al.*, 2016; Vera *et al.*, 2021) and exposing the joint to high loads which are often in direct contact with the soft tissue. This often results in injury to the hip or groin pain (Anderson, Strickland and Warren, 2001).

Groin or hip pain can indicate more serious underlying conditions such as osteoarthritis which may lead to eventual loss of function in the lower limb (Jackson

et al., 2015). Damage to the labrum is often used in identifying abnormal pathologies of the hip joint and can precede more severe pathologies. Approximately 22-55% of all patients who report hip or groin pain have some form of labral tearing (Groh and Herrera, 2009) presented before, or often with more serious hip conditions such as osteoarthritis (Neumann *et al.*, 2007).

Young and active patients aged between 20-40 are most prone to developing labral tears due to femoroacetabular impingement (FAI) or hip dysplasia (Austin *et al.*, 2008; Gerhardt *et al.*, 2012). Prolonged damage from these conditions is thought to be a precursor to early-onset hip osteoarthritis (Beck, 2005; Neumann *et al.*, 2007; Ganz *et al.*, 2008; Hosseini *et al.*, 2013; Fairley *et al.*, 2016), which is especially concerning for patients under 50, who may need total hip replacements and would require subsequent revision surgeries.

When the labrum is torn, it can cause microinstability, subluxation or dislocation in the joint (Harris *et al.*, 2016; Kraeutler *et al.*, 2016). While a torn labrum is often found in asymptomatic patients, it is more often found in those with abnormal joint morphologies and elderly patients with osteoarthritis. Labral tears rarely occur in the absence of structural osseous abnormalities and labral tears are frequently associated with lesions of acetabular cartilage such as delamination (Beaulé, O'Neill and Rakhra, 2009; Gdalevitch, Smith and Tanzer, 2009; Cho *et al.*, 2022).

Although there has been some success in managing symptoms caused by labral tears, the long-term outcomes are poorly understood, and there is little underpinning evidence of the best surgical strategy. There is a growing need for understanding the structure and function of the labrum and how it can become damaged with structural abnormalities. Moreover, while arthroscopic and radiographic evaluations can reveal labral pathology (Martin *et al.*, 2006; Shindle *et al.*, 2008; Reiman *et al.*, 2014; Barros *et al.*, 2019), these procedures can be invasive and only provide information at a single point in the care continuum of the patient, revealing little detail of the damage mechanism or the mechanical cause of damage observed clinically.

The lack of studies characterising the labrum and the pathogenesis, challenges in accessing the tissue, and the lack of resolution to visualise the microstructure resulted in the labrum being excised or resected (Greaves, 2008; Philippon, 2010; Cadet *et al.*, 2012; Miozzari *et al.*, 2015). More understanding of its functions and structure has led surgeons to opt for preservative interventions which promote repair and restore the mechanical functions of the labrum. Surgeons now prefer arthroscopic labral repair or debridement, but there is still a lack of consensus on the best surgical technique or management for labral tears and cartilage pathology (Amanatullah *et al.*, 2015; Harris *et al.*, 2016; Su, Chen and Yang, 2019).

With increasing importance being given to the acetabular labrum, with treatments that promote repair and healing, long-term outcomes still need to be clarified as the developments have been relatively recent (Bowman, Fox and Sekiya, 2010). This is particularly concerning, considering the number of hip arthroscopy procedures being performed yearly which are only set to increase with time with an increasingly active and ageing population (Palmer *et al.*, 2016). The number of hip arthroscopic procedures performed in the UK was recorded from 2002 to 2013, the procedures were projected to increase steadily by 1400% in 2023 from 2002 (Palmer *et al.* 2016). On a global scale, hip arthroscopy procedures have increased significantly in Korea (Sienko, Ekhtiari and Khanduja, 2023) and the United States (Degen *et al.*, 2022; Zusmanovich *et al.*, 2022), this trend could be attributed to the growing understanding and diagnosis of hip pathologies, especially in preserving the acetabular labrum and improved clinician training (Cevallos *et al.*, 2021; Holleyman *et al.*, 2023; Malviya *et al.*, 2023; Novoa-Parra *et al.*, 2023). The Non-Arthroplasty Hip Registry (NAHR) has reported the yearly arthroscopy procedures in the UK per year from 2012 to 2022, arthroscopic procedures reported included all acetabular and femoral procedures (Holleyman *et al.*, 2018). From 2012 to 2022, there was an increase in the total acetabular procedures (arthroscopic labral debridement and repair) by approximately 150% (Malviya *et al.*, 2023). The recorded surgeries are

based on registered surgeons who submit to the joint registry and this figure could be underreported across the UK.

Studying the acetabulum labrum and the interface with articular cartilage can help uncover the mechanical degradation caused by structural deformities on the labrum itself or by the altered. If this damage can be recreated and studied *in vitro*, it would allow the altered biomechanics to be better understood, helping overall understanding of the damage and how it could potentially be relevant to early onset of osteoarthritis.

The performance of the hip joint is dependent on an interplay of complex structural, biomechanical, and biochemical factors. Deformities such as Femoroacetabular impingement (FAI) and hip dysplasia change the normal biomechanics of the joint – creating an unnatural and altered mechanical environment in the joint. The change in joint geometry is hypothesised to increase shear forces at the peripheral load bearing regions found at the anterior-superior rim of the acetabulum. These regions do not make the same degree of contact as when these deformities were absent. Understanding the influence of static, dynamic, and biochemical changes during loading in this altered state can help develop current treatments.

The change in mechanical environment is difficult to study and measure in practice, as the hip is difficult to access and image. The femoral head sits deep in the pelvis, enclosed with musculature and capsuloligamentous support. Changes are usually found much later when patients are examined physically or radiographically when they present with hip or groin pain, where damage to the labrum or soft tissue may have already occurred. This makes it quite difficult to determine the cause of the changes and the events that trigger the changes to the biomechanics and joint tribology, as well as determine if these changes are permanent.

There have been developments in experimental and computational studies investigating the hip joint. Experimental anatomical joint simulators which house cadaveric, or animal hip joints have been used to study the biomechanics of the joint

and allow various aspects of the joint tribology. These methods have rarely been applied to study chondrolabral damage. The progression of degeneration of labral or chondral damage once a tear is present is undetermined. Additionally, it is unclear where damage first appears in response to an altered mechanical environment, and if labral tearing precedes articular cartilage damage.

Finally, knowing the best surgical intervention which would restore mechanical function and prevent further degeneration through experimental studies would complement the clinical consensus and help optimise care for patients and prevent the need for future joint arthroplasty.

Therefore, the focus of this thesis was to investigate the acetabular labrum with altered mechanical environments and characterise the changes to the structure, especially at the interface between the cartilage and labrum transition – the chondrolabral junction.

This thesis describes the development of an experimental *in vitro* simulation testing setup of the natural hip joint (Chapter 3), used to recreate, and study chondrolabral damage (Chapter 4). Chondrolabral damage was generated to match clinical observations of labral tearing and chondral delamination. The changes to the labral structure before and after simulation were examined and imaged using histology (Chapter 2 and 5), multiphoton imaging, Raman spectroscopy and polarised multiphoton imaging (Chapter 5 and 6). The prospect was to develop the experimental simulation to recreate chondrolabral injuries, which can be used for pre-clinical testing of early interventions to aid in managing labral tearing and associated chondral injury.

Literature Review

1.2 Hip Anatomy and Biomechanics

1.2.1 The hip joint

The human hip forms an important articulation of the lower limb, contributing to the overall stability required to keep humans upright during bipedal gait and carry out activities of daily living. The joint is located at the pelvis (Figure 1.1). The hip consists of paired hip bones which join each other at the pubic symphysis and to the sacrum through the sacroiliac joints.

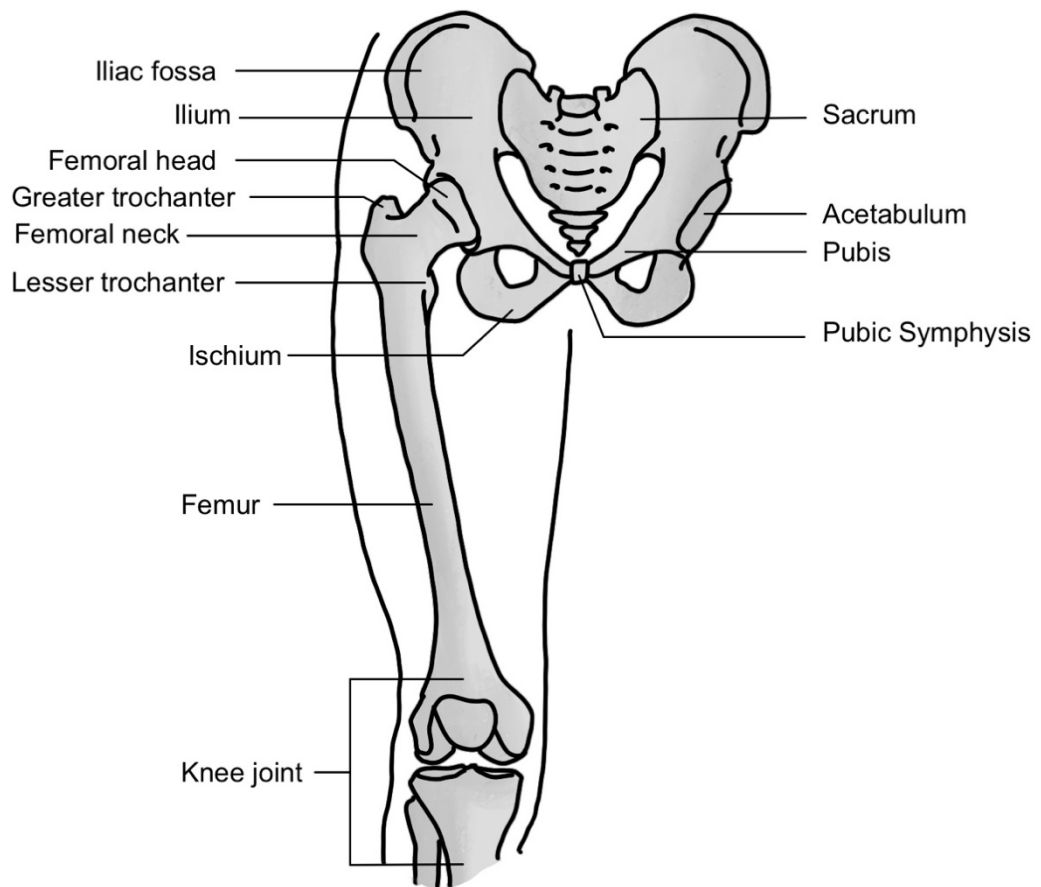


Figure 1.1 – Bones from the Pelvis to the Knee. Drawing adapted from McGraw Hill. The hip joint comprises the femoral head found superiorly from the femur (thigh) bone which articulates within the joint cavity of the pelvis known as the acetabulum (Figure 1.2). The hip joint is considered a diarthrodial or synovial joint as it has a joint cavity, the articulating surfaces are covered in smooth articular cartilage, it possesses a synovial membrane producing synovial fluid and it is surrounded by a ligamentous capsule (Byrd, 2005).

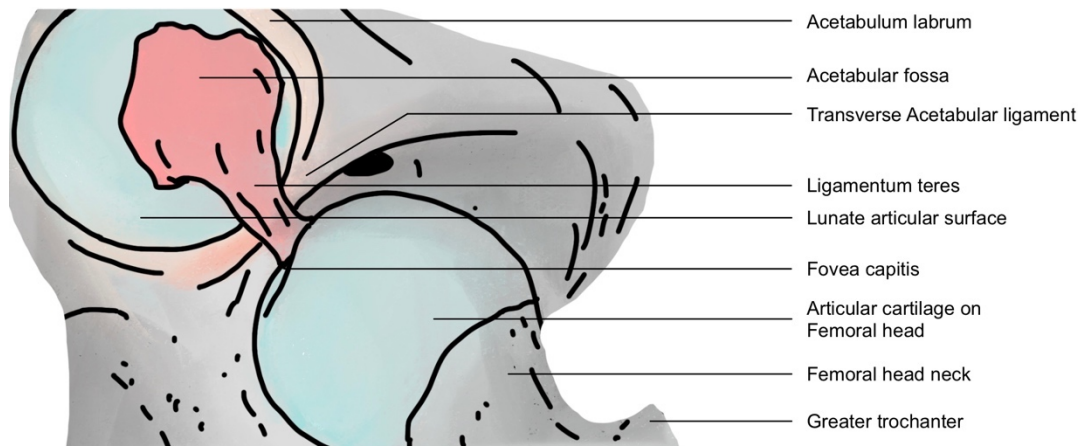


Figure 1.2 – Lateral view of the dislocated right hip joint. Drawing adapted from McGraw Hill.

1.2.1.1 Acetabulum

The acetabulum is found at the intersection of the ilium, ischium, and pubis bones (Melluso and Mansi, 2017). The acetabulum is a deep cavity lined with a horseshoe shaped surface covered in articular cartilage, which extends to a rim of fibrocartilage termed the acetabular labrum. Structurally, the acetabulum has three identifiable features: the horseshoe-shaped lunate surface, acetabular notch, and acetabular fossa (Figure 1.3).

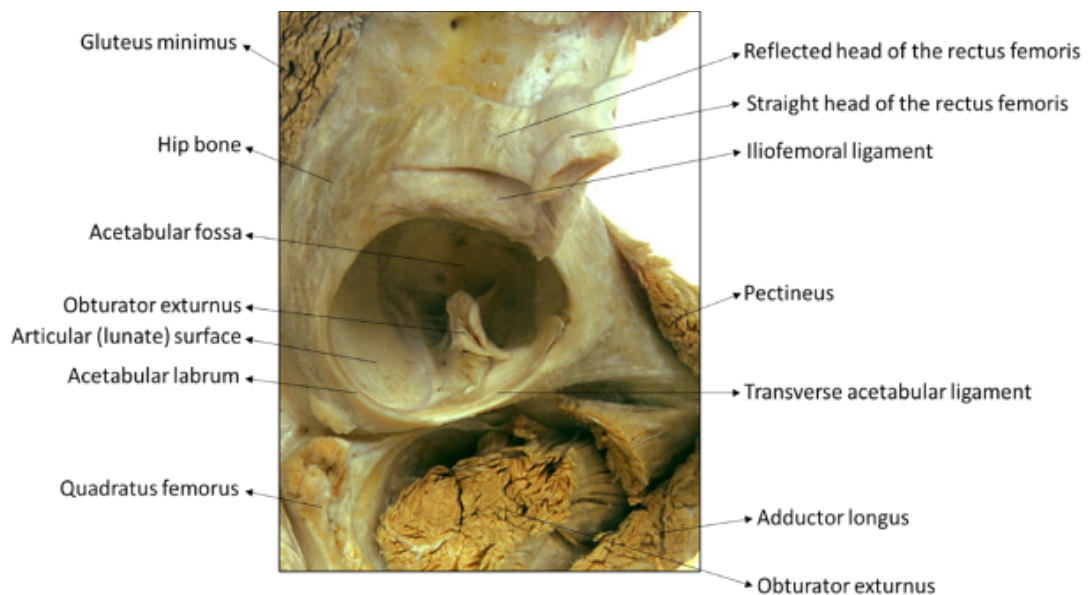


Figure 1.3 - Dissected human acetabulum (right hip). Lateral view showing the major muscle attachments, ligaments and surfaces that form the acetabular portion of the hip joint. Image adapted from Anatomy.tv, 2019, Primal Pictures, 2019.

The area covered by articular cartilage forms a horseshoe shape and is involved in weight bearing, with the maximum thickness occurring superiorly at the site of

maximum load bearing during motion. The central inferior non-articular cavity is termed the acetabular fossa. A synovial-covered fat pad and the acetabular attachment of the ligamentum teres are located at the fossa. The acetabular rim increases the depth and extension of the acetabular fossa. The non-articular portion found anteroinferiorly is the acetabular notch and is attached with the transverse acetabular ligament (TAL) which is continuous with the acetabular labrum. The TAL supports against tensile strains during motion (Löhe *et al.*, 1996).

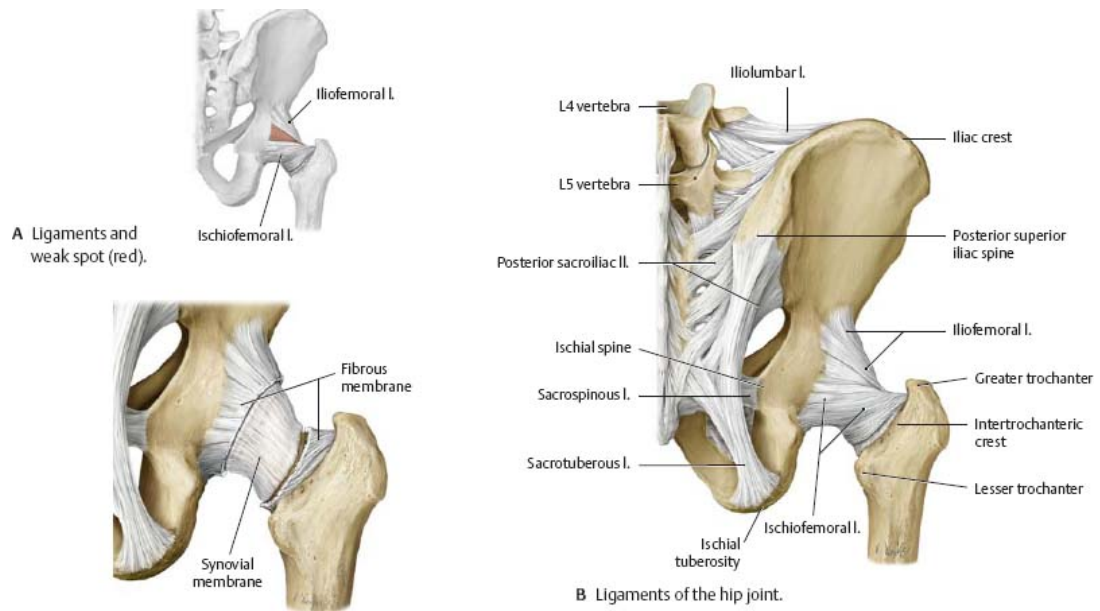
The head of the femur articulates within the acetabulum. It is roughly spheroidal in shape except for a small area called the fovea capitis where the ligamentum teres is attached to the acetabular fossa. The average radius of curvature of a human femoral head is reported to be around 250 mm (Melluso and Mansi, 2017). The articulating surface of the femoral head is also covered in smooth articular cartilage. The smooth articular cartilage covering the articulating surfaces reduces the friction through several million cycles of motion.

The stability of the hip joint depends on three factors: the acetabular depth, associated with the size and narrowing provided by the acetabular labrum, the strength of the iliofemoral, pubofemoral and ischiofemoral ligaments and surrounding musculature which reinforce the joint capsule, and, the length and shape of the neck of the femur.

1.2.1.2 Joint capsule

The joint is encapsulated in thick fibrous sac called the capsular ligament which extends from the intertrochanteric crest enfolding the neck of the femur to the superior of the acetabular rim (Figure 1.4). The capsule is thicker anterosuperiorly compensating for increased stresses experienced in the anterosuperior aspect, for example when standing (Melluso and Mansi, 2017). The capsule is thinner toward the posteroinferior aspect, and the cartilage fibres are loosely connected. The variation in thickness anteroposteriorly correlates with other supporting tissues such as the labrum and ligaments of the joint capsule (Horner, 1846; Cruveilhier, 1847).

The interior aspect of the fibrous capsule is lined with a thin synovial membrane containing synovial fluid which provides the nutrition and lubrication to reduce the friction between the articulating surfaces and through its viscoelastic properties, can dampen the loads experienced through daily activities.



C Joint capsule.

Figure 1.4 - Joint Capsule and Ligamentous support. A – Iliofemoral and Ischiofemoral ligaments with the weak spot highlighted in red. B – The major ligaments of the hip joint contributing to the overall stability of the joint. C – The joint capsule which is a combination of the synovial and fibrous membranes. Image adapted from Melluso and Mansi, 2017, and Ricciardi, 2015.

1.2.1.3 Ligaments of the hip joint

There are six major ligaments of the hip joint which contribute to stabilising and supporting the hip including the capsular ligament, the iliofemoral ligament, the pubofemoral ligament, the ischiofemoral ligament, the transverse acetabular ligament and ligamentum teres femoris (Figure 1.4; Figure 1.5) (Wagner *et al.*, 2012; van Arkel, Amis and Jeffers, 2015). Additionally, the congruency of the bones and the extracapsular support keep the hip joint stable and prevent unnecessary dislocation.

The iliofemoral ligament is located anteriorly and close to the joint capsule, it connects the lower half of the inferior iliac spine and acetabular margin to the intertrochanteric line on the femur (Figure 1.5). The iliofemoral ligament is composed

of thick and strong fibres which prevents the torso from falling backwards during a standing position. The ischiofemoral ligament is relatively weaker than the iliofemoral ligament and provides posterior support.

The ischiofemoral ligament is attached from the greater trochanter to the ischium. The pubofemoral ligament is a triangular ligament located inferomedially and is combines with the anteroinferior part of the capsule and medial aspect of the iliofemoral ligament.

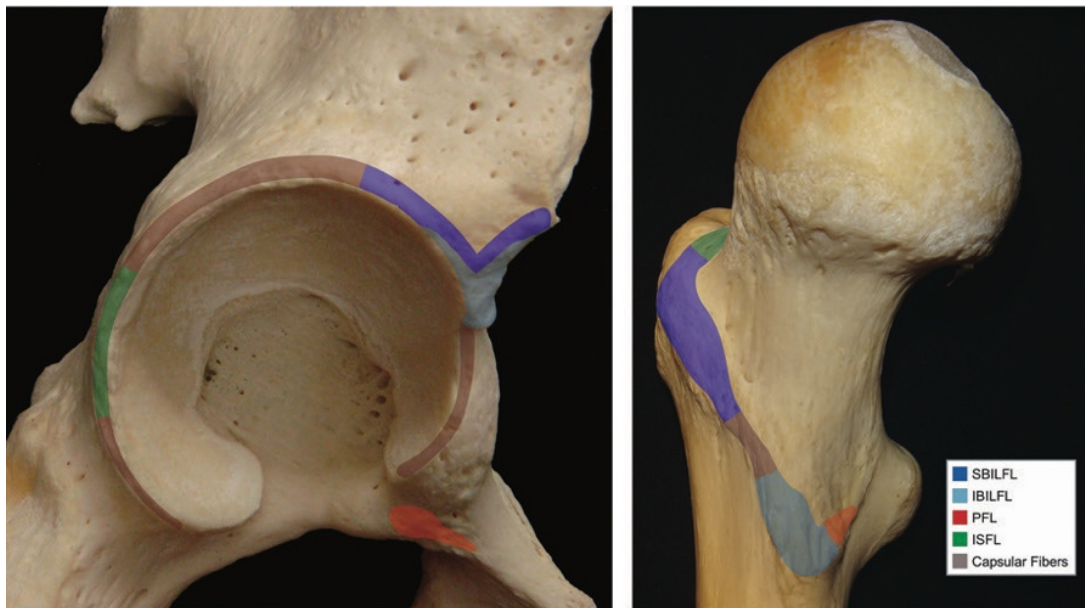


Figure 1.5 – Hip joint model with overlays of the proximal and distal osseous attachments of the articular capsule and capsular ligaments of the hip, respectively, in the acetabular rim and anterior portion of the proximal femoral epiphysis. Key: CLH capsular ligaments of the hip, IBILFL inferior band of the iliofemoral ligament, ILFL iliofemoral ligament, PFL pubofemoral ligament, SBILFL superior band of the iliofemoral ligament, ZO zona orbicularis. Image adapted from Wagner *et al.*, 2012.

The round ligament of the head of the femur or the ligamentum teres femoris is a flat triangular ligament which connects from the fovea of the head to the transverse acetabular ligament (TAL). The ligamentum teres carries arteries to the femoral head which branch originate from the acetabular branches of the obturator and medial circumflex femoral arteries (Mikula *et al.*, 2017).

The acetabular labrum is a fibrocartilaginous rim connected to the acetabular margin. Previously, the labrum was referred to as the cotyloid ligament as it formed a round band which connected the cotyloid cavity (acetabular notch) however it is more

appropriate to think of the labrum as two continuous structures, the labrum (the rim) and the transverse acetabular ligament which completes the labrum but is devoid of cartilage cells.

1.2.1.4 Femoral head

The femoral head is predominantly spherical in shape forming two-thirds of a sphere, being more oval during development. The head is attached at its base separated near the epiphyseal line to the femoral neck which is located distally to the femoral shaft (Figure 1.6).

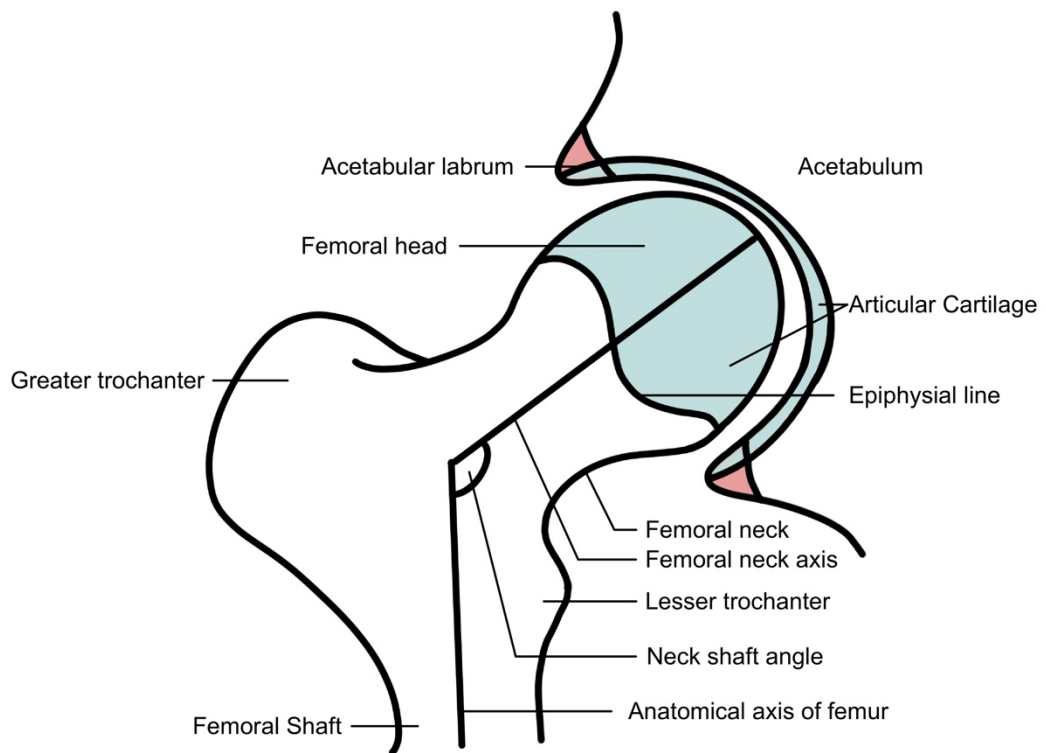


Figure 1.6 – Cross section of the hip joint showing the femoral neck axis and anatomical axis of the femur.

The femoral head is covered with articular cartilage except at the posterior-inferior depression termed the fovea capitis. The ligamentum teres contains a blood supply and is covered in synovium. The fovea capitis is the femoral insertion site of the ligamentum teres(Keene and Villar, 1994).

The size of the femoral neck varies in length and is dependent on the size of the body. The femoral neck is normally narrowest towards the middle. The neck-shaft

angle is the angle between the anatomical axis of the femur running through the femoral shaft with the femoral neck axis.

The neck shaft angle is typically $125\pm 5^\circ$ in adults (Byrne, Mulhall and Baker, 2014). A decreased femoral neck angle is termed coxa vara where the angle is less than 120° , while an increased femoral neck angle is termed coxa valga where the angle exceeds 130° . A significant deviation in neck angle can result in a change in the lever arms used to produce motions by the abductor muscles being too small or too large depending on the condition (*D'lima et al., 2000; Ng et al., 2019*). The femoral neck is also rotated medially (anterior to the coronal plane) this is termed femoral anteversion. The angle of anteversion forms between a mediolateral line through the knee and a line through the femoral head neck and shaft. The angle of femoral anteversion is typically between 15 to 20° (*D'lima et al., 2000; Byrne, Mulhall and Baker, 2014; Bouma et al., 2015*).

1.3 Hip Joint Biomechanics

The joint provides multiaxial mobility and stability during load-bearing activities and the transmission of forces from the upper body to the lower limbs.

1.3.1 Kinematics

The hip joint allows movement in three planes: sagittal/transverse (flexion and extension), frontal/anteroposterior (abduction and adduction) and transverse/vertical (internal and external rotation). The average range of motion in a normal adult hip is summarised in Table 1.1, the variance is subject to age, sex and anatomical differences.

Table 1.1 Average range of motion of the human hip joint. Adapted from (Paul, 1967; Burstein, 2001; Netter, 2006; Torricelli *et al.*, 2016).

Movement	Range of Motion
Flexion	0° to 120°-140°
Extension	0 to 10-30°
Abduction	0° to 30-50°
Adduction	0° to 10-35°
Medial-lateral rotation	0° to 45°

During walking, flexion-extension can range between 45° and 60° per stride, resulting in average sliding velocities of up to 50 mm/s (Brinckmann, Frobin and Hierholzer, 1981; Ipavec *et al.*, 1999). The largest range of motion (ROM) occurs in the sagittal plane during flexion and extension. The total range of motion becomes limited and the measured angles for each movement are lower in patients suffering from osteoarthritis or other pathological conditions (Burstein, 2001). (Kotzar *et al.*, 1991) reported a minimum hip flexion of 120° and 20° abduction/external rotation were crucial for enabling essential activities of daily living.

The human body is highly efficient in ambulation, subtle changes in torques, motion or stability can lead to a loss of efficiency and suggest abnormalities may be present. The stability of the hip depends upon several factors such as the joint kinematics, loading experienced by the joint during static or dynamic activities, unique morphology of bony structures, the action of large muscle groups, the labrum, articular congruence during loading, synovium and capsuloligamentous support.

Paul, (1967) described loading patterns in the hip and knee joints. The force fields during walking are complex, three-dimensional, time dependant and vary considerably with the speed of walking (frequency). In the hip, loading patterns of the walking cycle can be divided into different phases, commencing with heel strike (Figure 1.7).

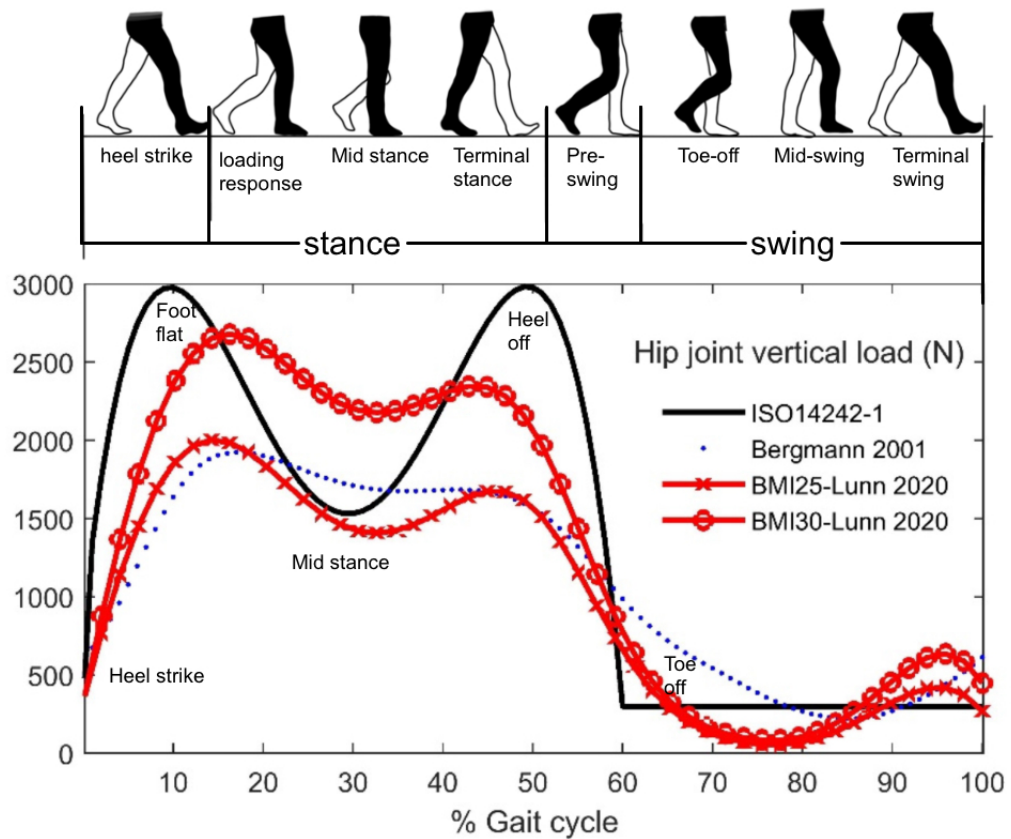


Figure 1.7 – Human walking gait cycle based on three different profiles measuring the joint reaction force on the hip and its relation to the stance and swing phases. Adapted from (L. Gao *et al.*, 2022).

The human walking cycle is divided into two distinct phases, the duration the foot is in contact with the ground is known as the stance phase, while the time the foot is off the ground is known as the swing phase. Figure 1.5 summarises the ground reaction force experienced by the hip during this cycle. The human walking cycle is the most studied gait pattern among other activities of daily living. Both healthy natural hip and artificial joints undergo three-dimensional loads and motions in different activities. The walking cycle from the international organisation for standardisation (ISO) for the operation of wear simulators on joint loading and movements is ISO 14242-2 for human hip replacements. This standard is based on a human model weighing 75kg. The stance phase of the walking cycle is divided into two peaks, at heel strike and toe-off where loads can reach up to four times body weight and between peaks, the load drops below 2 times body weight. The peaks are associated with dynamic

(intertrial forces, acceleration and deceleration of body segments) and static forces (Burstein, 2001). Factors that affect the contact force of the hip joint include age, gender, body mass index (BMI), the frequency of walking, and abnormal walking conditions such as stumbling (Bergmann, Graichen and Rohlmann, 1993; Bergmann *et al.*, 2001, 2016; Pieri *et al.*, 2019; L. Gao *et al.*, 2022).

1.3.2 Contribution of Muscles of the Hip

Muscles play an important role in controlling the movement of the hip joint. An unrestricted hip joint permits rotational motion in all directions. 22 muscles provide the forces required for movement of the hip and contribute to stability. The major muscle groups involved in the hip are summarised with the motion they control in Table 1.2. Muscles of the hip also act to prevent large bending stresses on the femur. As a vertical load passes through the femoral shaft, the medial-lateral sides of the bone experience tensile and compressive stresses. While the effects of muscles are significant to physiological hip mobility, they are not discussed in greater detail in this thesis as the hip simulator used to assess the joint replaces the functionality of the muscle groups *in vitro* using electromechanically controlled actuated motors and hydraulics.

Table 1.2 - Muscles of the hip joint and their axis of motion. Adapted from (Anderson, Strickland and Warren, 2001; Ramage and Varacallo, 2022).

Muscle group	Muscles	Axis of motion
Hip flexors	Iliac and psoas Pectineus Rectus femoris Sartorius	Flexion-Extension
Hip extensors	Gluteus Maximus and Hamstrings	Flexion-Extension
Adductors	Adductor brevis and longus Adductor magnus Gracilis	Adduction- Abduction
Abductors	Gluteus medius and minimus Tensor fascia lata	Adduction- Abduction
External rotators	Gluteus maximus Piriformis Obturator externus Obturator internus Superior and inferior gemelli	Internal-External rotation

1.3.3 Kinetics

The hip forms the structural link between the lower extremities and the axial skeleton; therefore, the hip transmits forces from the ground up, but also some forces from the trunk, head and neck, and upper extremities. During athletic activities, the hip joint is exposed to increased axial and torsional forces (Byrne, Mulhall and Baker, 2014). During a single-leg stance, static forces equate to approximately twice the body weight due to the moments involved in the lever actions of muscles required to counteract body mass forces. During certain activities of daily living such as running, jumping, or climbing stairs, forces acting at the hip, and knee, are greater still.

The static loading of the hip joint has can be simplified using a two-dimensional analysis viewed from the frontal plane. When the body weight is distributed on both legs in a standing position, the centre of gravity is centred between the two hips and the force exerted is equally distributed. The body weight is equal to the sum of weight on both legs, supported equally on the femoral heads, with the resultant vectors being vertical. In a single-leg stance, the effective centre of gravity moves away from the centre between two hips and is now distal from this point. This is due to the non-supporting leg being added to the body mass acting upon the weight-bearing hip (Figure 1.8). The downward force exerted on the weight-bearing hip creates a moment about the centre of the femoral head. The force of the abductor muscles also creates a moment around the centre of the femoral head, the combined force of abductors is typically a multiple of the body weight.

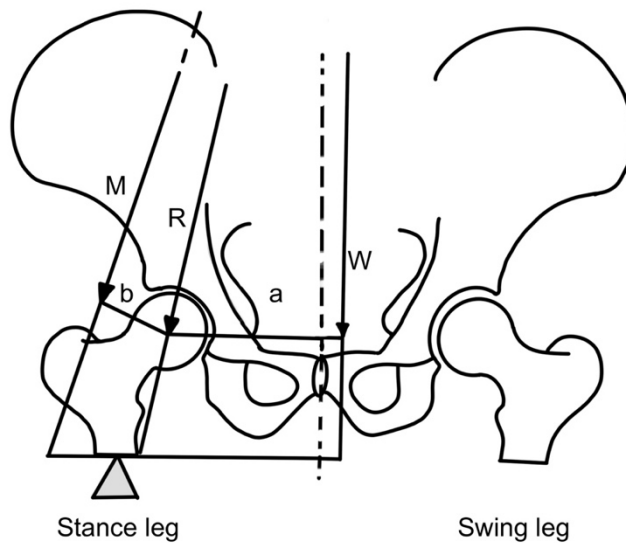


Figure 1.8 – Free body diagram for calculation of the hip joint force while walking. **W** body weight. Moment arm **a** (the distance from the femur to the centre of gravity). Muscles **M** (abductor muscles which resist the movement). Moment arm **b** (caused by the force of the abductors from the centre of the femoral head). **R** joint reaction force.

The lever-arm ratio between the body weight moment arm and the abductor muscle moment arm ($a:b$) contributes to the overall joint reaction force. If the lever-arm ratio increases the force required for gait from abductor muscles increases in addition to the forces on the femoral head. This puts people with shorter femoral necks or a wider pelvis at greater risk of high hip forces when other values are the same (Greenwald and O'Connor, 1971; Greenwald and Haynes, 1972; Greenwald and Nelson, 1973). This may also explain why women are at higher risk for hip fractures and hip replacements due to the wider pelvis, resulting in larger hip forces experienced compared with men due to anatomical differences (Hunt, Clohisy and Prather, 2007; Byrne, Mulhall and Baker, 2014).

Increased body weight is another key contributor to a higher risk for injury as it would increase the total compressive forces applied to the joint. (Zaghloul, 2019) reported that the joint reaction force can be reduced by approximately 50% when 15% of the body weight is applied to a walking stick or cane, this is because the total joint forces can be reduced by bringing the centre of gravity closer to the centre to the femoral

head thereby reducing the moment arm b . This is supported by obesity being a key risk factor for osteoarthritis (Lievence *et al.*, 2002; King, March and Anandacoomarasamy, 2013; Raud *et al.*, 2020). (Felson and Zhang, 1998) estimated that the risk of hip osteoarthritis would decrease by 25% when obesity was managed. Other risk factors include activities which expose the hip joint to higher load bearing, such as jogging, running and contact sports (Rydell, 2014; Martin *et al.*, 2015). Rydell (2014) reported force magnitudes of 2.3 to 2.9 times the body weight for a single leg stance and 1.6 to 3.3 times the body weight for level walking. Similar *in vivo* measurements have been conducted on prostheses and endoprosthesis with strain gauges to record hip joint forces in the body. This suggests overloading as a key mechanism for exposing the joint to experience high joint forces, which over time could expose the joint-to-joint damage or degeneration.

1.4 Tissue structures of the Hip Joint

1.4.1 Types of cartilage

Cartilage is a specialised form of connective tissue made up of cells termed chondrocytes and an extracellular matrix (ECM) of different fibres and ground substance. Mature cartilage is typically found to be avascular and lacks nervous supply leading to poor healing potential. Cartilage can be classified as smooth, hyaline, or fibrous (Figure 1.9).

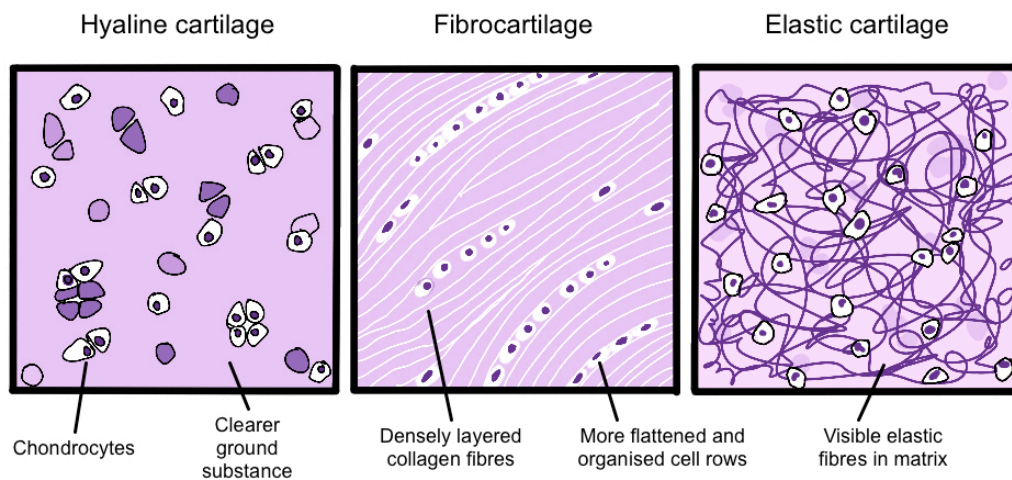


Figure 1.9 – Types of cartilage featuring histological differences typically observed with H&E staining. Hyaline cartilage contains rounded chondrocytes in columns known as lacunae, collagen fibres are not visibly stained in the matrix. Fibrocartilage contains thick, collagen bundles layered on top of one another with rows of chondrocytes intertwined between the fibres. Elastic cartilage contains darkly stained elastic fibres in the matrix. Adapted from Hu and Nukavarapu, 2019.

Chondrocytes are distributed within the ground substance in cavities called lacunae (Tallitsch, 2009). The ground substance is gelatinous and highly elastic allowing the ECM to withstand large amounts of pressure and shear (Tallitsch, 2009). The ground substance comprises a low concentration of glycoproteins and a high concentration of glycosaminoglycans including hyaluronic acid, chondroitin sulphate, and keratan sulphate (Figure 1.10). The chondroitin and keratan sulphates combine with a protein core to form proteoglycans which interact with the collagen and elastic fibres present in the matrix. Approximately 80 chondroitin 4-sulfate and chondroitin 6-sulfate chains bind to the core protein and make up a major portion of the dry weight of hyaline

cartilage (Sophia Fox, Bedi and Rodeo, 2009; Eschweiler *et al.*, 2021). Other components include chondronectin which is a glycoprotein found in cartilage and is responsible for the adhesion of chondrocytes to type II collagen. Laminin and fibronectin are also common glycoproteins involved in cell adhesion and migration (Cramer and Bakkum, 2014).

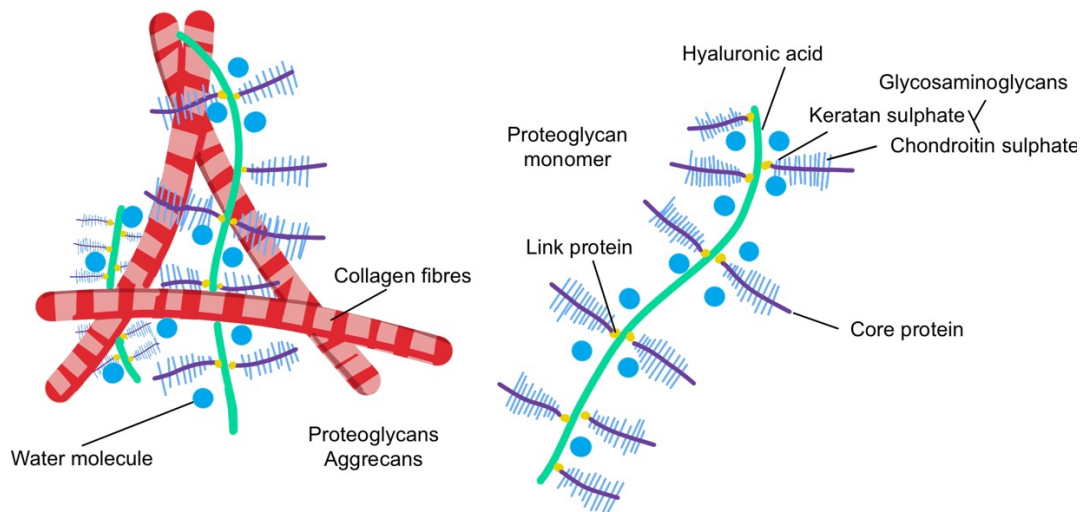


Figure 1.10 – Schematic diagram of the articular cartilage collagen and proteoglycans (aggrecan). The proteoglycan monomer consists of a protein core with covalently bonded glycosaminoglycan side chains consisting of keratan sulphate and chondroitin sulphate. The proteoglycan monomers are non-covalently attached to the hyaluronic acid backbone stabilised by the link proteins. The negatively charged GAG side chains attract water molecules with associated cations. Adapted from Gahunia and Pritzker, 2020.

Hyaline cartilage is commonly surrounded by dense regularly arranged connective tissue known as the perichondrium. The perichondrium is important in the growth and repair of hyaline cartilage and is composed of a fibrous outer layer and a chondrogenic inner layer. The outer layer is made of dense irregular connective tissue hosting spindle-shaped cells called fibrocytes, while the inner layer is made of larger, rounder cells called chondroblasts. Chondroblasts secrete the components of the ground matrix of hyaline cartilage including collagen fibres, hyaluronic acid and chondroitin sulphate. As the cartilage develops and chondroblasts continue to secrete these components they become confined in restricted places called lacunae

and start to differentiate into chondrocytes responsible for maintaining the collagen matrix. A mature cartilage is observed when the chondrocyte completely fills the lacuna.

Fibrocartilage also contains chondrocytes trapped within lacunae, however, unlike hyaline cartilage, the distribution of the lacunae is highly organised in rows. Additionally, the extracellular matrix of fibrocartilage is less homogeneous and collagen fibres within the collagen matrix are arranged regularly. This regular arrangement seems to predict its function for resisting compression and shear forces upon the collagen fibre matrix and the areas it tends to occur in tissues. In most cases there is an absence of the perichondrium in fibrous cartilage, however in regions of articulation, the perichondrium exists, for example in the glenoid labrum and may explain the limited capacity for cartilage repair at articulating joints. Fibrocartilage is found in the knee meniscus and acetabular labrum but also in transitional areas between the cartilage and the bone-forming links between tendons and bone such as the ankle and the annulus fibrosus in the spine.

1.4.2 Articular Cartilage

Articular cartilage is a type of hyaline cartilage lacking a perichondrium, found at the articulating surface of the hip known as articular cartilage. Fibrocartilage is typically found in areas under high stress. Articular cartilage differs from typical hyaline cartilage in the arrangement of the chondrocytes and the collagen fibres of the matrix. The chondrocytes of articular cartilage near the surface are superficial layer are flattened (Figure 1.11), while they are rounder mid to deep zones similar to those in hyaline cartilage shape. In the deepest layers, the chondrocytes are stacked in columns and the matrix is calcified (Cohen, Foster and Mow, 1998; Poole et al., 2002).

Articular cartilage possesses high tensile strength and low compliance because of Glycosaminoglycans (GAGs) which attract cations and water causing the surface to swell after being held in place by the fibrillar network. The arrangement of collagen fibres is suspected to ref

lect the response to the mechanical pressures put on the tissue(Maynard and Downes, 2019). The fibrillar network comprises fibres orientated in different directions amongst 3 zones (Figure 1.12). The arrangement of fibres within the ECM allows the cartilage to withstand compressive and shearing forces more than other forms of cartilage (Figure 1.12).

The articular surface maintains a low coefficient of friction allowing for almost frictionless motion during load bearing. However, the articular cartilage has poor healing capacity, making it susceptible to acute injuries and degenerative changes such as osteoarthritis (Sophia Fox, Bedi and Rodeo, 2009). Historically, ageing and mechanical loading influence the homeostasis of articular cartilage and are important in the pathogenesis of the degenerative joint disease (Musumeci, 2016).

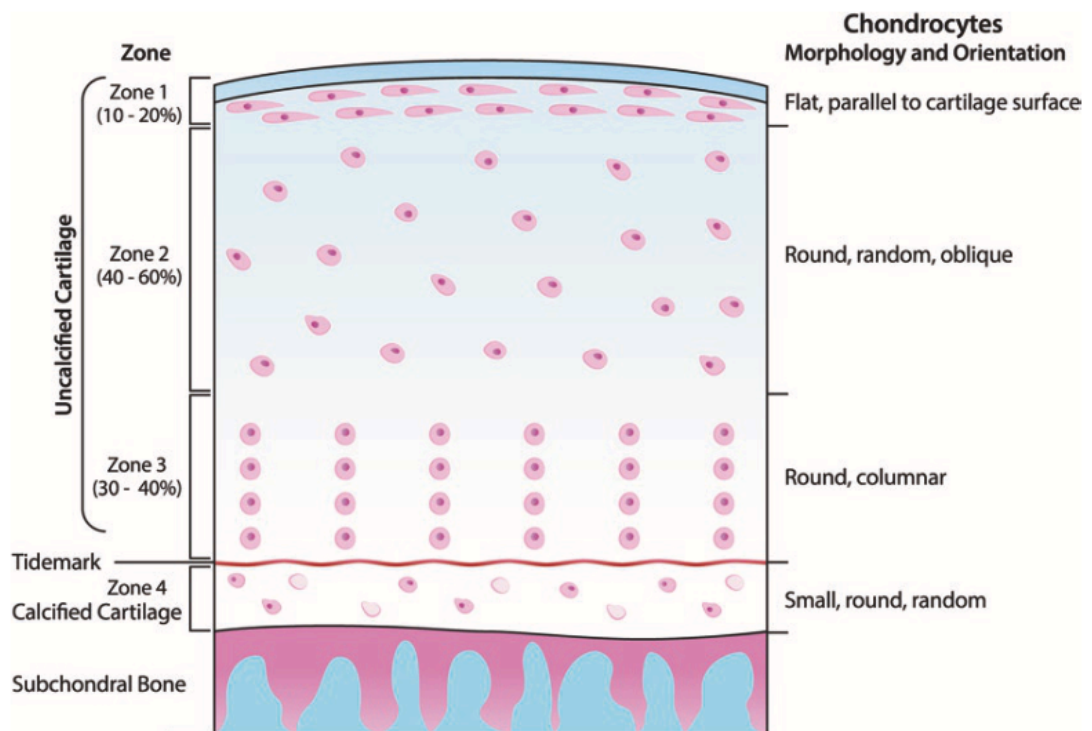


Figure 1.11– Cellular composition and arrangement of the articular cartilage. Taken from Gahunia and Pritzker, 2020.

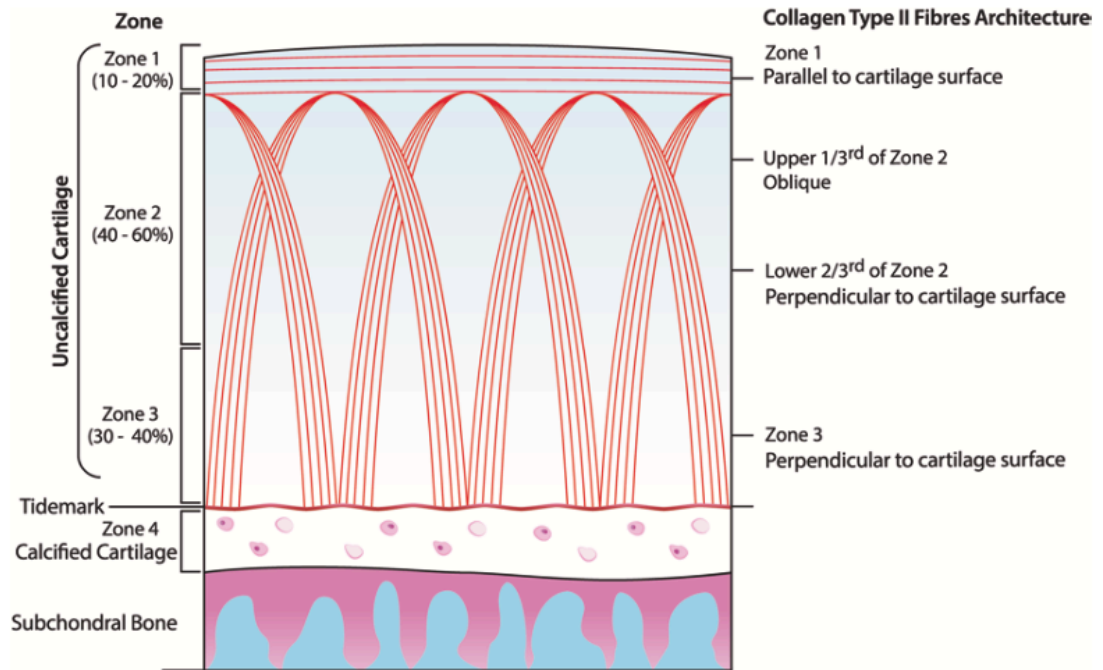


Figure 1.12 – Arrangement of Type II collagen in articular cartilage. The characteristics of the collagen orientation are provided for the superficial, transitional and radial zones. Taken from Gahunia *et al.*, 2020.

1.4.3 Acetabular Labrum

1.4.3.1 Structure of the labrum

The labrum is made up of fibrocartilage and dense connective tissue which merges with the articular cartilage of the acetabulum termed the chondrolabral junction. The labrum transitions from the smooth articular cartilage. The structure is composed of radially oriented collagen fibres attached to subchondral bone of the acetabulum. The acetabular labrum possesses a triangular cross section (Figure 1.13) and the structure is larger with higher coverage in children than adults or mature labrum (Schmerl, Pollard and Hoskins, 2005).

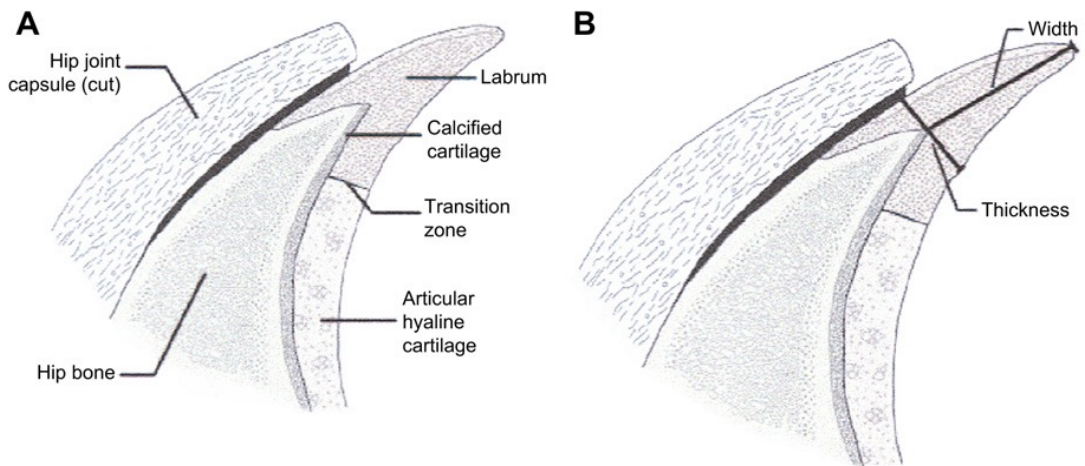


Figure 1.13 – Structure of the human acetabular labrum as defined by (Lewis & Sahrman, 2006). **A** Cross-section of the posterior labrum, showing the boundaries between different zones of subchondral bone, articular cartilage, and labrum. **B** Definitions of the width and thickness of the labrum where the labrum was found to be wider and thinner in the posterior region through arthroscopic examination (Lewis and Sahrman, 2006).

The structure of the acetabular labrum resembles the structure of the meniscus and the glenoid labrum (Alzaharani *et al.*, 2014; Alashkham *et al.*, 2018). The labrum is thought to be like the meniscus, as it is found at the margin of the acetabular cartilage and the joint capsule, furthermore, it assumes a triangular cross-section with a free atypical border and is elastic to touch (Kim, 1984).

Due to the lack of extensive characterisation of the acetabular labrum from literature, it is difficult to definitively define the labrum as a complete fibrocartilaginous structure as it does not match the observed structure of fibrocartilage. However, the composition closely resembles that of cartilaginous, fibrocellular fibrocartilaginous and dense connective tissue. This difficulty in defining the structure is similarly faced with the glenoid labrum (Ockert *et al.*, 2012; Alashkham *et al.*, 2018) as it too has several arthroscopic reports but not enough immunohistochemical or histological analysis. Additionally, it is often difficult to obtain human labrum tissue from donors for thorough characterisation, most studies include structures extracted from surgeries treating labral pathologies.

The labrum deepens the acetabulum increasing the overall surface area, volume, congruity, and stability of the hip joint. The labrum also maintains a fluid seal

(Ferguson *et al.*, 2003; Cadet *et al.*, 2012; Nepple *et al.*, 2014; Philippon *et al.*, 2014), producing negative intra-articular pressure which is important in distributing contact pressure across the articulating surfaces, which lowers the stress on the articular cartilage.

While the labrum has some microvasculature at the base, the labrum is largely believed to be avascular and must utilise diffusion for nutrition and waste transfer. The rate of transfer is dependent on mobility, as the more restricted range of motion can compromise the nutrient flow. Restoring the natural joint range of motion can promote labral healing through hip joint tractional manoeuvres or arthroscopy (Schmerl, Pollard and Hoskins, 2005).

1.4.3.2 Vascularity of the labrum

The healing capacity of tissue is dependent on the presence and location of a vascular supply as has been shown in the meniscus and Achilles tendon. When considering the healing potential of labral lesion, it has remained unclear due to debates upon the presence of vasculature in the acetabular labrum.

Schuck, Noble and McCarthy (2000), examined 10 fresh acetabulae dyed with india ink in the femoral circumflex and internal iliac arteries using a modified spalteholtz clearing technique to make any vasculature visible through layers of soft tissue. Utilising stereomicroscopy and immunohistochemical methods, they found small blood vessels of 0.3-0.5 mm diameter located between the outer surface of the acetabulum to the outer surface of the labrum, terminating at the labral-articular cartilage junction. These vessels seemed to stem from the internal iliac artery and extend into a small portion of the labrum, while most of the labrum was found to be avascular. Therefore, the labrum seems to possess three nutrient pathways linked to each side, the non-articular portion is supplied by synovial vessels, the base is supplied by vessels originating from the subchondral bone and the articular surface from the surrounding synovial fluid. Therefore, between the three sides, the largest potential for healing lies at the base of the labrum. At the same time, damage to the

articular and non-articular surfaces is avascular and has the least potential to heal (Schuck, Noble and McCarthy, 2000).

The vascularity of the acetabular-labrum complex has been found in adults, however, needs to be better understood in the developing child or foetus to understand the development of the supply to the labrum. Masloń *et al.*, (2011) assessed the vascularity of 21 foetal labra and found most of the blood supply was arising from the capsular attachments. The greatest number of vessels were found in the posterosuperior and anterosuperior quadrants. Additionally, the group counted the number of vessels in the capsular and articular areas aged 5-10 lunar months. It noted that the number of labral vessels decreased during foetal development and is expected to decrease in adult life. The lack of vessels could contribute to labral degeneration and poor healing, this finding correlates to the large proportion of patients over 60 with labral tears while they are rarely observed in young and healthy patients. In addition, the lowest number of vessels were found in the posteroinferior quadrants of both regions of the labrum, this is believed to be a result of the pressure changes in this part of the labrum due to a tight fit between the femoral head and the acetabulum when the foetus is in the uterus (Masloń *et al.*, 2011).

The vascular arrangement and supply at the developmental stages can reveal important information about the consequence of micro stress caused to the labrum when comparing the developing labrum in normal hips to patients with developmental hip dysplasia.

1.4.3.3 Nerve supply of the labrum

Patients experiencing hip pain or mechanical related symptoms typically have some form of acetabular tearing. This is observed when patients present posterior hip pain especially during to weight-bearing or twisting motion. The hip pain observed is typically lumbosacral, thoracolumbar, or sacroiliac in origin. In older patients, this could be because of ageing and osteoarthritis. Younger patients may possess labral injuries yet show no signs of pain. They are largely asymptomatic, making it quite

difficult to determine to what extent the labrum signals pain and whether it even possesses a nervous supply (Schmerl, Pollard and Hoskins, 2005).

The most recent study to investigate the nervous supply of the labrum was conducted by Alzahrani *et al.*,(2014), where they harvested 20 specimens to test the presence of free nerve endings (FNE) and different types of nerve end organs (NEO). To reveal the structures, the specimens were stained using Hematoxylin and Eosin and followed with immunohistological staining using a rabbit polyclonal antibody directed against S-100 protein which is commonly used to identify cells of the nervous system. The study observed the presence of FNEs and NEOS in all labral specimen in superficial zones of the labra at the antero-superior and postero-superior zones of the labrum with lower nervous activity in the antero-inferior and little activity in the postero-inferior quadrant. In the deep zones there is almost no activity in all four quadrants (with very few free nerve endings in the antero-superior quadrant) (Alzahrani *et al.*, 2014). This suggests that the labrum does play an important role in transmitting nociception via FNEs and proprioception to the hip through NEOs. This could explain why for late-stage degeneration or deep tears, go unnoticed by patients so can appear to be asymptomatic and the most common area for small tearing or fraying is found in the antero-superior quadrant which had the highest nerve endings and could explain the reported groin pain. Importantly, the study noted the presence of microfilaments rich in fibroblasts with elongated cell processes or myofibroblasts –specialised contractile fibroblasts which are involved in tissue repair and secrete extracellular matrix and provide high contractile forces which help in healing the tissue.

It is therefore possible, that the labrum can have microtears occurring in healthy individuals but can maintain itself and close small tears through the myofibroblasts and neurosection through the synovial fluid. This similar system is found in the cornea of the eye (Seldes *et al.*, 2001a). Therefore, for management of early or less severe tearing, labral repair could retain the proprioceptive function of the hip and allow the

tears to heal with time, while surgeons operating on severe tearing may consider arthroscopic labral debridement (partial labrectomy) which could provide pain relief for patients experiencing sharp groin pain through the excision of free nerve endings.

1.5 ECM mechanics

The tissue microstructure in section 1.3 explains the arrangement and contribution of collagen fibre bundles and proteoglycans which form the articular cartilage and fibrocartilage of the labrum. These structures contribute to micromechanics and inform the gross mechanical behaviour of the tissue in resisting a wide range of forces. Collagen fibres resist tension where many fibres create a bundle arrangement or layer which resists tension in a particular direction, which is defined by the orientation of these fibres. For example, to resist shear forces experienced at the surface, collagen fibres are arranged parallel to the superficial surface layer forming a mesh layer known as the lamina splendens. In the middle deeper zone of articular cartilage, collagen fibres are arranged perpendicular to the surface as long fibres and help resist compression and shear stresses (Bowman, Fox and Sekiya, 2010). The intra and intermolecular cross-links inform the ultimate tensile strength of collagen fibres. The proteoglycans and glycosaminoglycans form a dense bottle brush structure which attracts and holds onto water molecules creating a gelatinous structure which is designed to withstand compression. The overall arrangement and composition of the extracellular matrix inform the bulk tissue mechanical properties designed to resist, tensile, shear and compressive forces during load bearing.

1.5.1 Synovial fluid

Synovial fluid is an ultrafiltrate from plasma & contains proteins derived from the blood plasma & proteins that are produced by cells within the joint tissues. Synovial fluid forms a thin layer (roughly 50µm) at the surface of cartilage and seeps into microcavities and irregularities in the articular cartilage surface (Gardner, 2008; King, March and Anandacoomarasamy, 2013).

Synovial fluid acts as the lubricant in articulating joints reducing the overall friction during joint motion. As a dilatant fluid, synovial fluid functions as a powerful shock absorber as it becomes more viscous under applied pressure. In the hip, synovial fluid becomes thicker when shear is applied to protect the joint. The fluid thins out to its normal viscosity between shocks to resume its function as a lubricant. Synovial fluid is also important for nutrient and waste transport to the avascular cartilage, it supplies oxygen and nutrients while removing CO₂ and metabolic waste from the chondrocytes within the surrounding cartilage. Finally, the fluid is also involved in molecular sieving, as pressure within the joint forces hyaluronan in the fluid against the synovial membrane forming a barrier, preventing cells from migrating into or fluid from migrating out of the joint space (King, 1966; Gardner, 2008).

1.5.2 Lamina Splendens (Superficial Layer of Articular cartilage)

The lamina splendens comprises interwoven collagen bundles which lie parallel to the surface of the articular cartilage (Figure 1.14) and integrate with perpendicular oriented collagen fibres and those in the deeper region to form a 3D collagen scaffold, which anchors to the subchondral bone. Peeling off the surface layer of the lamina splendens reduces the wear and shearing resistance of the articular cartilage. It can also lead to a change in the osmotic pressure in the articular cartilage and therefore gradual release of proteoglycans to the joint cavity. This effect may be determined by assessing the reduction of GAGs using histochemical investigation or biochemical analysis using GAG assays or spectroscopy. The mechanical strength and integrity of the interwoven collagen bundles have not studied extensively and however, it would be characteristic of delamination-type damage where the most superficial layer is peeled off.

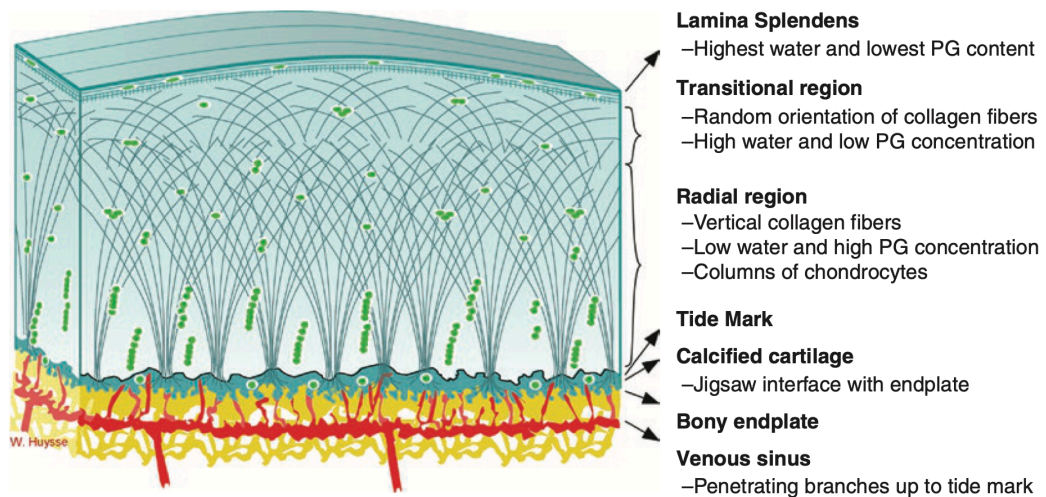


Figure 1.14 Schematic of the articular cartilage, showing the arrangement of collagen fibres within the different regions. Notice the superficial layer arranged with fibres parallel to the surface known as the lamina splendens. This would suggest this layer is particularly important for shear resistance. Taken from Huysse and Verstraete, 2021.

1.5.3 Collagen

Collagen is a major component of the dry weight of the extracellular matrix with collagen fibres being predominantly resistant to tensile forces. The orientation and arrangement of these fibres can affect the functions of the tissue. Table 1.3 details the main characteristics of collagen types I and II as they are the most abundant fibrillar collagens present in articular and fibrocartilage (Hill *et al.*, 2008; Wu, Kirk and Zheng, 2008; Rieppo *et al.*, 2009; Exposito *et al.*, 2010; Eleswarapu, Responde and Athanasiou, 2011; Hosseini *et al.*, 2013; Ross *et al.*, 2013; J. Li *et al.*, 2016; Ravanfar *et al.*, 2017; Copes *et al.*, 2019; Kistenev *et al.*, 2019; Mansfield *et al.*, 2019).

Table 1.3 – Main characteristics of collagen types I and II. Adapted from (Ricard-Blum, 2011).

Collagen	Presence	Optical appearance through microscopy	Ultrastructure	Interaction with GAGs	Main function
Type I	Fibrocartilage, tendon, dermis	Closely packed, thick, strongly birefringent yellow or red fibres	Densely packed fibroblasts, thick fibrils	Low level of interaction, typically only with dermatan sulphate	Resistance to tension
Type II	Hyaline and elastic cartilage	Loose, collagenous network typically visible only through PicoSirius red staining and polarisation microscopy	No large fibres, Very thin fibrils embedded in an abundant ground substance	High level of interaction, mainly with chondroitin sulphate	Resistance to intermittent pressure, compression

1.6 Labral tearing, Cartilage degeneration and Bony abnormalities

Groin pain can result from intra or extra-articular hip joint pathologies such as labral tearing or through anatomical deformities (Table 1.4).

Table 1.4 : Intra and extra articular pathologies of the hip joint resulting in groin pain (Suarez *et al.*, 2013).

Intra-articular hip joint pathology	Extra-articular hip joint pathology
Acetabular labral tears	Apophyseal avulsion fractures
Osteonecrosis of the femoral head	Lumbar radiculopathy
Femoroacetabular impingement	Pubic ramus stress fracture
Pethes disease	Muscle strains
Oncologic processes	Nerve entrapment
Osteoarthritis	Osteitis pubis
Osteochondritis dissecans	
Septic Arthritis	
Slipped capital femoral epiphysis	
Synovitis	

Two major structural abnormalities lead to most reported pathomechanical hip conditions which are femoroacetabular impingement (FAI) and hip dysplasia (or structural instability of the hip).

FAI causes regular undesirable contact between the femoral head-neck junction and the acetabular rim, and the contact has been associated with labral detachment and intra-articular cartilage delamination. Abnormal contact between the proximal femur and acetabular rim causes lesions at the acetabular labrum and can even affect the adjacent articular cartilage. FAI is commonly classified into two subcategories cam or pincer type. Hip dysplasia is a form of structural instability of the joint which causes shear overloading and damage to the acetabular rim (Ross *et al.*, 2013). Typically, biomechanical evaluation of osteoarthritis (OA) indicates that concentric or eccentric overloading of the anterior superior portion of the labrum, lead to cartilage degeneration due to axial overload caused by a disorientated articular surface with reduced contact areas due to instability from a condition such as developmental dysplasia of the hip. Typically, this leads to excessive eccentric loading at the anterosuperior portion of the acetabular labrum (Mak *et al.*, 2011; Weiss *et al.*, 2013; Samaan *et al.*, 2017). Proteoglycan disorientation in the labrum and articular cartilage is thought to alter osmotic swelling and other interactions associated with the biomechanical properties of the articular cartilage (Han *et al.*, 2011; Alcaide-Ruggiero, Cugat and Domínguez, 2023).

1.6.1 Femoroacetabular impingement

Femoroacetabular impingement (FAI) occurs when there is abnormal contact between the femur and the acetabular rim as a result of abnormal morphology of the proximal femur and/or the acetabulum, or in the case of patients with normal anatomy, excessive and extreme ranges of motion outside of the normal physiological range. Unlike with hip prostheses, the natural hip joint is considerably constrained and, therefore is subject to direct contact and shearing forces with fewer abnormal motions. FAI is further distinguished into two main subtypes based on the

loading pattern and areas of damage that are linked with the condition (Figure 1.15).

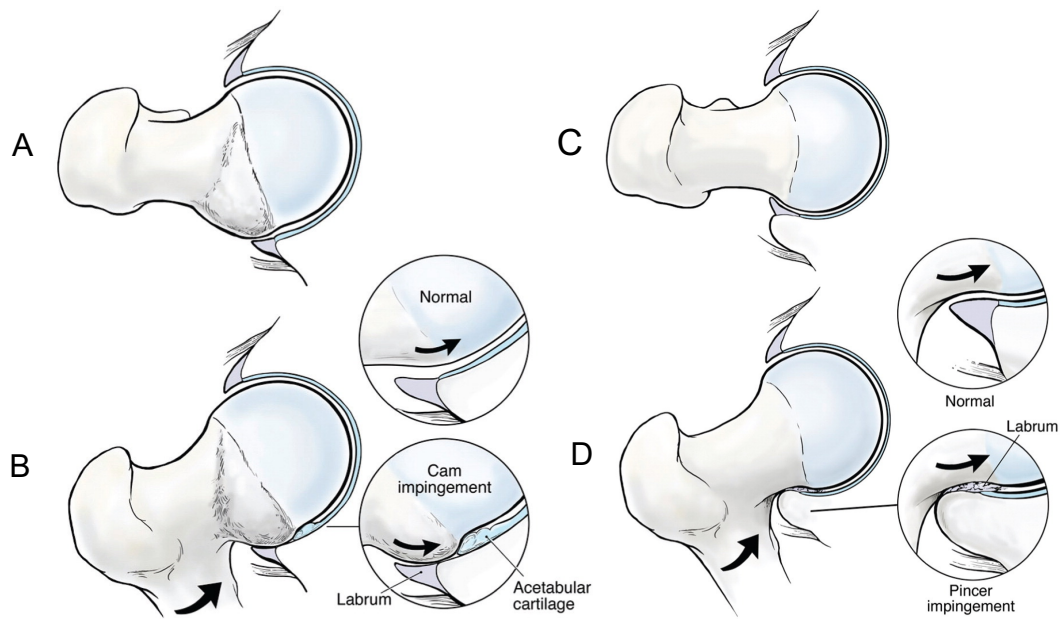


Figure 1.15– A – Bony prominence found centred on the anterolateral femoral head-neck junction (cam lesion). B Cam impingement is when the aspherical cam lesion glides under the labrum during flexion, making contact with the edge of the articular cartilage, resulting in progressive delamination. C Bony overcoverage of the anterior labrum results in pincer impingement. D The anterior labrum gets crushed by the pincer lesion against the neck of the femur. Adapted from (Byrd, 2014).

Ross *et al.*, (2013) reported that FAI is the major contributor in developing early osteoarthritis for non-dysplastic hips due to the motions involved rather than the axial loading on the hip. Physical examination of the hip revealed limitation of motion in terms of internal rotation and adduction during flexion. FAI is believed to precede OA in younger patients as it is typically observed in young and active adults with a slow onset of groin pain initiated from minor trauma. Initially, patients report intermittent pain aggravated under intensive athletic or prolonged daily activities such as walking or sitting.

When comparing the chondral lesions between the two types of impingement, the lesions in pincer type are often benign, limited to a small rim area compared to deeper lesions and widespread tearing of the labrum found in cam type. Additionally, cam

type seems to be more commonly found in young males compared to pincer type which is found in middle aged women with abnormalities to the acetabulum.

It is widely debated whether labral injuries precede impingement or if chondral injuries can cause detachment and damage to the labrum. Ross *et al.*, (2013) reported that cam impingement resulted in deep chondral injuries followed by labral detachment. Arthroscopic examinations by surgeons revealed that the labral detachment occurs at the articular margin and not the capsular margin. Additionally, chondral injuries in the absence of labral tears can be observed at the early stages of the impingement process but not the opposite. If there is labral tearing without chondral injury not due to pincer impingement, is quite rare and could be explained by acute trauma to the labrum. In the case of early pincer impingement there is labral tearing prior to chondral injuries. Labral tears initiated by impingement often occur in the anterosuperior region of the acetabulum as observed during arthroscopic examination of the hip. It is possible however that chondral lesions remain undetected during hip arthroscopy which may account for the high number of isolated labral tears typically found in the literature.

1.6.1.1 Cam type deformities

Cam impingement is a result of an abnormal femoral head with an increasing radius or at the neck junction which impinges on the acetabulum during flexion. This leads to shear forces on the surface between the articular cartilage and the acetabular labrum leading to abrasion of the cartilage and avulsion from the labrum and subchondral bone. While the damage is in the anterosuperior rim area, the damage is not constantly directed at the rim and the chondral avulsion is suspected to cause tearing or detachment of the non-contact labrum.

1.6.1.2 Pincer type deformities

Pincer impingement is a result of direct contact between the acetabular rim and the femoral head-neck junction where the abutment is a result of an abnormal acetabulum commonly a coxa profunda or over coverage termed acetabular

retroversion. This type of FAI leads to direct damage to the acetabular labrum before affecting the surrounding structures. Repetitive damage leads to degeneration of the labrum with intrasubstance ganglion formation, or ossification of the rim leading to additional deepening of the acetabulum and worsening of the over coverage. The damage typically occurs in the anterior region where the abutment occurs and, in the opposite (posteroinferior) side of the acetabulum because of the contact from the femoral neck.

1.6.2 Labral damage

Labral tears are classified with respect to location, morphologically and etiology, tears are usually classified as either radial flap, radial fibrillated, longitudinal peripheral and unstable, they occur anterior, posterior, or superior and etiologically as degenerative, dysplastic, traumatic or idiopathic (Schmerl, Pollard and Hoskins, 2005).

The highest number of labral tears occur in the anterosuperior region, followed by anterior and superior regions of the acetabular rim (Amanatullah *et al.*, 2015). A common feature of anterosuperior tears is with patients reporting a catching type pain from slipping or twisting injuries. In Asian countries, there was higher incidence of posterior tears which could be linked to certain motion such as hyperflexion or squatting motions, however the evidence for this is limited as no large-scale study has been conducted to confirm these differences. Posterior tears are more likely when the patient has posterior subluxation or dislocation. McCarthy *et al.*, (2001), termed lesions found in the anterior labrum as watershed lesions which are found following anterior acetabular chondral injury (Schuck, Noble and McCarthy, 2000).

There is significant evidence for the occurrence of labral lesions from cadaveric studies alone. Typically, around 93-95% present at least one labral lesion with around 80% of older patients (above 30) presenting some form of labral detachment from the articular cartilage termed a bucket handle lesion (Schmerl, Pollard and Hoskins, 2005).

Degenerative tears can affect multiple regions of the labrum and are associated with inflammatory arthritis. The typical morphology of labral tears involves detachment from the articular cartilage commonly observed as radial flap tears and radial fibrillated tears. Tears which are a result of instability followed no real pattern but triggered mechanical symptoms (Schmerl, Pollard and Hoskins, 2005).

The tears tend to fray and are commonly found in patients older than 60. For older patients over 60 years, tearing is believed to be a part of ageing leading to eventual osteoarthritis; however, there has been no large-scale study confirming the presence of labral tears or symptomatic hip pain as part of the normal ageing process. The labrum is thought to possess weight bearing function therefore it is sensible to assume that asymmetric force distribution could eventually lead to cartilage erosion and possible erosion of the joint space with other degenerative changes to the joint (Schmerl, Pollard and Hoskins, 2005).

Labral tears resulting from trauma typically benign, and do not implicate other areas depending on the type of loads or motion affected. Axial loading of the femoral head into the acetabulum with posterior dislocation tend to create posterior labral tears. Anterior labral tearing typically results from axial trauma without dislocation. The most severe form of labral tearing is linked with hyperextension and femoral external rotation. Although there is a lack of strong evidence from studies relating to the function of the labrum, it is believed that the labrum takes on a weight-bearing role under extreme motion or loading and results in tearing or detachment. Therefore, young adults and athletes who partake in repetitive twisting motions, hyperflexion, hyperextension, or abduction are at the highest risk of causing trauma to the labrum (Schmerl, Pollard and Hoskins, 2005).

1.7 Visualisation of labral damage

There are very few methods capable of assessing early changes in osteoarthritic cartilage in a non-destructive manner. Magnetic resonance imaging (MRI) is one of the most common radiographic methods used to visualise soft tissue and changes

for diagnosis and treatment, especially in the assessment of cartilage degeneration and detection of early OA in a non-destructively (Alhadtaq *et al.*, 2004).

While MRI has been used to detect abnormalities in cartilage morphology and measure changes in cartilage volume, it is limited to a lower resolution relative to some of the newer imaging methods and is prone to some artefacts such as partial volume averaging which can lead to compromised detection of microstructural changes of cartilage degeneration in the clinic (Alhadtaq *et al.*, 2004; Amanatullah *et al.*, 2015). Furthermore, studies have shown that in early OA, the collagen fibril network can remain largely intact using MRI and may appear healthy, hence can lead to misdiagnosis and requires the use of high-resolution imaging techniques. In fact, in older patients, it is only at the more advanced stages of OA where the cartilage will appear to fray and lose its trilaminar appearance, looking fibrillated in MRI and due to the anisotropic nature during MRI imaging, the damage may cause artefacts which are overlooked at the clinic.

A pelvis MRI with intra-abdominal and intra-pelvic structures is not enough when diagnosing more subtle pathologies of the hip such as cam deformity. For higher resolution a dedicated hip MRI with a hip coil and intravenous/intra-articular contrast is necessary. This method is called MRI arthrography and can help distinguish any labral or chondral lesions and morphology of the acetabular rim and femoral head-neck junction. Healthy labrum tissue appears triangular with sharp margins and low signal intensity on T1 and T2 weighted images. Gradient echo sequences (GRE) show the labrum with higher signal intensities, much like fibrous tissue. On the contrary, degenerated labrum has an increased signal on T2 weighted and GRE sequences. The labrum may also be increased in volume and tears are distinguished by a linear band of high signal intensity in the labrum or near the chondrolabral junction. Furthermore, with increasing degeneration, thinning of the labrum is observed with ossification occurring near the articular side, typically observed in

chronic pincer FAI. At advanced stages, the entire outline of the labrum is ossified and is observed at signal intensities close to bone.

1.8 Classification of labral tearing and damage

Labral tear classification was initially based on location of the tear, referred to as the clock face model around the acetabulum. In terms of histological evaluation tears were divided into type 1 where there was detachment of the labrum from the articular surface, and type 2 where there was intrasubstance injury. The Lage scale is based on the etiology to define whether the tear occurred as a result of traumatic, degenerative, idiopathic or congenital basis or on the morphology of the tear. McCarthy *et al.*, (2001) classified damage by including the adjacent cartilage damage on a scale from 0 to 4 based on severity. The most recent method for classification is based on the MAHORN system which considers both the morphology and the pathology of the tear through its histological appearance, gross appearance, morphology, and etiology.

1.9 Surgical management of labral tearing

Arthroscopy represents the gold standard in both the diagnosis using MR arthrography and in the treatment of labral tears. The procedure is considered minimally invasive as it requires only two entry points. The surgeon can visualise and access of all quadrants of the acetabulum using arthroscopy (Schmerl, Pollard and Hoskins, 2005). The process of labral repair (Figure 1.16) involves restoring the integrity of the labrum through anchoring or suturing the labrum in place.

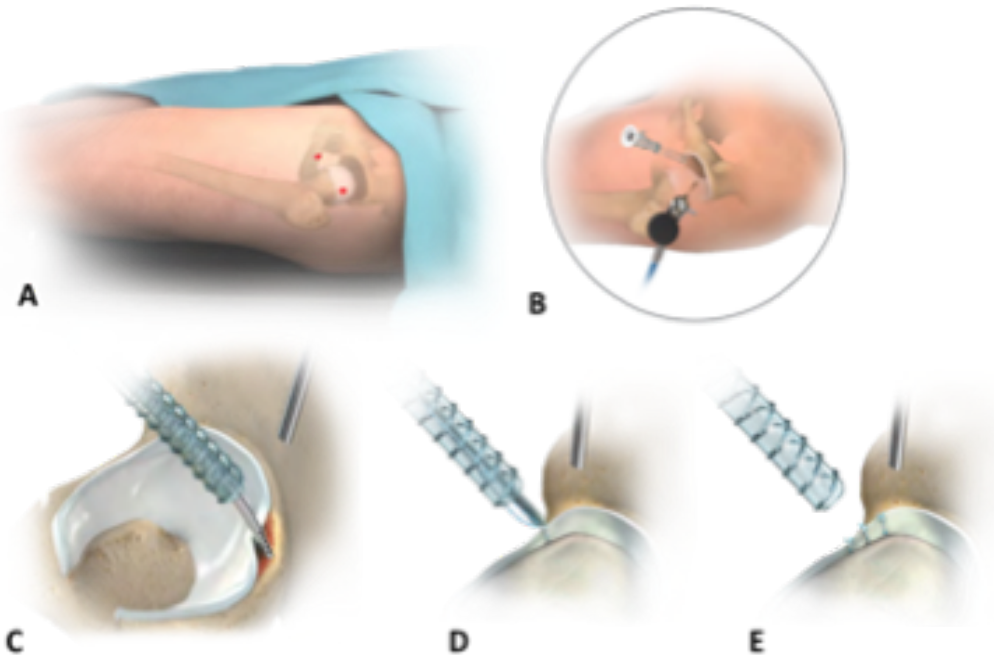


Figure 1.16 - Hip Acetabular Labral Repair. A - the entry portals chosen during hip arthroscopy. B - the two-portal technique. C - the use of a shaver to debride the torn labrum. D shows the drill and suturing procedure. E shows the completed sutured labrum. Adapted from (Matsuda, Hurst and Biomet, 2016).

While the procedure is routinely performed and is accepted to be better option than labrum resection (complete removal of the labrum) as the labrum plays several important functions in maintaining the hip joint, the outcome measures are typically only observed for a year and resection is still widely performed. The non-arthroplasty hip register found comparable levels of resection to repair surgeries being performed in the UK.

A recent systematic review of the outcomes for hip arthroscopy, measuring common indications for arthroscopy including FAI, labral tearing, septic hip, loose bodies, extra-articular lesions, and mild to moderate osteoarthritic lesions, revealed that there was considerable evidence supporting arthroscopic repair of labral tears and for treating symptomatic FAI. On the other hand, they reported poor-quality of evidence to support arthroscopic procedures to treat extra-articular impingement, septic arthritis, mild/moderate osteoarthritis and labral reconstruction. Additionally, they could not make any recommendations for treatment of asymptomatic FAI. The

outcome measures and indication for arthroscopic surgeries therefore needs to be observed over time and the scientific evidence behind many of these procedures must be re-evaluated to allow better patient outcomes.

Finite element models are particularly useful at investigating parameters which cannot be examined easily in-vitro, such as fluid support or to consider more complex factors to investigate the mechanical properties of cartilage. For example, Harris et al 2012 used finite element analysis (FEA) to predict hip joint contact stress during gait and other activities of daily living. When the cartilage was modelled as hyper-elastic, the hip was found to experience a peak contact stress of 8.66 MPa during walking gait, which increases by up to 4MPa during stair climbing. Studies like this can help prototype and predict behaviours rapidly. Moreover, several variations or conditions can be tested with input of clinical gait data or CT scans to predict and plan strategies for surgery and predicting how impingement may occur.

Early studies investigated artificial acetabular cups implanted into cadaveric femoral bones to test micromotion, however, these studies were limited by the lack of a full range of motion i.e. 6DOF as they only used single or limited directions of motion which were assumed to be dominant. Additionally, these studies did not factor the effect of dynamic hip motion observed during daily activities. Hips were placed at fixed angles throughout the testing period to replicate single stance or heel strike modes. These limitations also translate to several studies investigating the whole human hip joint which used inconsistent loading regimes, static loads which were relatively low and with motion limited to a single axis or stationery.

1.10 Experimental and computational approaches for investigating the natural hip joint

Turley *et al.*, (2013) investigated different CT range of motion to determine the range for osseous impingement of the bony geometries of the hip joint and the effect of soft tissues on the natural bony structures. They showed that pure flexion motion was at the highest risk of osseous impingement, followed by flexion with adduction. These

motions help understand where damage from femoroacetabular impingement is likely to occur or of prosthetic impingement post-THA. By comparing the extremes of motion experienced by the hips of subjects who took part in a series of activities of daily living, they recorded the arc of motion predicted by the osseous structures of the joint. When overlapping these motion arcs, they found a reduced functional range of motion compared to the osseous motion possible (Figure 1.17). They noticed a significant reduction in extension and flexion with adduction which suggests that soft tissues play a major role in controlling extension as opposed to reaching osseous impingement with an anteverted acetabular cup. Furthermore, osseous impingement was noted at the extremes of adduction and abduction, corresponding to osseous impingement of the lesser trochanter on the pubis and the superior-lateral acetabular rim.

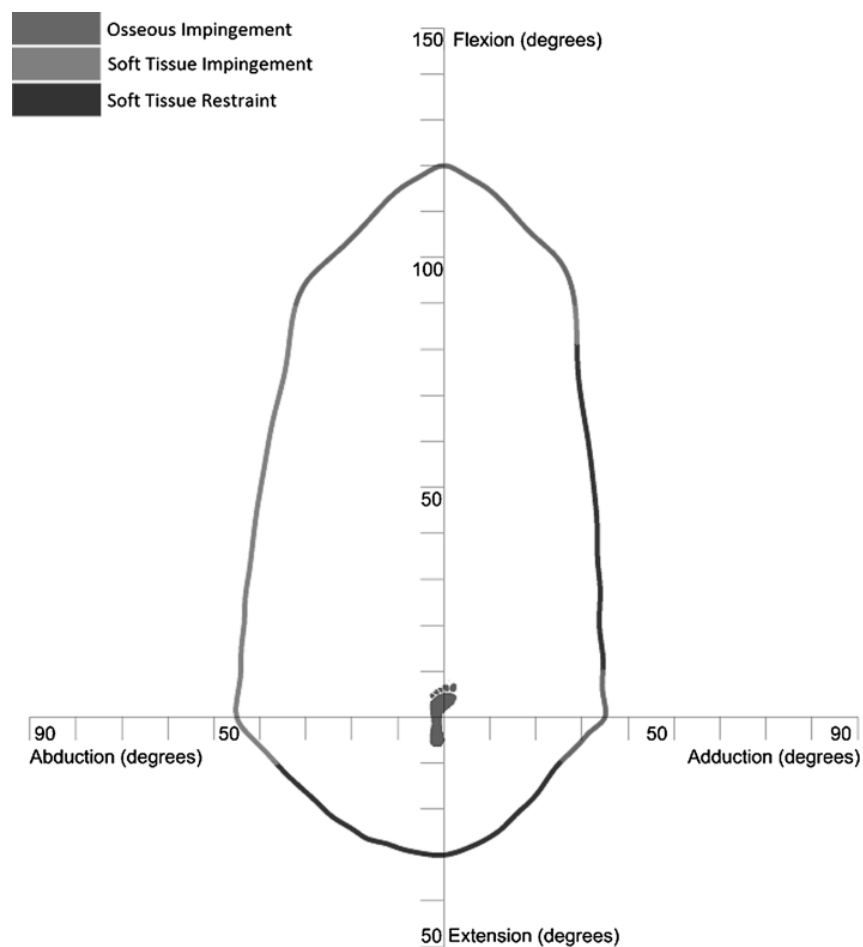


Figure 1.17 - Evaluation of range of motion restriction within the hip joint. This graph shows the range of motion benchmark recorded and the associated impingement

zones. Osseous impingement was most likely with flexion and flexion-adduction. Soft tissue impingement was most likely with abduction and flexion-abduction, and flexion-adduction. Image adapted from (Turley *et al.*, 2013).

1.10.1 Mechanical Hip Simulation

Electromechanical hip simulators can produce mechanical environments for tribological assessment of artificial hip or hemiarthroplasty implants. These implants are tested *in vitro* in a physiologically relevant loading environment with control over the interaction between structures, motions, loading, lubrication, and temperatures like the human hip joint.

Hip joint simulators can reproduce millions of human gait cycles representing the performance of the artificial joint if it was implanted *in situ*. Surfaces of the components can then be assessed using tribological measurements and qualitative analysis. Thus, they permit human hip joint sized components to be studied in an experimentally controlled environment over a long period of time.

While clinical and *in silico* studies have assessed mechanical environments (Miozzari *et al.*, 2004; Moores *et al.*, 2007; Pascual-Garrido *et al.*, 2018), there is a considerable gap in experimental models which can study natural hip joints *in vitro*. Experimental models which have studied natural hip joints *in vitro*, have yet to investigate in detail how abnormal mechanical environments can degrade the soft tissue. A comparison of natural hip simulation studies has been provided in Table 1.5

Table 1.5 - Comparison of studies conducting mechanical simulation.

Study	Tissue	Tissue Type	Simulator	Load/Pressure	Motion	Duration	Comments
Macirowski, 1994	Hemiarthroplasty model	Human cadaveric	MIT Hip Simulator	225-900N	Stationary	1800 seconds	Inverted Endoprosthesis setup for total surface stress measurements and analysis of intact acetabular cartilage topography. Very short test, no motion due to assumption. Only considered the viscoelastic nature of cartilage. Physiological loading was used however the motion was limited to recording movement of articular cartilage after the application of axial force rather than a test for natural loading and motion experienced from a hemiprosthesis upon cartilage.
Konrath <i>et al.</i> , 1998	Whole hip joint	Human cadaveric	Instron materials testing machine	2060N	Stationary	-	Study setup model to simulate loads experienced by the labrum and TAL during a single leg stance where the joint was loaded with axial and abductor forces. Study

							had a small sample size and use of pressure films was unreliable. Study reported that the removal of the labrum or TAL did not significantly increase the pressure or load in the acetabulum with only a small decrease being recorded in the posterior aspect of the acetabulum.
Ferguson <i>et al.</i> , 2003	Whole hip joint	Human cadaveric	MTS Bionic srvo- hydraulic test frame	Static + Dynamic conditions (200- 550 N)	Stationary	3600 seconds	Investigated the labral seal function. Measured fluid pressure within acetabulum using pressure film and hydraulic actuators. Applied constant and cyclic sinusoidal load of 0.75x BW. Found that labrum adds extra resistance to the flow path for interstitial fluid expression. Potting was not physiological.
Miozzari <i>et al.</i> , 2004	Whole hip joint	Ovine	Custom built	Body weight	Stationary	-	Study showed that the labrum regenerated to the extent that dense fibrous scar extending from the surgically denuded origin filled the defect. Recreated

							loads described by Bergmann.
Smith <i>et al.</i> , 2011	Whole hip joint	Human cadaveric	Custom testing apparatus with a pulley system.	10-200 N	Anterior translation till dislocation	-	Custom testing apparatus with a pulley system designed to adjust compressive loads by altering the weight of the pulley. Load increased incrementally. Poor repeatability due to anatomical variation between samples.
Cadet <i>et al.</i> , 2012	Whole hip joint	Human cadaveric	Custom fluid infusion device and mount	2-4 psi	Stationary	120 seconds	Fluid infusion testing apparatus using 0.9% normal saline from a fluid-filled canister and outflow tubing into the hip central compartment at different labral-tested conditions under regulated infusion pressures. Flow rate was determined by the calculated weight reduction of the fluid canister measured by a scale.
Song <i>et al.</i> , 2012	Whole hip joint	Human cadaveric	Servo-hydraulic materials	Static 700 N	9° rotation position prior to testing,	13 seconds	A servo-hydraulic materials testing system was used to provide an axial compressive load and angular displacement to the specimen. The friction

			testing system		stationary when testing		of the articular cartilage was measured using the measuring the resistance to rotation (RTR) of the hip. The study showed the labrum provided a low friction environment possibly through its fluid seal..
Philippon <i>et al.</i> , 2014	Whole hip joint	Human cadaveric	Instron E10000 Instron Systems Corp	Static 218N	Stationary	300 seconds	Hip was compressed with a force of 2.7 times body weight (2,118 N) while intra-articular pressure was continuously measured with 1.0 9 0.3 mm pressure transducers. Partial labral resection resulted in significant decrease in intra-articular fluid pressurization. Labral reconstruction significantly improved pressurization to levels similar to the intact state. Hip was aligned with the proximal femur at a 30° angle relative to the loading axis in a tensile testing machine.

Lertwanich <i>et al.</i> , 2016	Whole hip joint	Human cadaveric	Robotic manipulator	80N	Six axis joint serial articulation	-	At 30° of flexion, under axial load, the displacement of the hip with capsulotomy and labral resection (9.6 ± 2.5 mm) was significantly larger than the hip with capsulotomy alone. Study limited to testing under axial load or combined loading in a second axis.
Groves, 2016	Hemiarthroplasty	Porcine	Pendulum friction simulator	25-750 N	Flexion and extension Dynamic	7200 seconds	Setup is able to apply only one axis of motion and an axial load and may result in some abnormal stresses being applied to the joint. Moreover, the samples being anatomically inverted mean that the axial loading applied to the hip joint in vitro is through the femur rather than through the acetabulum of the pelvis, as it is in vivo.
Pallan, 2016	Whole hip joint	Porcine	Single Station Hip Simulator	750 N-3000N dynamic	Physiological, 6 axes	10800 seconds	Whole natural simulation using porcine tissue under dynamic load and physiologically relevant loading. Limited in terms of damage creation and

							adaptability for human tissue in simulator.
Koh and Gupta, 2017	Whole hip joint	Human cadaveric	Instron 871 materials testing machine	132-756N Dynamic	Stationary, Axial force	100 cycles at 1Hz	Single leg stance chosen for alignment. "3 cadaveric pelvises underwent creation of a 1.5 cm anterior-superior labral tear in each hip. The tears were then replaced using 2 suture anchors, following repair, the hip joint underwent axial cyclic loading to 756N and were inspected for separation of the labrum from the acetabulum. The mean failure force of the 12 anchors was 154N. Labral repair may be able to tolerate axial weight bearing immediately after repair. Only the anterior superior portion was tested, with little knowledge of the exact loads experienced by the regions of the labrum.
Angsutanasombat <i>et al.</i> , 2018	Whole hip joint	Human cadaveric	Custom simulator with single load cell capable of	Static 350N	Adduction- Abduction single axis, then flexion extension,	-	Whole natural joint simulation for comparing contact pressures on labrum to compare surgical methods.

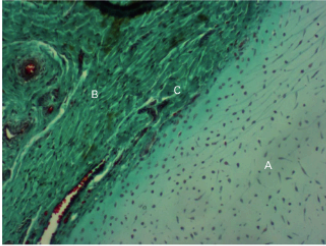
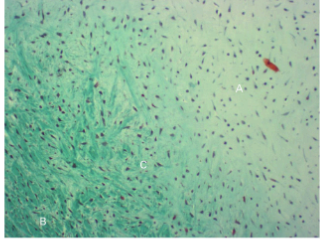
			loading in 6 axes		then external- internal rotation		Constant load of 0.5 times body weight (71kg) applied throughout testing. Testing was limited to one axis per test between tests e.g. first flex-ext then proceed to abd-add. Therefore, natural simulation is quite limited. Contact pressures measured using film piezoresistive load sensors. Method unreliable due to curvature of labrum.
--	--	--	----------------------	--	--	--	--

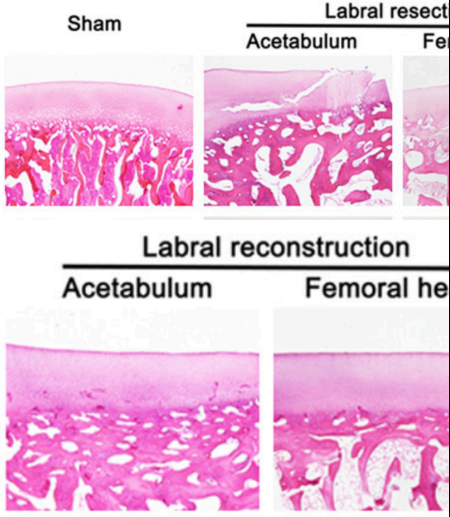
1.10.2 Characterisation of the chondrolabral junction using histology

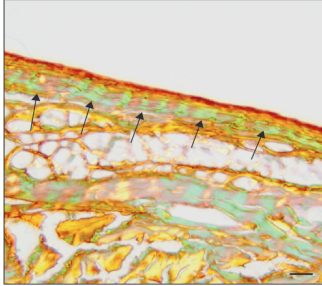
Cashin *et al.*, (2008) studied the prenatal development of the human acetabular labral-chondral complex in 11 fetal hips, aged from 8 weeks of gestation to term. They found consistent differences between the anterior and posterior chondrolabral complexes throughout all gestation ages. The Anterior labrum had a marginal attachment to the acetabular cartilage with an intra-articular projection. The interface was sharp and abrupt. Collagen fibres were arranged parallel to the chondrolabral junction. The marginal attachment and the orientation of collagen fibres parallel to the chondrolabral junction is why it may be more prone to damage than the posterior labrum where the collagen fibres are anchored in the acetabular cartilage. The Posterior labrum was attached and continuous with the acetabular cartilage. The interface was gradual and interdigitated. Collagen fibres were aligned perpendicular to the chondrolabral junction.

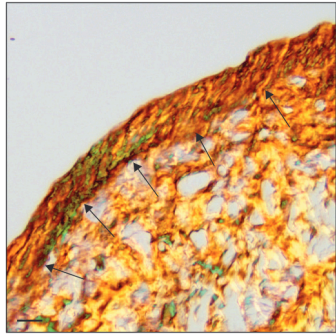
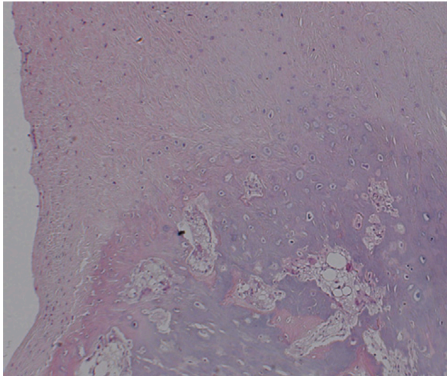
Neumann *et al.*, (2007) noted that 66% of patients with mechanical symptoms in their hip were found to have labral tears seen on MR arthrography, with most being located anteriorly. Schuck, Noble and McCarthy, (2000) noted that most tears of the anterior labrum are associated with degenerative changes in the articular cartilage. Which one precedes the other is unclear (Beck, 2005; Beck and Universitätsspital, 2015; Anwander, Beck and Büchler, 2018). Bony deformities are often present in the presence of labral tears which suggests there is a relationship between mechanical damage due to structural deformities and the presence of associated anterior labrum tearing and degenerative changes to the articular cartilage (Wenger *et al.*, 2004; Beck, 2005; Pritzker *et al.*, 2006). Table 1.6 comprises all current reported studies characterising the histological and immunohistological characterisation of acetabular labral tissue.

Table 1.6 - Comparison of studies reporting histological or immunohistological examination of acetabulum labral tissue. (Continued overleaf)


Paper	Design	Data used	Section and stains used	Results	Comments
Cashin <i>et al.</i> , 2008	To analyse the embryology of the acetabular labral-chondral complex	Hips were removed from aborted fetuses (eight weeks of gestation to term), decalcified in ethylene diamine tetra-acetic acid	11 sections Sectioned in frontal, transverse, and sagittal planes, mounted on glass slides stained with H&E and azan.	 <p>Anterior transition zone (top)</p>  <p>Posterior transition zone (bottom)</p>	Anteriorly, there was an abrupt transition at the junction of the cartilaginous acetabulum with collagen fibres running parallel to the junction while the posterior acetabular labral-chondral complex in the same specimen showed a gradual and interdigitated transition zone with collagen fibres more haphazardly arranged.

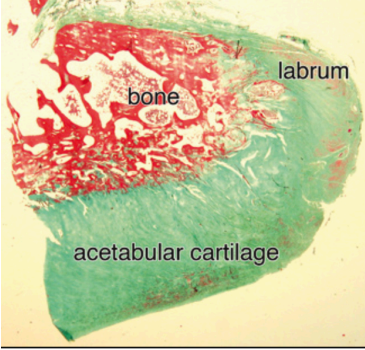
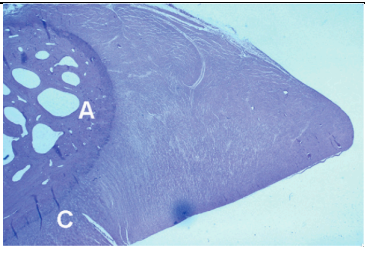
<p>Shi <i>et al.</i>, 2019</p>	<p>Investigation of labral reconstruction or labral resection (n = 6 for each group) on porcine labrum to determine capacity for healing and repair</p>	<p>n=12 porcine joints</p>	<p>5µm thick samples. H&E, toluidine blue, Masson's stain and immunohistological stains for type I, II and X collagen</p>	 <p>The figure displays four histological sections of porcine joints. The top row shows a Sham control joint on the left and a Labral resection joint on the right. The Labral resection joint is further divided into Acetabulum and Femoral head views. The bottom row shows Labral reconstruction joints, also divided into Acetabulum and Femoral head views. The Sham and Labral reconstruction joints exhibit smooth, homogeneous cartilage surfaces. In contrast, the Labral resection joints show significant surface abrasion, with loose, irregular, and broken cartilage layers, and exposed collagen fibers.</p>	<p>Abrasion of cartilage surface of the acetabulum and femoral head in resected joints. Reported discontinuous and delaminated cartilage surface with loose, irregular, broken, or exposed collagen fibres. In contrast, the cartilage surface of in the reconstructed joints were smooth and homogeneous, without cracks or delamination. Decreased proteoglycan content in resected joints. Type II collagen fibre staining in the resected joints</p>
--------------------------------	---	----------------------------	---	---	--

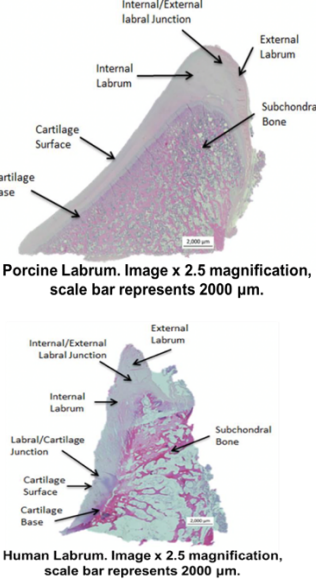
					<p>was weak and uneven with a disordered structure, Type X collagen is a sign of cartilage hypertrophy, which increases significantly when the cartilage is damaged. Reported higher in resected joints.</p>
Schon <i>et al.</i> , 2020	To investigate the expression of matrix metalloproteinases (MMPs) in labral tissue with symptomatic FAI	n=4 symptomatic patients with labral tears	Samples extracted anterior-superiorly using H&E and Picosirius Red		<p>The collagen fibres in the adjacent area are composed of both thick and thin fibres. c) Collagen fibres in the superficial region of the normal labrum are oriented in parallel with the labrum surface. d) Collagen fibres in the superficial region of the FAI</p>

					labrum are disoriented and more heterogenous in the makeup of collagen fibres
Audenaert <i>et al.</i> , 2012		Biopsy specimens retrieved from 6 patients were available for histologic assessment. median age of these patients was 37 years (range, 30 to 40 years). All patients had a longitudinal bucket-handle tear.	H&E	 <p>Labral cleft observed in the deep zone towards the subchondral bone</p>	Biopsy specimens were retrieved from 6 patients during total hip arthroplasty after clinical failure of the index arthroscopic procedure. All patients were diagnosed as having Femoroacetabular impingement with a concomitant labral tear. In all cases severe chondral damage was observed

					<p>during arthroscopy (Beck grades 3 to 4). Despite successful technical repair of the labral tear, chondral damage in these patients was so advanced that the clinical progress after the procedure was unsatisfactory and arthroplasty of the joint was required. In the superficial and deep parts of the labral body, small clefts were observed in all cases.</p>
--	--	--	--	--	--

<p>Seldes <i>et al.</i>, 2001a, p. 20</p>	<p>Investigation into the gross, histologic, and microvascular anatomy of the adult acetabular labrum and tears of the labrum.</p>	<p>n = 55 cadaveric hips. 50% were female and mean age recorded was 78.</p>	<p>H&E and Stain factor VIII Immunohistological stain.</p>	 <p>Type I tear (top) at AS junction</p> <p>Type II tear (bottom) at labrum and vascularity within labrum</p>	<p>Reported incidence of labral tears, characterising labral tears histologically into 2 types, an intra-substance tear found in the labral portion, and a tear found between the articular cartilage and labrum. Generally, the articular cartilage remained intact with minor changes recorded. Hip function or history was not provided so it is unclear if donors with labral tears had symptomatic FAI or other pathologies outside of labral tearing.</p>
---	--	---	--	--	---

<p>Kohl <i>et al.</i>, 2011, p. 2</p>	<p>Investigated articular cartilage damage by extracting tissue from patients undergoing treatment for symptomatic cam, pincer or mixed femoroacetabular impingement.</p>	<p>n=20 patients (5= cam-FAI, 6=pincer-FAI, 9=mixed-FAI)</p>	<p>H&E, Safranin O and Masson's trichrome.</p>	 <p>A histological section of a human hip joint stained with H&E, Safranin O, and Masson's trichrome. The image shows a cross-section of the joint with labels for 'bone' (red), 'labrum' (green), and 'acetabular cartilage' (green).</p>	<p>Provided valuable insight into damaged anterior-superior chondral damage in human samples from severe symptomatic Cam, Pincer and mixed FAI. Not possible to compare with in-tact structure of the junction. Low sample size. Patient variability and extracted samples depend on surgery. Damage reported could be due to processing.</p>
<p>Philippon, Arnoczky and Torrie, 2007</p>	<p>Histology was used to evaluate labral repair in ovine model</p>	<p>N=10 female sheep underwent unilateral arthroscopic repair for acetabular-labral detachment.</p>	<p>Transverse cross sections from Anterior labrum were stained using H&E.</p>	 <p>A histological section of an ovine labrum stained with H&E. The image shows a cross-section of the labrum with labels 'A' and 'C'.</p>	<p>This study showed the anterior labrum to be largely avascular and showed the ovine labrum to have a similar triangular</p>

				<p>Triangular shape of the anterior labrum. Found to be avascular.</p>	<p>shape to human acetabular labrum.</p>
<p>Pallan, 2016</p>	<p>Analysed porcine and human acetabular labrum samples using histology and immunohistochemistry</p>	<p>n=6 porcine samples n=6 human samples, aged 55-70, generally overweight and equal mix of male to female.</p>	<p>3 sections from porcine and anterior region from humans. Stained with H&E, Sirius red and Miller's elastin, Alcian blue. Immunohistological stains for collagen I and II.</p>	 <p>Porcine Labrum. Image x 2.5 magnification, scale bar represents 2000 µm.</p> <p>Human Labrum. Image x 2.5 magnification, scale bar represents 2000 µm.</p>	<p>Characterisation of native porcine labral and human samples provides some useful insight into morphological differences, the immature porcine tissue is rounder while the labrum is triangular in human acetabulum, there is also a distinct margin found anteriorly in human samples.</p>

1.10.3 Non-linear imaging methods for advanced investigation of chondrolabral tissue

Collagen fibres provide tensile strength while proteoglycans provide compressive resistance to articular cartilage and labrum. The arrangement and distribution of different types of collagen fibres and proteoglycan concentration, varies throughout the zones of cartilage and labrum, giving the tissue their functional properties in distributing loads during motion.

Second harmonic generation (SHG) multiphoton imaging uses the natural asymmetry of biological molecules, reflecting the molecular asymmetry and supramolecular organisation of polarisation dependent proteins and membranes. Collagen is one of the major constituents of the cartilage matrix. The highly non-centrosymmetric molecular assemblies of fibrillar collagen make it an extremely bright second-harmonic generator allowing SHG microscopy to be used (Helmchen and Denk, 2005). Polarised SHG can allow structural and morphological modifications in the collagen network within the collagen matrix to be visualised with additional capabilities to identify the different types of collagen fibres based on their susceptibility value (Yeh *et al.*, 2005) allowing for a semi-quantification without the need of imaging markers as with immunohistochemistry.

By utilising optical signals from the extracellular matrix and chondrocytes, images can be taken from intact tissue without the need for sectioning or staining, thereby preserving the state of the tissue being investigated. It can allow the microscopic composition of the labrum and articular cartilage to be determined which can aid in studying the collagen fibre organisation or disruption in response to dynamic mechanical loading as conducted *in vitro*, using anatomical hip simulation using mechanical hip simulators.

The advantage of using non-linear microscopy includes deep penetration of tissue allowing sub-micron resolution in which collagen fibre and bundle arrangement can be clearly defined using a non-destructive methodology. When compared to other imaging modalities, multiphoton microscopy enables high-resolution imaging with increased imaging depth with the advantage of being non-invasive and non-destructive compared to MRI, Ultrasound, High-resolution CT and Confocal microscopy (Kumar *et al.*, 2017; Kumar and Kumar, 2019).

Previously, healthy cartilage has shown a characteristic pattern of polarisation sensitivity with depth which has detectable changes when lesions are present indicative of disrupted collagen architecture (Macirowski, 1994). By investigating damaged or degenerated tissue taken from different loading conditions representing increasing severity, the underlying mechanisms can be determined. Degeneration likely occurs at the microscale, leading to intraarticular damage before the macroscopic or extraarticular damage can be visualised. Moreover, this approach would complement previous histological examinations of tissue allowing a complete representation of damaged or torn acetabular labral tissue to be formed.

Petersen, Petersen and Tillmann, (2003) reported initial findings of the microstructure and arrangement of collagen fibrils using scanning electron microscopy (SEM) for microstructural examination of the acetabular labrum revealing differences between the inner and external labrum separating structures into dense connective tissue and fibrocartilage. Vascularity was present in the inner regions of the labrum, which suggested healing potential and would help select appropriate treatment strategies. SEM images of collagen bundle and fibre arrangement in zones throughout the labrum cross-section were shown; however, processing methods during extraction of the labrum were undesirable and may have led to artefacts in the collagen arrangement. Non-linear imaging methods such as multiphoton imaging minimised processing artefacts and reduced artefacts due to processing requirements with stains or fixatives. Unlike SEM which can provide very high-resolution details, there was no requirement for fixatives. To better understand damage progression due to abnormal loading, combining multiphoton with complementary non-linear imaging methods can provide detailed insight into the microstructure.

1.11 Summary of Literature and Aim of the thesis

Previously, the labrum was considered as the non-functional rim of the acetabulum of the hip joint and was resected when damaged or causing pain. However, there is increasing evidence suggesting the labrum plays a vital role in healthy functioning of the hip joint.

Contact stresses in acetabular articular cartilage increase significantly when the labrum is torn or has been removed. The intact labrum reduces these stresses as it deepens the acetabulum, thus increasing the overall surface area, volume, congruity, and stability of the hip joint. The labrum also maintains a fluid seal, producing negative intra-articular pressure which is important in distributing contact pressure across the articulating surfaces, which lowers the stress on the articular cartilage.

Underlying structural abnormalities such as Femoroacetabular impingement and dysplasia of the hip increase the risk of labral tearing. Labral tearing can lead to loss in mobility, joint degeneration and is often found in degenerative conditions like osteoarthritis.

Although there has been some success in managing symptoms caused by labral tears, the long-term outcomes are poorly understood and there is little underpinning evidence of the best surgical strategy.

There is a growing need for understanding the structure and function of the labrum and how it can become damaged with structural abnormalities. Moreover, while arthroscopic and radiographic evaluations can reveal labral pathology, these procedures can be invasive and only provide information at a single point in the care continuum of the patient, revealing little detail of the damage mechanism or the mechanical cause of damage observed clinically.

The following research questions were used in the design of the thesis:

- Can literature inform the main mechanical parameters which can be applied to natural hip simulation for the generation of labral tearing and the generation of chondral delamination?
- Can clinically relevant chondrolabral damage be recreated *in vitro* using natural hip simulation?
- Can this approach help aid surgeons to make choices when deciding surgical treatments to improve patient outcomes for hip arthroscopy?
- How does the loaded structure of the labrum compare with the unloaded labrum?

- Can novel non-linear imaging be used to investigate the microstructure of damaged labrum to inform the mechanism of damage and degeneration that occurs with labral tearing?
- How do collagen fibrils (responsible for the mechanical response to loads in cartilage/fibrocartilage) respond to abnormal loading environments and how are they disrupted as a result of loading?
- If changes to the collagen microstructure can be visualised, how may this help in the repair strategy for chondrolabral damage?

The overall aims were:

- To characterise the native structure of the acetabular labrum using histology and non-linear imaging methods.
- To experimentally induce chondrolabral damage on porcine natural hip joints using a natural hip simulator, particularly labral tearing, and chondral delamination.
- To investigate the chondrolabral junction at the anterior-superior region and determine the effects of applied mechanical damage to the orientation and arrangement of collagen fibres.

Chapter 2 Histological Characterisation of Porcine Labrum, Articular Cartilage and Chondrolabral Junction

2.1 Introduction

The articular cartilage of the human and animal acetabulum has been well characterised with respect to its biochemical and histological appearance (Horvai, 2011; Fermor *et al.*, 2015; Maynard and Downes, 2019; Gahunia and Pritzker, 2020). The extracellular matrix (ECM) is rich in collagen and proteoglycans, which are arranged in a specialised manner directed by chondrocytes (Rathnayake *et al.*, 2021). The structure of the articular cartilage relates to its function in resisting compressive loads, joint articulation, and lubrication. In contrast, there is limited biological characterisation of the acetabular labrum (Seldes *et al.*, 2001a; Cashin *et al.*, 2008; Pallan, 2016). Chapter 1 reviewed the current state of biological characterisation of the acetabular labrum, revealing that a more comprehensive analysis was required to determine how the structure, cellular and matrix components of the acetabular labrum differ from articular cartilage and other fibrocartilaginous tissue such as the meniscus (Prokopi *et al.*, 123AD) or glenoid labrum (Ockert *et al.*, 2012).

Functions of the labrum have been discovered over time, such as its contribution to hip stability (Boykin *et al.*, 2011), forming a fluid seal between the joint capsule and femoral head (Cadet *et al.*, 2012). The detailed tissue microstructure and contribution to mechanical function are still not understood (Bedi *et al.*, 2011; Fairley *et al.*, 2016; Alcaide-Ruggiero, Cugat and Domínguez, 2023). Many structure-function relationships are based on predictions of labral structure because of similarities with the glenoid labrum (Hill *et al.*, 2008; Ockert *et al.*, 2012; Alashkham *et al.*, 2018; Como *et al.*, 2021), annulus fibrosus (Hoy *et al.*, 2020) and meniscus (Prokopi *et al.*, 123AD; Fox, Bedi and Rodeo, 2012; Zhang *et al.*, 2012).

This chapter discusses the specific methods by which histological examination was conducted and the subsequent findings of the gross microstructure of porcine labrum sections characterising the labrum structure, comparison with the articular cartilage surface and the interface between the anterior, superior, and posterior acetabulum.

By macroscopically and histologically assessing acetabular labrum tissue, key tissue features could be identified. Areas of interest, such as the anterior-superior region of the labrum, the most common site for labral tears (Malviya *et al.*, 2023), were characterised to support work in Chapters 4 and 5, where damage is generated to see how the structure is altered in response to abnormal loading.

The focus of the characterisation was on the chondrolabral junction and the anterior-superior region of the labrum, and the arrangement and alignment of collagen fibres and proteoglycan concentration in different areas of the extracellular matrix. These components are thought to provide the labrum with its functionality to stabilise tensile and compressive loads respectively. The anterior-superior region is the most observed region with labral tearing (Groh and Herrera, 2009; Kaya, 2014; Lee *et al.*, 2015; Cho *et al.*, 2022) and hence was of focus to determine why the structure exposes this area to a higher likelihood of tearing. The native unloaded porcine labrum was characterised to understand how mechanical damage presents at the chondrolabral junction and how experimental simulation would alter this structure.

2.1.1 Chapter aim

The main aim of this chapter was:

- To characterise freshly dissected porcine acetabular tissues (n=6) macroscopically and histologically from multiple regions (anterior, superior, and posterior).
 1. To serve as a baseline for histological analysis of damage in future chapters.
 2. To understand better understand how tissue microstructure contributes to function.

2.1.2 Objectives

The main research objectives for this study were:

- To characterise the gross appearance and histological appearance of the porcine chondrolabral junction: anterior-superior and posterior-superior chondrolabral junctions to compare with previous findings from Pallan, (2016) in porcine tissue.

- To assess gross differences between the structure of the anterior, superior, and posterior regions of the labrum in morphology, distribution of GAGs and orientation of collagen fibres.
 - To characterise the general histological structure of acetabular labrum tissue using Haematoxylin & Eosin (H&E) staining.
 - To determine the distribution of glycosaminoglycans (GAGs) present in native porcine labrum using Safranin-O and Fast green staining.
 - To determine the arrangement of collagen fibres, present in native porcine labrum using Sirius red and Miller's elastin staining and under polarised light microscopy.
- To determine if there is a relationship between the structure and why the anterior-superior region is more likely to be damaged than the posterior labrum.

2.2 Preparation of tissue for histological examination

The following section describes the general methodology for extracting samples for histological examination on freshly dissected porcine hip joints (n=6).

2.2.1 Selection and acquisition of porcine tissue

Porcine tissue was selected for this research due to tissue availability and general reproducibility in age and weight as they were supplied from the food chain, reducing variance between porcine hip joints. Porcine right hind limbs were readily available and sourced from the food chain supply via local abattoirs. As a result, ethical approval was not required in this study.

Furthermore, the relative structure of the porcine hip joint is comparable to the human joint. Animal hip joints typically have a relatively similar morphology to human hip joints (Bergmann, Graichen and Rohlmann, 1999; Thorup, Laursen and Jensen, 2008; Mirkiani *et al.*, 2022), where the articular surfaces are similar in thickness (Horvai, 2011). Immature porcine tissue was also found to have a higher GAG content compared to ovine and bovine models (Fermor *et al.*, 2015; Cone, Warren and Fisher, 2017; Bowland *et al.*, 2018) which would support use

for longer simulation cycles and for assessing joint tribology. Therefore, porcine tissue was chosen as the animal model for testing.

2.2.2 Dissection

The following section describes the general dissection used throughout the studies featured in Chapters 3-6. Approximately six months old porcine right hind limbs (Figure 2.1) were obtained from a local abattoir and dissected by removing all surrounding soft tissue, muscle and fat leaving only the acetabulum and labrum, femoral head, transverse acetabular ligament, acetabular fat pad and articular surfaces in-tact (Figure 2.3). Specimens were then wrapped and stored in tissue soaked in phosphate-buffered saline (PBS) and stored at -20°C until necessary.

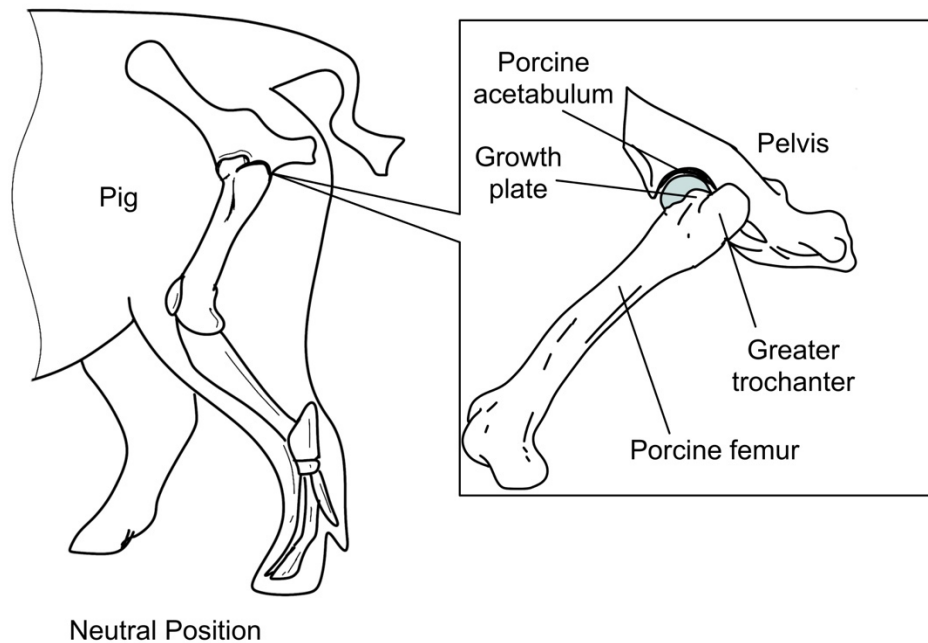


Figure 2.1 – Schematic drawing of the porcine hip joint in a neutral position.

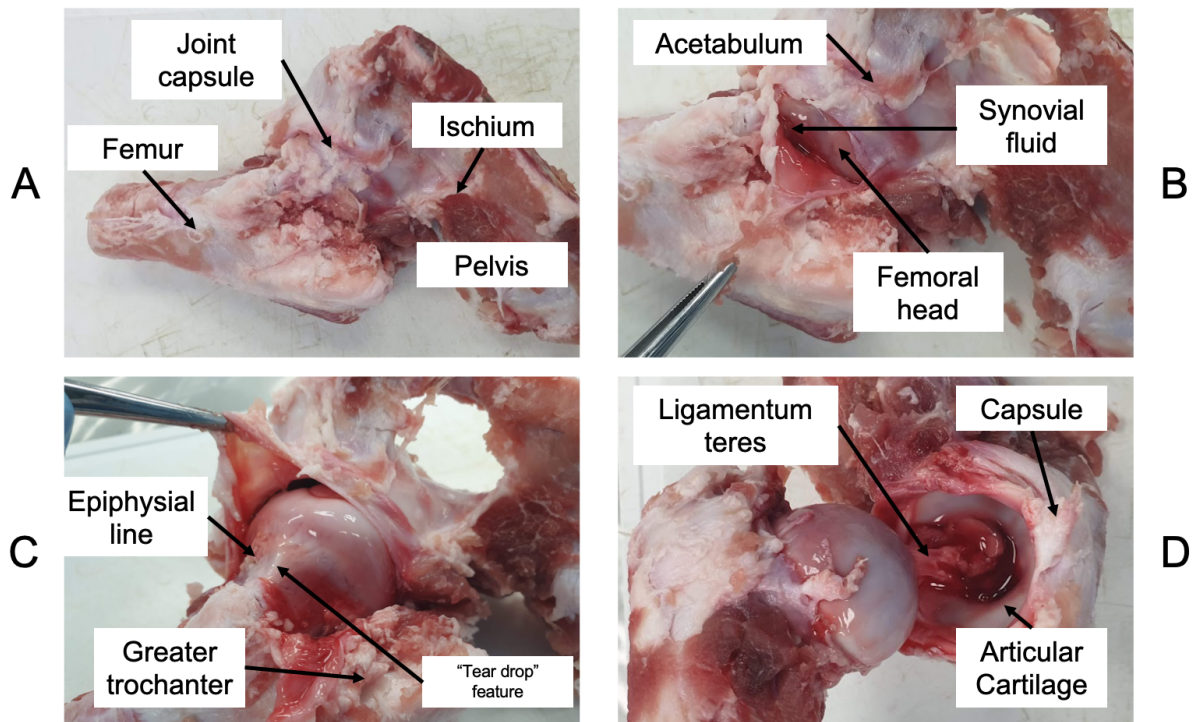


Figure 2.2: Dissection of a right hind pig leg. **A** Skin, musculature and soft tissues were removed after identifying the location of the hip joint until the joint capsule was exposed. **B-C** Surrounding soft tissue, ligaments and joint capsule were removed preserving the articular surfaces. The joint capsule was carefully excised following the attachment points close to the base of the femoral head avoiding any cartilage, releasing the synovial fluid, and destabilising the femoral head. **D** The femur and acetabulum were disarticulated by separating the ligamentum teres and remaining capsular connective tissue.

The major structural differences to consider when using porcine tissue in place of human tissue were due to the age of the tissue, as at six months the porcine femur had growth plates intact. The femoral head of the porcine femur is more aspherical compared to a human and due to the pig being quadruped, the joint itself is more restricted, mostly being used for flexion-extension.

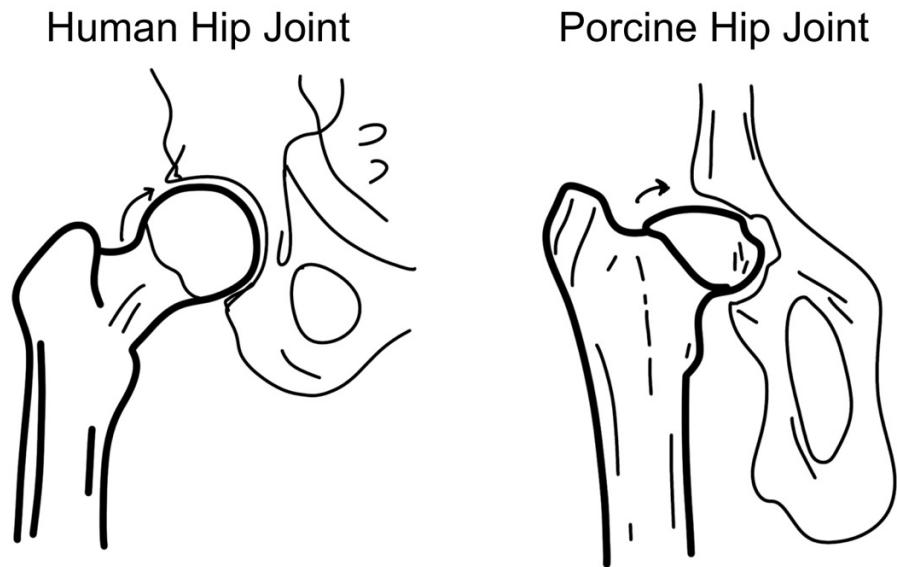


Figure 2.3 - Schematic drawing showing the difference between the geometry of the human and porcine hip joints. The greater trochanter protrudes further in the porcine femur with an aspherical femoral head.

This difference was lessened by cutting off the excess bone from the trochanter (Figure 2.4), the growth plate, and the femoral stem to reshape the femur to appropriately represent the human femur. The acetabulum was reshaped to model human hip joint morphology and to accommodate the working volume of the hip simulator used in Chapter 3. The greater trochanter of the porcine femur was much larger than a human femur, resulting in a protrusion that would impinge or be restricted in the range of motion and, therefore was also reduced using a bone saw. This feature was considered in detail for the simulation conducted in Chapters 3 and 4 to increase the reliability of simulations when using porcine hips.

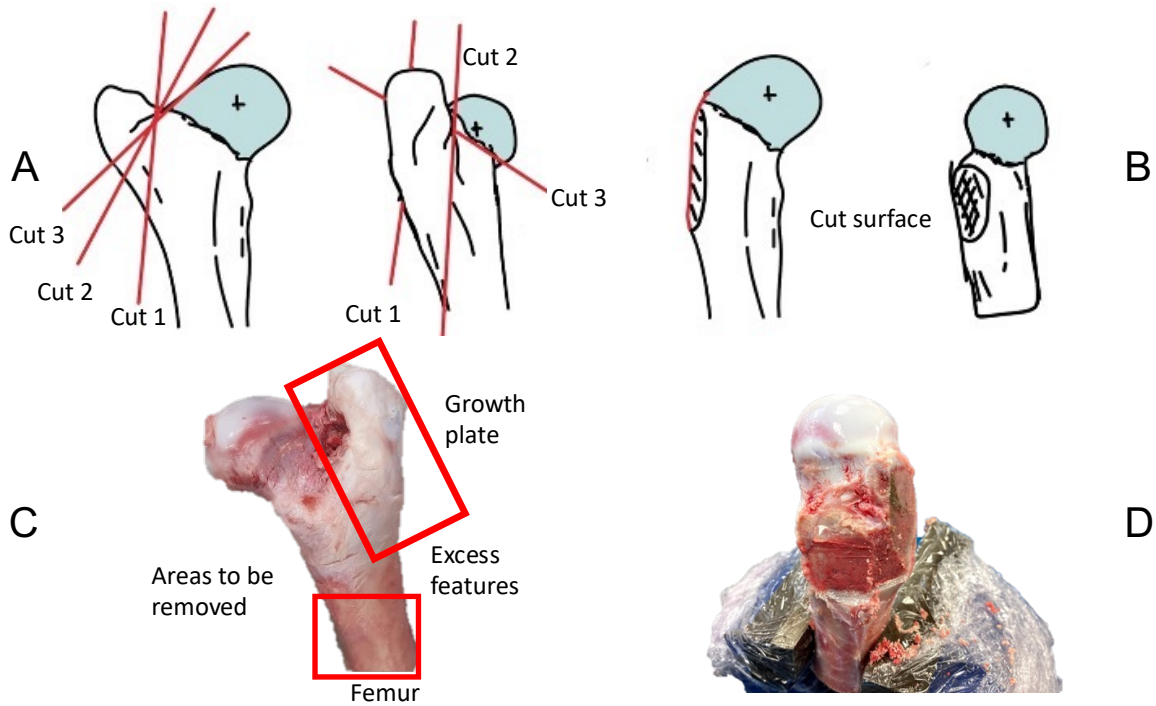


Figure 2.4 – Reduction of the greater trochanter. **A** – Red lines indicating where on the porcine femur cuts were made using a bone saw. **B** – Schematic of a resected femur. **C** – Natural porcine femur with large greater trochanter. **D** – Resected Porcine femur.

Some natural intra-variance of acetabulum morphology was seen between samples during dissections. However, to establish the general histoarchitecture of the labrum and articular cartilage of native unloaded samples, samples were only excluded when major structural deformities or abnormal pathologies were present. This natural variance in acetabulum morphology was explored further during mechanical testing discussed in Chapter 3 as the morphological features could influence the simulations in mechanical testing.

2.2.3 Extraction of porcine labrum samples

Six porcine hip joints were dissected and prepared for gross and histological examination. Only the acetabulae were used for histological examination as the focus of this investigation was to characterise the acetabular labrum and cartilage hence, the femurs of each joint were kept frozen at -20°C . For conducting histological characterisation, labral sections had to be extracted from the joint. Clinically, the acetabulum is divided into a clockface model which helps surgeons diagnose features. Similarly, the acetabulum and labrum were divided into

four quadrants to represent the major regions of the labrum, these being the superior, anterior, posterior, and inferior regions (Figure 2.5A).

After the porcine hip joint had been carefully disarticulated by removing the ligamentum teres from the femur and acetabular fossa, labral sections were extracted using a 2A scalpel blade and with a handheld bone saw.

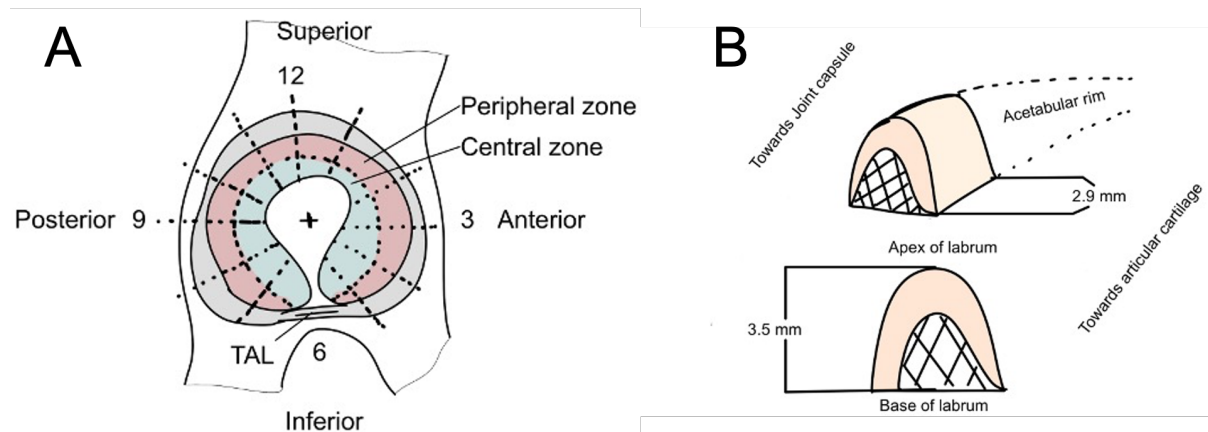


Figure 2.5: **A** Quadrants of the acetabulum as defined in this project, the schematic shows the clockface model used by surgeons as well as the definition of the peripheral and central zones of the acetabulum **B** Schematic drawings of extracted labral sample and acetabular labrum cross-section viewed from a transverse plane.

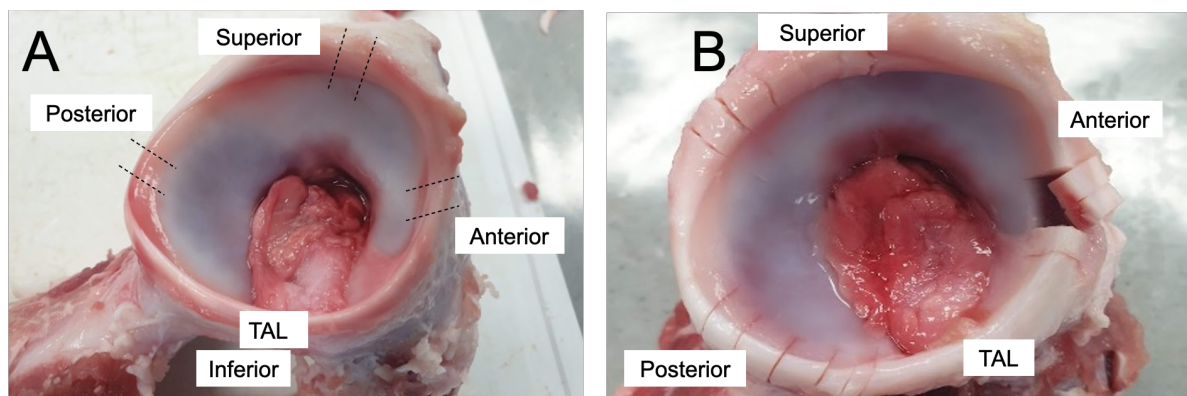


Figure 2.6: **B** Dissected porcine acetabulum with the joint capsule resected. Note the morphological differences between the posterior and anterior regions. The posterior labral rim at 9° clock is deformed and extends beyond the bony margin. This was a common feature observed in some **B** extraction of porcine labral sections.

Superiorly, the labrum was deeply integrated with the joint capsule, and this was resected to leave the labral rim intact before extraction of samples. Sections were extracted from the anterior, superior, and posterior regions of three porcine acetabulum. Small portions of subchondral bone were used to identify the base of the samples to distinguish between the articular and capsular sides of the labrum.

For each region, to extract a single section, a scalpel blade or handheld bone saw was used to make two incisions 2-3mm apart from the apex of the acetabulum to the subchondral bone around 5-7 mm in depth. This resulted in labral sections which were approximately 2-5mm x 2-5mm (Figure 2.5C). The size of labral sections varied between porcine hips due to some variations in the shape and overall size of the acetabular rim in porcine acetabulae.

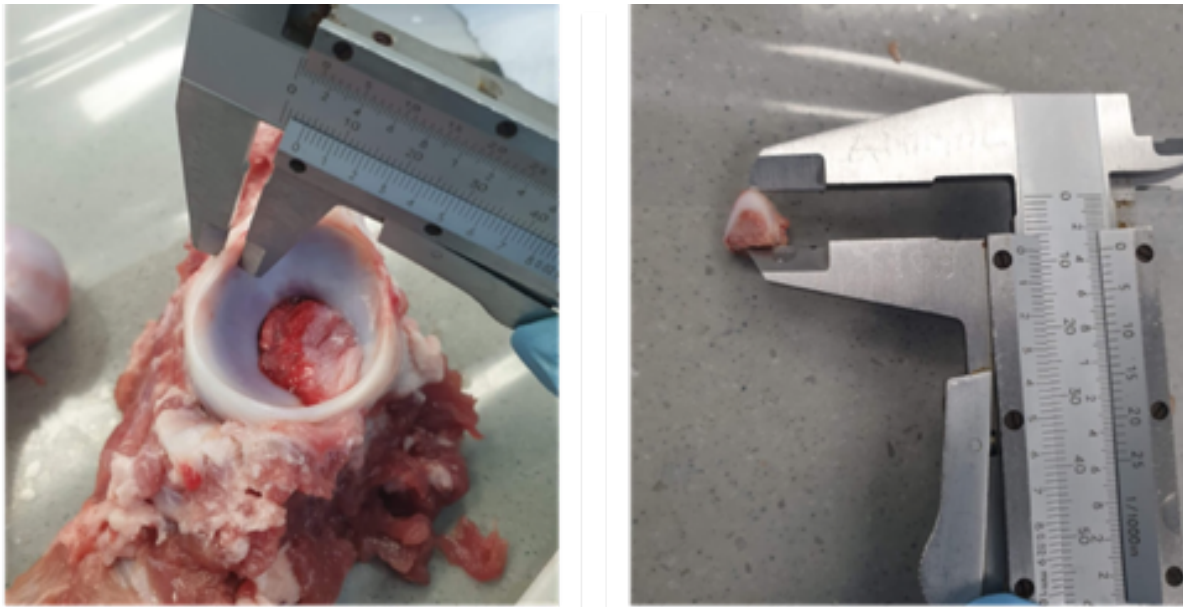


Figure 2.7 labral sections extracted for use in histology. The triangular-shaped sections measured approximately 2-7mm in depth.

Cross-sectional samples were imaged immediately after extraction from the acetabulum to highlight features before further processing required for histology. A digital SLR camera (Canon, EOS 750D) was used to assess cross-sections for gross inspection of shape, morphology and tissue features as viewed macroscopically as described in Chapter 3.4.2.5.

2.3 General materials and methods for histological examination

2.3.1 Fixation of labral sections

For the structure and constituents of the labrum to be visualised, the tissue was fixed to ensure no constituents were washed out or damaged during sample preparation. Any calcified tissue such as bone was decalcified to be soft enough to section with a microtome in further steps. After decalcification, the tissue sections were embedded in paraffin wax to enable them to hold their shape during sectioning.

Sections to be used with histological stains were fixed in 10 % (v/v) Neutral Buffered Formalin (NBF). NBF was used to fix the tissue and maintain tissue morphology through the histological procedure. Sections were placed in plastic histology embedding cassettes (Histosette®). and labelled using a lead pencil. The plastic cassettes were immersed in EDTA fixative for 3 days for decalcification.

After decalcification, an automated tissue processor (Leica TP1020, Milton Keynes, UK) was then used to sequentially immerse the cassettes in:

- 70% (v/v) ethanol,
- 90% (v/v) ethanol,
- Absolute ethanol,
- Xylene (Genta Medical, York, UK),
- Molten paraffin wax

After processing sections were removed from the automated tissue processor and placed into metal moulds with the cross-section surface on the base, the moulds were filled with molten wax and set overnight at room temperature. Once the wax had hardened, the blocks were removed from the mould and the excess wax over the cassettes was removed.

Prior to sectioning the wax blocks were cooled to -20 °C for 30 minutes and sectioning wax blocks were kept on ice in-between blocks to retain their temperature. The wax blocks were then sectioned using a manual microtome at a thickness between 6-12 µm and an angle of 2 ° to the blade. The cut sections were then transferred to a paraffin section mounting water bath maintained at 40 °C and transferred onto Superfrost Plus slides. Slides were left to dry on a

hot plate at 45 °C for at least 3 hours. This process was very difficult due to the thickness of samples, and the speed at which samples must be sectioned without letting the wax blocks to get closer to room temperature which would cause the wax to roll up and then result in the sections to tear or have folds.

2.3.2 Reagents for histology

2.3.2.1 Safranin O & Fast Green

0.02% w/v aqueous Fast Green was prepared by dissolving 100mg of fast green dye into 500ml of distilled water. The solution was filtered to prevent the formation of any precipitates. 1% v/v acetic acid was then prepared by mixing 5ml of glacial acetic acid with 495 ml of distilled water.

0.1% w/v Safranin O was prepared by dissolving 500 mg of Safranin O dye in 500 ml of distilled water. The solution was filtered to prevent the formation of precipitate before use.

Table 2.1 Chemicals and Reagents required for preparing Safranin-O and fast green stains.

Chemical/Reagent	Cat No.	Supplier
DPX mountant	RRSP29	Atom Scientific
Ethanol	E/0555DF/25	Fisher Scientific
Weigert Haemotoxylin Solution A Solution B	RRSP72-D RRSP73-D	Atom Scientific
Hydrochloric Acid	H/1200/PB17	Fisher Scientific
Fast Green	F7258	Sigma
Acetic acid (glacial)	A/0400/PB17	Fisher Scientific
Safranin O	S305-2 S305-3	Raymond Lamb
Xylene	GPS1001-G	Atom Scientific

2.3.2.2 Sirius red/Miller's elastin

The following section describes the preparation of specific reagents required for Sirius red and Miller's elastin staining using the chemicals and reagents shown in Table 2.2.

5% (w/v) potassium permanganate

Prepared by adding 15g potassium permanganate into 300 ml of distilled water. The solution was stirred using a magnetic stirrer until dissolved. The resulting solution was filtered before use.

1% (w/v) oxalic acid

Prepared by adding 1g of oxalic acid to 100 ml of distilled water. The solution mixture was stirred with a magnetic stirrer until dissolved.

Weigerts haemotoxylin

Prepared by mixing equal volumes of solution A and solution B. The resulting solution can be stored at 4 °C for 1 month.

1% acid alcohol (1% conc. Hydrochloric acid in 70% Ethanol)

Prepared by adding 5 ml of concentrated Hydrochloric acid to 495ml of 70% Ethanol.

0.1% (w/v) Sirius red

Prepared by weighing out Sirius red in the fume hood in the carcinogens room. Picric acid solution should be handled extremely carefully as contact with metal is explosive due to the formation of metal picrate. 0.1g of Sirius red was dissolved into 100ml of aqueous saturated picric acid solution using a magnetic stirrer. The resulting solution should be filtered before use and can be stored at room temperature for up to six months.

Table 2.2 Chemicals and Reagents required for preparing Sirius red/Miller's elastin

Chemical/Reagent	Cat No.	Supplier
DPX mountant	RRSP29	Atom Scientific
Ethanol	E/0555DF/25	Fisher Scientific
Miller's stain	LAMB/080-D	Raymond A Lamb
Oxalic acid (dihydrate)	20562.234	VWRI
Picric acid	36011	Sigma-Aldrich
Potassium permanganate	P/6520/53	Thermo Fisher Scientific Ltd.
Sirius red	F3B	VWR International
Weigert Haemotoxylin Solution A Solution B	RRSP72-D RRSP73-D	Atom Scientific
Xylene	GPS1001-G	Atom Scientific

2.3.2.3 Haemotoylin and eosin

Scott's tap water substitute was prepared to create a 1x solution by diluting Scott's tap water by adding 50 ml of the 10x solution to 450 ml of distilled water.

Table 2.3 Chemicals and Reagents required for preparing Haemotoylin and eosin

Chemical/Reagent	Cat No.	Supplier
DPX mountant	RRSP29	Atom Scientific
Ethanol	E/0555DF/25	Fisher Scientific
Mayer's Haemotoxylin (Mayer's Haemalum)	RRSP60	Atom Scientific
Eosin Y	1.09844.1000	Merck Millipore
Scott's tap water substitute 10x concentrate	RRSP190	Atom Scientific
Xylene	GPS1001-G	Atom Scientific

2.4 Methodology for Histological Characterisation

Tissue sections were decalcified and fixed and embedded in paraffin wax before being sectioned and stained. The staining procedure consisted of five stages consisting of dewaxing, rehydration, staining, dehydration and mounting. Sections were then imaged using an upright light microscope.

The purpose of histology was to highlight the general tissue architecture and use stains to highlight key features of the extracellular matrix (ECM) and cells present in the tissue to determine the nature of the cartilage type and characterise the features of the matrix, which would relate to biomechanical function which is relevant to this study. For this, the following stains were used.

- 1. Haematoxylin and eosin** – a common stain used for interpreting general tissue histoarchitecture. Haematoxylin stains negatively charged cell nuclei a dark blue or violet while eosin binds with proteins in the cytoplasm and ECM stains pink or red.
- 2. Sirius red and Miller's elastin** – a specialised histochemical stain visualises collagen and elastin structures. Sirius red binds with collagen fibres staining them red under brightfield illumination. Miller's elastin stains elastin fibres blue/black. The tissue can be examined under polarised light to highlight the birefringence of collagen fibres to determine the direction of the long axis of the collagen fibre at that polarisation angle and plane. (Bryan, 1955; Rosenberg, 1971)
- 3. Safranin-O and fast green** – a specialised histochemical stain using a cationic dye to assess the abundance of proteoglycans in the matrix. The stain is highly sensitive to acidic polysaccharides. The dye reacts with both carboxylated and sulphated polysaccharides. This stain can detect sulphate groups on chondroitin sulphate or keratan sulphate, providing a distribution of GAGs across the tissue (Bryan, 1955; Rosenberg, 1971). A positive produces an orangish red hue while the background is stained blue. (Safran *et al.*, 2011)

2.4.1 Dewaxing

The slides were immersed in a series of pots intermittently, the first set was immersed in xylene for dewaxing for 10 minutes, followed by a new pot for 10 minutes.

2.4.2 Rehydration

The slides were immersed in a series of pots intermittently, the first set was immersed in 100% ethanol for 3 minutes, 100% ethanol for 2 minutes, 100% ethanol for 2 minutes, 70 % ethanol for 2 minutes and in a new pot with running tap water for 3 minutes.

2.4.3 Dehydration

The slides were immersed in a series of pots intermittently, the first set was immersed in 70% ethanol for 5 seconds, 100% ethanol for 1 minute, 100% ethanol for 2 minutes, and 100 % ethanol for 3 minutes.

2.4.4 Staining

2.4.4.1 Haematoxylin and eosin

Each slide containing a section of a sample was placed into a slide holder and dewaxed following the steps in section 2.4.1. Next, the slides were rehydrated following the steps in section 2.4.2. Slides were then immersed in a new pot containing Mayer's haematoxylin for one minute. The slides were rinsed using tap water until the water ran clear. The slides were then immersed in a new pot containing in Scott's tap water for three minutes. The slides were rinsed using tap water for three minutes. The slides were then immersed in a new pot containing eosin for three minutes and then left in a pot containing running tap water for one minute. After staining was completed, the slides were then dehydrated following the steps in section 2.4.3.

2.4.4.2 Sirius red and Miller's elastin

Each slide containing a section of a sample was placed into a slide holder and dewaxed following the steps in section 2.4.1. Next, the slides were rehydrated following the steps in section 2.4.2. Slides were immersed in a new pot containing into 5 % (W/V) potassium permanganate for five minutes. The slides were rinsed using distilled water. The slides were immersed in a new pot containing 1 % (w/v) oxalic acid for two minutes. The slides were rinsed twice using distilled water for one minute then four minutes. The slides were immersed in a new pot containing 70 % (v/v) ethanol for one minute. The slides were immersed in a new pot containing 95 % ethanol for one minute. The slides were stained with Miller's stain for one hour. The slides were rinsed using 95 % (v/v) ethanol until running clear. The slides were immersed in a new pot containing 70 % (v/v) ethanol for one minute. The slides were rinsed using tap water for two minutes. Stain sections using Weigerts haematoxylin for ten minutes. The slides were rinsed using tap water for one minute. The slides were differentiated in 1% acid alcohol for 1 minute. The slides were rinsed using distilled water for 30 seconds. The slides were stained using picosirius red for one hour. The slides were rinsed using distilled water and blot dried. After staining was completed, the slides were then dehydrated following the steps in section 2.4.3.

2.4.4.3 Safranin-O and fast green

Each slide containing a section of a sample was placed into a slide holder and dewaxed following the steps in section 2.4.1. Next, the slides were rehydrated following the steps in section 2.4.2. Slides were immersed in a new pot containing Weigert haematoxylin for 3 minutes. The slides were immersed in a new pot containing tap water for 10 minutes. The slides were differentiated in 1% acid alcohol for 1 minute. The slides were washed in tap water for 3 minutes. The slides were stained in 0.02% aqueous Fast Green for 5 minutes. The slides were washed in 1% acetic acid and drained. The slides were then stained in 0.1% Safranin O for 4 minutes. After staining was completed, the slides were then dehydrated following the steps in section 2.4.3.

2.4.5 Mounting

All slides were then prepared for mounting, by immersing slides in xylene for ten minutes, and a further ten minutes. For mounting, a Pasteur pipette was used to drop a small amount of DPX mountant on top of the section. A glass coverslip was placed on top of the section. The slide was air-dried for four hours. The sections were imaged using an upright microscope under normal Koehler illumination and polarised light.

2.5 Results

To determine how damage would alter the gross macroscopic and microscopic appearance of the acetabular labrum tissue, labral sections were initially characterised using. After labral sections were prepared, macroscopic photography was used to investigate the gross appearance of the labrum from the anterior, superior, and posterior regions.

2.5.1 Gross examination of the labrum of the acetabulum

Porcine acetabular cross-sections from the posterior, superior and anterior labrum were photographed before they were examined using histology (Figure 2.8). The acetabulum labrum sections varied in size and cross-section across the circumference of the porcine acetabulum (Figure 2.8, top). The labrum sections were round in cross-section at the apex and wider at the base toward the subchondral bone with the posterior and superior sections appearing more triangular (figure 2.8). The sections had a distinct fibrous appearance

toward the capsular side of the external labrum (Figure 2.9, white cross) compared with the smooth and greyish-white opaque appearance towards the articular cartilage (Figure 2.9, black square). The transition between the whiter, more fibrous appearance to the cartilage was most noticeable in the posterior labrum (Figure 2.9, red line). The sections had varying transitions separating the smooth and fibrous regions, where the posterior section had the largest visible fibrous region, followed by the superior and anterior regions.

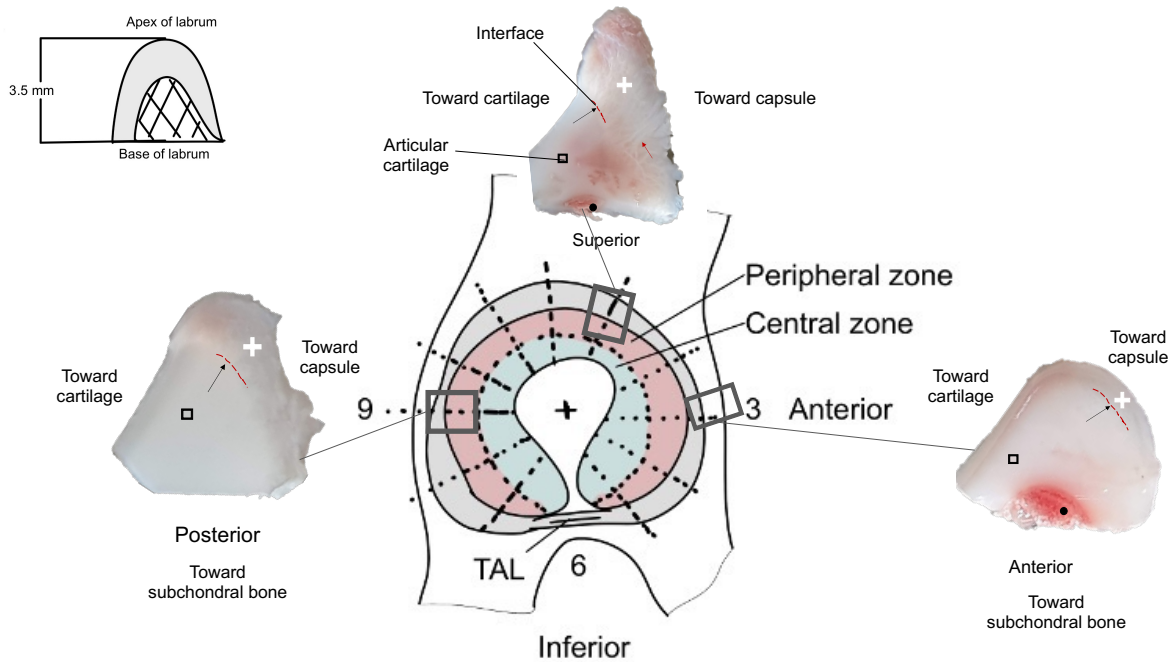


Figure 2.8: Gross examination of labral sections extracted from porcine acetabulum.

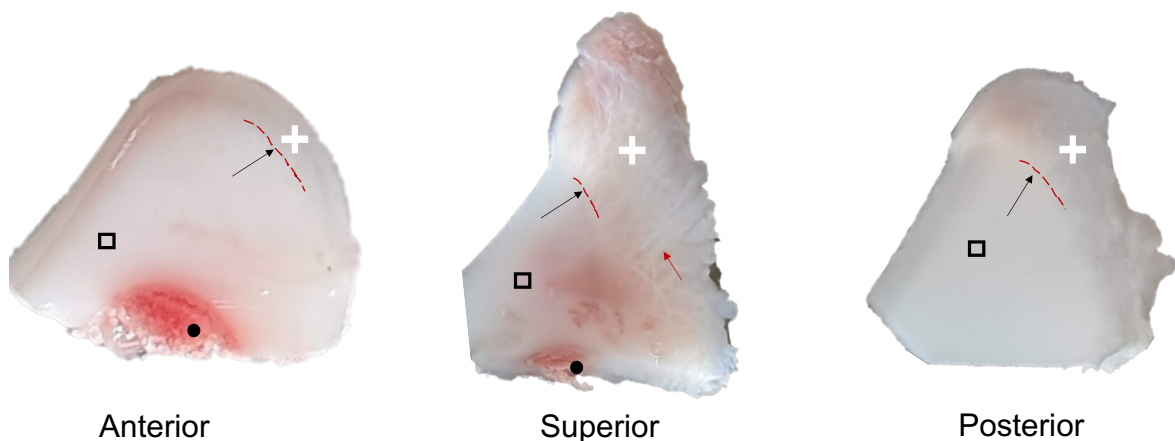


Figure 2.9: Gross examination of labral sections extracted from porcine acetabulum from anterior, superior, and posterior regions. Black square: cartilage, plus-sign: dense fibrous connective tissue in external labrum, Black circle: subchondral bone, red dotted line: interface between internal and external labrum, red arrow: large fibres visible in the fibrous portion

towards the capsular side. Black arrow: margin separating more fibrous and fibrocartilaginous regions.

2.5.2 General tissue architecture using H&E staining

Haematoxylin & Eosin (H&E) staining was used to characterise the general tissue histoarchitecture of acetabular labrum tissue. The labral cross-sections (Figure 2.10; Figure 2.12) were stained blue-purple for the subchondral bone and nuclei, the extracellular matrix was stained pink, and air spaces appeared white. Eosin stains collagen pink as it is eosinophilic. The acetabular labrum sections contained articular cartilage, fibrocartilage, thick dense layers of collagen fibres, dense irregular connective tissue toward the external labrum and subchondral bone. Small holes were observed within the tissue structure that resembled small blood vessels (Figure 2.11, Figure 2.13). Finally, there was a high number of chondrocytes and cells present in all tissues (Figure 2.13). Comparing the regions, the anterior labrum was triangular, while the posterior and superior were rounder. The subchondral bone was structured similarly, with the anterior region being arranged triangular while the posterior section was wider at its base. The superior labrum section had torn and fragmented tissue in the articular cartilage (Figure 2.12A). The posterior labrum had a large deeply red stain in the tissue. Similar deep red streaks were present in all sections.

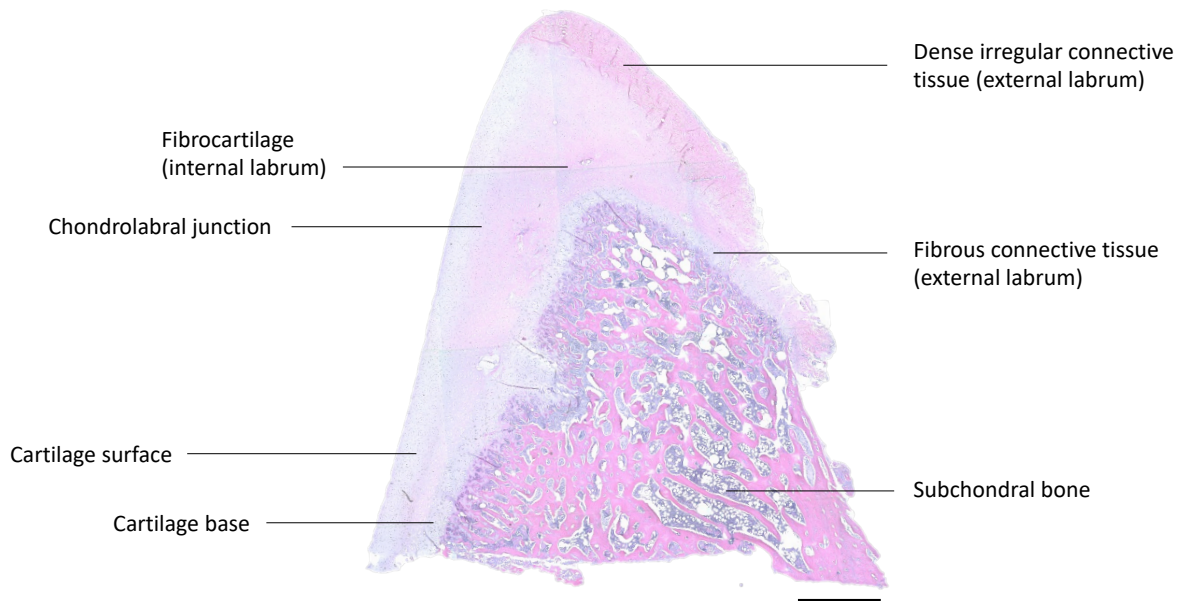


Figure 2.10 – H&E-stained anterior porcine labrum with labels showing the various regions found in the cross-section. The acetabular labrum was found to be continuous with the articular cartilage and capsule hence had the presence of fibrocartilage internally. At the same time, there was more dense irregular connective tissue and fibrous connective tissue found towards the capsule.

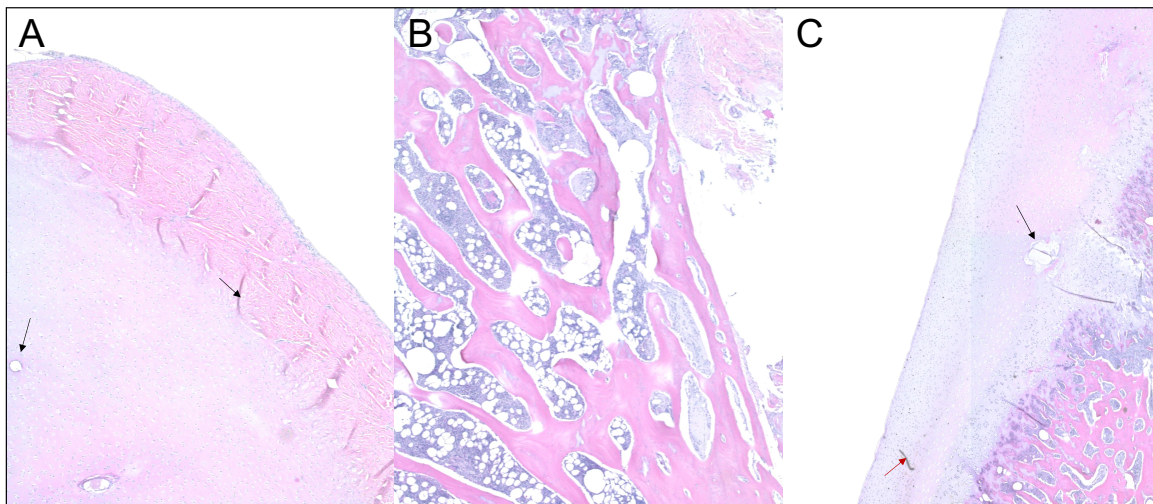
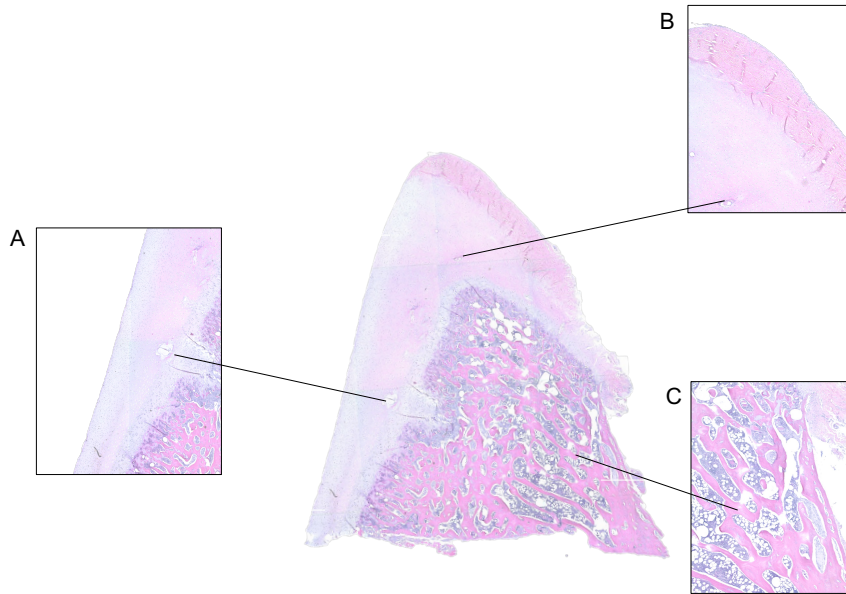


Figure 2.11 – A representative set of H&E stained anterior porcine labrum. A – a magnified view of the external labrum. B – the subchondral bone structure. C – The cartilaginous region of the labrum and articular cartilage. Red arrow – artefact. Black arrow – the presence of holes or features resembling blood vessels.

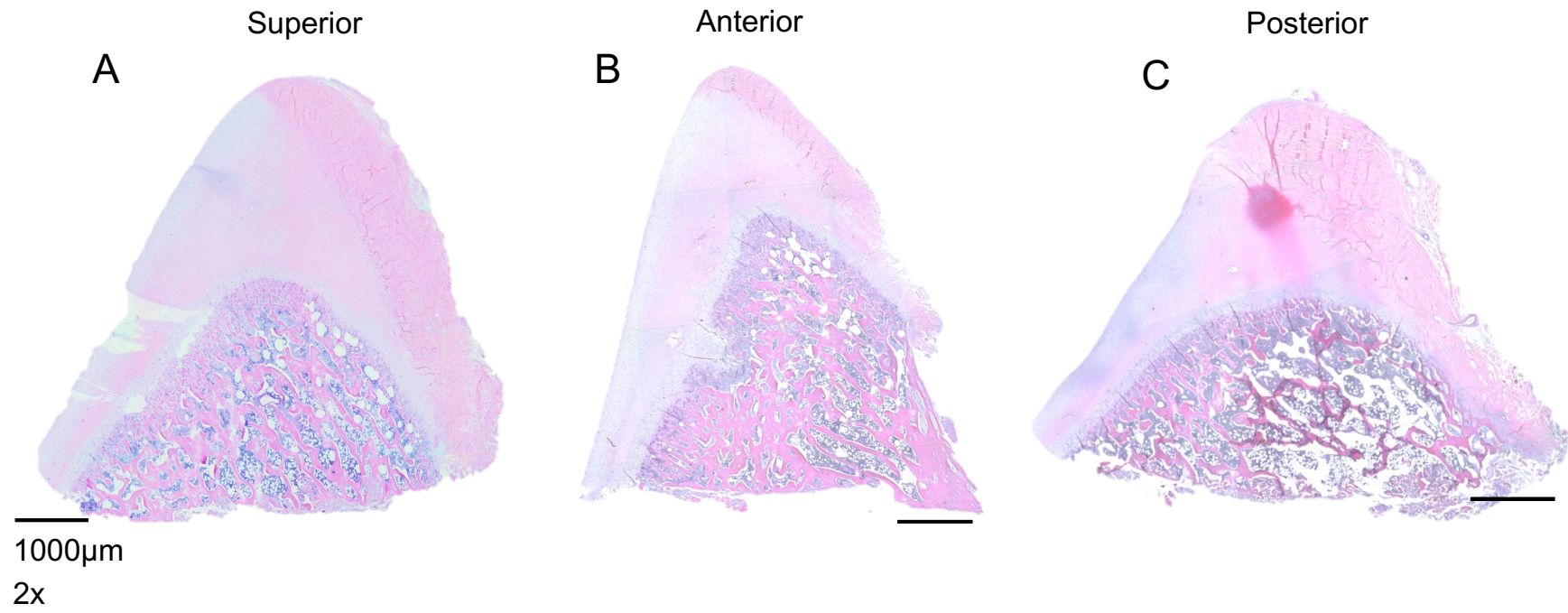


Figure 2.12 – A representative set of H&E stained native porcine labrum from anterior, superior, and posterior regions.

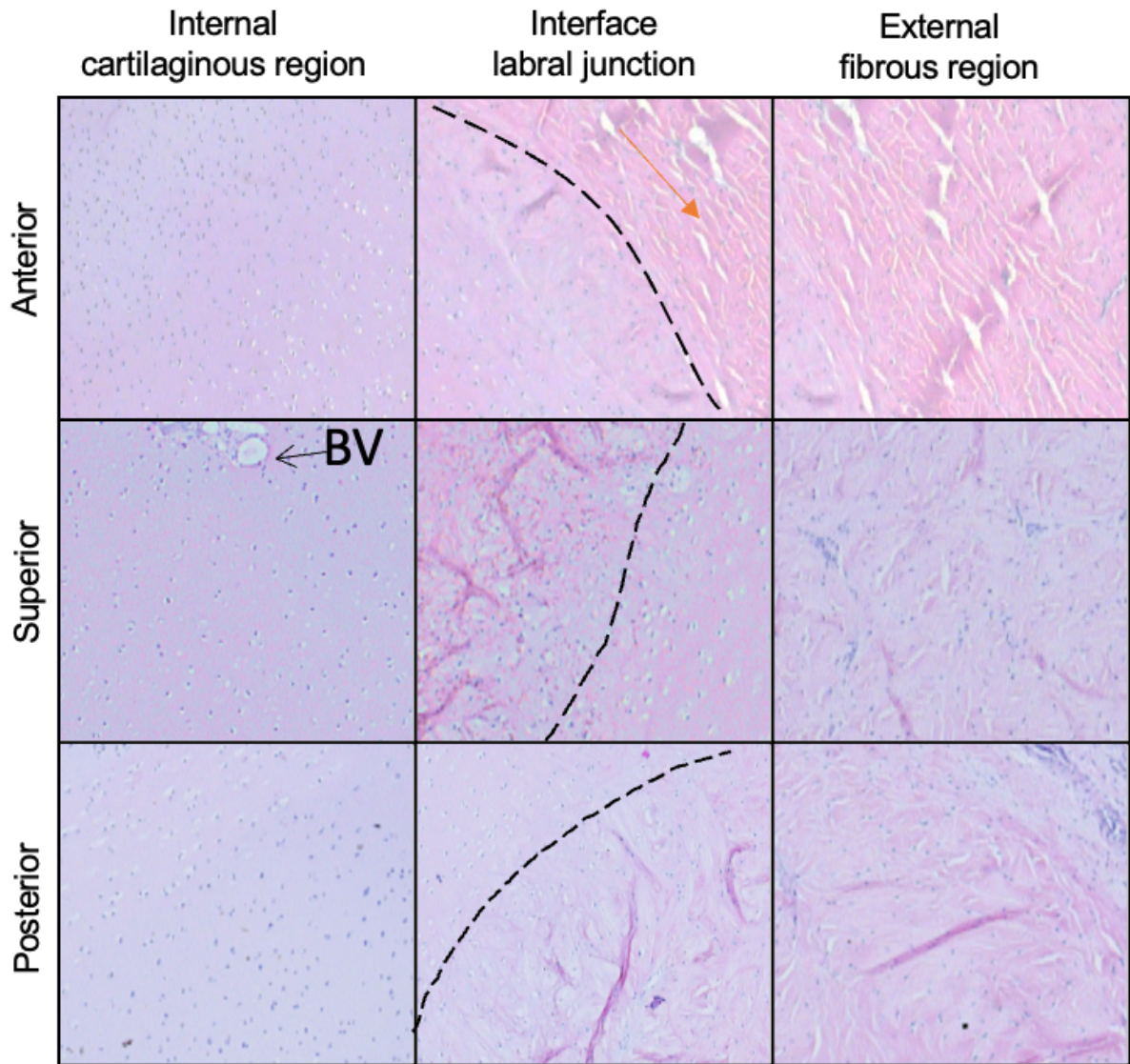


Figure 2.13 – An image table comparing the key regions from Figure 2.11 of H&E-stained native porcine labrum from anterior, superior, and posterior regions. The black dashed line represents the transition between the fibrous and cartilaginous regions. The orange arrow represents the general direction of collagen fibres found in the anterior labrum in the fibrocartilage. BV represents the blood vessels found.

2.5.3 Distribution of proteoglycans using Safranin-O & Fast green staining

Safranin-O and Fast green staining allowed for visual assessment regarding the distribution of glycosaminoglycans (GAGs) present in the native porcine labrum. This allowed comparisons between the different regions of the acetabular labrum related to function.

The background stain and cytoplasm were stained grey-green due to fast-green dye. Cartilage, mucin, and mast cell granules were stained due to safranin-o with shades of red and indicate presence of GAGs due to the proteoglycans being positively stained. A higher intensity is indicative of a higher proteoglycan content in normal cartilage (Camplejohn and Allard, 1988). The external labrum was stained blue-green in all samples, this is the site where the labrum integrates with the joint capsule which is composed of dense connective tissue. The posterior labrum (Figure 2.14C) had the largest blue-green appearance in the external labrum suggesting a more fibrous structure compared to the anterior labrum (Figure 2.14B), which had the least green staining in the external labrum. Examining the chondrolabral junction (Figure 2.15) in the native porcine labrum revealed a transition between the red and green stains with fibre like structures integrating from the external to internal sites. The posterior labrum had parallel alignment of collagen fibres across the external labrum (Figure 2.15) and had a large transition between the internal and external labrum which appeared pink (Figure 2.14C). The anterior and superior labrum had a distinct margin at the interface which separated the red/pink stain from the blue-green stain of the external labrum (Figures 2.14A and 2.14B). The collagen fibres around the interface in the anterior and posterior labrum were aligned perpendicular to the margin (Figure 2.15, orange arrows), while the integration of fibres at the superior labrum was more anisotropic. All labrum sections had a higher distribution of GAGs toward the cartilage than the peripheral capsular side. The highest concentration of GAGs was found anteriorly, superiorly, and then posteriorly in the native porcine sections which was based on the concentration of red stain. Holes were present in the cartilage and external labrum which resembled blood vessels. These sites were surrounded by a cluster of flattened cells in a ring (Figure 2.15).

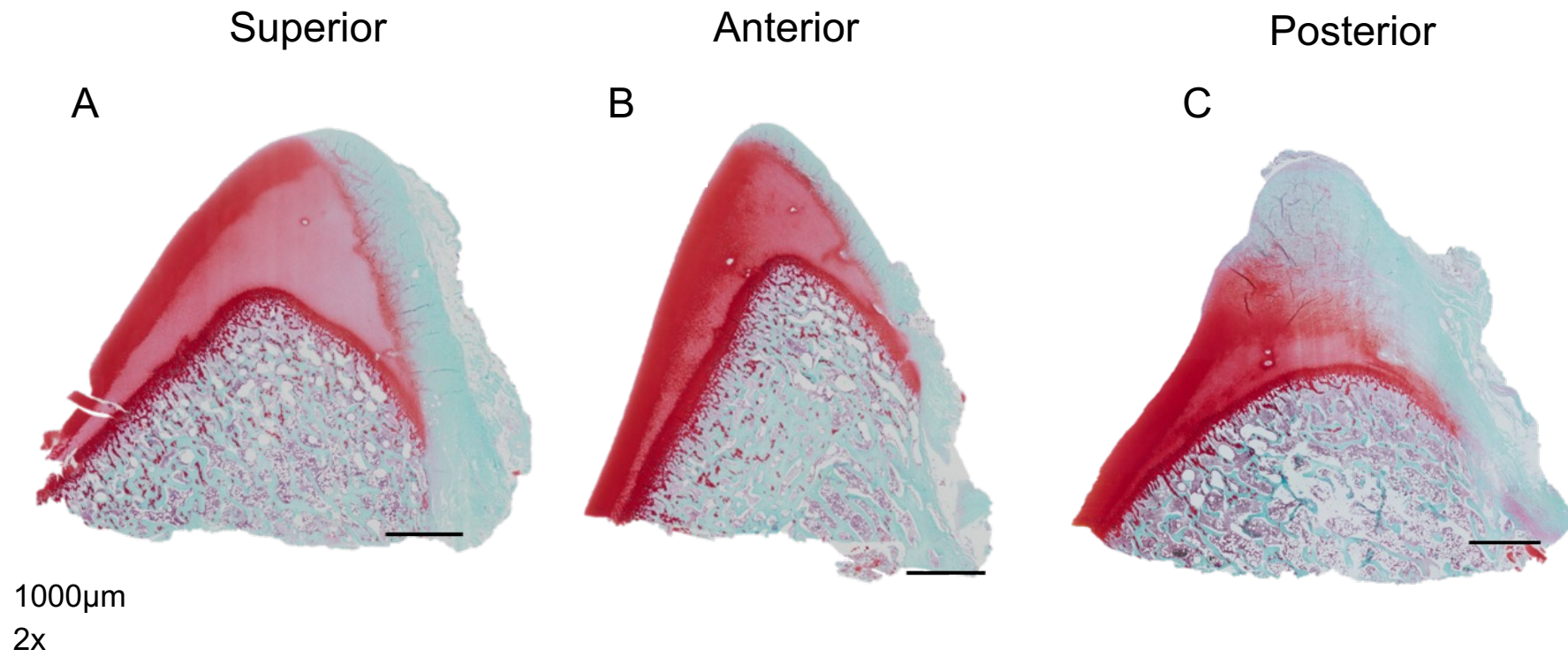


Figure 2.14 – A representative set of Safranin-O & Fast green stained porcine labrum from anterior, superior, and posterior regions.

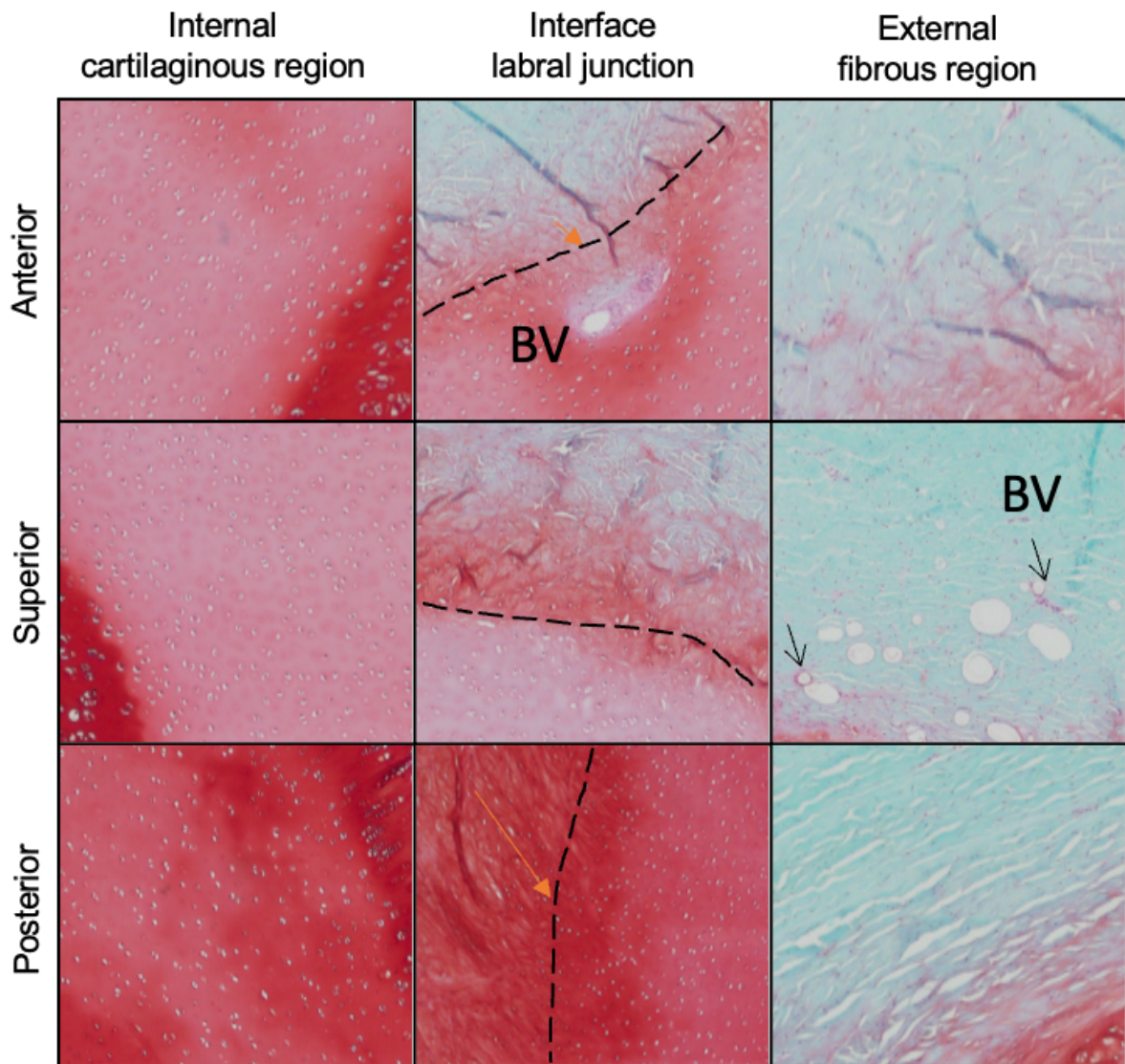


Figure 2.15 – An image table comparing the key regions from Figure 2.14 of Safranin-O & Fast green stained porcine labrum from anterior, superior, and posterior regions. The black dashed line represents the transition between the fibrous and cartilaginous regions. The orange arrow represents the general direction of collagen fibres. BV represents the blood vessels found.

2.5.4 Distribution of collagen fibres using Sirius red & Miller's elastin staining

Sirius red and Miller's elastin staining was used to determine the arrangement of collagen fibres present in native porcine labrum. Under brightfield light microscopy, Sirius red stained collagen red. Elastin was detected where the tissue was stained dark purple around the lacunae and in some blood vessels observed in the cartilage of all porcine sections (Figure 2.16). The cartilage was stained pink at the periphery of all the porcine sections (Figure 2.16). The external labrum was stained a dark red colour suggest strong positive staining for type I collagen fibres, which appeared thick non homogenously arranged in all samples (Figure 2.17). Chondrocytes were identified in their lacunae with arrangement typically seen in articular cartilage (Figure 2.17, internal cartilaginous region). Collagen fibres were detected running parallel to each other and perpendicular to the chondrolabral junction in the superior and posterior labrum (Figure 2.17, orange arrow). This followed a non-homogenous array of large collagen fibre bundles across the external labrum (Figure 2.17). Black circles represent bubbles created during the fixation process when applying a coverslip. A tissue artefact was present in the cartilage near the base in the posterior labrum (Figure 2.16C), where some subchondral bone appeared on top of the cartilage.

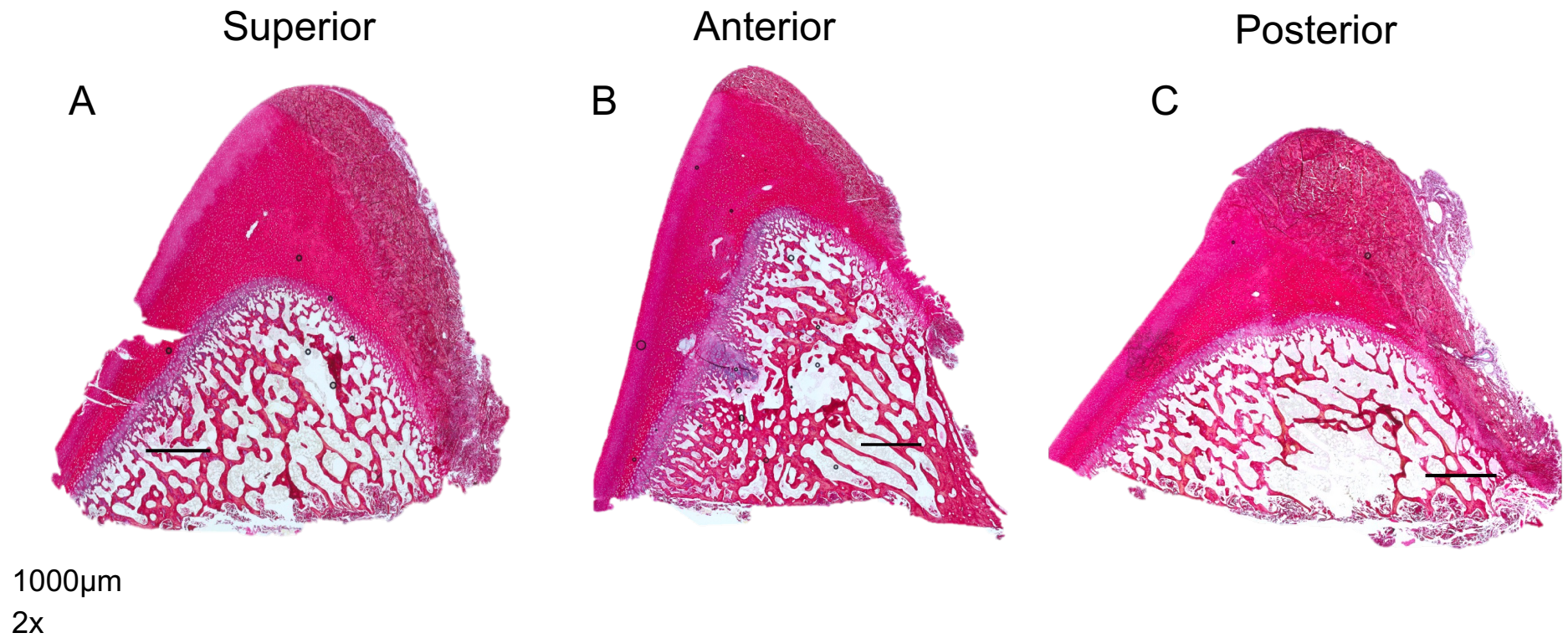


Figure 2.16 – A representative set of Sirius red and Millers' elastin-stained porcine labrum from anterior, superior, and posterior regions. Black circles represent bubbles created during the fixation process when applying a coverslip. A tissue artefact was present in the cartilage on the bottom right of C in the posterior labrum, where some subchondral bone appeared on top of the cartilage, which may have occurred during processing.

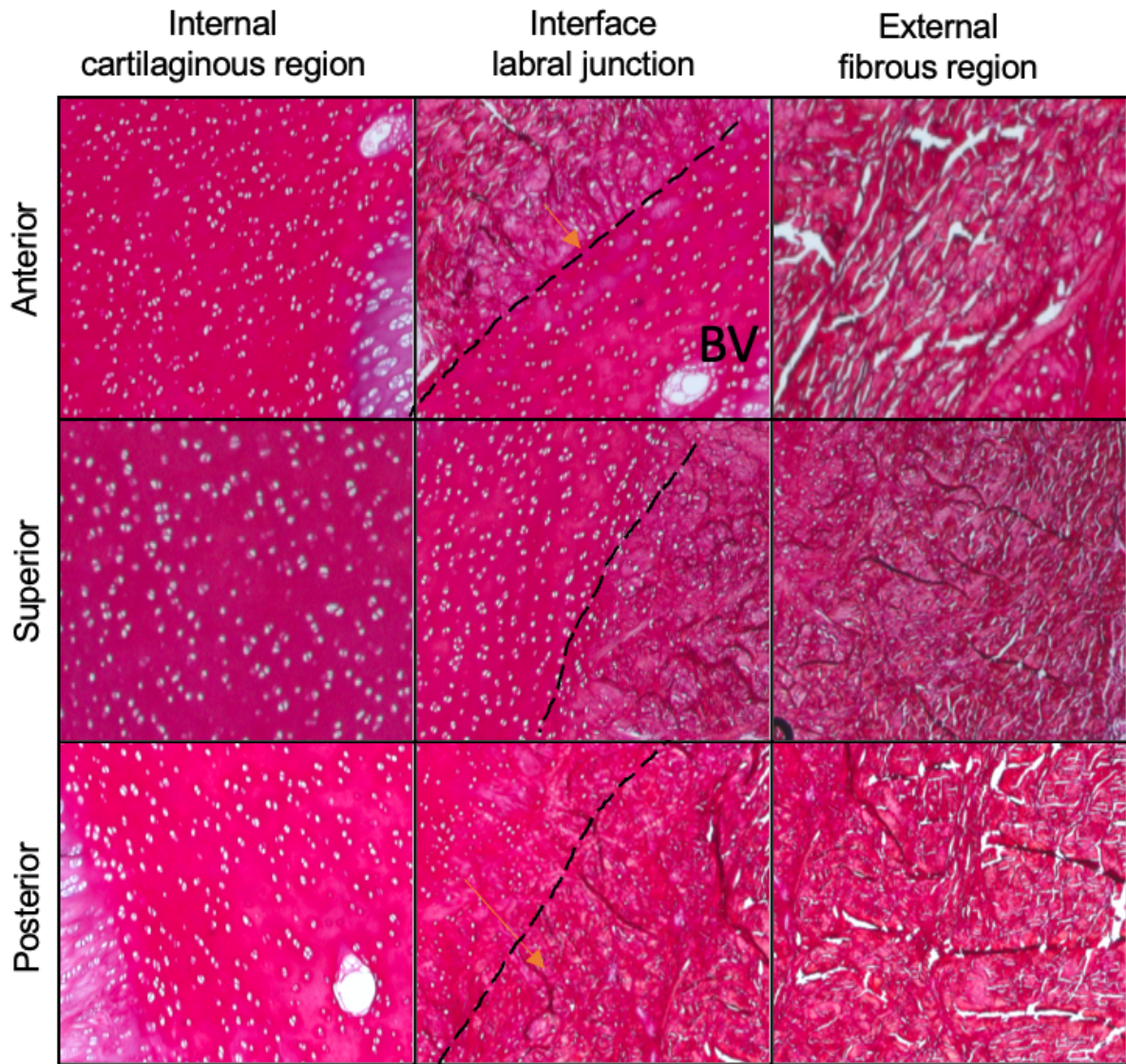


Figure 2.17 – An image table comparing the key regions from Figure 2.16 of Sirius red and Millers' elastin-stained porcine labrum from anterior, superior, and posterior regions. The black dashed line represents the transition between the fibrous and cartilaginous regions. The orange arrow represents the general direction of collagen fibres. BV represents the blood vessels found.

2.5.5 Investigation of collagen fibre alignment using Polarised light

Polarised light microscopy was used to visualise the same sections from 2.5.4 stained with Sirius red and Miller's elastin determine the organisational arrangement of collagen fibres present in native porcine labrum sections. Collagen responds to polarised light where certain collagen fibres become visible and the alignment of such fibres or bundles can be detected due to the birefringence of collagen(Liu *et al.*, 2021). Type I collagen appears bright red or a red-yellow when detected with polarised light in contrast to type III collagen and elastin which stain green. The external labrum of all native porcine sections-stained bright red (Figure 2.18) where large type I collagen bundles and fibres were observed. There was a sharp transition and a loss of red colour at the transition near the chondrolabral junction appearing black with thinner red fibres interspersed in the articular cartilage (Figure 2.19, interface). Type I collagen fibres were aligned parallel to each other in the interior articular cartilage of the posterior and superior labrum sections. The anterior labrum section did not stain as bright red as the superior or posterior sections and had the smallest margin of type I fibres in the external labrum. Some yellow and green fibres were detected in the internal cartilaginous and external fibrous region (Figure 2.19, internal cartilaginous region) suggesting presence of elastin or type III collagen. At the chondrolabral junction interface and throughout the internal cartilage, there was strong alignment of fibres (Figure 2.19, blue arrow). Bright red collagen type I fibres were arranged perpendicular to those in the cartilage in the anterior and posterior labrum sections (Figure 2.19, yellow arrow). There was some alignment of collagen fibres in between the transition and periphery of the external labrum in the anterior porcine labrum (Figure 2.19, green arrow), whereas the collagen fibres present in the superior and posterior region appeared non homogenous in arrangement and alignment.

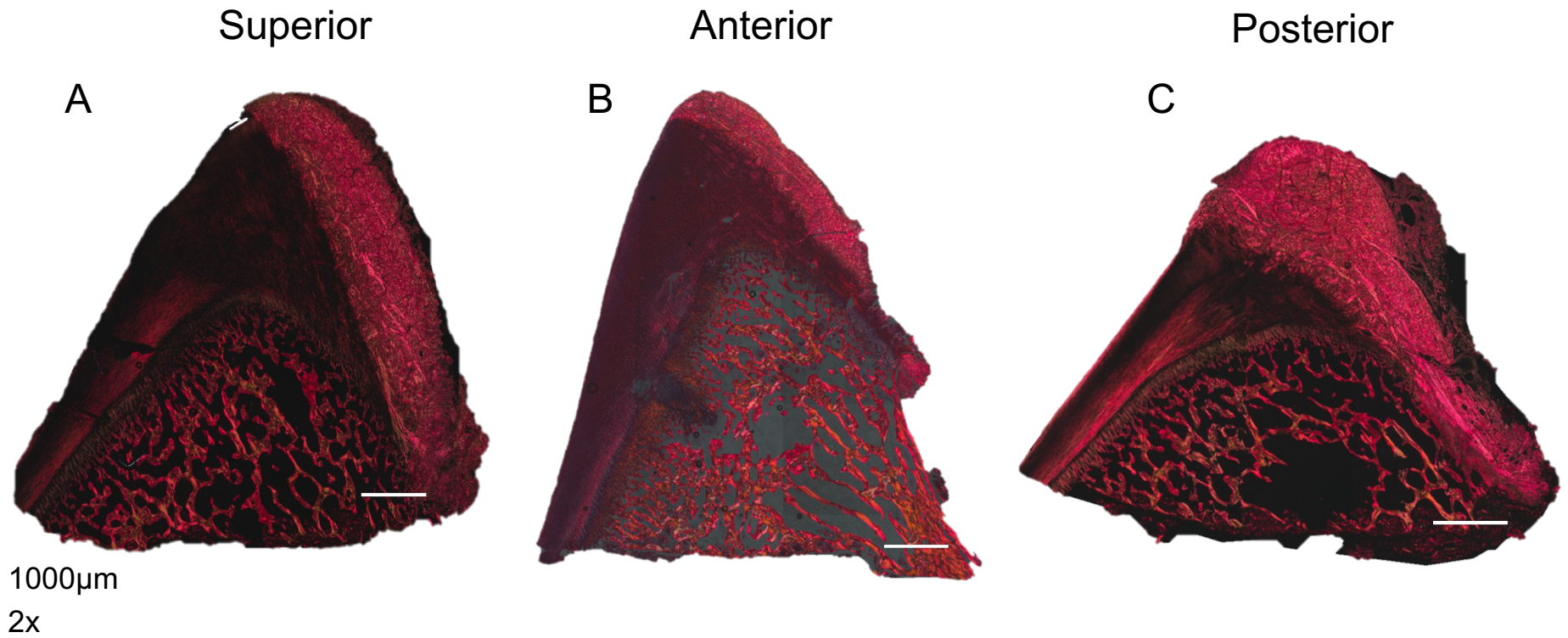


Figure 2.18 – A representative set of Sirius red and Millers' elastin-stained native porcine labrum viewed under polarised light from anterior, superior, and posterior regions.

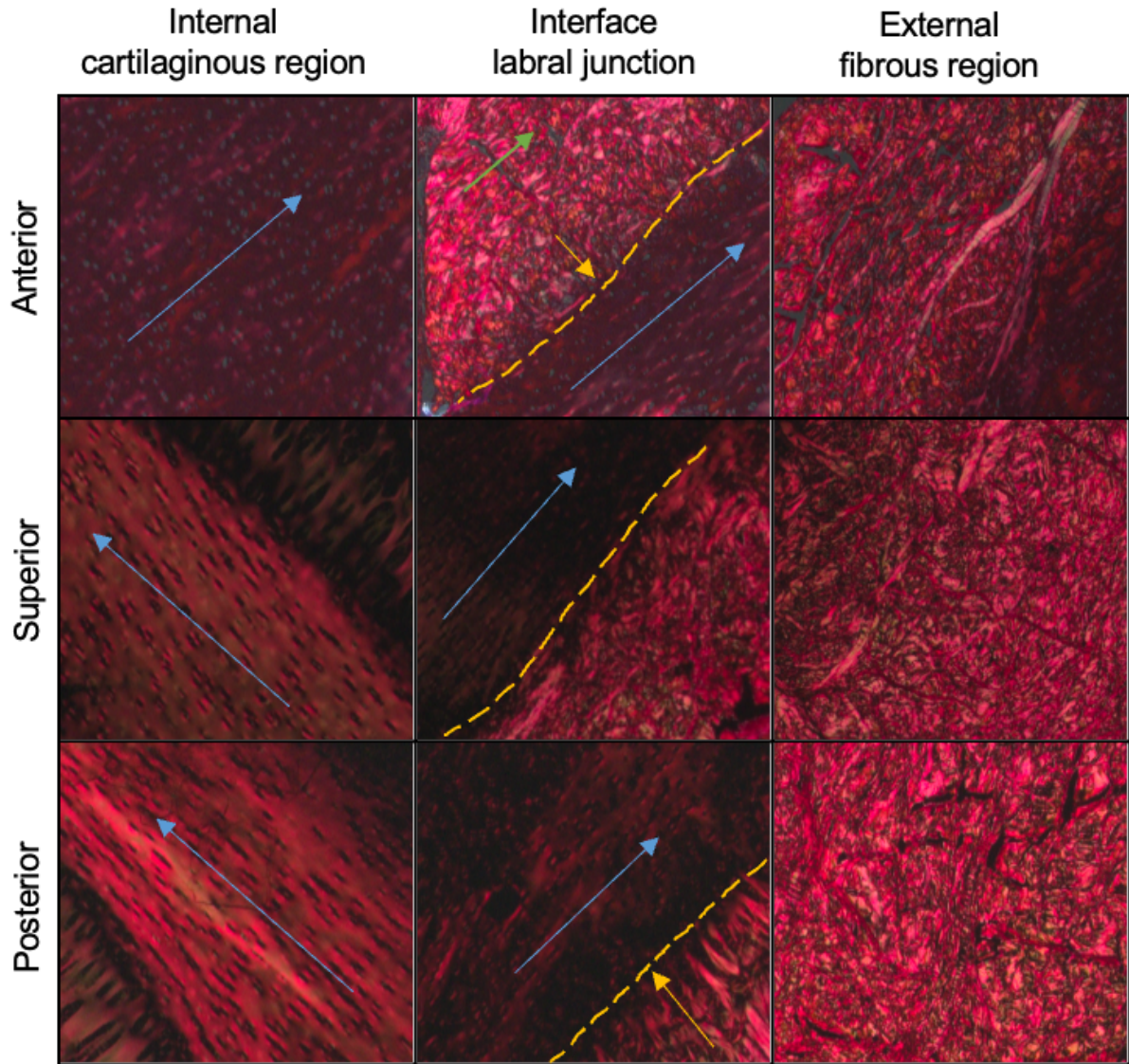


Figure 2.19 – An image table comparing the key regions from Figure 2.18 of Sirius red and Millers' elastin-stained porcine labrum from anterior, superior, and posterior regions. The yellow dashed line represents the transition between the fibrous and cartilaginous regions. The blue arrow represents the general direction of collagen fibres.

2.6 Discussion

This study aimed to characterise unloaded porcine acetabular tissues (n=6) macroscopically and histologically from multiple regions (anterior, superior, and posterior) of the acetabulum.

The acetabulum labrum sections varied in size and cross-section across the circumference of the porcine acetabulum (Figure 2.8, top). The labrum sections were round in cross-section at the apex (tip of the cross sections from the subchondral bone base) and wider at the base with the posterior and superior sections appearing more triangular (figure 2.8). This differed from the H&E staining where the anterior labrum was found to be triangular, while the posterior and superior were rounder. Pallan, (2016) reported a rounder shape of immature porcine labrum and a triangular shape in human labrum. Kohl *et al.*, (2011) found that the human anterior-superior labrum were rounder in shape. (Philippon, Arnoczky and Torrie, (2007), reported a triangular shape of the anterior labrum.

When comparing the structure of the internal and external labrum. The sections had a distinct fibrous appearance toward the capsular side of the external labrum (Figure 2.9, white cross) compared with the smooth and greyish-white opaque appearance towards the articular cartilage (Figure 2.9, black square). The external labrum was stained blue-green with Safranin-o and fast green staining in all samples, which suggests this area is dense with collagen fibres and lacks proteoglycan content in this region. This is expected anatomically as the external labrum integrates with the joint capsule which is composed of dense connective tissue comprising of thick collagen type I fibres. The posterior labrum (Figure 2.14C) had the largest blue-green appearance in the external labrum suggesting a more fibrous structure compared to the anterior labrum (Figure 2.14B), which had the least green staining in the external labrum.

The sections had varying transitions separating the smooth and fibrous regions, where the posterior section had the largest visible fibrous region comprising of collagen type I fibres, followed by the superior and anterior regions. At the chondrolabral junction interface and throughout the internal cartilage, there was strong alignment of fibres (Figure 2.19, blue arrow). The presence of type I collagen in the external labrum agreed with the findings

reported through immunohistochemistry conducted on porcine native samples by Pallan (2016). There was some alignment of collagen fibres in between the transition and periphery of the external labrum in the anterior porcine labrum (Figure 2.19, green arrow), whereas the collagen fibres present in the superior and posterior region appeared non homogenous in arrangement and alignment. Collagen fibres were detected running parallel to each other and perpendicular to the chondrolabral junction in the superior and posterior labrum (Figure 2.17, orange arrow). There is a relationship between the Sirius Red dye and the collagen which enhances the birefringence detected. The dye is affixed to the collagen fibre such that their long axes are parallel to elongated dye molecules (Junqueira, Bignolas and Brentani, 1979). The external labrum was stained a dark red colour under Sirius red staining suggesting strong positive staining for type I collagen fibres, which appeared thick non homogeneously arranged in all samples (Figure 2.17). This followed a non-homogeneous array of large collagen fibre bundles across the external labrum (Figure 2.17). The external labrum of all native porcine sections-stained bright red (Figure 2.18) where large type I collagen bundles and fibres were observed. There was a sharp transition and a loss of red colour at the transition near the chondrolabral junction appearing black with thinner red fibres interspersed in the articular cartilage (Figure 2.19, interface).

In addition, the shade of red observed from polarization microscopy of PSR stained sections may be attributed to various factors, including the size, alignment, and packing of fibers, the cross-linking of fibers, the presence of interstitial ground substance, and the water content (Gopinathan et al., 2020). It has been observed that collagen molecules that are tightly packed and well-aligned exhibit a shift towards longer wavelengths in the polarization colours. This shift is characterized by a predominance of green to greenish-yellow hues in both thin and thick fibers. This suggests that the collagen molecules in these fibers are loosely packed and may consist of procollagens, intermediates, or pathological collagen, rather than tightly packed normal fibers (Gopinathan et al., 2020).

Schon et al., (2020) investigated anterior-superior labrum using H&E and picrosirius red reporting that collagen fibres in the external labrum contained thick and thin collagen fibres.

Pallan, (2016) reported no difference in collagen structure between the anterior, superior, and posterior porcine regions. This conflicts with this study's findings as there were distinguishable differences apparent through both Safranin-o and Sirius red stains. It is unclear which region of porcine labrum was stained with Sirius red and miller's elastin, by Pallan (2016) who reported an overall duller labrum with much higher green-yellow birefringence at the cartilage with lack of birefringence detected at the internal labrum. The external labrum was stained red. This lack of colour could be explained due to processing methods as decalcification was not used to prevent loss of GAGs with alcian blue samples, which may impact the strength of red colour observed.

The anterior labrum section did not stain as bright red as the superior or posterior sections and had the smallest margin of type I fibres in the external labrum. Some yellow and green fibres were detected in the internal cartilaginous and external fibrous region (Figure 2.19, internal cartilaginous region) suggesting presence of elastin or type III collagen. The posterior labrum had parallel alignment of collagen fibres across the external labrum (Figure 2.15) and had a large transition between the internal and external labrum which appeared pink (Figure 2.14C). The collagen fibres around the interface in the anterior and posterior labrum were aligned perpendicular to the margin (Figure 2.15, orange arrows), while the integration of fibres at the superior labrum was more anisotropic.

Cashin *et al.*, (2008) reported there was an abrupt transition at the junction of the cartilaginous acetabulum with collagen fibres running parallel to the junction while the posterior acetabular labral chondral complex in the same specimen showed a gradual and interdigitated transition zone with more collagen fibres more haphazardly arranged. Stained with H&E and azan. The study was limited as only the transition between cartilage and fibrocartilage was imaged. Additionally, the samples were human fetal labrum which may be further different from the immature porcine labrum and the typical mature human labrum reported in wider literature.

Schon *et al.*, (2020) investigated anterior-superior labrum using H&E and picosirius red reporting that collagen fibres in the superficial region of the labrum were oriented parallel with the labrum

surface and with damage, while human labrum from patients with symptomatic FAI were disoriented and more heterogeneous.

All labrum sections had a higher distribution of GAGs toward the cartilage than the peripheral capsular side. The highest concentration of GAGs was found anteriorly, superiorly, and then posteriorly in the native porcine sections which was based on the concentration of red stain.

Pallan, (2016) found that the internal labrum and cartilage was stained positively for GAGs across all the porcine regions. However, her stains were not able to pick up differences in the shade of blue as all samples were the same colour. Only the external human anterior labrum was stained which did not positively stain for GAGs.

The structure of the acetabular labrum is often compared with the fibrocartilaginous structure of the meniscus or the annulus fibrosus. The acetabular labrum is quite different due to its inherent interface with the articulating surface which is composed of articular cartilage. While labral tears have been well characterised radiographically (McCarthy *et al.*, 2003; Laumonerie *et al.*, 2021), there needs to be more information regarding the intact acetabulum labrum. Part of the lack of research in this area is due to the need for detailed studies investigating the microstructure of the labrum, to understand how this fibrocartilaginous tissue behaves and functions in the highly stable hip joint.

This means the structure is complex and the nature of this transition zone, the morphology and where the interface begins needs to be clarified. It is most like the glenoid labrum in terms of its structure and function which similarly has a transition from articular cartilage to a fibrocartilaginous structure which transitions to the capsular portion consisting of dense irregular connective tissue.

Posteriorly, the labrum can withstand tensile loads from different directions, while anteriorly is more designed to compressive forces, which could mean it is more susceptible to tensile or shearing forces, which can cause labral tearing. The anterior region had the least fibrous section and was duller in stain when compared with the other regions. This supports the theory that it is more designed to withstand compressive forces, which matches the literature (refs) as it is the main load-bearing region where the femur will interact during deep flexion in the

gait cycle and the labrum will help dissipate some of this load. This is also supported by the shape which is more triangular compared with other regions to prevent the femur from dislocating. Therefore, the excision of labrum may increase the forces experienced at the rim. Bioimaging and histological examination of the macro and microstructure can help determine the vital arrangement of this tissue, which likely differs from the other joints. While the results are representative of the general structural differences in different regions of the acetabular labrum, it would be useful histologically examine unloaded cadaveric human acetabulum samples. Additionally, comparing findings with mature porcine acetabulum samples in the future could further help validate using porcine tissue as a suitable model for whole natural hip joint testing.

Small holes were observed within the tissue structure that resembled small blood vessels (Figure 2.11, Figure 2.13). Holes were present in the cartilage and external labrum which were surrounded by a cluster of flattened cells in a ring (Figure 2.15). Elastin was detected where the tissue was stained dark purple around the lacunae and in some blood vessels observed in the cartilage of all porcine sections (Figure 2.16). There were also some holes in the capsular side of the labrum and in the articular cartilage however it was not possible to confirm if these structures were in fact blood vessels as they lacked the presence of endothelial cells surrounding the structure. It is not unexpected to find vasculature in developing porcine tissue as similar structures have been observed previously (Julkunen *et al.*, 2009, 2013; Al-Talalwah, 2015; Alashkham *et al.*, 2018). Philippon, Arnoczky and Torrie, (2007) also reported avascular anterior ovine labrum using H&E. Su *et al.*, (2023) found major blood supply of the native labrum at the capsular side, while fewer vascular structures were observed toward the articular cartilage.

It should be noted that while it is not completely accurate, Sirius red and millers' elastin can confirm the presence of blood vessels in porcine tissue samples as it stains dark purple and was detected in the external labrum at the joint capsule of porcine cross sections. Pallan (2016) was able to detect blood vessels in porcine labrum samples through Sirius red and Miller's

elastin staining but was not able to detect the presence of elastin in the human labrum likely reflecting the maturity of tissue.

The posterior labrum had a large deeply red stain in the tissue. Similar deep red streaks were present in all sections which may be an artefact of the section folding or due to processing. Black circles represent bubbles created during the fixation process when applying a coverslip. A tissue artefact was present in the cartilage near the base in the posterior labrum (Figure 2.16C), where some subchondral bone appeared on top of the cartilage. The superior labrum section had torn and fragmented tissue in the articular cartilage (Figure 2.12A). These artefacts could be explained by difficulties in sectioning the samples as they contained some small amount of subchondral bone, which aids in identifying and knowing where the base of the labrum is to select the appropriate orientation when preparing slides. Unfortunately, the bone results in uneven thickness and obtaining the optimal thickness for sections was difficult. Sections were between 6-12 μ m and, in some instances, resulted in folding or tearing of wax-embedded samples which appeared as artefacts in the final images.

The characterisation reported in this study can be further improved by increasing the sample size, comparing with more mature porcine tissue to better compare with human labrum and secondary analysis using immunohistochemistry or other more resolving methods.

2.7 Conclusion

In this study, the gross appearance of native porcine acetabulum and acetabular labrum was visualised, and histological examination was used to characterise the structure of the acetabular labrum, articular cartilage and chondrolabral junction.

It was found that the histoarchitecture of native porcine labrum varied across the anterior, posterior, and superior regions of the acetabular labrum which may relate to the function of the labrum regionally across the acetabulum.

The anterior labrum had the thinnest external labrum and subsequently less visible collagen type I bundles while the chondrolabral junction at this site had a distinct transition which may explain why it is more likely damaged compared to the superior or posterior region which

appear more fibrous due to a larger proportion of collagen type I detected through polarised Sirius red and miller's elastin staining.

These findings will form the basis for the unloaded, native structure of the porcine labrum from these regions. Additionally, Safranin-O and polarised Sirius red staining allowed features of glycosaminoglycan distribution and collagen distribution to be characterised.

These findings contribute to the understanding of how the labral microstructure contributes to function, especially due to morphological and compositional differences found, particularly between the anterior and posterior labrum.

Chapter 3 Developments in *In Vitro* Cyclic Whole Hip Joint Testing

3.1 Introduction

The hip is a highly stabilised joint located in the pelvis, making it difficult to access and assess experimentally (Bedi *et al.*, 2011). This has resulted in a limited number of experimental *in vitro* studies, where most findings have been made through clinical examinations and hip arthroscopies (Aydingöz and Öztürk, 2001; Bouma *et al.*, 2015; A.L *et al.*, 2016; Battistelli *et al.*, 2023) resulting in a limited understanding of the mechanisms behind damage. To study the mechanical environment and how different hip pathologies affect the natural anatomy, motion or mechanics, experimental studies are still required and would greatly help develop suitable interventions.

3.1.1 Motivation

Due to the lack of capable experimental whole joint testing models of the hip, there have been more predictions of the mechanics and contact stresses of the hip through computational studies (Ipavec *et al.*, 1999; Charbonnier *et al.*, 2009; Chegini, Beck and Ferguson, 2009; Mak *et al.*, 2011; Julkunen *et al.*, 2013; Turley *et al.*, 2013; Hodaei, Farhang and Maani, 2014; Arndt *et al.*, 2017). However, due to the need for more understanding of the exact biomechanical behaviour to investigate damage found *in vivo*, there must also be more reliable and repeatable methods incorporating the natural physiology using animal or human cadaveric tissue. While there are fewer natural hip studies, *in vitro* experimental studies of artificial hip joints or joint prostheses have been possible through the design and development of hip simulators.

Joint simulators have been adapted to test natural hips (Lizhang, 2010; Taylor, 2012; Pallan, 2016) experimentally *in vitro*; however, studies in this area are limited and often oversimplified, limiting their potential for studying abnormal mechanics of the joint and the associated damage mechanisms. The use of a cadaveric or animal hip joint can help understand how abnormalities in mechanical parameters such as structure, shape, orientation, or excessive motions or loading can result in degeneration of hip tissue and result in the generation of labral

tears or cartilage injury, and aid in the selection of interventions that promote natural hip preservation.

A suitable animal model which can use the hip geometry to allow the mechanical environment to be controlled and altered would allow simulation of the abnormal mechanics created from conditions which alter the natural geometry of the hip joint or altered contact between the femoral head and the acetabulum.

Whole natural hip joint testing by adapting an artificial hip simulator was first shown by Groves, (2016) who tested Cobalt Chrome (CoCr) metal femoral heads with natural acetabulae cemented in testing pots mounted on the simulator in a hemiarthroplasty model. Matched porcine femoral heads were cemented and mounted in the simulator with cemented acetabulae in a pendulum hip simulator.

Pallan (2016), indicated that altered parameters led to increased damage to natural porcine hip joints, but these early tests were inconclusive and lacked assessment into the progression of damage. Therefore, this chapter aimed to develop the experimental hip testing methodology to allow it to be used as a consistent tool for *in vitro* cyclic whole hip joint testing.

3.1.2 Chapter aim

To develop an existing experimental simulation model for generating chondrolabral damage using a hip joint simulator.

The objectives were:

- To initially replicate previous methods (Pallan, 2016) and identify the issues which lead to failures, make adaptations to optimise the process and compare findings.
- To develop the experimental simulation model to allow adverse mechanical loading environments.
- To assess which mechanical parameters can be implemented using the single station hip simulator to generate clinically relevant forms of damage.

- To determine the effect of simulator inputs in generating a specific type of chondrolabral damage and propose the simulator constraints for generating types of chondrolabral damage.

3.1.3 Background to Whole Natural Hip Joint Simulation

Methods used in this study were initially developed using components and models of a hemiarthroplasty model using a pendulum simulator (Lizhang, 2010) as in Figure 3.1, and for tribology studies (Taylor, 2012), which was adapted further into a protocol for whole joint testing in a pendulum simulator (Groves, Fisher and Williams, 2017).

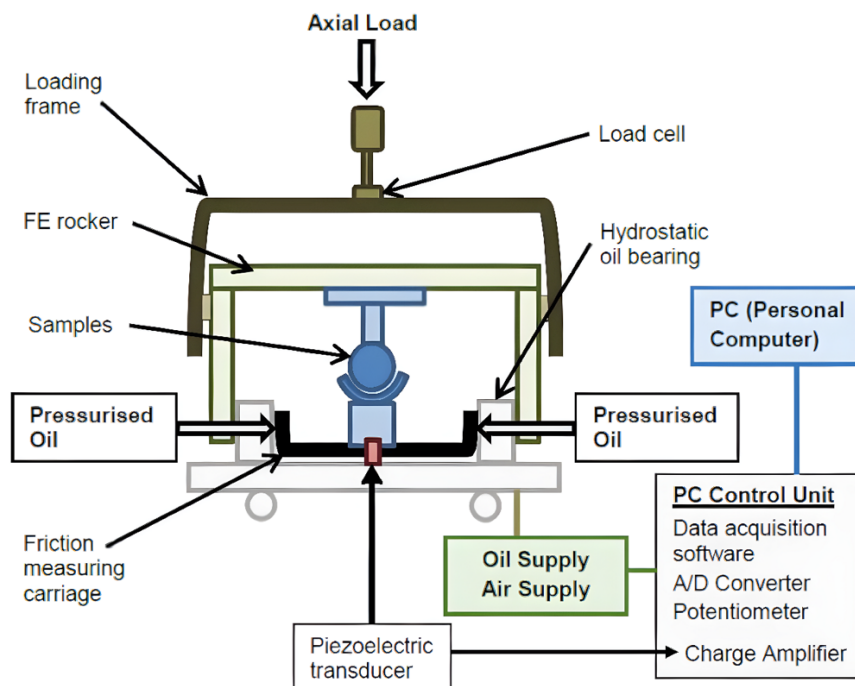


Figure 3.1 Schematics of pendulum friction simulator (Groves, Fisher and Williams, 2017)

The initial hemiarthroplasty model consisted of an artificial femoral head, paired with an equivalent diameter porcine acetabulum (Figure 3.2), where the joint was aligned based on human orientations of the joint as opposed to porcine acetabular orientation.

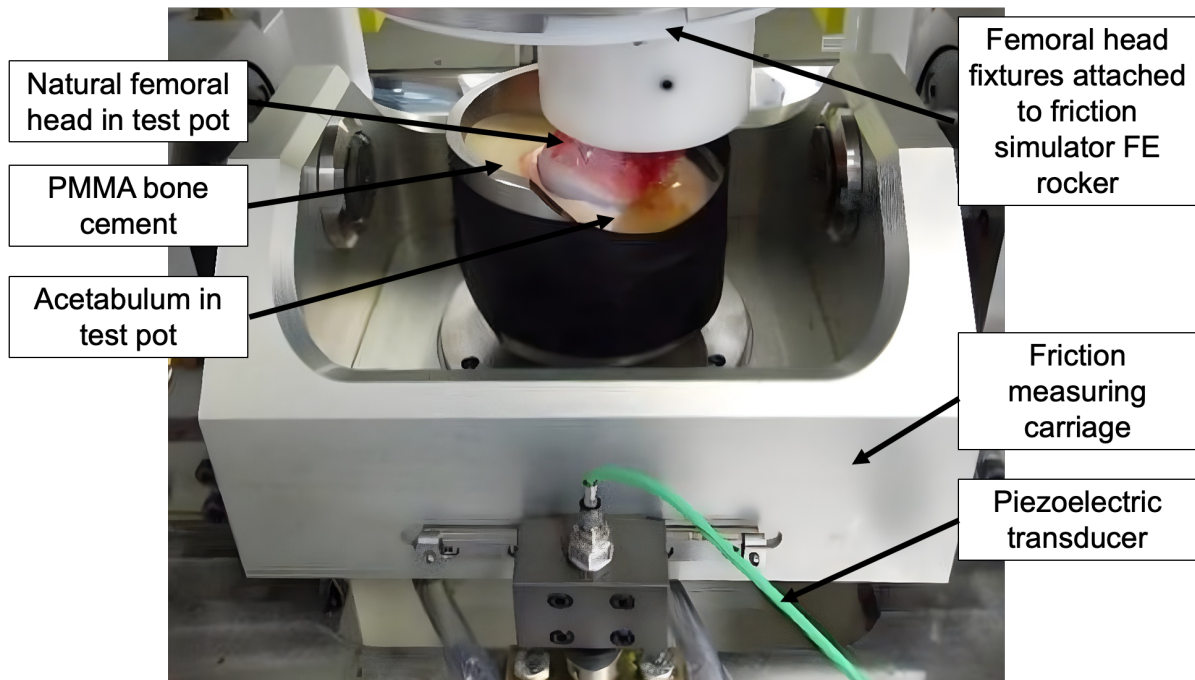


Figure 3.2 Mounted whole natural porcine hip joint components in the pendulum friction simulator limited to flexion extension (FE) motion(Groves, Fisher and Williams, 2017)

The model was simulated with axial loading following human gait cycles based on (Paul, 1967) and the International Organisation for Standardisation (ISO) 14242-2, however was limited to one axis of motion in flexion-extension. Loading of these joints ranged from 25N to 800N, with a frequency of 1Hz tested for 7,200 cycles or 2 hours. 25% bovine serum lubricant was used to represent synovial fluid. The joint was enclosed in a polymer gaiter to hold the lubricant simulating the physiological loading environment.

Pallan (2016) adapted the components used for these studies by creating polyethene and metal fixtures which would allow existing components to be mounted on a more advanced hip simulator (Figure 3.3) The *in vitro* testing method using the hip simulator was chosen for its ability to replicate three degrees of freedom motion and more advanced control of tuning, loading parameters and frequency used with a larger working space, which would suit the goals of this project in creating more extreme loading environments for natural joints.

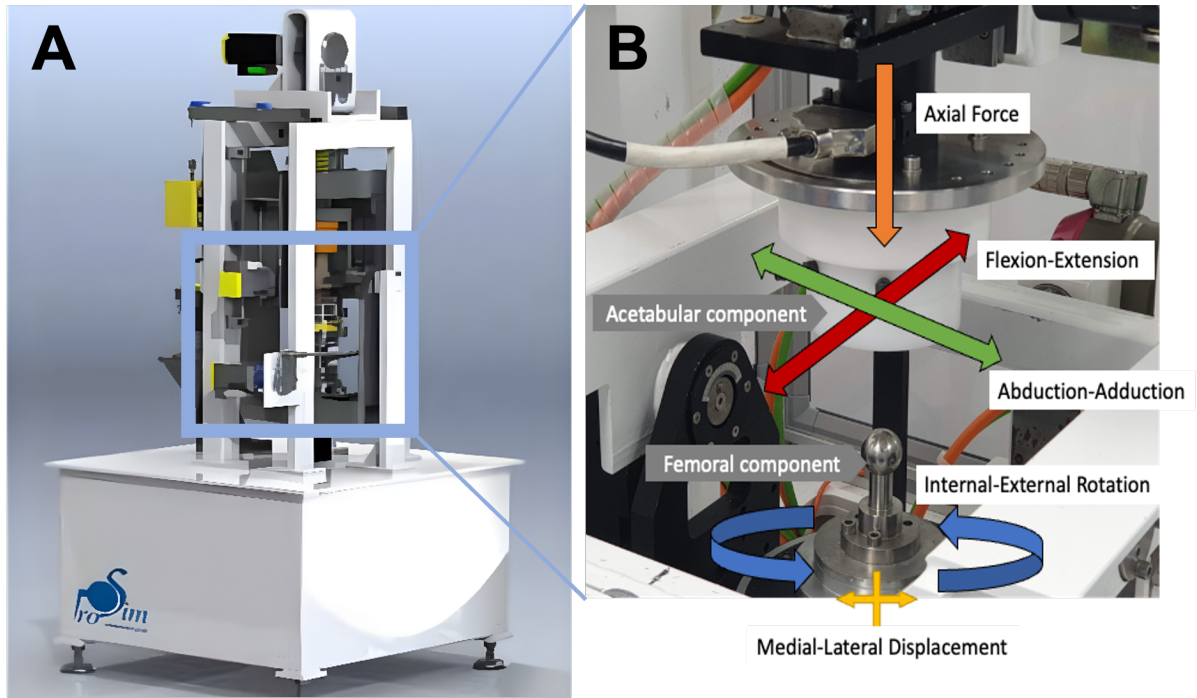


Figure 3.3: Hip Simulator used in this project and by Pallan (2016). **A** - Schematic of Prosim 1-Station Deep Flexion Hip Simulator (Simulator Solutions, Stockport, UK). **B** – Photograph of the working environment and three degrees of freedom labelled within the hip simulator with a dummy femoral head and cup.

3.2 Materials

The following section describes the materials used for natural hip simulation and any changes that were made to improve the existing methods, equipment or process previously used by Pallan (2016).

3.2.1 Materials and equipment required for cementing

Table 3.1 Table of the cementing equipment, consumables, and simulator components

Simulator Components	Consumables	Equipment
Acetabular base plate attachment	Clear plastic sheet	Glass beaker
Acetabulum head pot component	PBS (Phosphate buffered saline)	Hex keys
Femoral head base plate attachment	PMMA bone cement powder	Nitril gloves and PPE
Femoral head pot component	PMMA curing agent	Handheld bone saw
	Scalpel blade remover	Scalpel blade remover
	Scalpel blades and holders (Size 11)	Stirring rod
		Vice Clamp

3.2.2 Solutions and Media

Initially, the lubricant of choice was Bovine Foetal calf serum (FCS) (Harlan Bioproducts for Science, United States) as it contained a variety of proteins which help maintain joint lubrication that natural synovial fluid would provide. 25% (v/v) FCS was diluted with PBS for natural hip simulation. This provides a protein concentration of 16 – 18 mg/ml, similar to a natural synovial fluid protein content of approximately 20 mg/ml. However, since the duration of tests was shorter than in vitro testing of THR and typically for up to 4 hours, an alternative lubricant was chosen. Ringer’s Solution is relatively easier to prepare, and economical and has also been found to have similar biomechanical properties as synovial fluid(Forster and Fisher, 1996; Charbonnier *et al.*, 2009; Bortel, Charbonnier and Heuberger, 2015). The cartilage-specific modified ringer’s solution was based on (Urban, 1994) and used the following preparation:

- 130 mM Na⁺ solution with each salt mass is per 10 mL of distilled H₂O

- Potassium Chloride (KCl): 5.22 mg, 7 mM
- Calcium Chloride (CaCl₂): 5.55 mg, 7 mM
- Sodium Chloride (NaO): 51.43 mg, 88 mM
- Sodium Bicarbonate (NaHCO₃): 35.28 mg, 42 mM

There were no noticeable changes when switching to Ringer's solution compared to serum for short-term testing as used in the following chapters. Importantly, using Ringer's solution was sufficient to keep the cartilage hydrated as required for *in vitro* simulation.

- Double strength Ringers' solution:
 - 8 Ringer's Solution Tablets ¼ strength (Sigma-Aldrich, UK) composed of:
 - g/l Sodium Chloride,
 - 0.105 g/l Potassium Chloride,
 - 0.12 g/l Calcium Chloride 6H₂O,
 - 0.05 g/l Sodium Bicarbonate
 - Distilled Water (1l)
- Phosphated buffered saline
 - 10 Oxid Phosphate Buffered Saline Tablets (ThermoScientific, UK)

3.2.3 Photogrammetry equipment

A DSLR camera mounted on a tripod with an extensible arm set with a light tent. The light tent housed an acetate template at the base of the tent with markings for the acetabulum and femoral head mounting pots to be centred and aligned with the camera overhead (Figure 3.4).

Table 3.2 Table of the photogrammetry equipment, consumables, and simulator components

Simulator Components	Consumables	Equipment
Cemented acetabulum in acetabular pot	Clear Plastic sheet	Canon 750D DSLR camera
Cemented porcine femur in femoral pot	Nitril gloves and PPE PBS (phosphate buffered saline)	Acetate templates for femoral/acetabular base Light Tent (70x70x70cm) Macro lens (Canon, EF 100 mm f2.8 USM Macro lens) Tissue forceps Tripod with extendable arm Wide lens (Canon, EF-S 28-70 mm f3.5-5.6 IS II USM lens)

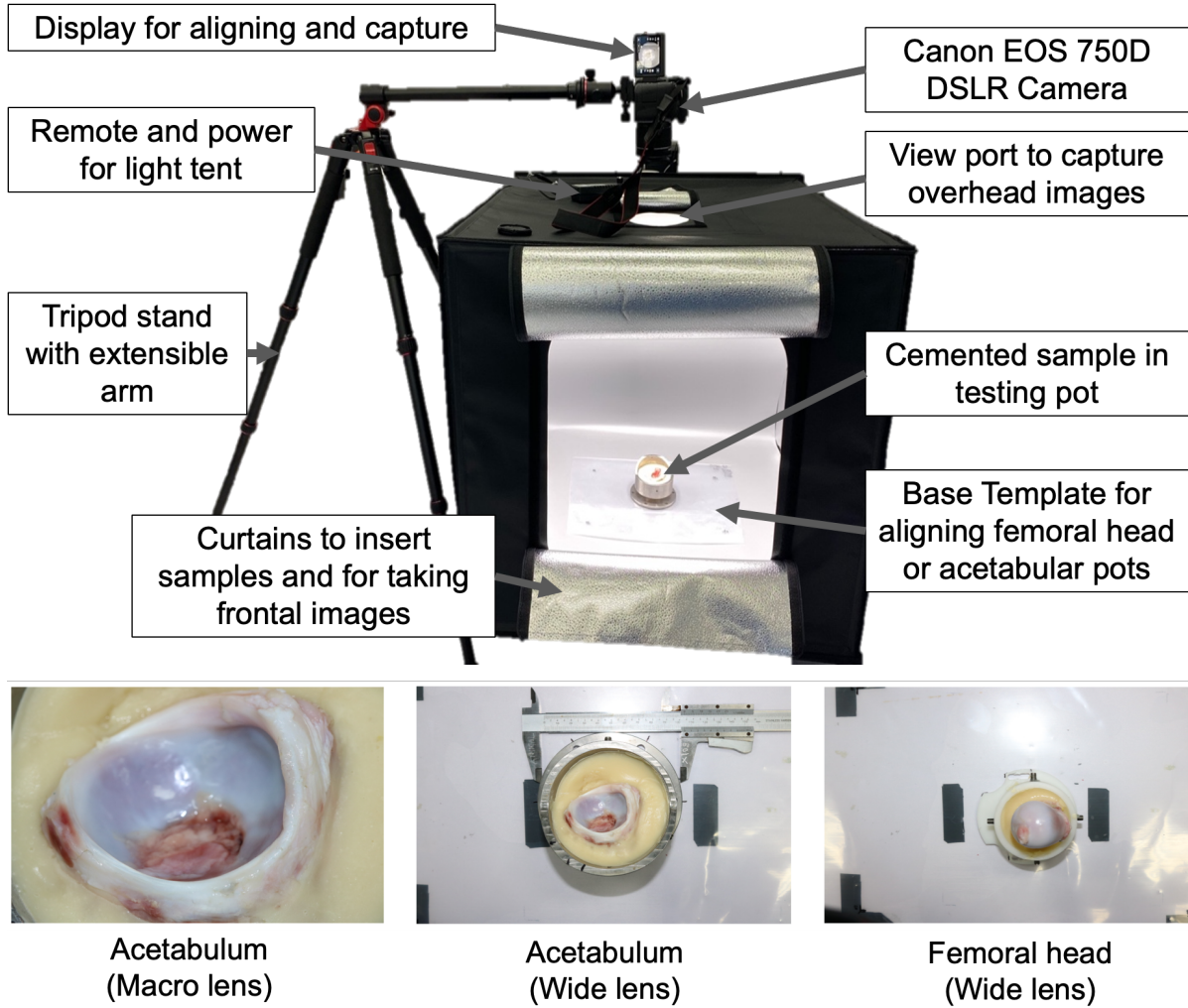


Figure 3.4 – Photogrammetry Set-up: a light tent used with acetate templates to position acetabular and femoral components. Wide and macro lenses were used with a digital camera to capture surface details of porcine acetabulum and femoral head at different stages of simulation.

3.2 4 Simulation equipment

Table 3.3 Table of the simulation equipment, consumables and simulator components required for mounting and running an experimental hip simulation.

Simulator Components	Consumables	Equipment
Cemented acetabulum in acetabular pot	Clear Plastic sheet	Acetate templates for femoral/acetabular base
Cemented porcine femur in femoral pot	Nitril gloves and PPE	Tissue forceps
Delrin	PBS (phosphate buffered saline)	Funnel with pipe attachment
Femoral/Acetabular Base components	FBS/Lubricant 1l	Gaiter
PBS (phosphate buffered saline)		Hex keys
Ringers Solution 1l		Jubilee clips
Tape		
Tissue forceps		
Waste bucket		

3.3 Methods

3.3.1 Joint dissection(Pallan, 2016)

The hip joints were harvested from skeletally immature porcine right hind legs following slaughter at a local abattoir (JPenny, Rawdon, Leeds). The legs were typically 24 to 26 weeks old at the time of slaughter, and the average weight of the whole animal was roughly 80 kg, with the right leg typically weighing between 12-15kg. The porcine leg was dissected as described in Chapter 2. Initially, the weight of the whole pig found on an attached tag was recorded and used for specimen identification. The leg was then dissected under non-sterile conditions using a large size 5 scalpel holder with a 22A shape blade for larger and deeper cuts and a small size 3 scalpel holder with an 11-shape blade for more precise and sharper cuts. The hip joint was felt for and marked. Bulk tissue was excised from around the hip joint, such as the superficial soft tissue e.g., skin, muscle, fat, and tendons. Once the proximal aspect of the femur and pelvic bones could be seen, the deep muscle and soft tissue were

carefully removed to reveal the synovial joint capsule. At this stage part of the capsule was kept sealed. At the same time, small excisions to the femoral side were made to remove the capsular ligaments (iliofemoral, ischiofemoral and pubofemoral) from around the joint.

On immature porcine femurs, there was dense fibrous tissue between the growth plate and the greater trochanter which had to be removed to enable the joint to be distracted properly before separation of the head from the acetabulum. The joint capsule was opened, and fibrous tissue attached to the labrum and articular margin of the femoral head was carefully removed, leaving the femur attached to the acetabulum via the ligamentum teres, which is attached from the acetabular fossa to the fovea capitis on the femoral head. Extra care was taken at this stage to avoid any cuts or damage to the articular surfaces or labrum tissue which may impact the latter stages of experimentation. Phosphate Buffered Saline (PBS) was used during tissue storage to maintain articular cartilage hydration during dissection, cementing and before testing. One PBS tablet (MP Biomedicals, United States) was dissolved per every 100 ml sterile water. Once separated, the surfaces were covered in PBS-soaked tissue for hydration. The tissue was then stored in a fridge or frozen until needed for further testing.

3.3.2 Potting and Alignment

Prior to potting, the pelvis was separated from the rest of the leg where any residual soft tissue around the acetabulum had been excised. Any excess pelvic bone (ischium, ilium, and pubis) was removed (Figure 3.5) by clamping the ilium and pubis bones and removing the excess pelvic bone surrounding the acetabulum using a handheld hacksaw or electric saw. Finally, the articular surface, transverse acetabular ligament, and intra-articular fat pad were inspected to ensure they were not damaged and intact before cementing.

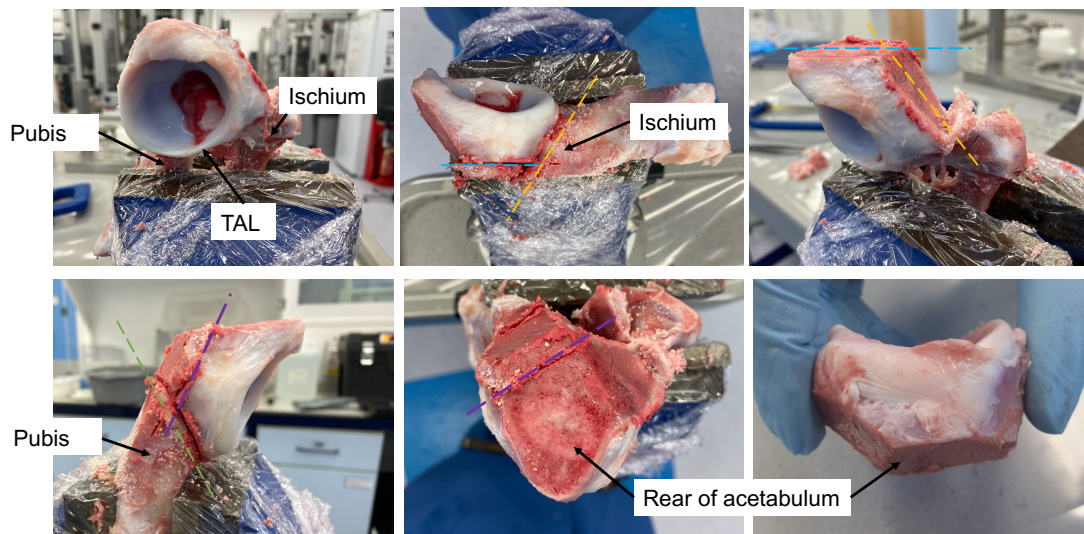


Figure 3.5 Cuts made to reduce features around the acetabulum to fit the acetabular pot. The acetabulum was separated by making four cuts along the pubis and ischium bones of the pelvis. The yellow and blue lines represent cuts along the ischium while the green line represents the cut made along the pubis. The purple line was made along the base of the acetabulum and coincident with where the abattoir cuts the limb. This feature was reduced to allow more control when positioning the acetabulum during cementing.

Similarly, to allow the femur to be used with the femoral head pot developed by Groves et al. (2015), the femur was also excised as described in Chapter 2 (Figure 2.4). The main feature necessary for removal for use with the hip simulator was the excess growth plate and greater trochanter (Figure 3.6) which would impinge with the cement, acetabulum, and acetabular pot during testing.

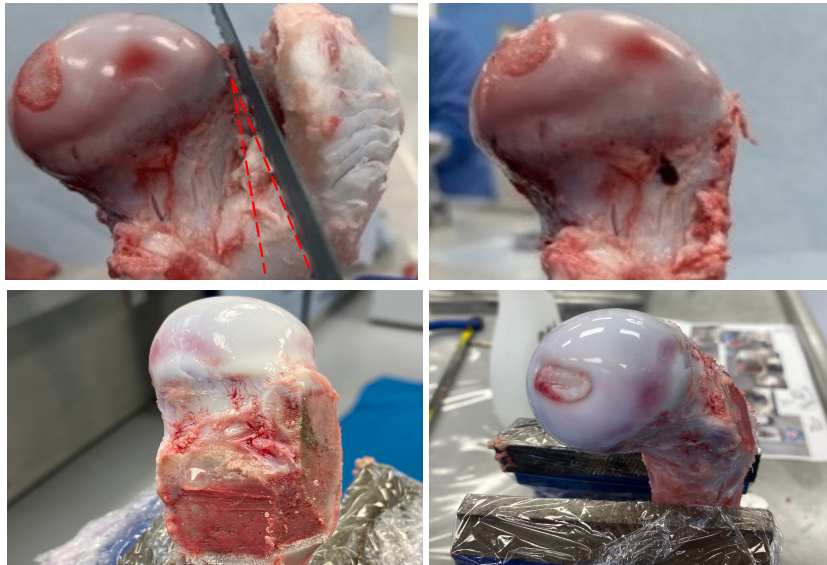


Figure 3.6 – Left - Cuts made on porcine femur to remove the attached growth plate. The length of the femur was also shortened. This allowed the femoral head to fit the femoral head pot required to fit the dimensions of the simulator to prevent impingement

Before cementing into acetabular and femoral pots, the size of the natural femoral head and acetabulum diameters were measured. The main diameter required for simulation was the femoral head diameter. This was measured and matched using templates initially used for standard sizes of CoCr head prosthesis (Figure 3.7). The centre of the head was kept parallel to the epiphyseal line, where a tear drop like marker was used to ensure consistency in taking head diameters across samples. This marker was used to align the femur with the centre of the transverse acetabular ligament and was apparent through all the dissections of porcine right hind limbs. The site was also where the epiphyseal line aligned with attachment site of the joint capsule. The diameter of the acetabulum was measured using a vernier calliper taking the measurement at the interior edge of the labrum which was aligned horizontally and parallel to the inferior TAL. This was recorded and checked with the femoral head diameter to assess how well the femoral head and acetabulum matched as there were occasions where the acetabulum was dissected and had deformities resulting in a mismatched pair which could introduce damage during testing.

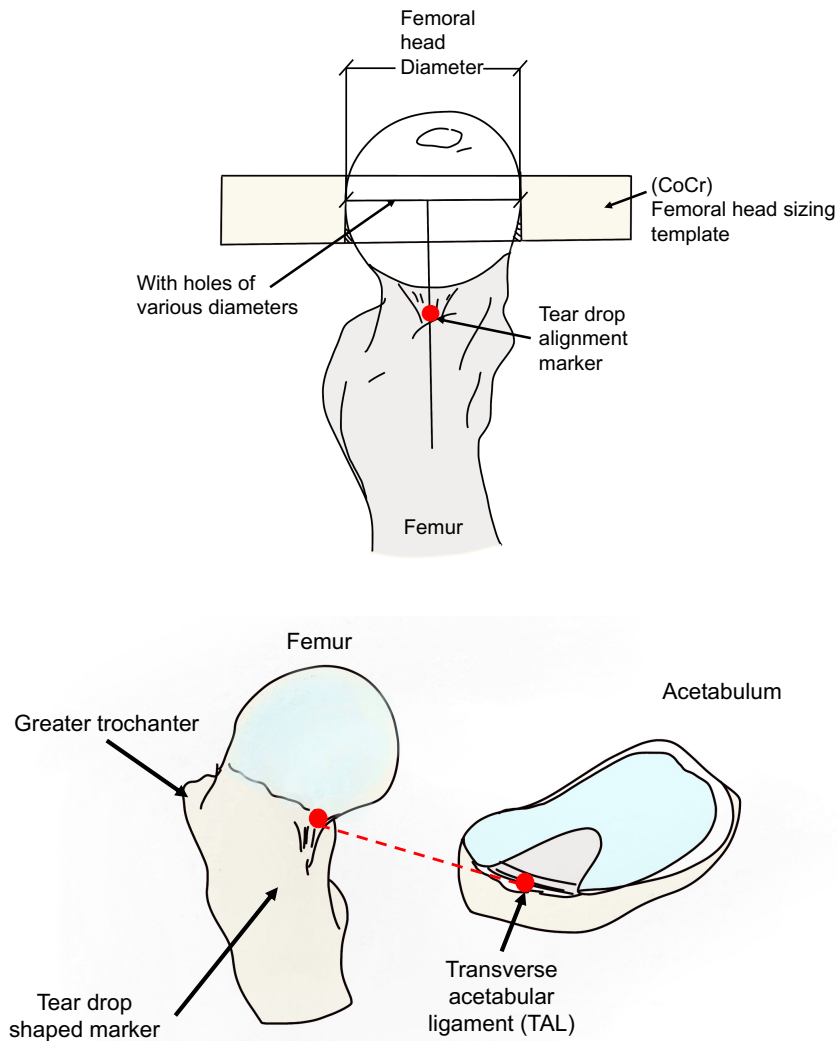


Figure 3.7 Schematic showing how the femur was placed in sizing template (top). The femur was placed into different diameter holes in the template to get a good match with the spherical diameter the simulator was designed to be used with. The epiphyseal line of the femoral head and the tear drop shaped marker (bottom) found above the lesser trochanter were used to align the head parallel with the template. This tear drop shaped marker was found in nearly all porcine femurs and was coincident with the centre of the TAL of the acetabulum which made it useful for setting appropriate alignment of the natural joint.

Once the diameters were found, a CoCr femoral head was positioned with an inverted acetabular pot to maintain an equal centre of rotation between the simulator and the pots (68.24mm) as following the method described by (Groves, Fisher and Williams, 2017). The samples were covered with PBS-soaked tissue until needed.

Potting of the acetabulum required the acetabulum to be cemented in an anatomically inverted position using PMMA bone cement. The potting process was the same as when initially developed for the hemiarthroplasty potting model used in the pendulum simulator by Groves, (2016). The only difference was the inclusion of extra base plate adaptations developed by Pallan (2016), to fit with the single station hip simulator. For alignment of the acetabulum, the acetabular version was placed at 30° angle between the sagittal plane and the diametric line which passes through the centre of the TAL. The inclination angle was set at 35° between the acetabular rim and transverse plane.

Once the femoral head had been clamped in the correct position, it was held within the natural acetabulum and cemented in position. The position and orientation can be set at this stage and checked using an inclinometer. Once hardened, a jig developed to control and fix the precise orientation and positioning of the natural femoral head was used to mount onto the cemented acetabulum. At this stage, the femoral head would be positioned differently based on what condition was being tested. Once the position was selected, the femoral head would be inverted and placed into the femoral pot. A femoral head potting jig was used to set the centre of rotation of the femoral head. The cement could then be added with the holding jigs still in place. Once hardened, the jigs could then be removed. The articular surface and soft tissue of the potted acetabulum and femur were then wrapped with PBS-soaked tissue until mounting on the simulator.

3.3.3 Cementing

Non-sterile polymethyl-methacrylate (PMMA) bone cement is often used in orthopaedic procedures to aid in the fixation of artificial prostheses. The cement used for tests was formed using a 2:1 powder to liquid component ratio according to the manufacturer's instructions using cold cure powder (WHW Plastics, UK) and liquid monomer (Rapid Repair Liquid). The polymerisation was highly exothermic (Haas, Brauer and Dickson, 1975). Therefore, PBS-soaked tissue was used to reduce the risk of tissue damage caused by the temperature rise to the articular cartilage and labrum during the hardening of the cement.

Approximately 70g of powder was required for the cup while approximately 60g was required for the femoral pot. When potting with cement, the consistency would affect the pliability and the rate it will set. For the acetabulum, a thicker more viscous consistency was required as the acetabulum has no supporting fixtures to ensure correct positioning. For the femoral head, a loose runny consistency was required to allow pouring into the pot while avoiding the jig holding the femur.

3.3.4 Choice of peak loading for use with porcine hip joint

A porcine loading cycle was followed which was based upon an adaptation of the ISO standard 14242-1 (BSI, 2014) developed for THR wear testing however, it dictates the abduction-adduction, flexion-extension, and internal-external rotation motion with simultaneous axial loading during human gait. Following a study which measured joint reaction forces going through a porcine hip, it was estimated that a load of 900N and a peak moment of 24Nm for an average 6-month-old pig weighing 80kg (Thorup, Laursen and Jensen, 2008; Lizhang, 2010). In the cycle, the flexion/extension scaled down by 20%, abduction/adduction scaled up by 20% and the load was scaled down by 70% to match porcine neutral motion.

3.4 Preliminary studies for method development.

This section describes the preliminary studies replicating a whole natural hip simulation method to optimise methods and select criteria of conditions for generating damage.

An initial experimental design was created for generating chondrolabral damage, initially to create labral tearing at the anterior-superior quadrant of the acetabulum. By considering the mechanical factors involved in FAI, specifically, isolating the parameters involved in cam and pincer type impingement (Figure 3.8). Unloaded porcine tissue would be compared to the ISO standard loading and then applying the following changes based on the type of damage.

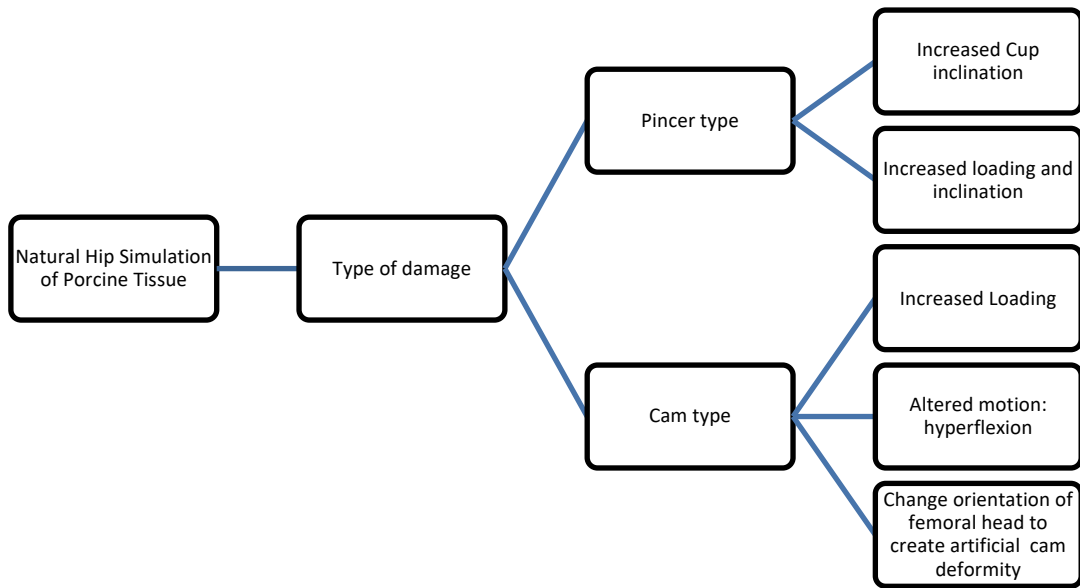


Figure 3.8 Flow chart showing the mechanical changes required to achieve damage associated with pincer and cam type impingement.

By replicating the methods described by Pallan (2016) for the generation of labral damage, it was clear that simulation would be difficult without making considerable changes to the methodology before it could be applied for more extreme loading scenarios. Initial testing using the ISO 14242 loading profile resulted in tests which were unsuccessful due to sample dislocation or extreme damage where the progression of damage could not effectively be captured. A summary of the issues found during testing are provided in Table 3.4, where the testing conditions are reported, and the subsequent changes are highlighted to optimise the methods for allowing a more controlled testing environment.

Table 3.4 Table of the issues which were addressed through experimentation.

Issue	Description	Testing conditions	Mitigation	Implementation
Pot Impingement	Vibrations during tests, and dislocations resulting in failed tests. Uncontrolled and unpredictable loading of tissue, cemented cups would loosen from holder	1 Hz, 7200 cycles, FE, IE, AA, FBS 20% Lubricant, ISO 14242 profile	Alter pot design, remove sharp edges which impinged during deep flexion.	New pots were created with altered dimensions which prevented pot contact and unwanted component engagement.
ISO loading	High loads applied on non-congruent samples resulted in dislocation. High peak axial loads resulted in damage therefore a control was hard to establish.	1 Hz, 7200 cycles, Peak 1500N, FE, IE, AA, FBS 20% Lubricant ISO 14242 profile	Determine physiologically relevant loading for porcine tissue and reduce testing parameters. Reject mismatched joint pairs.	A physiologically scaled loading profile was created as a control from which loads, or motions could be altered to create different severities of damage.
Acetabular orientation leading to dislocation	Steep angles >55° resulted in dislocation as the femoral head would slide out of the cup	1 Hz, 7200 cycles, FE, IE, AA, FBS 20% Lubricant ISO 14242 profile	Understanding the constraints of the simulator.	Other factors for generating damage were explored first before revisiting cup orientation.
Lack of defined sawing methodology and clear indications of sample size which could be potted.	Cutting too much of the acetabular mantle led to bone cement leaking into the joint space resulting in cement on cartilage damage	1 Hz, 7200 cycles, FE, IE, AA, FBS 20% Lubricant ISO 14242 profile	Improved sawing protocol to ensure enough bone is retained from acetabulum.	
Control over alignment during cementation	Lack of fine control of holding acetabular cups in the holder resulted in spillage of cement, cement debris an	1 Hz, 7200 cycles, FE, IE, AA, FBS 20% Lubricant, ISO 14242 profile	Cementing protocol was carefully reconsidered and pots were redesigned to allow more space.	Inclusion of holes for spokes in the redesigned acetabular pots reduced the errors in positioning and holding acetabulae during cementation

There were several issues when using the previous pot designed for the pendulum simulator in the single station simulator (Figure 3.9). This was due to the change in working space available in the single station simulator where pot impingement would occur during extension and rotation during testing, causing undesirable contact between components which could impact the study. This was resolved with a new potting design (Figure 3.10) which prevented pot impingement and allowed for consistent and improved cementing. In addition, the use of polymer spokes allowed the acetabulum to be held in position securely before cement was poured.

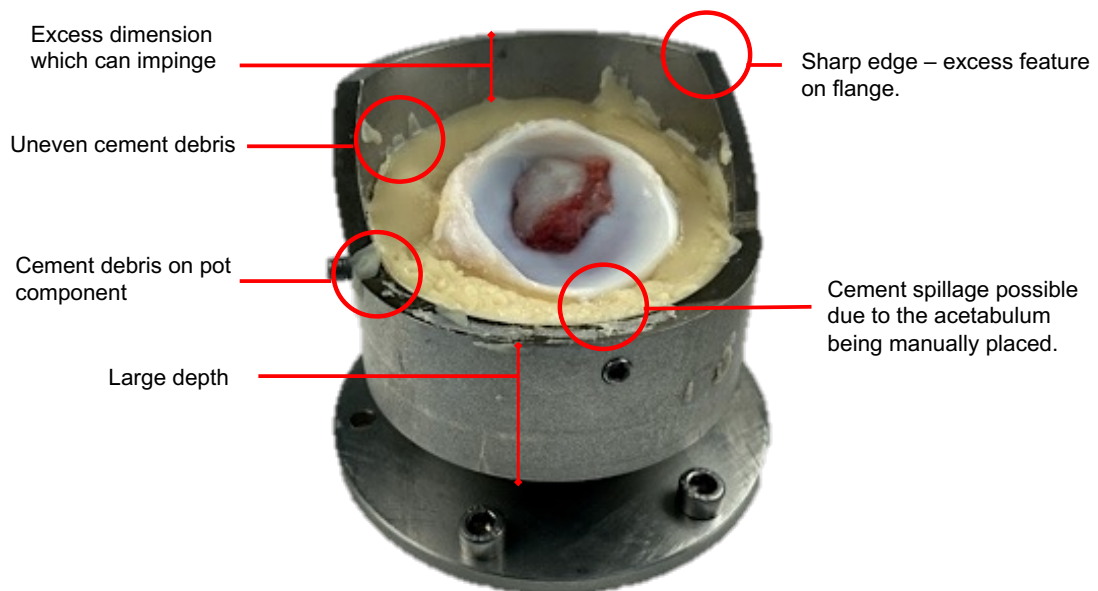


Figure 3.9 Issues with the previous pot used by Pallan (2016). The pot had a large flange which would impinge with the femoral pot due to its vertical height. Additionally, the deep pot would result in uneven cement pouring with some reaching the labrum and producing tiny cement debris which would impact the tests.

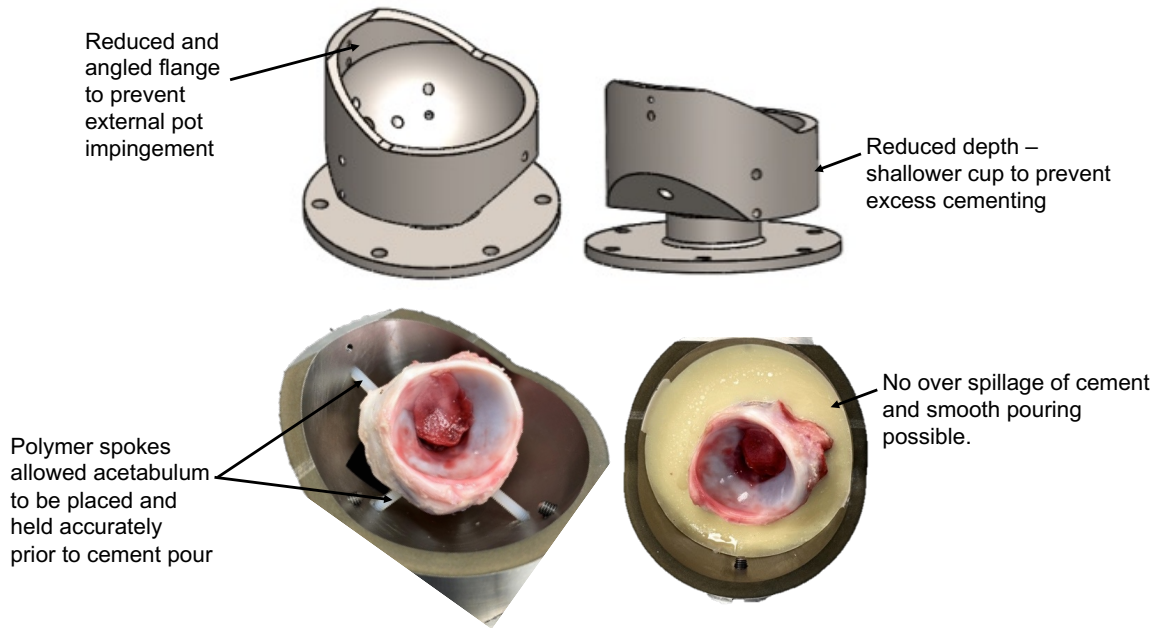


Figure 3.10 Updated acetabular pot had a lower lessened flange (top left) and a reduced vertical height (top right) to prevent contact with the femoral component. Additionally new threaded holes were included to allow polymer wires to be used to hold the acetabulum in place (bottom left) ensuring more even and consistent pouring (bottom right) preventing spillage onto the acetabular labrum.

Next, tests were redone to ensure that sample testing failure was minimised by applying the changes on the same condition, leading to the development of a standardised natural hip protocol suitable for porcine tissue for the assessment of joints. Subsequent tests reduced the failure of tested samples, however, there were still some optimisations to be made for preventing failures and dislocation during testing when applying extreme loading conditions and abnormal motions on porcine joints. Additionally, to evaluate the damage generated and evaluate the progression of damage in tissue, considerations had to be made for testing duration, stopping, and starting protocols and how to best evaluate the tissue after applying altered loading conditions. These investigations are summarised in Table 3.5.

Table 3.5 Table of the main considerations found through testing

Issue	Description	Testing conditions	Comments
Sample Selection	Variability of samples resulted in dislocations resulting in failed tests where abnormal acetabular morphologies would result in femoral head dislocation	Overloading, Scaled Porcine loading profiles, 1Hz, 14400 cycles, FE, AA, IE	The shape of the femur and acetabulum was important feature which could be used for creating damage. A matched pair where the relative diameters were similar (less than 1.5 mm difference) resulted in a reduction in failure of tests. Variability of acetabular depth was harder to control. Tests were inconclusive in terms of how acetabular depth affected potential to be damaged.
Test duration	Tested tissue for longer duration tests	Overloaded Porcine loading profiles, 1Hz, 0-28800 cycles, FE, AA, IE	It was found that after 28800 there was no noticeable changes to tissue macroscopic appearance, but tissue had deteriorated in quality. 14400 cycles were chosen as the maximum duration for tests and to allow comparison with Pallan, 2016.
Centre of rotation Alignment	Improper centre of rotation and alignment resulted in unnatural engagement of joint components.	Overloading, Scaled Porcine loading profiles, 1Hz, 14400 cycles, FE, AA, IE	Lack of engagement between femoral head with the cup, where damage should have occurred led to an examination of the components used in the hip simulator, Base plate was Off by 2mm
Cement and bony debris during tests	Cement debris and bony debris from the potting and cementation was evident at 7200 cycles, this may have introduced additional damage resulting from fine scratches during testing.	Overloading, Scaled Porcine loading profiles, 1Hz, 14400 cycles, FE, AA, IE	Prior to mounting, femoral head and acetabular components were placed in a PBS bath with a shaker to sediment any excess bony debris prior to testing.

3.4 Experimental Study: Assessment of the Natural Hip Simulation Methodology

The following section shows the final methodology used in later chapters in the form of a pilot study. The pilot study served as the control for future simulations by assessing the surface features and appearance of the articular cartilage and acetabulum labrum on a scaled porcine loading to resemble the physiological loads experienced by a porcine hip joint but modelled with human gait profile. This test aimed to assess if the simulation would introduce damage to the tissue during a normal walking cycle for a four-hour testing duration.

3.4.1 Study Design

A preliminary study was designed to simulate full loading and motion cycles to replicate physiological loading onto the porcine hip joint to act as a control for subsequent work altering the dynamic motion, axial force, orientation or positioning of the components could influence abnormal loading patterns replicating the biomechanical situation experienced in conditions like FAI.

3.4.2 Method

3.4.2.1 Joint dissection

To prepare porcine hip samples for simulation using the single station hip simulator, three immature porcine right hind limbs were dissected, where surrounding musculature, fatty tissue and ligaments were removed from the joint, excluding the transverse acetabular ligament. The joint was disarticulated by removing the ligamentum teres, leaving the femoral head and acetabulum with the pelvic bone. Samples with signs of previous articular cartilage damage or labral tears were excluded from the study. To fit the constraints of the loading area in the simulator, the femur was reduced to approximately 85mm from the femoral head using a hack saw. Additionally, excess surrounding bone, such as the growth plate was excised to resemble the natural shape of a human femur and to prevent abutment from the reduced head neck junction found in immature porcine femurs. Pelvic bone was removed from the acetabulum with approximately 40mm subchondral bone underneath. Excess fibrous capsular tissue was removed from the superior portion of the labrum and from the neck of the femur. Specimens

were then wrapped and stored in tissue soaked in phosphate buffered saline (PBS) solution and stored at -20°C until the day of testing.

3.4.2.2 Joint preparation and potting

Each joint was prepared for simulation by aligning and cementing based on anatomical markers found on the femoral head near the greater trochanter and the transverse acetabular ligament found on the acetabulum. The orientation of the acetabulum was positioned to match human orientation of 45°. The joint was held in place using a custom fixture and aligned such that the centre of rotation of the joint (at the femoral head centre) matched the centre of rotation of the simulator. The maximum vertical height of the test cell was 200mm and the centre of rotation was 120 mm up from the base of the test cell. Potting of the acetabulum requires the acetabulum to be cemented in an anatomically inverted position using non-sterile polymethylmethacrylate (PMMA) bone cement, which is often used in orthopaedic procedures to aid in the fixation of artificial prostheses. The cement was formed using a 2:1 powder to liquid component ratio according to the manufacturer's instructions using cold cure powder (WHW Plastics, UK) and liquid monomer (Rapid Repair Liquid) The potting process was the same as initially developed for hemiarthroplasty potting model used in the pendulum simulator by Groves (2015). An additional base plate adaptation was required and was developed by Pallan (2016), to fit the single station hip simulator.

3.4.2.3 Hip simulator and programming inputs

The Leeds single station hip simulator has the control over flexion-extension, abduction-adduction, internal-external rotation, axial load and medial-lateral displacement and anterior-posterior displacement (Figure 3.11). All axes of the single station simulator are driven by electromechanical actuators. The simulator allows for load and displacement control with a programmable range of up to ± 5 mm and ± 1 kN.

The medial-lateral displacement was set to neutral (0mm) from the centre of rotation. The simulator was programmed to follow an average walking cycle (Figure 3.12) at 1Hz as defined in the ISO-14242 standard. It was adapted to suit the porcine tissue by reducing the maximum load to account for differences in loading capacity. The loading profile was set to a scaled ISO

14242-2 profile which provides a general human gait cycle used in wear testing for hip joint replacement and was scaled to match physiological loads experienced by porcine hips.

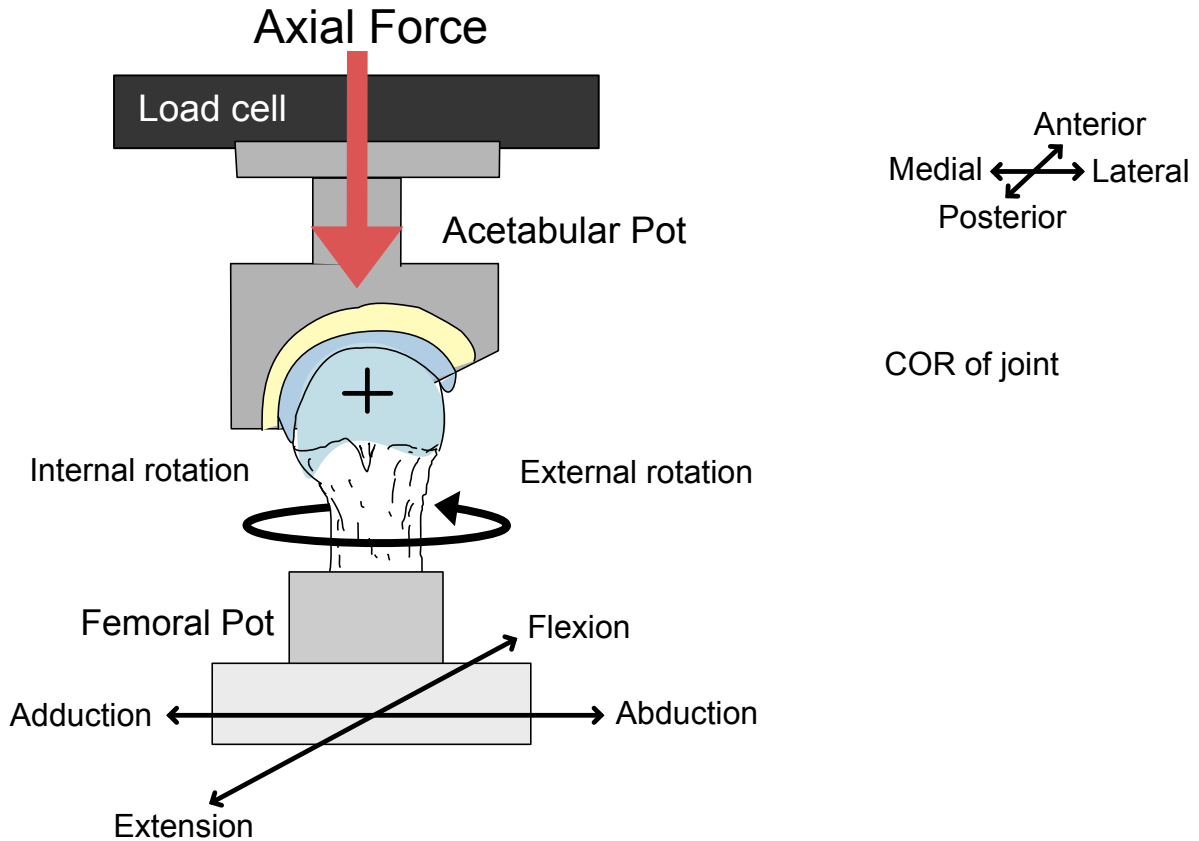


Figure 3.11 Single station hip simulator showing mounted natural porcine hip. The simulator uses a 6-axis load cell which can be used to apply ISO standard walking cycles or custom profiles. The walking cycle is applied using a demand wave cycle and can be monitored using a feedback wave cycle. The acetabular cup is mounted under the load cell while the femoral head is set on a cradle capable of moving in the simulator's three degrees of motion (FE, AA and IE).

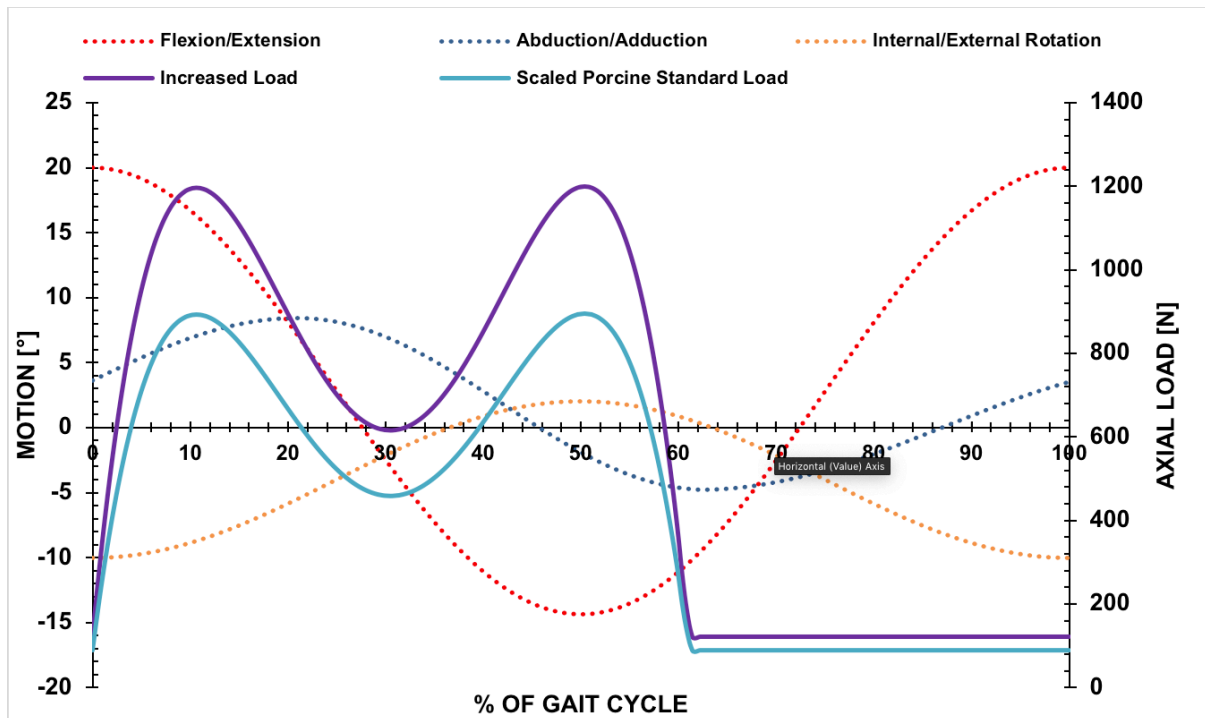


Figure 3.12 Simulator loading and motion input profiles used to simulate a standard walking cycle based on average human gait as per the ISO 14242-2 standard for wear testing and tribology of THR. Axial load was scaled down by 70% to match the typical load undertaken by a porcine hip joint during a walking cycle. The total load was increased to a maximum of 1200N for an equivalent representation of loading experienced by an overweight porcine hip. In both testing scenarios, human motion inputs were used for flexion-extension, abduction-adduction and internal-external rotation as the porcine geometry was used to represent human range of motion.

3.4.2.4 Simulation

Prior to simulation, the simulator load cell and the motors were calibrated using a dummy joint used for standard ISO-14242 specifications to ensure accuracy for the natural hip simulation. Next, the cemented porcine joint was mounted with the load cell driven at the acetabular cup and the femoral head being at the base of the simulator. The whole joint was sealed using a gaiter and was filled with Ringer's solution. Ringer's solution was used as the lubricant in place of synovial fluid to provide a consistent fluid environment during experiments. Each joint was mounted onto the simulator and tested for a total of 14400 cycles (4 hours). The simulation was paused at 7200 cycles (2 hours) to assess the tissue for changes and to replace the lubricating fluid. The simulation was then restarted and run for the remaining 7200 cycles. Photogrammetry was used to capture images of the tissue before, at 2 hours and at the end of the testing.

3.4.2.5 Photogrammetry and assessment of samples

All samples were assessed and graded using photogrammetry to measure the changes in condition of the acetabular labrum and the cartilage surface of the acetabulum and femur in a consistent manner using a Canon 250D camera with a wide and telephoto macro lens to cover the surfaces of the cartilage and labrum of the femur and acetabulum. Tissue appearance and damage was assessed based on visual changes to the tissue as described by literature using features characterising labral and chondral damage. A damage scale was created based on Czerny's classification of labral injuries (Czerny *et al.*, 1996) and the multicentre arthroscopy of the hip outcomes research network (MAHORN) classification of labral tears (El-Radi *et al.*, 2018):

Table 3.6 Grading system for visual characterisation of chondro-labral damage.

Grade	Description
I	Labrum is intact, with continuous attachment to articular cartilage. Surfaces are untouched.
II	Labrum surface or articular surface is bruised or scratched. Labrum is intact, with continuous attachment to the articular cartilage.
IIIA	Labrum surface or articular surface is bruised or scratched. Some separation at the chondro-labral junction (fine tearing).
IIIB	Labrum surface or articular surface is bruised or scratched. Distinct separation at the chondro-labral junction. Medium sized tears.
IIIC	Delamination of articular cartilage. Wave/crimping can be observed. Labral tearing.
IV	Detachment of labrum from articular cartilage and subchondral bone. Wave/crimping can be observed. Articular cartilage is delaminating.

3.4.3 Results

Three porcine hips were simulated under standard and increased loading conditions for a total of 14400 cycles where the simulation was paused to assess tissue for changes at 7200 cycles. The motion was defined as per the ISO-14242 human walking cycle with the peak loads being 900N and 1200N respectively. Photogrammetry was used to assess the nature of tissue before, after 2 hours and upon completion and recorded as per the grading scale (Table 3.7). Samples were generally similar in geometry however there was some natural variance between samples obtained as part of the food chain, with the average size of samples being between 36.5 mm. The tissue sourced was still developing and so their small differences in the shape of the femurs and the acetabulum as the femur was more rounded in some cases and the acetabulum asymmetric.

Table 3.7 Visual assessment of chondro-labral damage in simulated samples.

Sample	Weight (Kg)	Acetabular diameter (mm)	Femoral head diameter (mm)	Damage at 0 cycles	Damage at 7200 cycles	Damage at 14400 cycles
1 - Control	78.4	35.0	35.0	Grade I	Grade I	Grade I
2 - Control	97.2	38.5	37.5	Grade I	Grade I	Grade I
3 - Control	67.0	36.0	36.0	Grade I	Grade I	Grade I

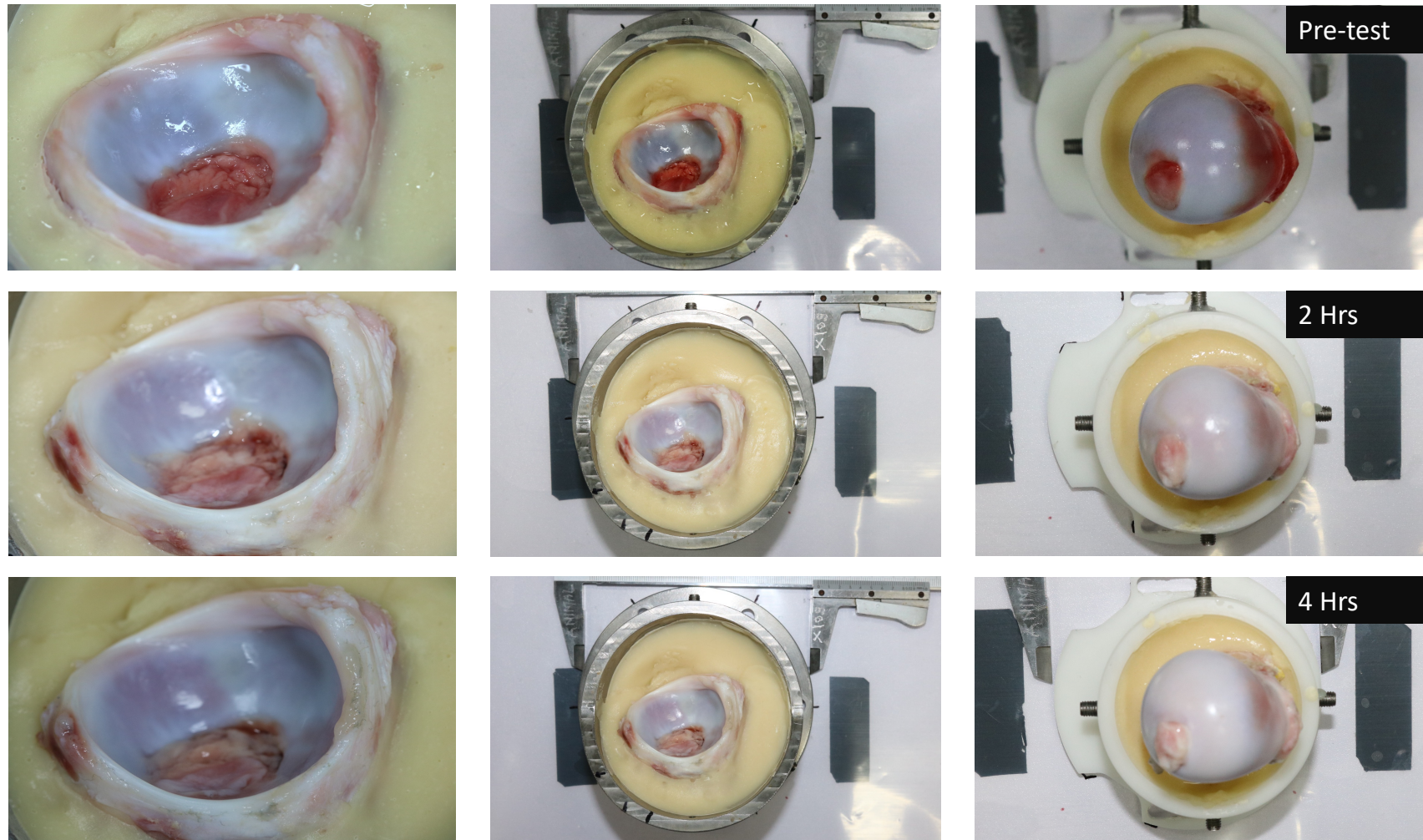


Figure 3.13 Photogrammetry of control samples which were simulated under standard loading (peak axial loading of 900N), with motion set to human walking cycle from ISO 14242 standard with Ringer's solution as lubricant. The telephoto image of the acetabulum (left), the whole acetabular pot (center) and the wide image of the femoral head surface (right) prior to testing, after 2 hours, and after 4 hours.

3.4.5 Discussion

The study aimed to develop the existing natural whole joint testing method initially used by Groves and Pallan (2016), to create a suitable existing experimental simulation model for generating chondrolabral damage using a hip joint simulator. The present study outlines a methodology that involves the development of a protocol for accurately and reproducibly setting up the natural hip in a simulator, while accounting for sample variations. The present pilot study was able to demonstrate no significant changes to the surface (Figure 3.13) after being simulated for 14400 cycles, with 45° inclination, ISO1424-2 input gait profile and ringers' solution. There were minor changes to the appearance of the acetabulum and femoral head, which included increased surface texture roughness at the articular cartilage (Figure 3.13) and very slight blushing after 4 hours.

To successfully create an in vitro whole natural joint testing model capable of simulating complex and abnormal mechanical loading environments, it was necessary to maintain the stability which gives the hip joint its unique characteristics (Crawford et al., 2007; Boykin et al., 2011; Kraeutler et al., 2016; Singleton and Leveau, no date). To assess changes caused by FAI or dysplasia and to generate damage, which is clinically relevant, several thousands of repeated abnormal loading cycles would need to be conducted while preventing unwanted dislocation or failure due to cement breaking or bone fracture during experimentation.

A limitation of the testing conducted by Pallan (2016) was the inclusion of multiple factors which influence damage but also instability which could result in damage or a failed test where the femoral head could dislocate. Cup inclination angle, ML displacement and load applied were investigated to generate chondrolabral damage using the electromechanical single station hip simulator. However, this was done before optimising the testing method and materials. The joint fixtures and pots were designed for use in the pendulum friction simulator to measure joint tribology and friction in hemiarthroplasty models adapted from Lizhang et al., (2013) and Groves, Fisher and Williams, (2017), not for whole natural joint testing under extreme testing conditions.

That is why initial tests were completed in this study to first optimise the standard testing model before progressing to more complex damage environments. This is because maintaining joint stability over the total duration of the simulation was important to prevent dislocation or unwanted movement such as the femoral head translating out of the acetabulum during tests. This could either impact the results due to introduced impingement or result in fracture of the femoral head as it abuts against bone cement or the metal pot housing the acetabulum.

By replicating previous methods of Pallan (2016), failures were experienced during testing of porcine tissue (Table 3.4), primarily the impingement of pots which held the acetabulum and femur and dislocation or fractures of the femur caused by inconsistent cementing methodology. Pallan (2016) reported several failures mainly specimens failing due to cement particles or debris being trapped between the articulating surfaces, resulting in artificial damage to the cartilage surfaces. It was also surprising that at reduced peak loads of 750° and an acetabular cup inclination angle of 45° where no damage to either the articular cartilage or labrum would be expected. However, there was still a failure reported due to cement being trapped during the test, suggesting there was issues with the methodology or specimen dislocation (Pallan, 2016).

Further studies were conducted to test the methodology with implemented improvements to the mounting equipment, cementing and photogrammetry methodology (Table 3.4). The most significant changes being the mounting pots which held the acetabulum samples and the improvements to the design to allow for more consistent cementation and prevent the generation of cement or bony debris during simulation.

The developments to fixtures allowed the centre of rotation (COR) of the natural hip joints to align with the COR of the simulator. Despite the disarticulation and removal of the greater trochanter during sample preparation, the joint maintained stability and dislocations were not experienced after making the changes described in Table 3.4

Finally, pilot studies were conducted to assess which mechanical parameters can be implemented using the single station hip simulator to generate clinically relevant forms of damage (Table 3.5). The shape of the femur and acetabulum was important feature which

could be used for creating damage. A matched pair where the relative diameters were similar (less than 1.5 mm difference) resulted in a reduction in failure of tests. Variability of acetabular depth was harder to control. Tests were inconclusive in terms of how acetabular depth affected damage to the tissue. Tauvqirrahman et al.,(2023) reported that changes to the size and diameter of joint components could impact the contact pressures experienced, where the use of a larger diameter femoral head within an acetabular cup oriented at 45° inclination would have the least contact pressure in a 3D model of dual mobility hip joint tested under simulated gait cycles.

It was found that after 28800 cycles there was no noticeable changes to tissue macroscopic appearance, but tissue had deteriorated in general quality. To date, this is the longest tested duration in vitro in a whole native joint simulator. Many tests were limited to a few 100 cycles (Macirowski, 1994; Koh and Gupta, 2017) to a few hours of testing (Ferguson et al., 2003; Groves, Fisher and Williams, 2017) the longest previous test was 10800 cycles (Pallan, 2016). Overall, 14400 cycles were chosen as the maximum duration for tests and to allow comparison with Pallan (2016), and because the proposed experimental testing methodology was to be used as a pre-clinical testing model for assessing interventions in the future, and so there should be a buffer to allow for retesting of samples without degrading tissue quality.

Lack of engagement between femoral head with the cup, where damage should have occurred led to an examination of the components used in the hip simulator, Base plate was Off by 2mm. This may explain the erroneous medial-lateral displacement experienced in physiologically scaled loading by Pallan (2016). The displacement may have resulted in vibrations or breakage of cement, resulting in wear and damage to the articular surfaces. Wear is a common reason for failure of artificial hip replacements (Dowson and Jobbins, 1988; Hodaei, Farhang and Maani, 2014; Viitala and Saikko, 2020). Hips which appeared aligned may have a slight misalignment which could impact the stresses experienced in the hip joints during testing. A study by Lizhang et al., (2013) identified that an increased clearance of 1 mm approximately doubled the contact stresses within a hemiarthroplasty model.

The photogrammetry method captured the different stages of the simulation process at an acceptable resolution, was framed consistently at the same height and distance and could show fine surface texture and details with the telephoto and macroscopic images. Under scaled physiological loads for porcine hips, the tissue appeared relatively unaffected by testing (Figure 3.13), and changes observed were generally due to differences in the lighting conditions and hydration of tissue as it was removed before or after testing. As the photogrammetry method was being developed, there were some differences in the exposure and focus of the labrum, however, with the wide frame, the cartilage and labrum remained completely intact, with no obvious scratches or signs of damage which may have occurred due to the simulation. Inspection with the macroscopic lens also revealed negligible scratches or surface damage. After 4 hours, the tissue was dull and had lost some of the blood and loose tissue that can be seen before the simulation. A limitation of the pre-test images was the reduced exposure presenting features, however, the surface characteristics remained noticeable.

Several damage scales, based on clinical findings and most applicable to MR arthroscopy and clinical examinations (Czerny *et al.*, 1996; Martin *et al.*, 2006; Kaya, 2014; A. E. Li *et al.*, 2016). OARSI grading scale is more relevant but is designed for histological evaluation of cartilage pathology (Pritzker *et al.*, 2006). Pallan (2016) used the Outerbridge scale of classification (Slattery and Kweon, 2018) for qualitatively assessing the acetabulum and labrum features after experimental joint testing, however this scale typically applies to grading of cartilage. The grading system used in the present methodology is more suited to in vitro experimental simulation it has adapted multiple grading and scoring systems which reflect that the tissue being graded is not as the in vivo condition, it is not radiographically imaged, and it is sensitive enough to differentiate between grades, incorporating the labral and cartilage pathologies which apply to surface characterisation of the tissue.

Despite the effectiveness of grading systems in discerning significant stages and categories of damage, their inherent limitations arise from the subjectivity of the grader responsible for analysing the damage. The assigned grades may exhibit variations among graders, especially

when the extent of damage approaches the boundary between two criteria, even in cases where prior training has been conducted.

A limitation of the damage presented in each image was the grading of porcine samples, as there may have been potential bias introduced as it was known at the time what loading condition, duration of test and the other inputs hence, there may have been bias towards grading the tissue to fulfil the intended type of test. For example, the tissue features being graded in this study was not expected to have any damage as it was a control.

Although all data was analysed as objectively as possible, variations in interpretation and grading can exist, as experienced graders such as clinicians or surgeons who routinely identify chondrolabral damage may grade the appearance differently. In future studies, the accuracy of the findings reported can be improved by increasing the number of graders for the data set and by randomised blinding when assessing porcine labrum samples to ensure objectivity.

Many clinical and in silico studies have provided evidence indicating that the mechanical environment plays a role in hip degradation (Ipavec et al., 1999; Ferguson et al., 2003; Bedi et al., 2011; Beck et al., 2012; Hunt, Gunether and Gilbert, 2013), these studies have not adequately addressed the impact of repeated loading cycles under different tuneable testing conditions. Repair techniques have primarily been developed based on short-term outcomes which may result in suboptimal approaches and uncertain long-term results. Previous efforts have been made to establish in vitro labral damage models for evaluating the impacts of labral damage and repair techniques. However, these models have thus far been constrained by limited ranges of motion, reduced loading conditions, and relatively short durations (Ferguson et al., 2003; Smith et al., 2011; Cadet et al., 2012; Philippon et al., 2014). A comprehensive labral damage model that is capable of mechanically assessing labral damage and repair techniques would offer a valuable tool for evaluating the long-term clinical outcomes of both existing and novel repair methods.

The developed methodology provides a suitable method for testing various parameters and can be used to generate and assess clinically relevant damage.

Chapter 4 Generating Chondrolabral Damage using Natural Hip Simulation

4.1 Introduction

In Chapter 3, porcine tissue was assessed under scaled physiological loading and resulted in minor changes to the surface condition. Following on from the developmental studies, the first type of damage to be recreated was labral tearing, followed by chondral delamination which can result in labral flaps. These forms of chondrolabral damage are commonly observed in patients (Wenger *et al.*, 2004; BURNETT *et al.*, 2006; Ganz *et al.*, 2008; Tannast *et al.*, 2008; Clohisy, John and Schutz, 2010; Fransen *et al.*, 2011) and this simulation model would allow the damage progression to be assessed *in vitro*. Labral tears were hypothesised to result from excessive loading of the rim (Wenger *et al.*, 2004; Hunt, Gunether and Gilbert, 2013; Miozzari *et al.*, 2015; Reyes *et al.*, 2016; Ng *et al.*, 2019; Raud *et al.*, 2020), where an increased axial force would result in increased compressive forces and contact at the rim (Mak *et al.*, 2011; Song *et al.*, 2021), causing wear at the anterior-superior margin of the acetabulum (Neumann *et al.*, 2007; Smith *et al.*, 2009; Mak *et al.*, 2011). Cartilage delamination was hypothesised to result from torsional loading (Ng *et al.*, 2019) where excessive shear forces and femoral head translation would damage the articular cartilage. This chapter presents two pilot studies designed by modifying the loading or motion profiles or by limiting the simulation to one or two degrees of motion to create a specific abnormal mechanical environment which would result in clinically relevant forms of chondrolabral damage. The relationship between the set parameters would allow for a better understanding of the altered mechanical loading environment which in turn would help recreate clinically relevant damage. This would aid in developing controlled and observable environments to assess how degeneration progresses over time and has the potential to be adapted in preclinical testing models in the future.

4.1.1 Chapter aim and research objectives

The main aim of this chapter was to use the experimental simulation model to generate chondrolabral damage using a hip joint simulator. The objective was to create adverse

mechanical loading environments, controlling different mechanical parameters to generate clinically relevant forms of labral tearing and chondral delamination.

4.2 Pilot Study 1: Generating labral tearing through overloading

4.2.1 Introduction

Stresses occurring in the soft tissue of the hip joint depend on joint geometry, motion, and loading. There is great potential in understanding the effect of these individual parameters on internal joint stress, destabilisation and the damage generated during hip impingement. Femoroacetabular impingement (FAI) is reported to be induced by an extreme range of motion-related activities in a well-constrained hip, and not directly through axial overloading of the hip, however, this has not been investigated *in vitro* under dynamic activities of daily living and the influence of stresses and joint dependent load testing has been limited. Thus, in this study, the effect of increasing axial force was tested *in vitro* for inducing impingement-like damage and assessing the effect of axial force at the chondro-labral junction in natural porcine hip joints. Cam-type impingement results in compression of the labrum between the aspherical femoral head and the acetabular rim, resulting in labral tears and subsequent detachment at the transition zone known as the chondro-labral junction. The effect of increased axial force during a standard walking cycle is hypothesised to promote similar compression of the labrum. This hypothesis is supported by studies reporting higher number of labral tears found in overweight or obese patients or joints which were exposed to unusually high axial forces during activities under a restricted range of motion (Martin *et al.*, 2006; Recnik *et al.*, 2009; King, March and Anandacoomarasamy, 2013; Turley *et al.*, 2013; Bliddal, Leeds and Christensen, 2014; MacLean, Callaghan and Maly, 2016; Reyes *et al.*, 2016; Raud *et al.*, 2020).

This study aimed to use the single station hip simulator to simulate a standard human walking cycle on porcine hip joints and investigate the effect of increased axial loading to generate labral tearing. Control data was generated using histological examination of unloaded porcine hip samples, to observe tissue structure and characteristics before simulation.

4.2.2 Methods

Six samples consisting of 6 months old porcine right hind limbs were dissected (Yorkshire Farms, North Yorkshire and prepared for simulation following the methods described in Chapter 3 (3.4.2.1 and 3.4.2.2) The acetabulum was orientated at 45° to the horizontal and mounted as shown in Figure 4.1.

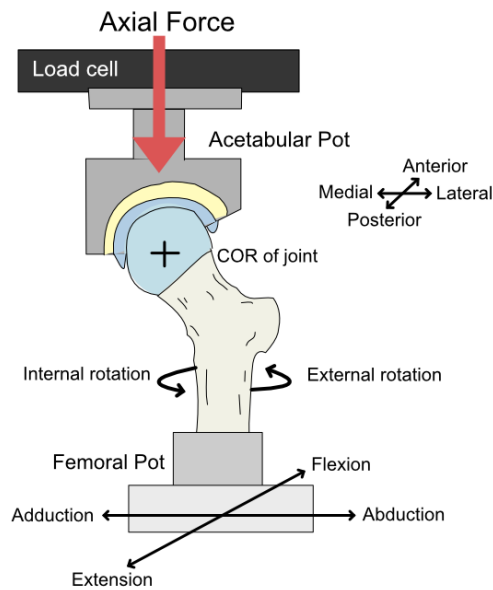


Figure 4.1: Single station hip simulator showing mounted natural porcine hip. The simulator uses a 6-axis load cell which can be used to apply ISO standard walking cycles or custom profiles. The walking cycle is applied using a demand wave cycle and can be monitored using a feedback wave cycle. The acetabular cup was mounted under the load cell while the femoral head was set on a cradle capable of moving in the simulator's three degrees of motion (FE, AA and IE).

For the scaled physiological loading, the axial load was scaled down by 70% to match the typical load undertaken by a porcine hip joint during a walking cycle which was estimated to be 900N for a pig weighing approximately 80kg (Thorup, Laursen and Jensen, 2008; Lizhang, 2010). The total load was increased to a maximum axial force of 1200N for an equivalent representation of the overloading of a porcine hip. In both testing scenarios, human motion inputs were used for flexion-extension, abduction-adduction and internal-external rotation as the porcine geometry was used to represent the human range of motion (Figure 4.2).

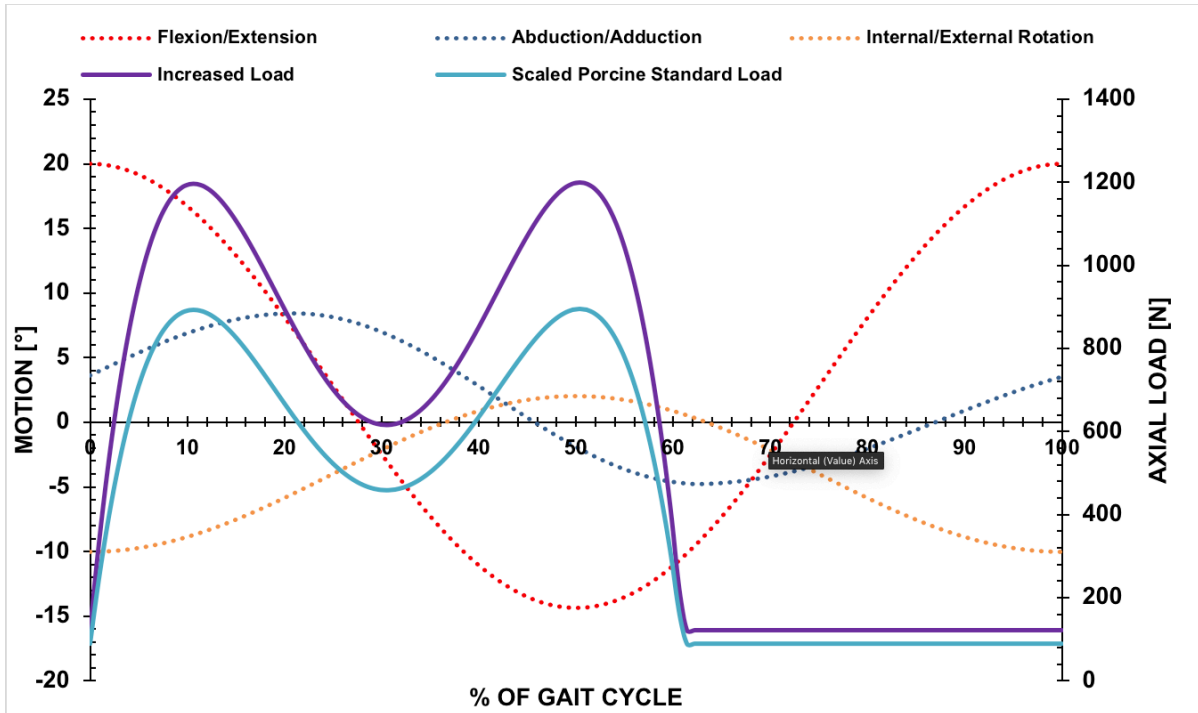


Figure 4.2: Simulator loading, and motion input profiles used to simulate a standard walking cycle based on a simplified human gait as per the ISO 14242-2 standard for wear testing and tribology of THR.

Following mounting, the cemented porcine joint in the simulator was sealed using a gaiter and filled with Ringer's solution. Ringer's solution was used as the lubricant in place of synovial fluid to provide a consistent fluid environment during experiments. Each joint was mounted onto the simulator and tested for a total of 14400 cycles (equivalent to four hours) where the simulation was paused to assess tissue for changes at 7200 cycles and fluid was replaced. The joint was remounted to complete the remaining cycles.

Photogrammetry was used to capture images of the tissue before simulation, at 7200 cycles and after completing 14400 cycles. All samples were assessed and graded using photogrammetry to measure the changes in condition of the acetabular labrum and the cartilage surface as described in Chapter 3 (3.4.2.5).

4.2.3 Results

Six porcine hips were simulated under standard and increased loading conditions for 14400 cycles where the simulation was paused to assess tissue for changes at 7200 cycles. The motion was defined per the ISO-14242 simplified gait cycle with the peak loads being 900N and 1200N respectively. Photogrammetry was used to assess the nature of tissue before running the test, after 7200 cycles (two hours) and upon completion of 14400 cycles (four hours) and recorded as per the grading scale in Chapter 3.

The shape of the acetabulae were generally similar in geometry (Table 4.2), with the average matched pair of acetabulum and femoral head diameter being approximately 36.5 mm. However, there were some natural differences between samples as they were obtained as part of the food chain. The tissue sourced was still developing so small differences in the shape of the femurs and the acetabulum were observed, as the femur was more rounded in some cases and the acetabulum asymmetric.

Table 4.1 Visual assessment of chondro-labral damage in simulated samples.

Sample	Weight (Kg)	Acetabular diameter (mm)	Femoral head diameter (mm)	Damage at 0 cycles	Damage at 7200 cycles	Damage at 14400 cycles
1 – Control scaled	78.4	35.0	35.0	Grade I	Grade I	Grade I
2 – Control scaled	97.2	38.5	37.5	Grade I	Grade I	Grade I
3 – Control scaled	67.0	36.0	36.0	Grade I	Grade I	Grade I
4 - Increased	74.1	35	35	Grade I	Grade I	Grade II
5 - Increased	90.6	38.5	38	Grade I	Grade I	Grade I
6 - Increased	86.8	38	38	Grade II	Grade IIIA	Grade IIIA

After *in vitro* simulator testing, the tissues were dull and had lost some of the blood and loose tissue that can be seen prior to simulation. The macroscopic appearance when considering the articular surfaces and labrum was unchanged when comparing pre-and post-test

appearance (Figure 4.3), and minor changes observed were generally due to differences in the lighting conditions and hydration of tissue as it was removed prior to or after testing.

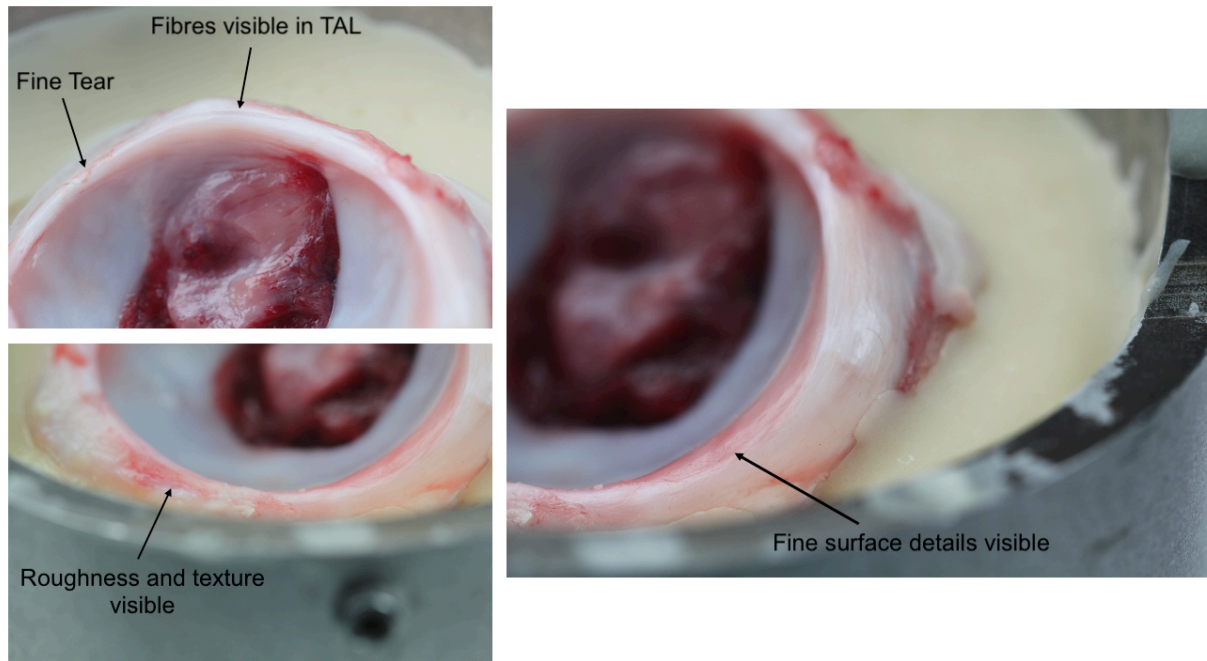


Figure 4.3: The telephoto images of the acetabulum showing the details of the articular surfaces and the acetabular labrum, fine details and tears can be identified as well as changes in surface topography.

With the wide frame, the cartilage and labrum remained completely intact, with no obvious scratches or signs of damage which may have occurred due to the simulation. Inspection with the macroscopic lens also revealed negligible scratches or surface damage. After 14400 cycles, the tissue was dull and may have lost some of the blood and loose tissue that can be seen before simulation.

In sample 4, there was an increase in visible blushing (redness) and dullness after 7200 (2 hours) and 14400 (4 hours) of simulation (Figure 4.4). The sample had increased scratching around the anterior-superior region of the acetabulum.

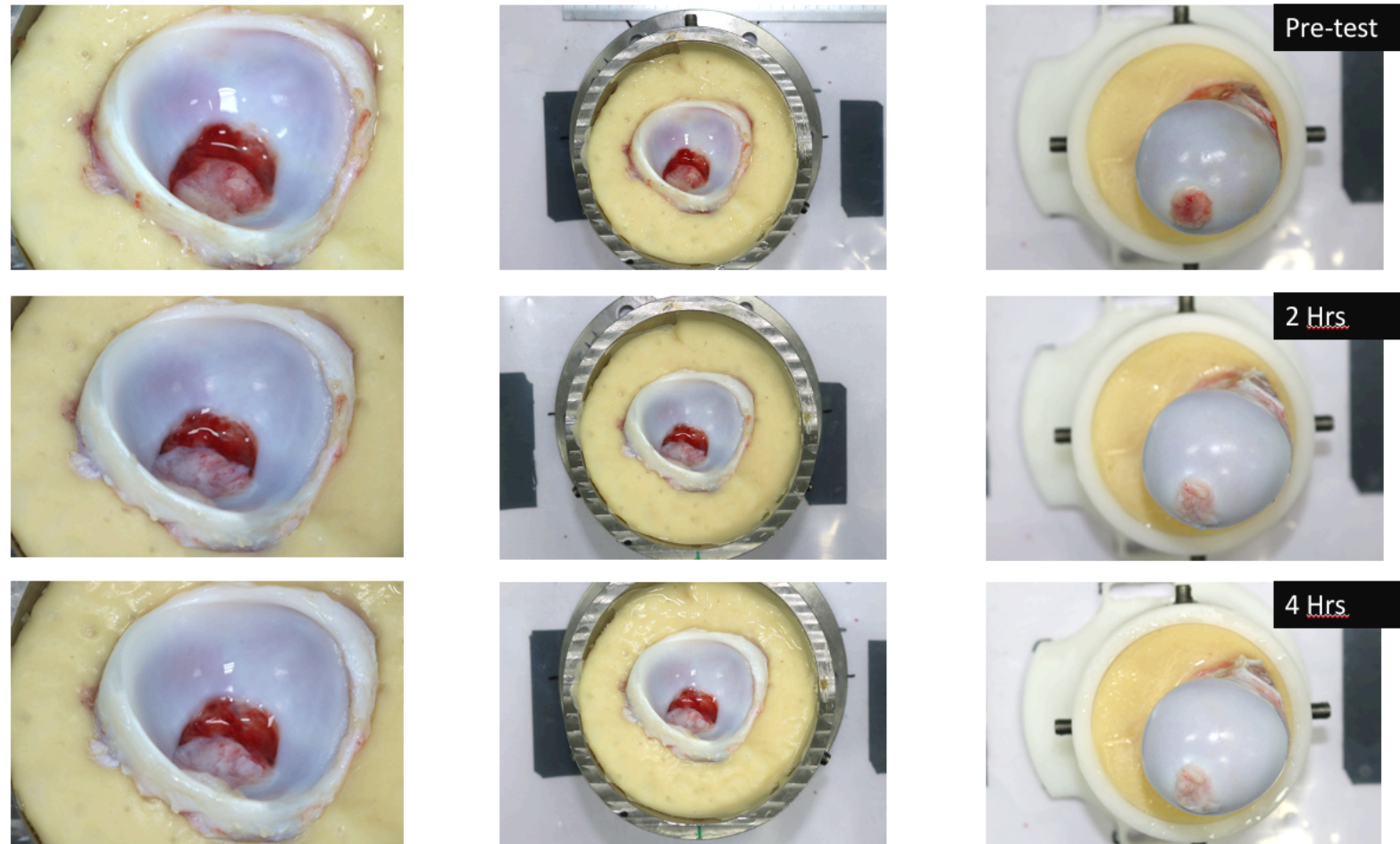


Figure 4.4: Photogrammetry of sample 4 which was simulated under increased loading (peak axial loading of 1200N), with motion set to human walking cycle from ISO 14242 standard with Ringer's solution as lubricant. The telephoto image of the acetabulum (left), the whole acetabular pot (center) and the wide image of the femoral head surface (right) prior to testing, after 7200 and 14400 cycles.

In sample 6, there was an increase in visible blushing (redness) and dullness after 7200 (2 hours) and 14400 (4 hours) of simulation (Figure 4.5). The sample had developed a peripheral labral tear and scratching around the anterior-superior rim of the acetabulum. The femoral head had significantly dulled at the end of the test compared to the pre-test suggesting signs of wear.

Under increased loading, some differences were found compared to control samples following two and four hours of in vitro simulation (Figure 4.4 and Figure 4.5). Signs of indentations or small scratches were observed on the articular surface of increased load samples (Figure 4.6) and were recorded as grade II (Table 4.2).

During these tests, lighting conditions were maintained which increased consistency in the method and resulted in sharper images. After 14400 cycles of in vitro testing, like the controls, the tissues were dull and had lost some of the blood and loose tissue that can be seen before simulation. In addition, in two out of three samples, the surface of the acetabulum had areas of damage with matching indentations observed on the femoral head suggesting signs of increased stress (Figure 4.6).

Sample 6 had a fine tear and scratch at the anterior side of the labrum which extended to the articular cartilage near the transverse acetabular ligament. At 7200 cycles this scratch grew and by 14400 cycles extended to the anterior-superior portion of the labrum just below the capsular attachment of the labrum. The scratch had grown from 4 mm to 15 mm (figure 4.7).

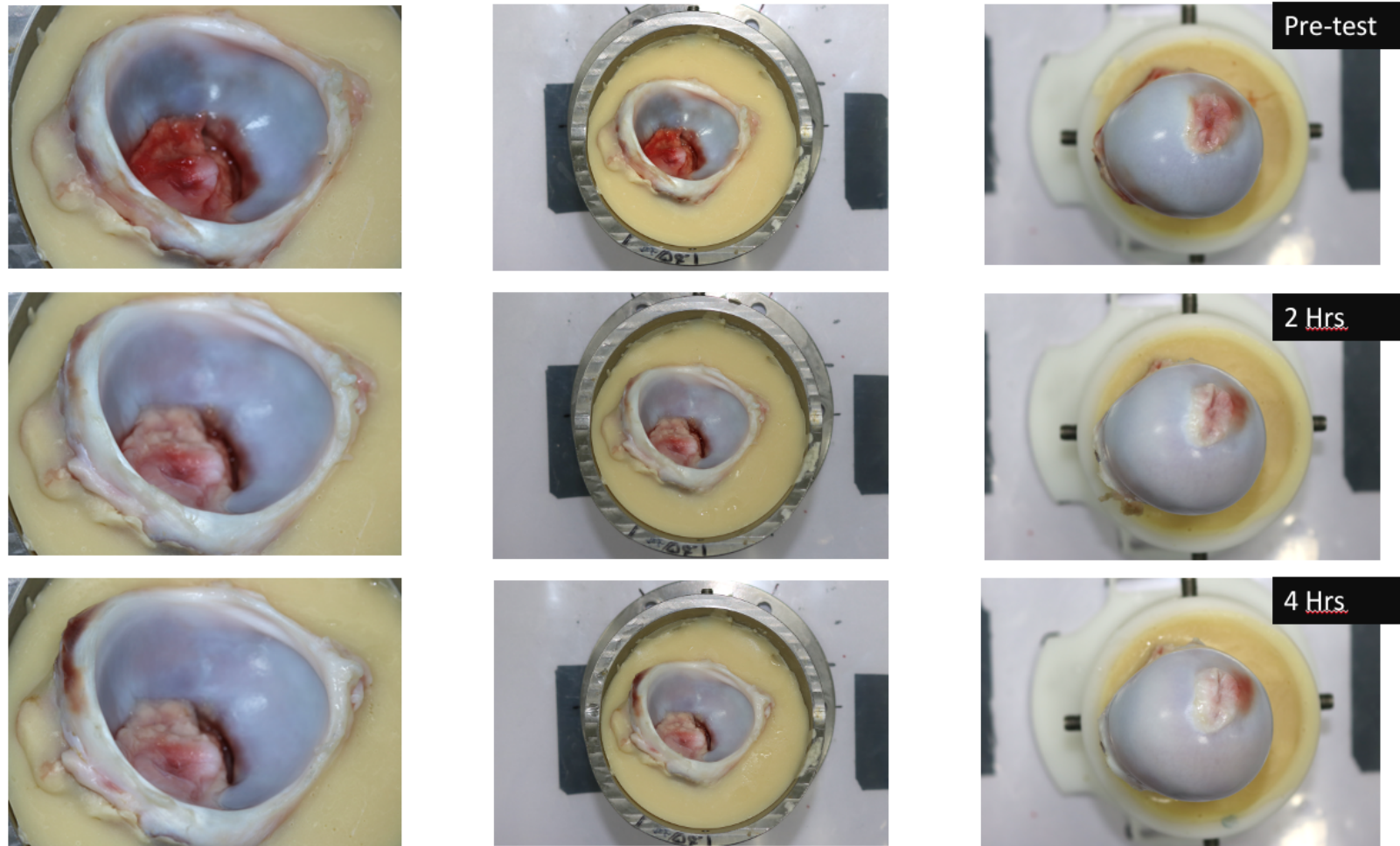


Figure 4.5: Photogrammetry of sample 6 which was simulated under increased loading (peak axial loading of 1200N), with motion set to human walking cycle from ISO 14242 standard with Ringer's solution as lubricant. The telephoto image of the acetabulum (left), the whole acetabular pot (center) and the wide image of the femoral head surface (right) prior to testing, after 7200 and 14400 cycles.

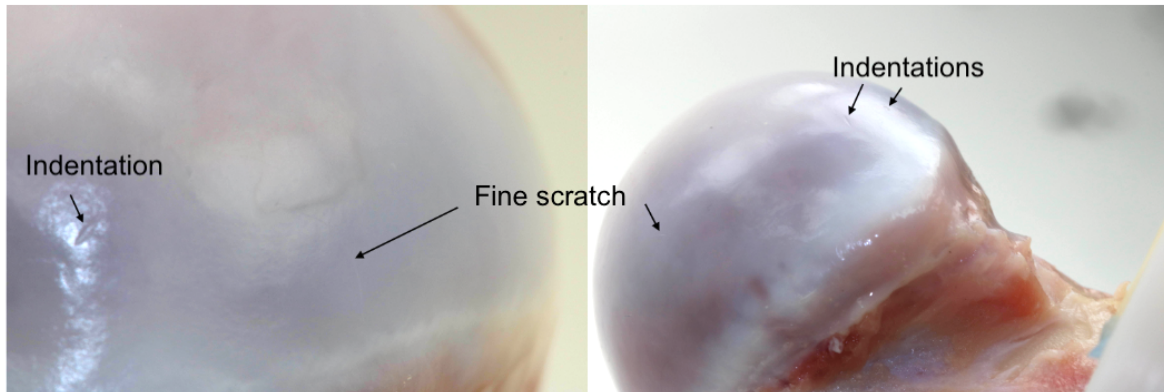


Figure 4.6: Dents and fine scratches observed on the femoral head which would align anteriorly near the transverse acetabulum ligament in sample 6, as seen with macroscopic lens with 1x magnification.

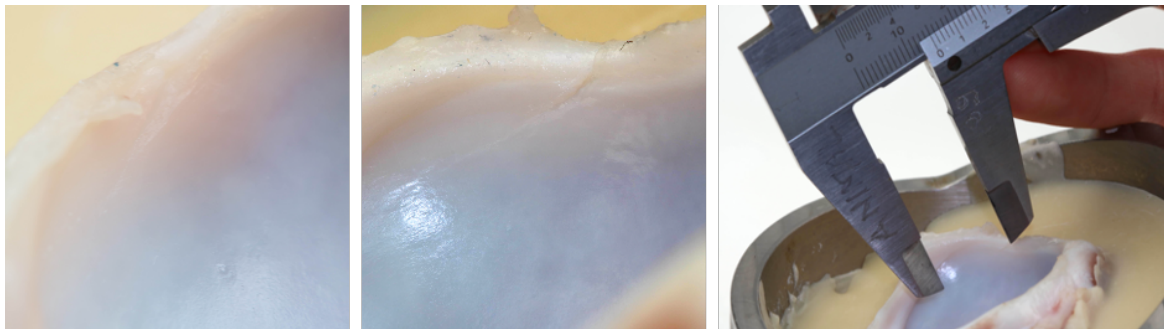


Figure 4.7: Fine scratches observed on sample 6 on the surface of the acetabulum labrum extending to the chondro-labral margin and acetabular labrum. As seen with the macroscopic lens with 1x magnification. Initial scratch found before simulation near the anterior portion of the labrum (left), and after four hours of simulation under increased loading.

4.2.3 Discussion

To the authors knowledge, this is one of the only studies to have simulated whole natural hip joints tested under increased loading in a controlled dynamic loading cycle.

The simulations resulted in observable differences in surface characteristics when the tissue was overloaded. Under increased loading the samples had a mild increase in surface roughness, blushing, fine scratches, and indentations after 7200 cycles (two hours) of testing. After 14400 cycles (four hours) of testing, anterior-superior peripheral labral tears were observed in two samples, both with chondrolabral separation. Blushing was more apparent

after 14400 cycles, where the anterior-superior rim had fine scratches and chondrolabral separation. One of the samples had a mild tear that increased in length after simulation and was observed as Grade II to Grade IIIA after 7200 cycles (two hours). This suggests prolonged overloading applied on the hip joint during motion, may be an important factor in the development of labral tearing and chondrolabral separation.

Increasing the load was expected to increase contact pressures and promote wear of the labrum/cartilage (Anwander et al., 2018; Bedi et al., 2011; Crawford et al., 2007; Diamond et al., 2016; MacLean et al., 2016) as studies have highlighted the effect of increased wear and damage with increases in a patient's body mass index (BMI) with higher possibility of developing early onset of osteoarthritis and tears when patients were overweight or obese (Chee et al., 2010; Recnik et al., 2009; Reyes et al., 2016). The findings of this pilot study suggest that overloading affects the appearance of the articular surface and labrum, as a 200N increase in load over 14400 cycles resulted in increased blushing and generation of clinically relevant anterior superior tearing.

The present study is consistent with prior *in vitro* investigations of natural cartilage or labrum specimens, which have revealed a correlation between increasing load and damage (Katta et al., 2007; Lizhang et al., 2013; Pallan, 2016). The majority of the observed damage was situated in the anterior-superior region of the acetabulae, a finding that is in line with clinically reported damage locations (Kaya, 2014; Kaya et al., 2016). Leunig et al. (2003) through clinical arthroscopic investigation demonstrated that joint degeneration was more commonly found at the anterior-superior site as observed in this study, this matches the clinical findings of joint wear occurring along the weight-bearing surface. This suggests that the present study was able to successfully generate a clinically relevant form of labral tearing as a result of hip simulation. One theory for this damage is likely due to the natural asphericity of the porcine head which likely caused damage at the anterior-superior junction as the porcine femoral head was placed to mimic that of a cam-type deformity in a neutral aligned human hip joint (Clohisy et al., 2011; Maquer et al., 2016; Ng et al., 2016, 2019).

Prolonged overloading of the hip likely occurs before labral tearing or articular damage, and overloading is one of the major factors that results in chondrolabral damage as has been shown by the results of this experimental study. It is still unclear whether cartilage damage precedes labral tearing however, it is more likely that a sudden or prolonged increase in pressure in the joint cavity would result in higher contact pressures at the anterior superior site resulting in chondrolabral damage.

It was expected that that overloading a pre-scratched hip would result in a further damage. One sample had a fine tear which was identified prior to simulation. The tear had grown from 4 mm to 15 mm and matches the look of a peripheral tear observed clinically (Cho et al., 2022; Martin et al., 2006b). The location of this tear was anterior-superior and was already present in the porcine hip, and under the increased loads experienced, this tear developed and extended to the anterior-superior portion of the labrum just below the capsular attachment of the labrum which suggests that increasing loading in the presence of tears could promote abnormal engagement of the femoral head.

By using a lower load and pausing the test at intervals allowed the progression of damage to be tracked and rather show the effect of prolonged overloading which is more representative to how a young active person may develop labral tearing. This was possible due to the developments made to the methodology described in Chapter 3. Compared to the damage generated by Pallan, (2016), there was a more controlled generation of damage. Pallan (2016) was able to produce clinically recognisable damage, but this was too severe with catastrophic changes detected too fast. This limited the ability to assess the progression of damage. With lower loads and more regular monitoring, this study showed the progression of damage with changes such as an increase in blushing with increased load over time, and the increase in size of tears already present in a sample. While more repeats are required, the present study has shown great potential to induce clinically relevant damage. Furthermore, Pallan (2016) could not generate damage at the anterior-superior acetabulum as tears were reported superiorly.

Overall, further repeats of the overloading simulation can increase the method's reliability for generating labral tearing. The study shows how experimental whole-natural joint simulation could be used as a preclinical model for studying how abnormal loading and motion scenarios affect whole-natural joint tissue experimentally. For example, after the generation of clinically relevant forms of damage and labral tearing, a surgeon performs a small repair of the labrum and assess different suture or anchor options (Philippon, 2010; Harris, 2016; Carton and Filan, 2017)

Due to the limited number of studies experimentally investigating whole natural hip joints, there is great potential for developing these methods for studying experimentally induced labral tearing or other forms of cartilage or labral damage in the hip. Overall, the effect of overloading resulted in fine damage and the presence of tearing after 14400 cycles, around the expected anterior-superior site where tears are typically observed.

It should be noted that the thickness of porcine labrum samples may affect the findings observed in this study and that labrum thickness should be recorded to evaluate the effect in future studies. Computational studies have shown how overloading can damage the glenoid labrum, while damage was not found under expected loads in daily living (Groh and Herrera, 2009; A.L *et al.*, 2016). Swanson, (2017) reported that the thickness of the labrum affected the transmission of stresses, where it was shown through finite element modelling that a thicker labrum had less chance of tearing. In practice, with natural simulation, it is not possible to control the natural anatomical variations between porcine labrum samples.

The size of the femoral head has also been shown to impact the contact pressures in the hip joint, where Tauviqirrahman *et al.*, (2023) reported that a smaller femoral head diameter could increase the contact pressures in dual mobility implants tested under gait cycles, where the acetabular cup orientation was set to 45° inclination. In this study, it was noted that there was some natural variation between the diameters of the femoral head and acetabulum, however, unnatural, or mismatched heads or cups were removed from the study to prevent dislocation. The size of the femoral head could be investigated intentionally, as a mismatch could result in additional damage. No conclusive relationship can be made between the size of the femoral

head and the acetabulum influencing the damage in the present study due to the low sample size. Interestingly samples 5 and 6 were of the same size and larger than samples 4 yet had differences in the damage which was observed.

The selective screening of samples worked as the damage detected appeared after the testing. It is possible that damage was introduced during the dissection of the porcine acetabulum. However, macroscopic photos of the femoral head and acetabulum were taken to avoid introducing damage before running simulations to ensure any minor indentations were a direct result of the mechanical simulation. In addition, fine scratches and indentations were not present after 14400 cycles in the scaled physiologically loaded samples. One sample with pre-existing tear damage was deliberately kept in for interest in the damage progression.

Some fine scratches were also observed on sample 4 at the labrum suggesting some wear may have resulted due to abnormal contact; however, this could also be a result of fine cement particles being trapped in the joint space due to the dissection process where the greater trochanter had to be removed. This may have left small loose sharp bony debris or bone cement debris in the ringer's solution causing some minor indentations and fine scratches as the tests ran. After 7200 cycles the simulation was halted to check for such particulates being collected. The tissues were also immersed in a PBS bath and shaken to collect and remove any remaining debris before the initial mounting and running the simulation during the simulation to minimise this effect.

The continuous overloading profile does not likely represent the in vivo case, as the simulation approximates how the tissue would respond to continuous prolonged overloading to accelerate the progression of damage and determine if overloading resulted in the development of anterior-superior labral tears. This approach has the advantage of showing a worst-case scenario of how abnormal loading would affect the articular cartilage and acetabular labrum.

Due to the limitations of the alignment of centre of rotation of the joint with the simulator, the joint capsule was removed along with the capsuloligamentous support. This limits the model as it is not like the in vivo state. In the future, a larger working space hip simulator designed to

hold natural tissue would allow features like the joint capsule to be preserved for investigations.

The experimental approach described in this study is also able to rapidly induce damage within two hours of testing an undamaged hip joint and can be similarly translated to a larger scale animal model such as bovine joint or to a human cadaveric model. It is worth noting that the tissue deteriorates over time and through simulation so there is a natural limit to the duration of tests. The choice of loading input parameters can account for this to accelerate the effects of simulation and obtain damage faster.

As the methods used in the pilot study were being developed, there were some inconsistencies with the photogrammetry and damage assessment methodology, and these could be further improved. Initially, there were some inconsistencies in colour temperature, sample height resulting in reflections and glare on the cartilage surface. It was also difficult to find a fixed focus plane due to the asymmetrical shape of the acetabulum. In addition, covering all sides of the acetabulum was not possible with the macroscopic lens in a fixed position as the shape and size of porcine acetabula differed.

As this study utilised qualitative assessment, identification of fine tears or damage was done using careful user examination, however, this may introduce interobserver errors and some fine tears may be missed. To resolve this, the raw data set could be included and random blind assessment against the damage scale by several observers to improve the reliability of the reported findings and observations.

As initial approach to assessment of damage, the current methodology is suitable for picking up Grade II and above classifications which do not require the use of complex imaging setup or microscopy. However, grading and interpretation remains a limitation of this type of study and to resolve this, having more graders and conducting the grading with randomised blinding would improve the objectivity of the interpretations provided.

4.3 Pilot Study 2: Compressive torsional loading for inducing chondral delamination

4.3.1 Introduction

Cartilage delamination is a common pathology in patients with femoroacetabular impingement (G. Gao *et al.*, 2022). Chondral lesions, fissures and chondral delamination have been associated with altered mechanical environment and degenerative changes in the joint. Since articular damage occurs due to increased frictional effects, changes in fluid pressure, and excess shear forces are expected to increase wear and degeneration of articular cartilage. Delamination in the OARSI cartilage osteoarthritis histopathology grading system is classified as the loss of the superficial zone fragment due to shear forces (Waldstein *et al.*, 2016). Clinical findings also observe chondral damage occurring in the presence of labral tearing from FAI conditions (McCarthy *et al.*, 2001). Clinicians observe delamination when the cartilage surface is relatively smooth but subjacent tissues have the appearance of mid-zone/superficial zone cartilage organisation. The delamination of the articular cartilage is theorised to produce a cartilage flap adjacent to the labral lesion and cause global chondrolabral pathologies (Groh and Herrera, 2009).

In this study, increasing axial loads were applied under internal-external rotation to apply shear and compressive forces on the articular cartilage and accelerate wear to the articular cartilage to generate delamination-type damage i.e., the femoral head would articulate within the acetabulum with increasing torsional loading. It was hypothesised that this altered mechanical environment would result in excess shear forces on the surface. Increasing the axial force would result in damage beneath the cartilage surface up to the subchondral bone. If sufficient, this loading scenario would result in a chondrolabral flap. Hence, to generate shear forces, the hip simulator was used to generate a twist compression test, where the femoral head was set to rotate and simultaneously apply pressure on the static acetabulum, resulting in friction produced at the contact area, creating lateral shear forces. Moreover, due to the femur naturally having the greatest contact anterior-superiorly, it was hypothesised that delamination or chondrolabral damage would be expected at the anterior quadrant of the acetabulum.

Loads were based on Pallan (2016) who had applied a maximum load of 2350N throughout her testing which could generate catastrophic damage to the labrum and cartilage in conditions where the femoral head was less likely to dislocate. The joint was potted with neutral human hip joint alignment, and abnormally shaped femoral heads or acetabulae were excluded from this study. Initially, the maximum load of 2350N, which is more extreme than the physiological loading experienced by the porcine hip was tested to compare if similar catastrophic damage would occur with the new changes to the methodology described in Chapter 3. In addition, to make comparisons with the previous overloading study 4.3.2 and to assess the impact of applying increased torsional loading, moderate and low loading conditions were chosen, at 900N and 1300N respectively. The input profile for the simulator would be the same as previous tests excluding motions such as flexion-extension and abduction-adduction were omitted from the test. In contrast, other motions such as internal-external rotation and axial force were used following the scaled walking cycle introduced in Chapter 3.

The aim of study 2 was:

- To determine if increasing axial loads with internal-external femoral head rotation (torsion) affects the articular surface of the acetabulum, resulting in delamination-type damage.
- To investigate the effects of delamination in influencing other forms of chondral or labral injuries.

4.3.2 Method

Nine immature porcine right hind limbs were dissected, and porcine hip joints were prepared following the methodology in Chapter 3 (3.4.2.3-3.4.2.2). Before testing, the femoral head diameter and acetabulum diameter were recorded to ensure no significant abnormalities in the shape that would result in dislocation during testing. Samples with previous signs of articular cartilage damage, or labral tears were excluded from the study. The joint was prepared for simulation by aligning and cementing based on anatomical markers found on the femoral head near the greater trochanter and the transverse acetabular ligament found on the acetabulum. The orientation of the acetabulum was positioned to match the human orientation

of 45°. The joint was held in place using a custom fixture and aligned such that the centre of rotation of the joint (at the femoral head centre) matched the centre of rotation of the simulator. Next, the cemented porcine joint was mounted with the load cell driven at the acetabular cup and the femoral head at the base of the simulator. The medial-lateral (ML) axis can be kept locked in a set position or removed. In this test, the ML axis was kept free throughout testing to allow natural head movements within the cup. The whole joint was sealed using a gaiter and was filled with Ringer's solution. The input for the test shown in Figure 4.8 represents the input profile used with the simulator. The testing frequency to repeat profiles was 1Hz, which simulates the frequency of human locomotion. Each joint was mounted onto the simulator and tested for 14400 cycles. The simulation was paused to assess tissue for changes at 7200 cycles and fluid was replaced and the joint was run again for the remaining cycles. Photogrammetry was used to capture images of the tissue before, at two hours and at the end of the testing.

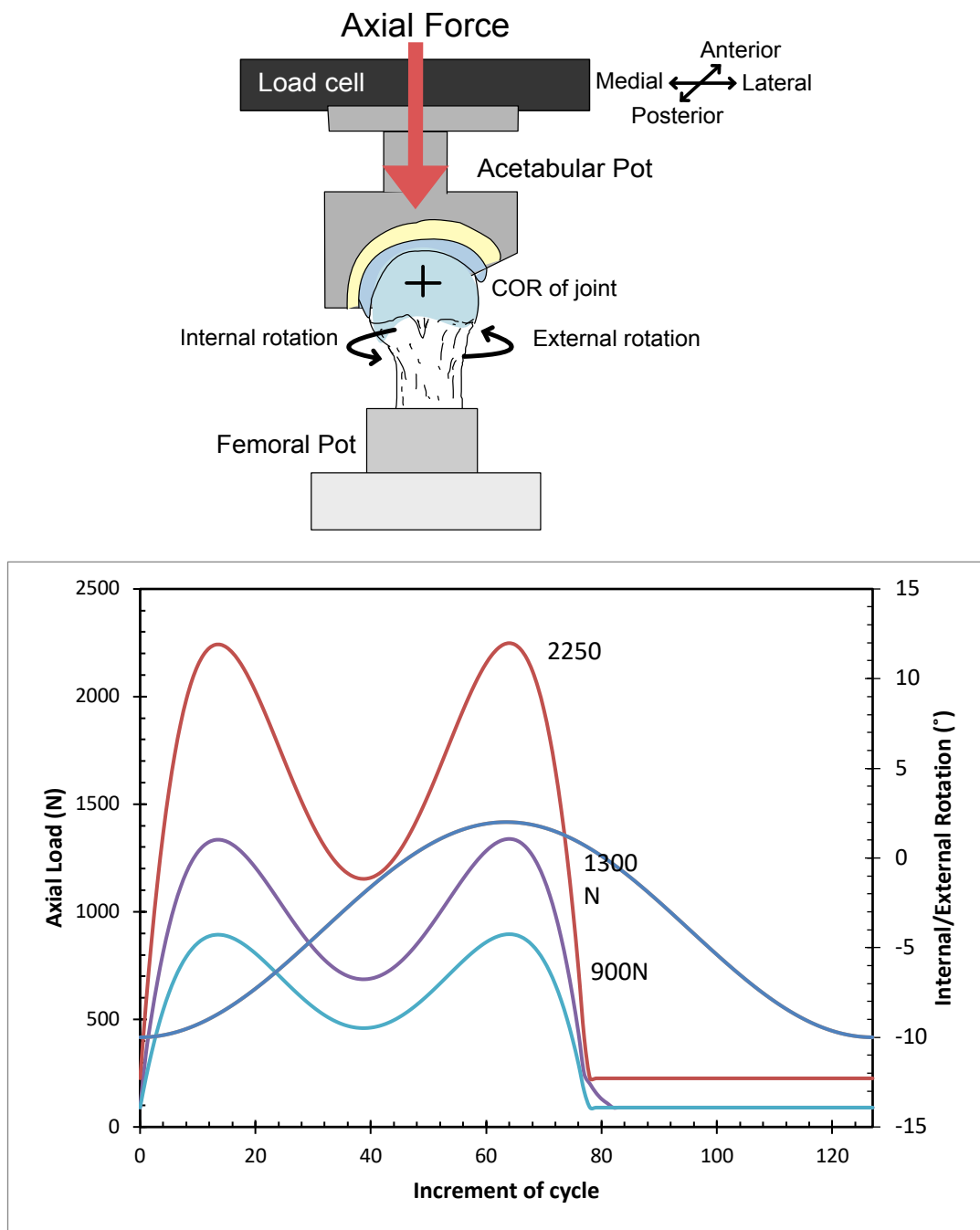


Figure 4.8 – Schematic of testing set-up, axial load was applied through the cup while the femoral head drove the motion. Input profile is shown by the graph representing the loads and motion profile used to generate compressive twisting (torsional) loading. The profile followed a simplified representation of human internal-external rotation and axial loading occurring during walking with the omission of abduction-adduction and flexion-extension.

4.3.3 Results

Surface photogrammetry was conducted as described in Chapter 3(3.4.2.5) using a macroscopic camera. Images were taken representing the condition of the cartilage and labrum in porcine samples before being simulated, at the middle of the testing phase roughly at 7200 cycles where the test was paused, and the joint was removed from the simulator for surface assessment before being remounted. and finally at the end of the test at 14400 cycles. In this study, blushing was defined as increased translucency of the articular cartilage, where the cartilage took a reddish hue. Under increased torsional loading, the visible damage was observed (Table 4.2; Figure 4.9). At 900N peak load, the tissue had a mild increase in blushing.

Table 4.2 – Surface Photogrammetry of porcine samples

Weight (Kg)	Acetabulum Ø (mm)	Femoral head Ø(mm)	Testing conditions	Total cycles run	Assessment		
					Pre-test	Mid-test	Post-test
93.7	39.0	36.0	900N AF + IE motion, Ringer's Solution, 45° cup orientation, central alignment, 1Hz, ML free	14400	Spherical, smaller head to cup, no damage on surfaces, labrum in-tact	Blushing on cartilage in small area superior region, labrum in-tact	Slightly increased blushing anterior- superiorly, with fine textured striations below cartilage, labrum in-tact
88.6	42.5	36.5	1300N AF + IE motion, Ringer's Solution, 45° cup orientation, central alignment, 1Hz, ML free	14400	Very Aspherical wider horizontally by 5mm, smaller head to cup, no damage on surfaces, labrum in-tact	Blushing anterior- superiorly, with fine textured striations below cartilage, labrum in-tact	Increased blushing anterior- superiorly, with fine textured striations below cartilage, labrum in-tact
91.1	39.5	37.5	2350N AF + IE motion, Ringer's	14400	Aspherical horizontally by 3.5 mm,	Blushing anterior- superiorly, with	Severe blushing anterior- superiorly, with

			Solution, 45° cup orientation, central alignment, 1Hz, ML free		relatively well-matched cup to head, no damage on surfaces, labrum in-tact	fine textured striations below cartilage, labrum in-tact, some fine indentations are present	well-defined textured striations below cartilage, fine tear at chondro-labral junction
88.4	38.5	38.5	2350N AF + IE motion, Ringer's Solution, 45° cup orientation, central alignment, 1Hz, ML free	14400	Spherical, well-matched cup to head, no damage on surfaces, labrum in-tact	Blushing anterior-superiorly, with fine textured striations below cartilage, labrum in-tact, some fine indentations are present	Severe blushing anterior-superiorly, with well-defined striations below cartilage, chondro-labral detachment and fine tears along labrum and cartilage, labrum is rougher in texture

After 14400 Cycles

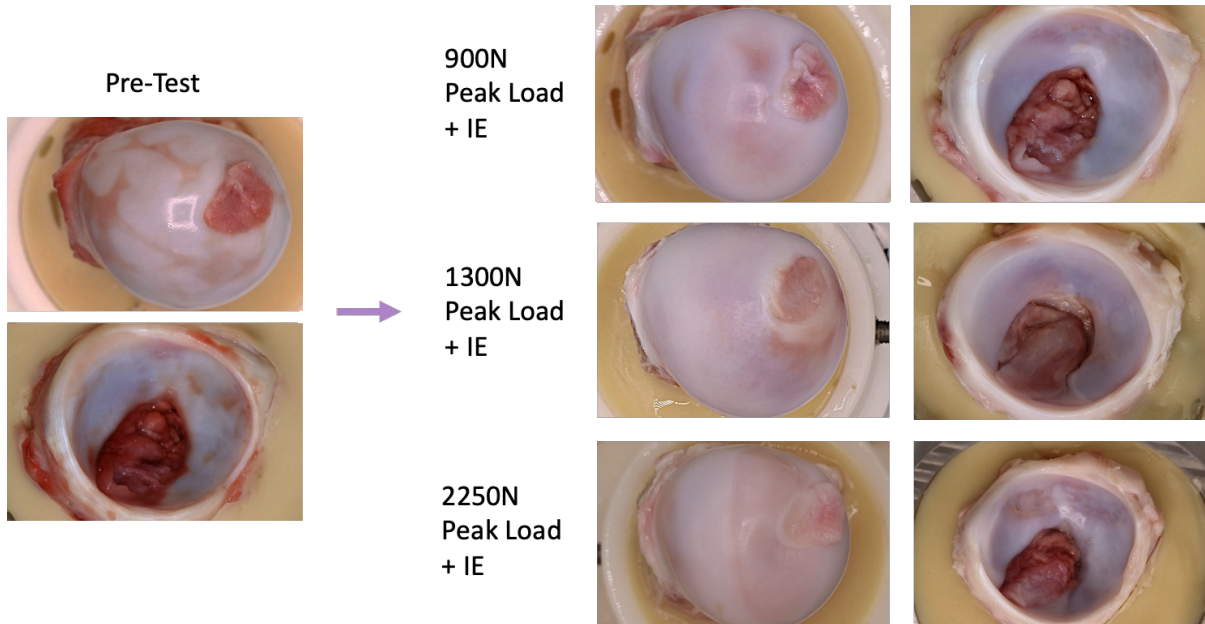


Figure 4.9 – Photogrammetry showing surface changes on the femoral head and acetabulum observed when comparing porcine hips unloaded to increasing levels of torsional loading. Images represent changes associated with the different axial loads where indentation,

blushing, blistering, and peripheral labral tears were observed, with the severity increasing with load.

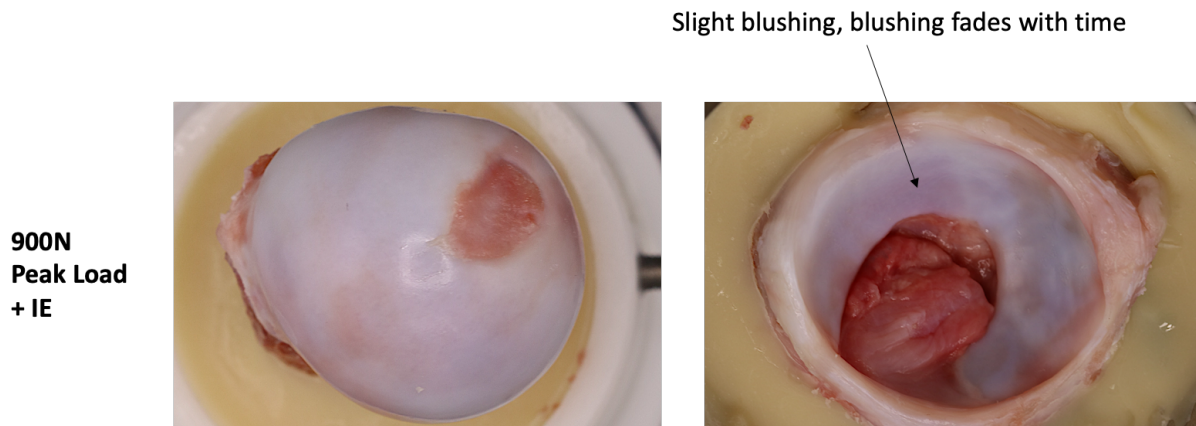


Figure 4.10 – Photogrammetry showing surface changes on the femoral head and acetabulum. At 900N peak load, the tissue had a mild increase in blushing.

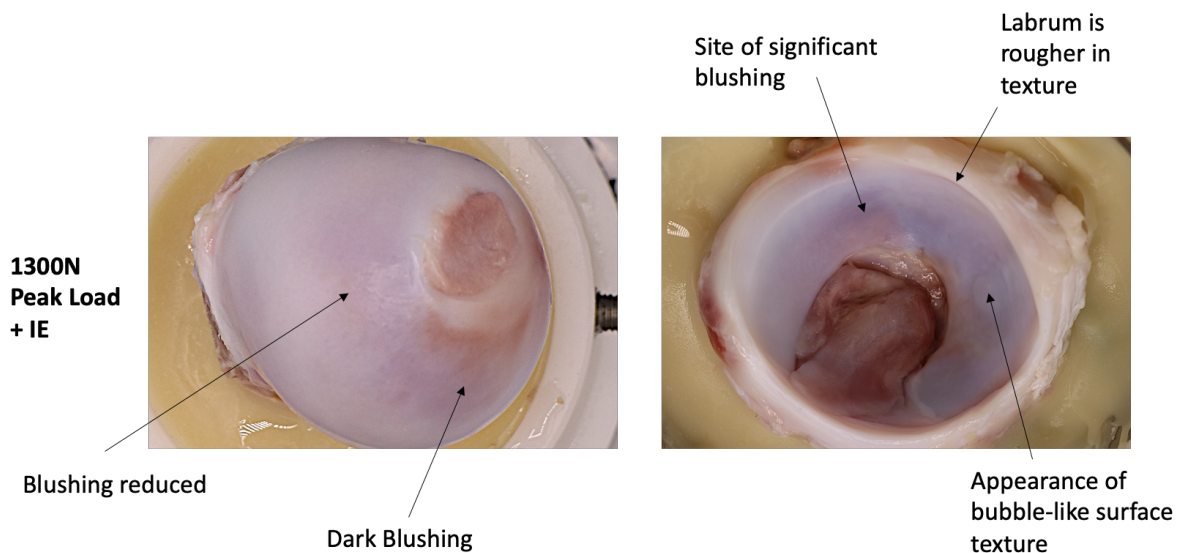


Figure 4.11 – Photogrammetry showing surface changes on the femoral head and acetabulum. At 1300N peak load, the tissue had a significant increase in blushing and the uneven wrinkled structure appeared like blistering on the articular cartilage surface.

Increased blushing was observed on the femoral head and the acetabular cartilage at 1300N peak axial load, with darker hues appearing at the point of most contact area during motion at the anterior quadrant of the acetabulum (Figure 4.11), a distinct pattern was found to be forming on the femur and the appearance of uneven, bubble or blister like structures were observed on the acetabulum (Figure 4.13). In some instances, this wrinkled texture was present in the posterior quadrant as well as the anterior quadrant.

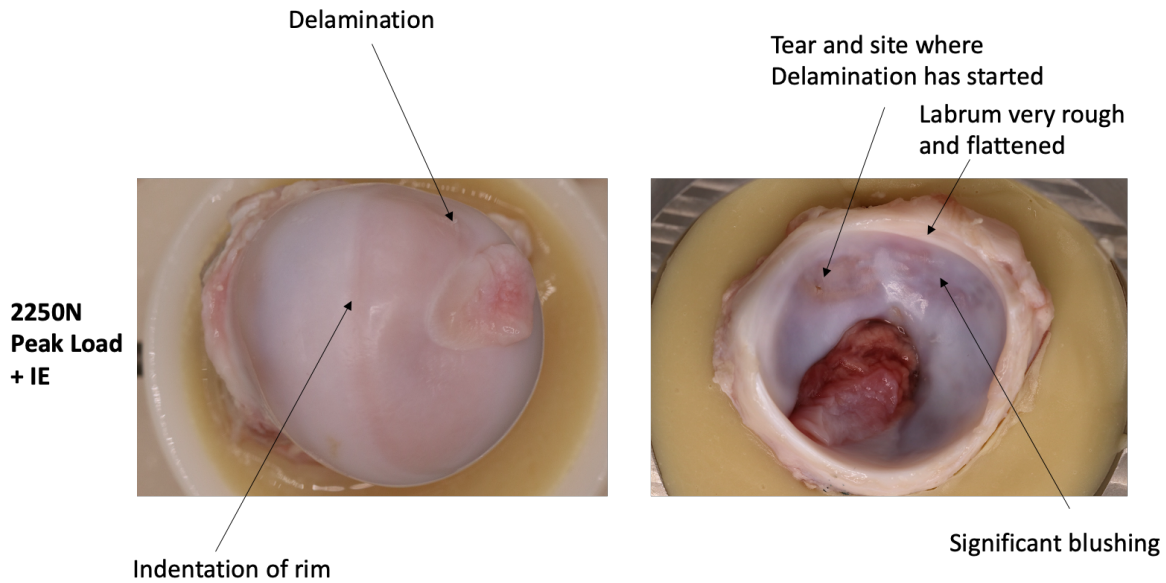


Figure 4.12 – Photogrammetry showing surface changes on the femoral head and acetabulum. At 2250N there was significant changes to the appearance of the femoral head and acetabulum. Delamination of the articular cartilage from the subchondral bone had occurred on the femoral head and cartilage. Fine tears and scratches were observed as well as significant blushing and blistered texture on the cartilage surface.

Increased blushing was observed on the femoral head and the acetabular cartilage with darker hues appearing at the point of most contact area during motion at the anterior quadrant of the acetabulum with signs of fine scratches, increased roughness, and flattened nature of the labrum. Small cartilage flaps and delaminated cartilage showed exposed subchondral bone underneath on the acetabulum (Figure 4.12). Similar damage was observed on the femoral head cartilage with a clear imprint of the site in most contact with the acetabulum (Figure 4.12).

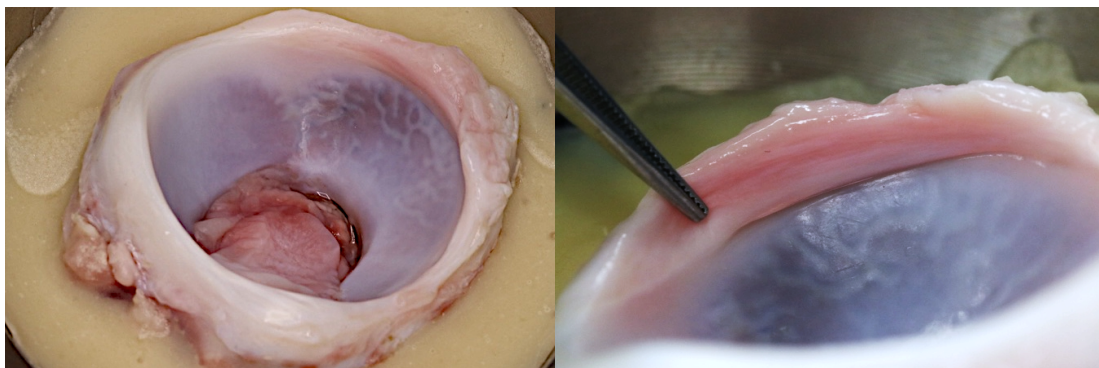


Figure 4.13 – Photogrammetry showing the uneven surface changes and appearance of bubble-like texture on the acetabulum observed at the end of testing. In some samples, chondrolabral tearing was observed at the anterior-superior rim.

When a scalpel was used to investigate the uneven blister-like structures found across the cartilage surface, the texture remained even when scored or when deep scratches were present (Figure 4.14). Forceps were used to investigate the blisters and found the surface layer hard when depressed. When a blister was punctured with a scalpel blade, the uneven texture remained (Figure 4.15).

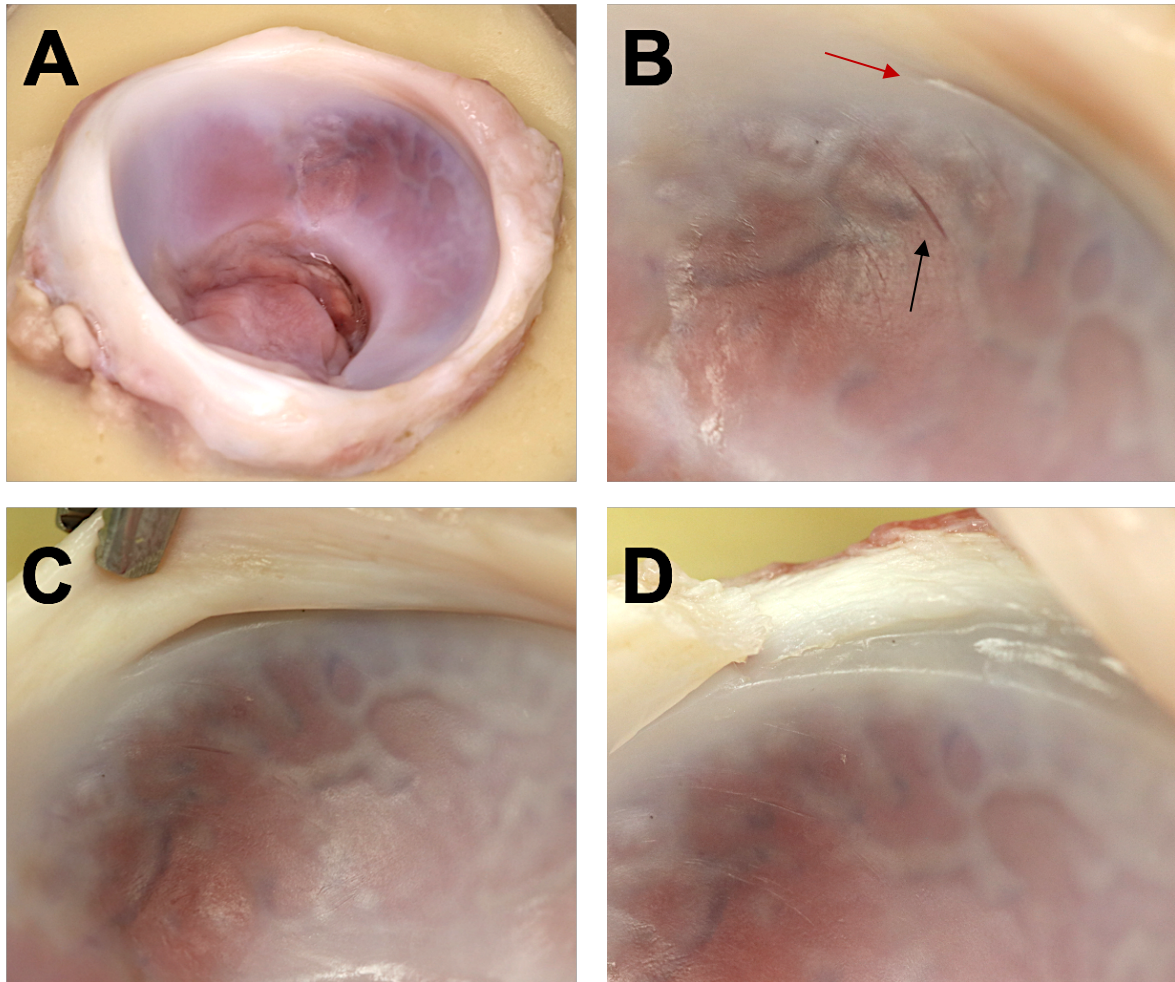


Figure 4.14 – **A** Photogrammetry showing an example of the uneven surface changes and appearance of bubble-like blistered texture on the acetabulum observed after 8 hours of testing under torsional overloading. **B** The blistered texture was observed even when there was a fine scratch running through the articular surface (black arrow). Chondrolabral separation was also present in the sample (red arrow). **C** The labral tear at the anterior-superior rim was lifted but had to change in the bubble like structure. **D** Removal of the labrum at the site of anterior-superior tear rim had no impact on the appearance of the bubble like structure.

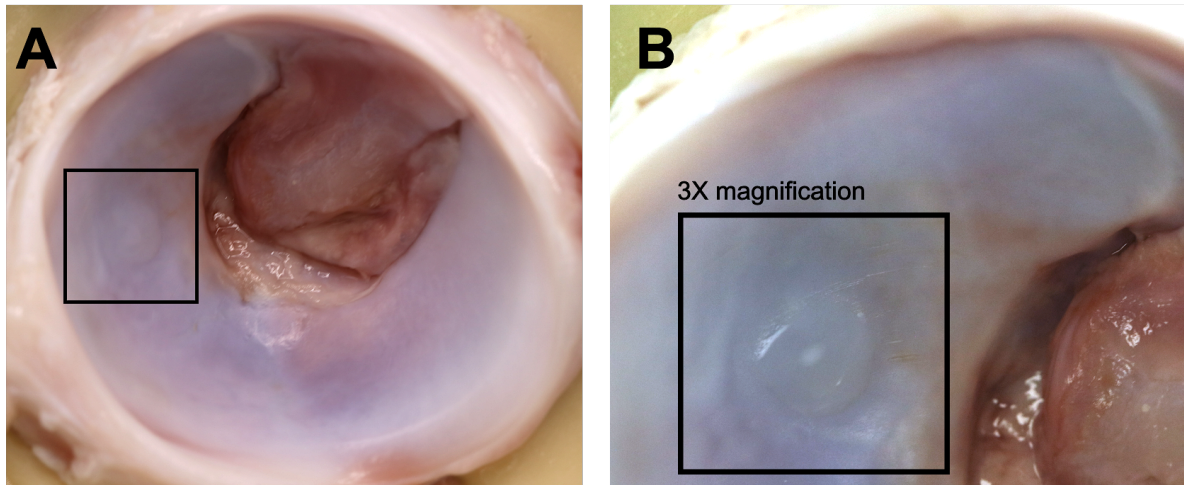


Figure 4.15 – A Photogrammetry showing an example of the uneven surface changes and appearance of bubble-like blistered texture on the acetabulum observed after 4 hours of testing under torsional overloading. **B** A 3x magnified image of the bubble which had been scored with a scalpel blade and had no change to the appearance of the blister-like surface.

4.3.4 Discussion

This study aimed to determine if increasing axial loads with internal-external femoral head rotation (torsion) would result in delamination of the articular cartilage. By applying increasing levels of torsional loading on the hip joint, the study found chondral damage on the articular cartilage, where there was an increase in blushing, a blistered and wrinkled surface texture. As per the author's knowledge this is the first-time chondral delamination has been investigated experimentally in the hip, and more significantly, the first time a whole natural hip joint has been used to induce delamination-type chondral damage.

While there are no comparable studies on the type of damage generated, it is suspected that chondral delamination occurred (Waldstein et al., 2016). The type of damage observed in the most severe torsional loading condition was closest to the cartilage grading score ICRS grade 3, and grade 4 in the Outerbridge scale (Cassar-Gheiti et al., 2017).

The uneven texture referred to as blistering was observed at the moderate load and suspected as an intermediary stage to visible delamination or generation of a chondral flap where the articular cartilage was detached from the subchondral bone below. The visual appearance matched that of ICRS grade IA where soft uneven surface was observed (Cassar-Gheiti et al., 2017).

Damage was observed in the articular surface beneath the top articular surface at the mid-zone of the cartilage. In contrast, the overall cartilage structure appeared intact. Investigation of the blistering revealed the surface layer was hard when depressed. A scalpel was used to make an incision at the labrum to excise the labrum covering the uneven surface to see if these blisters were being held at the anterior margin but remained intact due to the labrum, the cartilage layer remained fully intact suggesting the delamination occurred beneath the superficial layer of articular cartilage.

Studies have investigated delamination in the knee joint (Eleswarapu, Responde and Athanasiou, 2011; Liu et al., 2015; Gahunia et al., 2020) and patella (Goodfellow, Hungerford and Zindel, 1976). Blistering is rarely observed in hip arthroscopic investigations, and this may be due to the unique nature of how it presents. When samples were stored during or after completing simulations, the rough, uneven texture had gone leaving a smooth articular surface suggesting that the cartilage relaxes as it rehydrates which may be why surgeons are sometimes unable to see delamination in the hip and can only observe it when there is a noticeable wave or crimp sign or when the cartilage has completely torn such as a labral flap. Chondral delamination and blisters are most commonly reported in the knee (Goodfellow, Hungerford and Zindel, 1976; Zaltz, 2012; Cassar-Gheiti et al., 2017; Brittberg, 2022).

Goodfellow, Hungerford and Zindel, (1976) provided the closest explanation to the results observed in this study, when investigating chondromalacia in the knee patella. They proposed an explanation for the blistering observed. They described the cartilage deviating from normal cartilage in three stages, stage 1 or fasciculation where the articular surface was smoothly intact and the uneven surface would only be detected through palpation describing a spongy consistency. They hypothesised that it was the lack of cohesion between thick collagen bundles which resulted in the fasciculation. When collagen fibres of the midzone were broken, it resulted in a blistered appearance while the superficial layer remained intact.

This explanation may be supported by the fact that the superficial layer known as the lamina splendens forms a thick shear resistant layer of fibres (Aspden and Hukins, 1979; T Otsuka, 1995; Mansfield, Bell and Winlove, 2015; Rexwinkle, Hunt and Pfeiffer, 2017). It may be why

during the experimental simulation, which induced torsional loading and shear on the surface the collagen fibres of the midzone underneath were impacted, while the superficial layer remained intact.

It is possible that the delamination damage led to intra-articular damage, and the 'blushing' and striations led to damage beneath the superficial cartilage layer where collagen fibre organisation and cross-links holding the quaternary structure were broken resulting in denatured collagen being trapped. Subsequent damage would extend until the subchondral bone which when torn would result in the formation of a chondral flap as observed clinically in more severe cases of femoroacetabular impingement. Biological characterisation of the damage observed through imaging would be needed to examine the exact nature of the damage; however purely on surface assessment, the appearance of the damaged tissue matched the description of cartilage damage described in the OARSI histopathology scale as delamination type damage.

Since this test lacked the more dynamic motion required for walking, and focused solely on rotation and axial force, it would suggest that a cross-translation between the femur and the acetabulum was required to cause chondro-labral damage or tearing i.e., a rotation or shear effect and a translational effect (ML displacement or deep flexion/extension) as from the previous study in Chapter 4.2 for overloading, chondrolabral tears occurred under a full range of motion suggesting head translation/instability has an important role in damage to the rim.

In the study, at the highest load applied on samples, fine tears were observed along the articular surface and femoral head, with a rougher surface appearance of the acetabular labrum, and in some samples, there were instances of labral flaps and chondro-labral tearing at the anterior quadrant of the acetabulum suggesting the potential of delamination preceding other forms of chondral damage and degeneration. The uneven surface provided by the delaminated cartilage or bubble-like texture, could have resulted in the femoral head becoming unstable but prevented from dislocation due to the acetabular labrum rim, this overloading the rim and causing the flattened and rougher appearance was also observed at the anterior-superior labrum.

During the set-up, the ML axis was not locked to allow natural sliding and translation of the head in the cup. Further damage as a result of delamination could be due to the occurrence of medial-lateral (ML) displacement being noted to have changed from the feedback provided by the simulator during testing, which showed a net shift of 2-3 mm from the initial zero value (central alignment), which was present at pre-test, however, at higher loads, the ML reading suggested the oscillations which would have resulted in increased head translation which could explain the chondrolabral tearing observed on some samples.

Further testing would be needed to determine the exact effect instability has on the development of severe chondrolabral damage, and it is still unclear if articular damage precedes labral damage or if both occur in conjunction because of combined shear and compressive forces with a medial-lateral head translation.

As discussed in 4.2.3, the study was non-representative of an in vivo model condition, providing a complex set-up designed to simulate delamination-type damage. The grading and interpretation of the damage generated could also be improved by introducing random blinding and having more independent graders.

Due to the limited number of studies experimentally investigating whole natural hip joints, there is great potential for developing these methods for studying experimentally induced labral tearing or other forms of cartilage or labral damage in the hip such as fraying, rupturing or chondrolabral flaps (Groh and Herrera, 2009; A.L et al., 2016).

Chapter 5 Developments in Non-linear Microscopy for Imaging the Chondrolabral Junction

5.1 Introduction

There is a large gap in studies visualising labral damage or tearing at a microscopic level, as unlike the meniscus of the knee or the glenoid labrum, the arrangement of the collagen matrix is still unclear. It is believed that the orientation and arrangement of the collagen matrix are different throughout the labrum relating to the function. The overall distribution of loads across the labrum and the point of contact where the femur articulates within the acetabulum during motion was hypothesised to affect the structure of the collagen matrix based on function. It was hypothesised that the anterior-superior region was more prone to chondrolabral separation due to being more cartilaginous with a weaker attachment of collagen fibres at the chondrolabral junction.

Previously, few studies have investigated the microscale structure of the labrum. Most of the characterisation work conducted in recent years has been through histological imaging and immunohistochemistry using standard brightfield methods of the human labrum. Immunohistochemistry has revealed the type of collagen present in the labrum. Clinically, at the macro scale, MR arthrography, and CT scans have been used to determine damage to the labrum and cartilage, and bone shape respectively. This leaves a significant gap in the understanding of the progression of labral damage, which leads to labral tearing at a deeper level, especially when compared to similar tissues like the meniscus of the knee or the glenoid labrum, which have been studied in more detail.

Multiphoton imaging has been identified as a high-resolution imaging method capable of detecting collagen fibre alignment and orientation in cartilage and fibrocartilaginous structures like the labrum. Multiphoton imaging is a form of laser scanning microscopy which detects contrast information from non-linear optical properties of a sample. This type of microscopy can provide increased depth penetration and resolution than standard confocal imaging. During multiphoton imaging, a pulsed laser is used to excite fluorophores with two or three

photons of low energy to the same level as a single high-energy photon. By using low-energy photons, the method reduces the damage to the sample while allowing deeper penetration into scattering samples (Yeh *et al.*, 2005; Chen *et al.*, 2012; Novakofski *et al.*, 2016)

By studying the microstructure, detailed information can be revealed about the arrangement of collagen fibres at the chondrolabral transition which makes up the macroscale structure and how the structure relates to the function. This may provide insight (for example) into why labral tearing often occurs in the anterior-superior region, and if this is related to function alone, or a function induced change to the tissue. Observing how collagen and GAG arrangement is altered with loading can reveal important details on the mechanical behaviour of the tissue and how it degenerates.

This complex architecture is disrupted when damaged and subsequent degeneration can make the fibrocartilaginous structure weaker and prone to further deterioration which would start appearing at a macroscopic level. By studying the degeneration of the tissue at the microscale because of an abnormal mechanical environment, we can directly assess the degradation happening at a submicron scale and associate the structural changes to the collagen fibres which are difficult to visualise with conventional methods of imaging labral tearing such as MRI and ultrasound, due to the lack of resolution

Experimentally simulated samples from conditions described in Chapter 4 were characterised using multiphoton imaging without exogenous contrast agents. The materials, processing and methods and their developments to allow non-linear techniques to be applied to the porcine acetabular labrum and cartilage have been reported for the first time.

Chapters 4 and 5 involved the application of imaging techniques developed by Dr Jessica Mansfield (Mansfield, 2008) and were conducted at the University of Exeter. While the imaging conducted follows methods outlined by Mansfield *et al.*, (2009), the processing and image-capturing techniques and settings required for porcine acetabular tissue were different from Mansfield *et al.* (2008) and led by the author.

Chapter Aims

- To investigate the suitability of non-linear imaging techniques (multiphoton imaging, Raman spectroscopy and polarised microscopy) for imaging porcine acetabular tissue to visualise the collagen matrix within different regions of the labrum.
- To develop the methodology for imaging porcine labrum tissue and present preliminary results of unloaded porcine tissue.
- To image cross-sections of unloaded porcine tissue from the anterior, superior, and posterior quadrants of the acetabulum with multiphoton imaging, coherent Raman spectroscopy and polarised microscopy.

5.2 Working principles

Non-linear microscopy involves using laser scanning microscopy techniques built on the foundations of confocal microscopy. The focal point of a laser is emitted through a sample, and an output image is obtained from the signal through detectors. Non-linear microscopy has similarities to conventional confocal microscopy as both methods rely on powerful lasers to penetrate tissue optically. However, the depth penetration is typically between 50-200 μ m and requires fluorescently labelled molecules to observe features. Confocal imaging requires staining with fluorescent dyes, which has limitations of photo-bleaching and may induce processing damage, which would be unsuitable for characterising damage or degenerative changes at the microscale. Non-linear microscopy detects the scattering of a tissue in response to excitations produced by powerful lasers to produce images, thus is dependent on the inherent molecular properties of the tissue.

The main rationale for using this novel imaging approach for characterising the microstructure of the porcine labrum. This would allow higher resolution changes on the microstructure to be detected. Therefore, changes to the collagen fibre matrix structure due to the experimentally induced mechanical damage could be determined, particularly the anterior quadrant of articular cartilage, the acetabular labrum and the chondrolabral junction.

While Mansfield et al. (2008) reported the sources of contrast observed in equine articular cartilage, it was important to develop the microscopy setup and processing specific to labrum tissue. Captured images were used to reveal the structural composition of the collagen fibre network and organisation of the extra-cellular matrix at the chondrolabral junction of porcine acetabular tissue.

In non-linear multiphoton imaging, the depth and suitability of the technique used depends on the inherent tissue properties and the power of the laser used. The total depth penetration can be up to 500µm. This allows for thicker, intact sample imaging without needing several processing steps in staining and sectioning tissue before imaging. Additionally, the tissue can be investigated three-dimensionally, allowing changes in the z-axis to be observed, which is advantageous in this study as it can help track the alignment and trace the orientation of collagen fibres, especially at the boundary between the fibrocartilaginous labrum and the articular cartilage which has not been imaged with such high resolutions or depth to date. Porcine acetabulum samples can be imaged without exogenous stains as they contain the required sources of contrast for non-linear imaging methods.

Three main types of non-linear imaging approaches were used to examine tissue in this project, which included second harmonic generation (SHG), two-photon fluorescence (TPF) and coherent anti-stokes Raman scattering (CARS) multiphoton modalities. In addition, polarisation-sensitive non-linear microscopy (pSHG) was also used to observe collagen fibres and bundles' orientation and local arrangement. The difference in these methods is the wavelengths of the light produced from the interactions between the laser and molecules within the tissue. Different signals are produced and picked up via detectors which reveal various tissue features.

Multi-photon imaging of biological tissues involves multiple photons interacting with the key molecules of the tissue called sources of contrast, such as molecules which comprise in collagen. The interactions occur within the focal point of the laser beam, which has a large penetration depth, allowing thicker cross sections of samples to be used.

5.3 Sources of contrast in non-linear microscopy

When compared with other imaging techniques, multiphoton imaging has several benefits over other imaging techniques with higher lateral and axial resolution, depth penetration, without requiring the need for exogenous stains and complicated tissue preparation steps.

Spontaneous anti-stokes Raman spectroscopy requires infra-red laser excitation sources, and the signal produced is in the infra-red range at a shorter wavelength. The source of contrast is from molecular bond vibrations, e.g., CH₂ bonds found in key tissue components such as GAGs, water, lipids, DNA, and the conformational state of collagen.

SHG microscopy requires an infrared laser source to produce light in the visible range. The sources of contrast are molecules lacking inversion symmetry, a key feature of collagen. It is the current gold standard for imaging the microstructure of unstained collagen as it is a strong emitter of SHG light. pSHG microscopy is a subset of SHG microscopy, which relies on asymmetry and arrangement of molecules such as collagen fibres. This technique works on the same principles as SHG but with a rotating polarising film, and a signal is detected at each degree of rotation and then stacked to allow the overall features and all molecules to be highlighted. Along with the structure and compositional data, polarisation can report a measure of the organisation at the molecular scale. SHG light from collagen depends on the polarisation of the laser excitation beam compared to the long axis of the collagen fibres.

TPF microscopy requires an infrared laser source producing light in the visible range with a longer wavelength emitted than SHG. The source of contrast is from endogenous fluorophores such as elastin fibres and collagen cross-links.

5.4 Microscope Systems used for Multi-Photon Imaging

The multiphoton imaging conducted in this study used a Microscopy system 2 which is described in detail by (Mansfield, 2008). This microscope system involves simultaneous forward and epi-detection combining CARS with TPF and SHG multiphoton imaging. The Olympus FluoView microscope system was used for SHG, TPF and CARs imaging in forward and back-scattered directions. The system consisted of the Olympus IX71 inverted microscope and the Olympus FluoView 300 scanning system. Image acquisition was

controlled through FluoView version 5 software. For SHG and TPF imaging, the laser excitation light was from a Ti:Sapphire laser. The laser system (Coherent) consisted of a Mira 900 Ti:sapphire laser pumped by a Verdi (V10) laser (532nm). The maximum power output of the Mira was 1.5W and its wavelength is tuneable between (690nm and 990nm) with a repetition rate of 76MHz and pulse width of 200fs for both SHG and TPF imaging. The output of this laser was horizontally polarised. For CARS imaging, the laser excitation light was from a picosecond pulsed output from a Levante OPO pumped by a HighQ Picotrain laser which produces a 6 pico-second pulsed output at 532 nm, with a repetition rate of 76MHz and a maximum power of 10W. In the OPO the 532 nm is converted into two longer wavelength beams in a non-linear crystal.

5.5 Materials and Methods

For preliminary method development and assessment of the appropriateness of multiphoton imaging of porcine labrum samples, a porcine hip joint was dissected as described in Chapter 2 representing the unloaded native sample which would serve as the initial control to help understand the features which could be observed using multiphoton imaging and its compatibility in terms of sources of contrast. The following section describes the details of the tissue, which was imaged, the materials and equipment used to prepare the tissue for imaging, The preliminary findings are described in Section 5.6.

A freshly dissected native porcine hip joint (86.2 Kg, Yorkshire Farms) sourced and dissected as per Chapter 2.2.2. Only the acetabulum was used for imaging, the femur of the joint was kept frozen. It should be noted that as the nature of this study involved multidisciplinary work in multiple labs across two universities, the tissue underwent several freeze-thaw cycles between the mechanical testing, storage, and transportation to the University of Exeter from the University of Leeds.

Conventional photogrammetry was used to investigate the labrum and the chondro-labral junction during and after simulation to record any macroscopic features and changes during testing for features to be later aware of when using multiphoton imaging for example. Samples

were also investigated for chemical composition to identify changes in collagen and proteoglycan hydration content to investigate further the deterioration caused by overloading on the tissue microstructure. This would support the imaging findings provided by the multichannel multiphoton spectroscopy. Following the methods described in Chapter 5, between 9-12, single spectra were taken around the chondrolabral junction of each sample at the fibrous labrum, interface, and articular cartilage. Great care was taken to capture several spectra which best represented the three regions immediately around the chondrolabral junction of each sample. The single spectra were then averaged, producing an average single spectrum produced by the imaging software of the microscope.

Cryosectioning

A handheld bone saw was used to extend the cut to the subchondral bone and another cut was made approximately 20mm from the base of the acetabulum to remove the samples. Sections extracted from the acetabular labrum were taken from the anterior, superior, and posterior regions of the porcine acetabulum. For each region from a single sample, a scalpel blade was used to make an incision from the apex of the acetabulum to the subchondral bone around 5 mm in width as described in Chapter 2 (2.2.3).

Tissue sections for imaging were defrosted for approximately 20 minutes at room temperature before sectioning. Cross sections taken from four quadrants of the acetabulum: superior, posterior, anterior, and inferior were cryosectioned into samples of 7 μ m thickness using a cryotome. Tissue sections were then placed in Petri dishes separated for each region and hydrated with PBS solution.

Embedding media was placed onto a metallic chuck precooled in a cryostat (Figure 5.1). A labral specimen was placed on the semisolid chuck, and more media was added rapidly over the tissue covering the specimen. The chuck with the frozen tissue was placed inside the cryostat chamber, and the quick freeze function was used. Once fully frozen, the chuck was placed in the cryostat and sectioned. The labrum specimens were sectioned again at an optimal temperature between -18°C and -20°C. The optimal cutting thickness was 4-7 μ m for sectioning and 20-40 μ m for trimming. Thin sections were retrieved using a brush or tweezers

and placed immediately onto a glass slide. A PBS droplet was added on top of the specimen and was covered carefully using a coverslip avoiding any bubbles from forming (Figure 5.2). The process was repeated for the rest of the specimens and slides were imaged immediately.

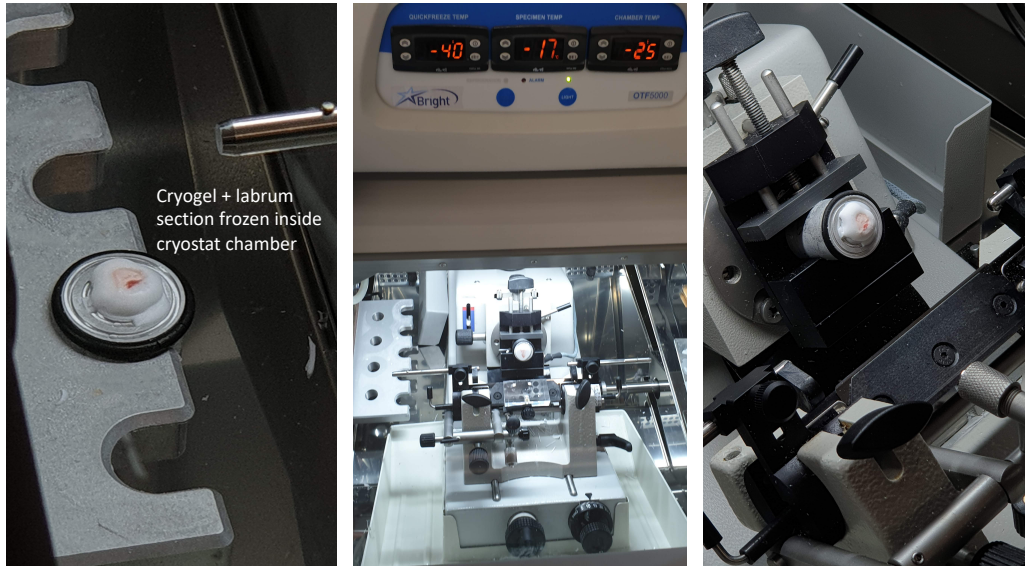


Figure 5.1 – A labral cross section was placed onto a metal chuck and frozen at -25°C using cryogel (left). A cryomicrotome was used to cryosection labral samples (centre). Samples were sliced using the cryomicrotome with $6\text{--}7\mu\text{m}$ sections (right).

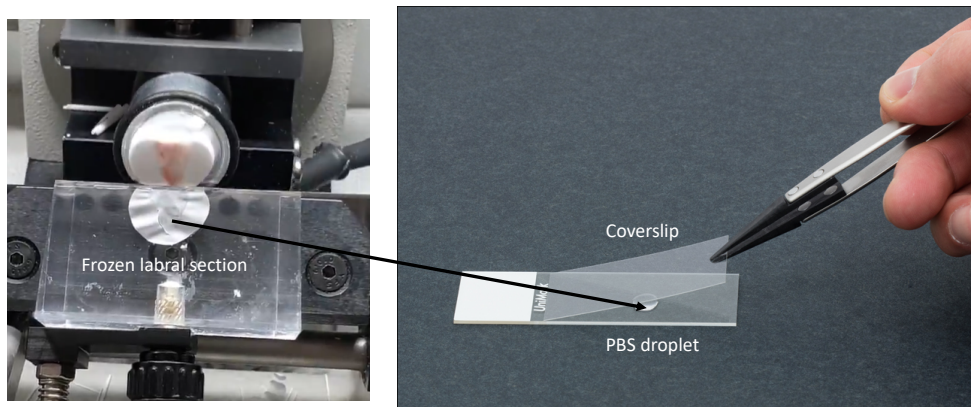


Figure 5.2 – After the frozen embedded labral samples were sectioned, they could frozen sections could be placed directly onto glass slide, hydrated with a PBS and covered with a glass coverslip.

5.6 Results

5.6.1 Multiphoton-imaging of the porcine acetabular labrum

The following section includes representative images of the native porcine labrum imaged using multi-photon imaging. All the images obtained using the multiphoton microscope were resolved at around $0.276\mu\text{m}/\text{pixel}$ providing detail of the collagen fibre bundles, cellular components and non-fibrous tissue. Large area strips were collected from the articular surface, through the chondrolabral junction to the fibrous/dense connective tissue. A full-scale image map was collected through a thinly sliced cross-section of the anterior labrum showing the rounded morphology of chondrocytes and a distinct shift in brightness from the presence of collagen present in the fibrous side of the labrum compared to the internal portion.

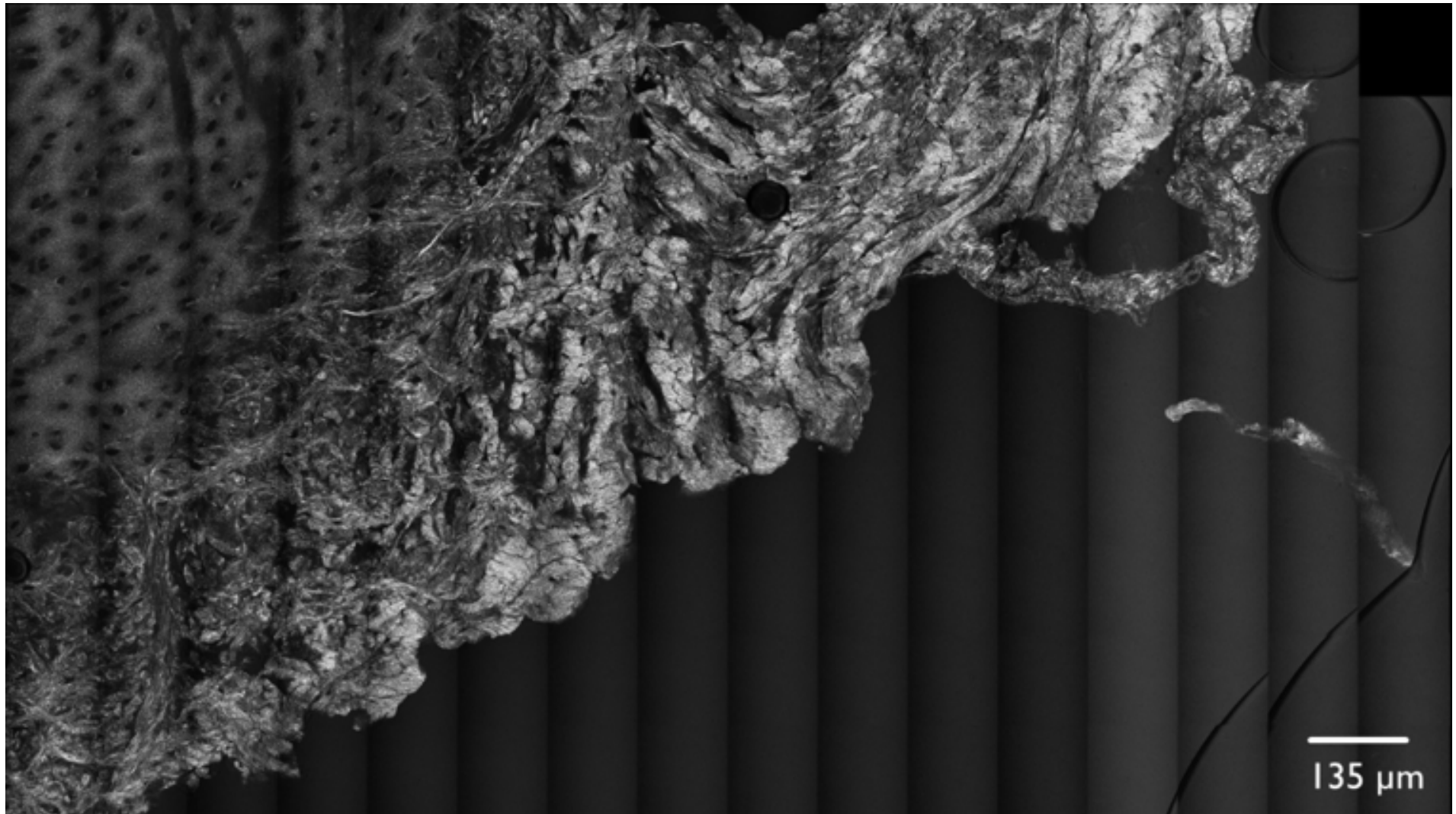


Figure 5.3 – Structure of the anterior acetabular labrum in porcine tissue. Large collagen type I fibres were observed in the external labrum which integrated with thinner fibres at the chondrolabral interface.

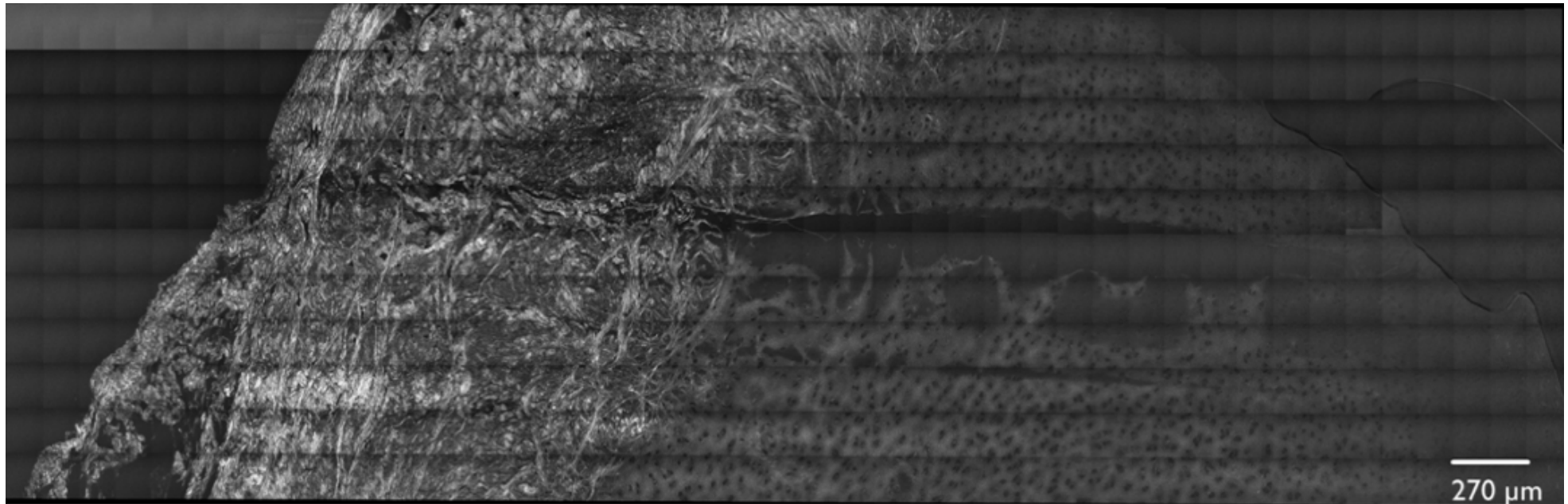


Figure 5.4 – Large map of the posterior acetabular labrum in porcine tissue spanning from the superficial external labrum to the chondrolabral junction and cartilage. A large tear in the form of a processing artefact was observed through the structure, which span across the specimen.

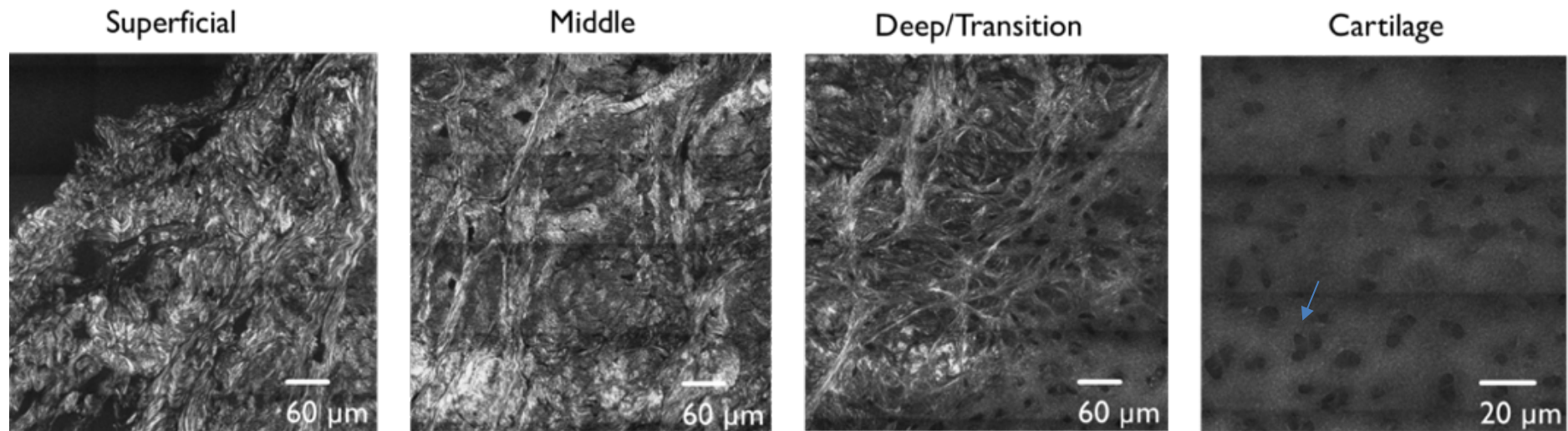


Figure 5.5 – Structure of the posterior acetabular labrum in porcine tissue. At the superficial labrum, large collagen fibres were seen in wave-like patterns. In the middle zone, there was the alignment of large type I collagen fibre bundles. In the deep transition zone, large fibres integrated into the cartilage in a layered arrangement with fibres entangled on each other. Cartilage showed the presence of thin type II fibres in the cartilage matrix.

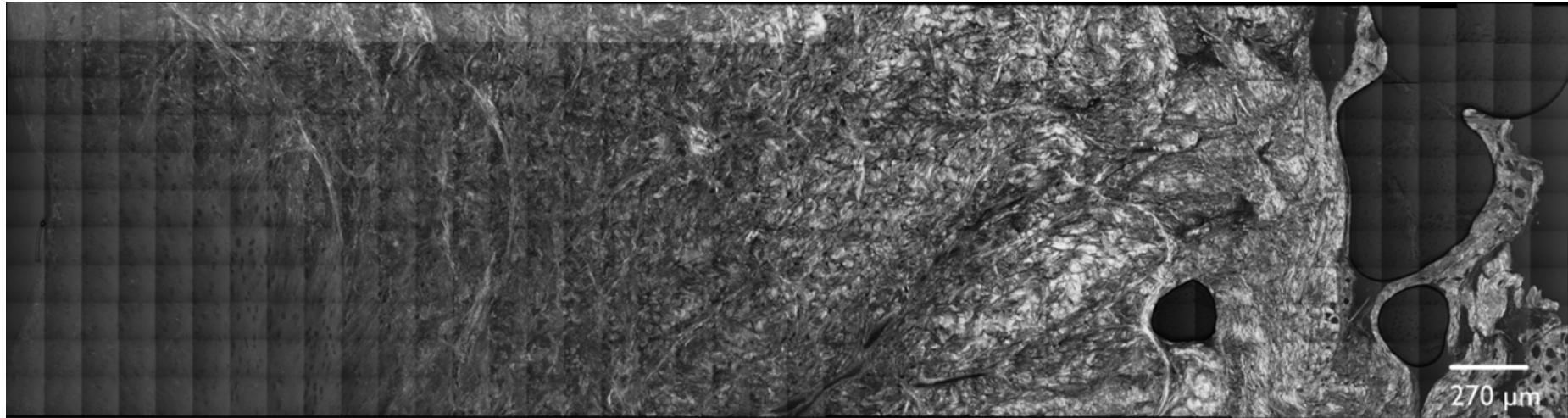


Figure 5.6 – Structure of the superior acetabular labrum in porcine tissue. Large collagen fibres were observed integrating with the cartilage at the interface. A higher signal intensity was observed in the external labrum, with fibres appearing much brighter in this region.

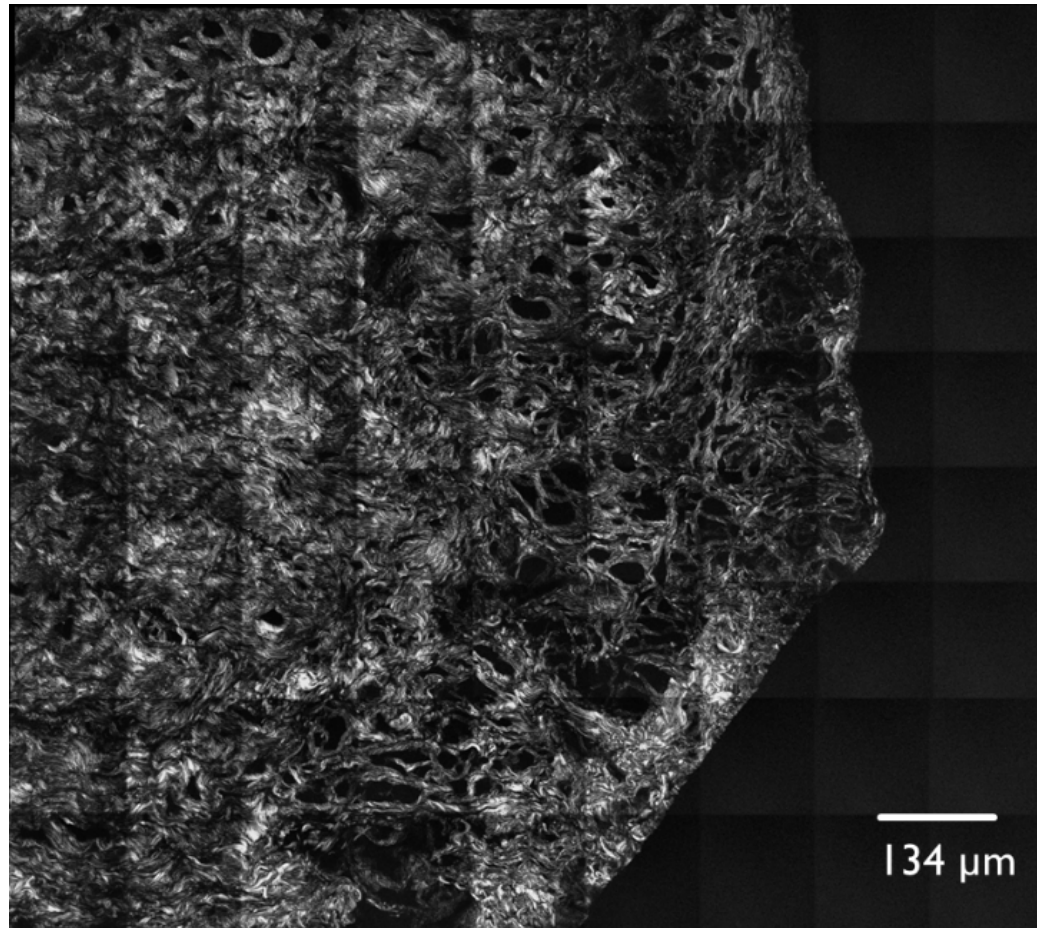


Figure 5.7 – Structure of the anterior acetabular labrum at the external-internal labrum interface. Small holes were observed throughout the structure at the periphery surrounded by collagen fibres. The collagen fibres were arranged in a wave-like pattern across this region.



Figure 5.8 – Full area map of the anterior acetabular labrum in porcine tissue. Banding was observed in the image due to the image capturing process.

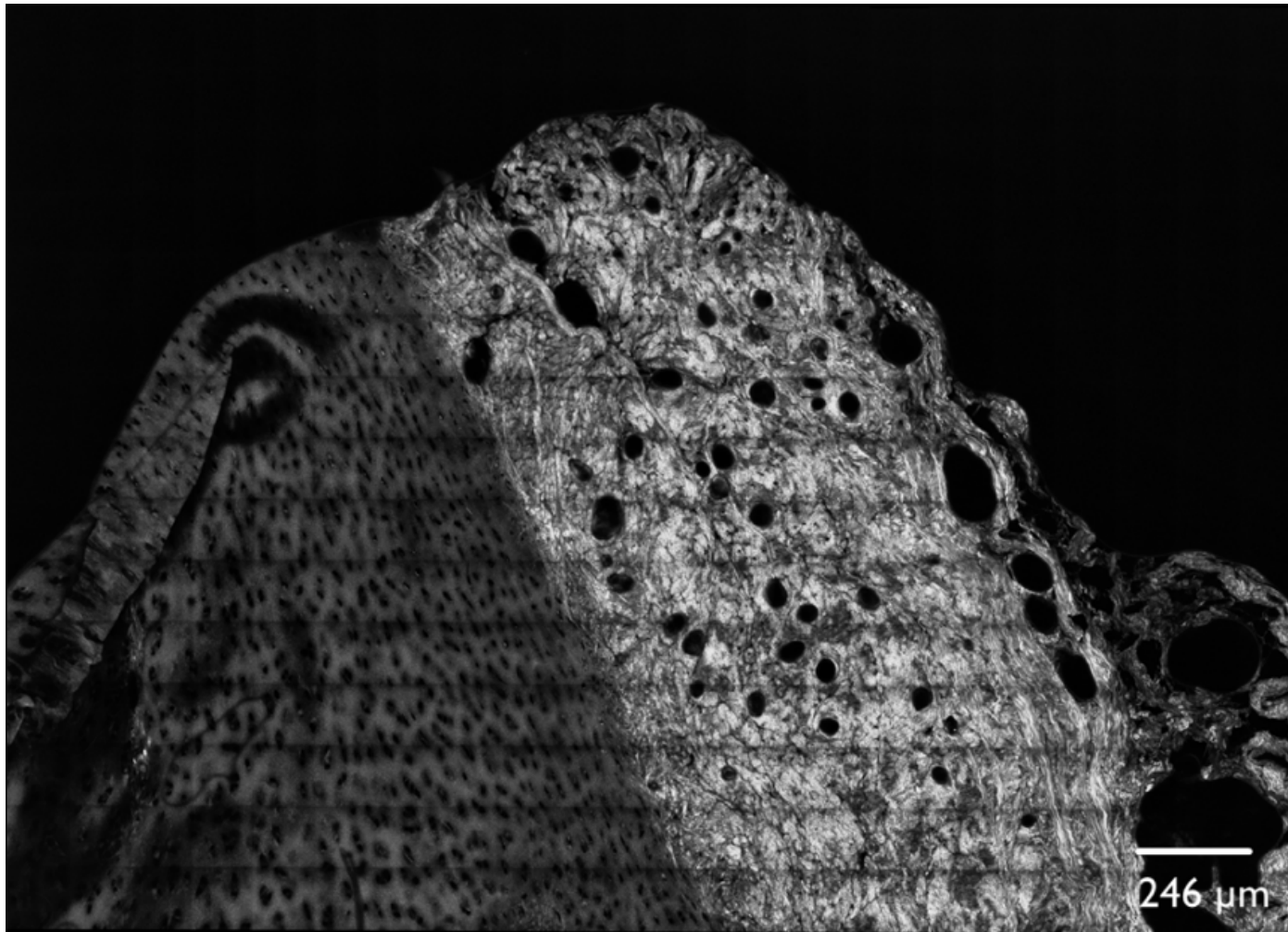


Figure 5.9 – Structure of the anterior labrum at the external-internal interface, small holes were observed in the external fibrous portion. There was a distinct boundary between the cartilage and the external labrum.

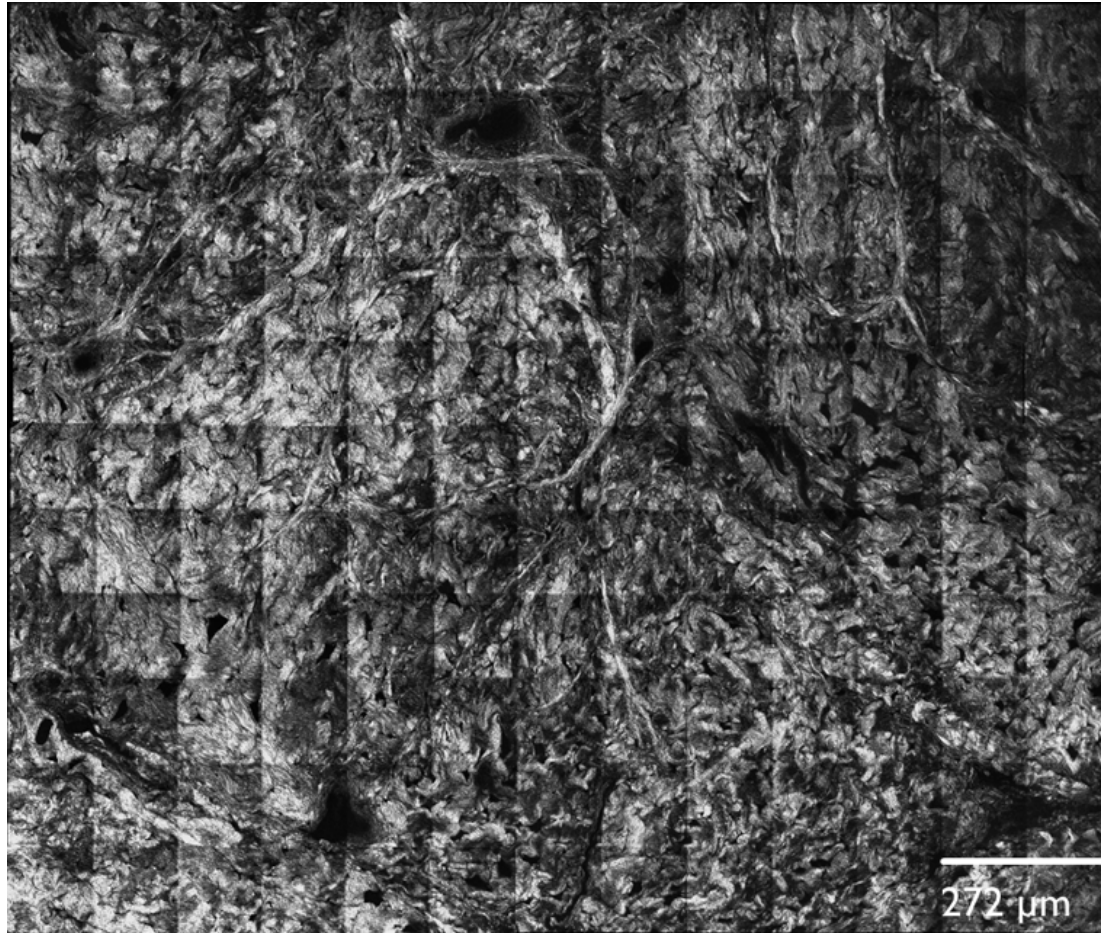


Figure 5.10 – Structure of the fibrous external labrum at the superior side. The external labrum had collagen fibre-like structures of various sizes arranged haphazardly.

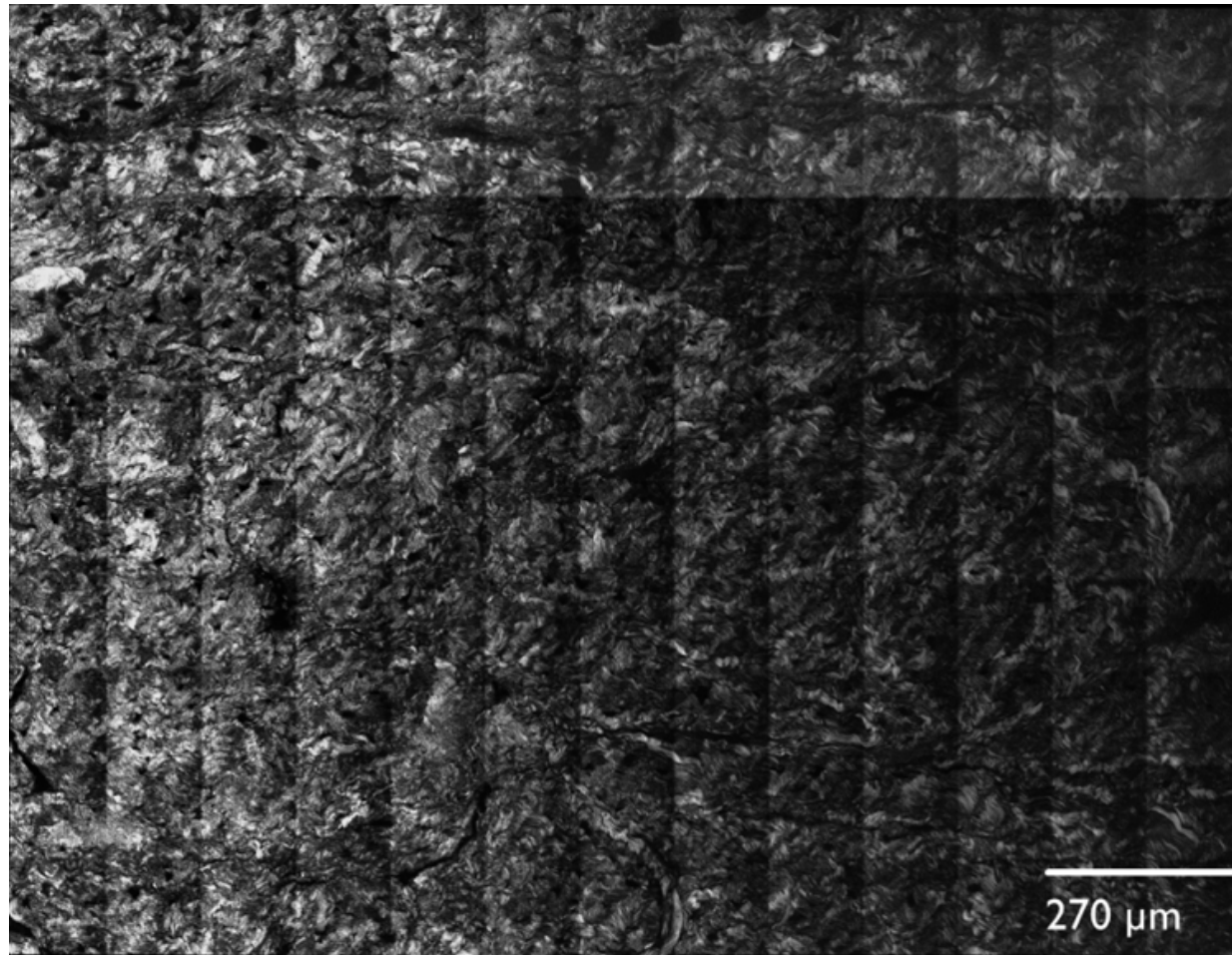


Figure 5.11 – Structure of the internal labrum at the superior side. There was more order and alignment of fibres in this region with fibres assuming a wave-like structure and most fibres being arranged parallel to one another, there were thicker fibres interspersed (bottom right).

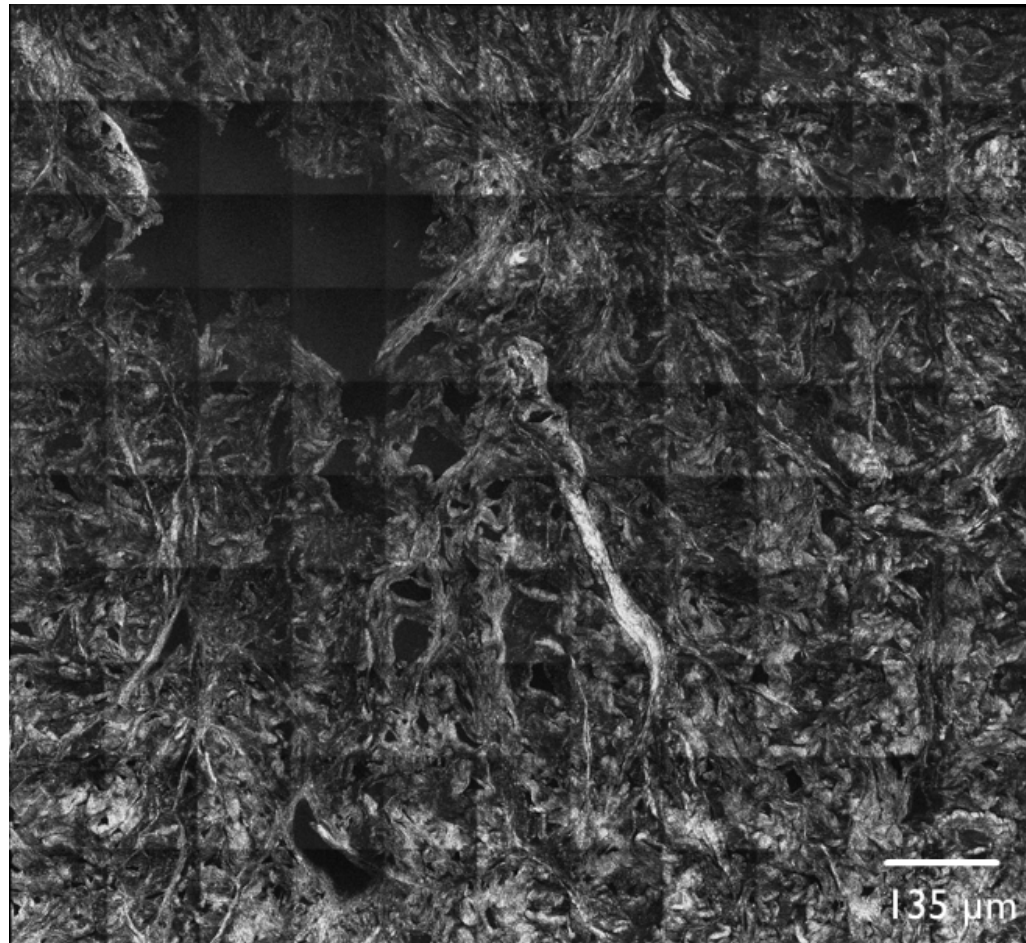


Figure 5.12 – Structure of the internal-external labrum interface at the superior side. The interface had a variety of different-sized collagen fibres arranged non-homogenously. A large, ruptured structure was present at the top left corner surrounded by smaller fibrous tissue structures.

5.6.1 Analysis of Multiphoton imaging of the porcine acetabular labrum

Large collagen type I fibres were observed in the anterior acetabular labrum at the external labrum (Figure 5.3), which integrated with thinner fibres at the chondrolabral interface. At the posterior external labrum, large collagen fibres were seen in wave-like patterns (Figure 5.4 and 5.5). Large type I collagen fibre bundles appeared more aligned in the middle zone in between the chondrolabral junction and external labrum. At the transition zone, large fibres were seen integrated into the cartilage in a layered arrangement with fibres entangled on each other. Thin type II fibres were observed in the cartilage matrix. Large collagen fibres were observed integrating with the cartilage at the interface of the superior labrum specimen (Figure 5.6). A higher signal intensity was observed in the external labrum, with fibres appearing much brighter in this region when compared with other samples. This higher intensity was generally present in the external labrum. The external-internal labrum interface had small holes throughout the structure (Figure 5.7) at the periphery surrounded by collagen fibres in the anterior acetabular labrum. The collagen fibres were arranged in a wave-like pattern across this region. Banding was observed in the image due to the image capturing process (Figure 5.8). There was a distinct boundary between the cartilage and the external labrum in an anterior labrum specimen (Figure 5.9). The external labrum had collagen fibre-like structures of various sizes arranged haphazardly (Figure 5.10). There was more order and alignment of fibres in the internal labrum at the superior region (Figure 5.11) with fibres assuming a wave-like structure and most fibres being arranged parallel to one another. The interface of internal-external labrum interface at the superior side had a variety of different-sized collagen fibres arranged non-homogeneously (Figure 5.12). A large, ruptured structure was present at the top left corner surrounded by smaller fibrous tissue structures.

5.7 Discussion

This chapter establishes the developments and methodology for imaging porcine acetabular tissue using non-linear imaging techniques. The multiphoton images revealed differences in structure present throughout the native labrum, as well as differences in composition in the different regions of the acetabulum. The images revealed a heterogeneous arrangement of collagen fibres, likely collagen I fibres due to their thick size and shape (Chen *et al.*, 2012) through different regions of the labrum. The thick collagen fibres detected in the external labrum were haphazardly arranged. The overall structure matches the previous findings of the H&E staining in Chapter 2 however, due to the increased resolution and magnification provided by multiphoton imaging, features of the microstructures such as cells, lacunae of the articular cartilage, small 5-20 μm sized blood vessels, collagen type I and II fibres along with larger bundles and fibrils were visible.

In nearly all samples, there was a higher presence of visible cells in the tissue likely caused by the age of the tissue reflecting immature porcine cartilage structure (Benjamin and Ralphs, 2004; Julkunen *et al.*, 2009; Eleswarapu, Responde and Athanasiou, 2011). Some of the heterogeneity of collagen fibres was hypothesised to change with age. As there are few studies available which compare the acetabular labrum structure to adult human acetabulum, the use of cadaveric samples would help differentiate any changes to the structure of the collagen fibres.

It would be beneficial to use multiphoton imaging to compare mature porcine tissue to cadaveric human acetabular labrums, with or without labral pathology due to the high resolution offered by non-linear imaging. In addition, this would allow comparisons with the human acetabulum presented in SEM images (Petersen, Petersen and Tillmann, 2003) and the morphology reported by (Seldes *et al.*, 2001b; Philippon, Arnoczky and Torrie, 2007; Kohl *et al.*, 2011; Pallan, 2016; Schon *et al.*, 2020).

Multiphoton has shown to resolve individual collagen fibres and ultrastructure of the extracellular matrix without the need for exogenous stains, it meets the proposed application for determining changes to collagen fibre alignment, orientation, arrangement, and general disruption. It can be applied as part of a methodology to understand the micromechanics and biomechanical response to load, as samples can be extracted and imaged after experimental hip simulation. This would allow features of chondrolabral damage such as fraying, fibrillation, and tearing to be studied in detail.

Studying the microscale structure of the labrum allows structural changes associated with degeneration to be observed. In the future, it may provide the link between labral tearing and progression onto the early onset of osteoarthritis (Battistelli *et al.*, 2023). Insight into why labral tearing often occurs in the anterior-superior region, and if this is related to function alone, or a function-induced change to the tissue can be determined. Observing how collagen and GAG arrangement is altered with loading can reveal important details on the mechanical behaviour of the tissue and how it degenerates. Clinicians use MR arthrography (Aydingöz and Öztürk, 2001) routinely to determine the condition of the labrum and cartilage, to identify labral tearing or chondral defects and to determine the bone shape. This technique cannot help the clinician to determine how femoroacetabular impingement resulted in a particular type of labral tearing, how the degeneration progressed with time or how it may link with associated chondral injury or early onset of osteoarthritis (Czerny *et al.*, 1996; Aydingöz and Öztürk, 2001; Stelzeneder *et al.*, 2012).

There are a limited number of studies which have investigated the arrangement of the collagen matrix structure in the acetabular labrum and how this is disrupted under abnormal loading conditions. Histological imaging and immunohistochemistry conducted through conventional brightfield imaging have been used in research to characterise the structure of the human labrum. Immunohistochemistry was used by

Pallan (2016) to reveal the collagen type present in the labrum, where the presence of type I and II collagen was detected in the acetabular labrum.

Petersen, Petersen and Tillmann, (2003) reported the first images and descriptions of the microstructure and arrangement of collagen fibrils using scanning electron microscopy (SEM). They reported differences between the inner and external labrum separating structures into dense connective tissue and fibrocartilage. Vascularity was present in the inner regions of the labrum, suggesting healing potential. SEM images of collagen bundle and fibre arrangement in zones throughout the labrum cross-section were shown; however, processing methods during extraction of the labrum were undesirable and may have led to artefacts in the collagen arrangement being reported due to the invasive nature of extraction and fixation required.

Compared to the findings of Petersen, Petersen and Tillmann, (2003), the acetabular labrum was found only to be aligned in specific regions of the labrum. Generally, there was nonhomogeneous arrangement of thick collagen type I fibres in the external labrum, as supported by similar findings in Chapter 2. These differences could be due to the regional variations found across the acetabular labrum, the age of tissue or the differences between human and porcine labrum. As human acetabulum has yet to be investigated with multiphoton imaging, it is difficult to compare the exact arrangement of collagen fibres.

Cartilage has been characterised before by Mansfield, (2008). The cartilage structure of the acetabular labrum sections was similar to the structure found in equine articular cartilage, thin type I collagen fibres were detected in the matrix of the cartilage, however, with SHG imaging, it was not determined if elastin was present (Mansfield *et al.*, 2009).

Non-linear methods such as multiphoton imaging provide similar or higher resolution than SEM. They can minimise the processing artefacts, as they are not dependent on using exogenous stains and do not require specialised fixation methods. Additionally, the imaging technique can use thicker samples exhibiting their

endogenous fluorescence, thus making live imaging possible. To better understand the progression of damage due to abnormal loading, combining non-linear imaging methods may provide detailed insight into the microstructure and allow visualisation previously not possible with other techniques.

As this was the first time porcine acetabulae have been imaged and processed for use with non-linear methods, there were challenges in development which can be further optimised in the future. While the tissue was suitable and largely like the cartilage from equine tissue which had been previously used with the same methods the main limitation for use was selecting the optimal thickness of the sample, holding the position of the sample, and keeping the surface flat for the duration of the capture duration.

There were limitations with the method; the samples must be as fresh as possible to have the highest image quality and signal. The samples in the current had undergone several freeze/thaw cycles, there were some issues with bubble formation and issues with adherence of the coverslips which were held by the surface tension between the tissue-PBS and glass.

While fresh labrum samples do not require staining, and samples can be excised and imaged immediately compared to the approximately 1.5 weeks required for imaging stained and paraffin-embedded samples. However, preparing these sections was difficult due to the cryosectioning requiring an optimal specimen temperature to cut the tissue effectively.

There were limitations with the method, the samples must be as fresh as possible to have the highest image quality and signal. The samples in the current had undergone several freeze/thaw cycles. Therefore, there were some issues with bubble formation and issues with adherence of the coverslips which were held by the surface tension between the tissue-PBS and glass.

Slides which were not immediately used were stored at -20°C until required. However, to keep samples as fresh as possible coverslips were added when the

tissue was fully thawed and were subsequently rehydrated, these samples were comparatively clearer and of higher quality. In the future, a z-stack would allow the preferred orientation of fibres to be visualised and by varying the polarisation angle, the ability to trace all the fibres (Borile *et al.*, 2021).

Furthermore, preparing these sections was difficult due to the cryosectioning requiring an optimal specimen temperature to cut the tissue effectively. Slides which were not immediately used were stored at -20°C until required. However, to keep samples as fresh as possible coverslips were added when the tissue was fully thawed and subsequently rehydrated, these samples were comparatively clearer and of higher quality. In the future, a z-stack would allow the dominant direction and orientation of fibres to be quantified and by varying the polarisation angle to trace all the fibres.

Chapter 6 Investigation of Chondrolabral Damage using Non-linear Imaging Methods

6.1 Introduction

After completing the initial pilot studies, labral tearing was hypothesised to occur when abnormal bony morphologies such as cam deformities rub against the anterior-superior margin where increased loading, shear forces and instability at the rim would result in chondrolabral separation.

In Chapter 4 peripheral labral tearing at the anterior-superior labrum was generated from overloading the chondrolabral junction.

The non-linear microscopy techniques established in Chapter 5 showed that it was possible to characterise the ultrastructure of the extracellular matrix at the microscale. Investigations into the anterior, posterior, and superior regions of the unloaded native porcine labrum, revealed differences in the distribution and arrangement of Collagen type I and II fibres adjacent to the chondrolabral junction. The fibrous margin was distinct and thicker posteriorly than the anterior-superior labrum samples. In addition, the anterior chondrolabral junction had a distinct interface separating large cartilaginous and fibrous regions with an unexpectedly high number of small blood vessels in the external fibrous region.

This suggested that there was potential for repair in a developing porcine labrum, and it was structurally designed for resisting compressive loads (due to a larger cartilaginous region), making it more flexible and compliant when the femoral head would make contact but more susceptible to tearing when exposed to shear or tensile forces at the margin.

This chapter addresses a major gap in the literature by characterising the porcine labrum which was mechanically overloaded using natural hip simulation to allow sub-micron level characterisation of the chondrolabral margin in anterior-superior and posterior labrum samples. This would allow microscale effects on the collagen matrix

microstructure to be studied, concentrating on changes to type I and type II collagen fibres present at the chondrolabral junction.

Understanding the disruption of the collagen matrix at the chondrolabral junction can improve our understanding of the damage to the anterior-superior rim of the acetabulum. This can allow damage generated via experimental simulation to be evaluated.

6.2 Chapter aims

The aims of the study were:

- To determine how overloading the acetabular rim changes the collagen matrix orientation and arrangement at the chondrolabral junction.
- To investigate differences in the microstructure surrounding the anterior-superior and posterior-superior chondrolabral junction.
- To determine how damage induced by mechanical loading appears in the microstructure of the chondrolabral junction.

The objectives were:

- To determine the type, orientation, and distribution of collagen fibres around the chondrolabral junction of unloaded and loaded labrum tissue using multimodal multiphoton (SHG, SRS and TPF) imaging.
- To determine if there was a change in the microscale orientation and alignment of collagen fibres in response to loading from mechanical simulation.
- To determine how damage altered the overall microstructure at the anterior-superior region and predict why the labrum is more susceptible to damage anteriorly.

6.3 Methods

This section contains the characterisation of porcine labral samples, where the chondrolabral junction was imaged with non-linear imaging techniques. The mechanical testing and simulation were conducted at the University of Leeds, and samples were then imaged and characterised at the University of Exeter. This characterisation focused on determining the effects overloading had on the microstructure and the imaging techniques developed by Dr Jessica Mansfield (Mansfield, 2008). This study did not cover specific technical details and aspects of the biophysics required in applying non-linear imaging techniques to porcine labral tissue and the specific technical aspects of SHG that correspond to the observations that would be investigated in the future.

6.3.1 Samples available for imaging analysis

Initially, this study was designed to compare the samples tested in Chapter 4 to analyse those loaded under dynamic torsion and overloading simulations. Unfortunately, a large majority of these samples were lost or severely degraded due to being defrosted at room temperature where a Freezer containing samples from Chapter 4 was being held. This impacted the data set to be used for imaging. The initial aim was to determine the extent of deterioration to the glycosaminoglycan content and changes in the arrangement of collagen fibres from abnormal loading. Due to the deterioration, it was difficult to use these samples which were defrosted for up to a week at room temperature along with several freeze-thaw cycles which would compromise the analysis of the ECM. These challenges were explained in Chapter 5 where deteriorated samples are featured; fortunately, it was still possible to demonstrate how the collagen fibres were arranged where chondrolabral tearing is presented in some samples, as major structures remained largely intact and reflected the damage generated from the mechanical simulation. Some of these samples were included in the results as they showed examples of intrasubstance and peripheral anterior-superior labral tearing.

To allow a more thorough examination without external factors influencing the ECM architecture and composition, four porcine samples were freshly dissected following methods described in section 2.2.2. The tissue included:

- One porcine joint which was freshly prepared was unloaded with no observable damage present.
- Three porcine hip joints (one per experimental condition) consisting of:
 - Sample 1 - Scaled loaded tissue – twin peak axial load of 900N, motion: flexion-extension 20°, abduction-adduction 8.8° to -4.8°, internal-external rotation -10° to 2°, duration 4 hours (14400 cycles), frequency 1 Hz. Ringer's solution as a lubricant. Potted at 35° acetabular inclination.
 - Sample 2 Overloaded loaded tissue – twin peak axial load of 1130N, motion: flexion-extension 20°, abduction-adduction 8.8° to -4.8°, internal-external rotation -10° to 2°, duration 4 hours (14400 cycles), frequency 1 Hz. Ringer's solution as a lubricant. Potted at 35° acetabular inclination.
 - Sample 3 Overloaded loaded tissue – twin peak axial load of 1340N, motion: flexion-extension 20°, abduction-adduction 8.8° to -4.8°, internal-external rotation -10° to 2°, duration 4 hours (14400 cycles), frequency 1 Hz. Ringer's solution as a lubricant. Potted at 35° acetabular inclination.

These samples were re-tested using the overloading testing profile developed in Chapter 4 of pilot study 1. They were immediately sectioned into smaller cross-sections as described in section 2.2.3 and stored at -20°C prepared for storage and transport to the Biophysics lab at the University of Exeter. In total, these samples were exposed to two freeze-thaw cycles and were expected to generate better clearer signals during testing, especially for characterisation with CARS. The four porcine labral samples were divided into three main regions (anterior-superior,

posterior-superior, and superior samples). All samples were then processed and prepared for multiphoton imaging as described in Table 6.1.

6.3.2 Photogrammetry of mechanical testing repeats used for characterisation

A porcine acetabular sample was dissected, and small labral sections were extracted following methods detailed in Chapter 2. Unstained specimen slides were prepared for imaging as detailed in Chapter 5. Similarly, three porcine samples were dissected and tested using methods described in Chapter 4.2 for overloading to induce labral tearing through overloading.

Porcine joints were subjected to experimental simulation testing, with peak axial loads of 1130N and 1340N. This generated anterior-superior tearing in the porcine chondral labral junction as described in Chapter 4.3. after four hours of testing, consistent with the findings reported in Chapter 4. Thus, four samples were investigated for multiphoton imaging, of which some had tears or damage because of the testing as shown in Table 6.1.

Table 6.1: Macroscopic observations of tissue after 14400 cycles (four hours) of simulation.

	Sample	Observation from mechanical simulation
1	Unloaded porcine hip joint (only dissected, control)	Acetabular cartilage surface was smooth and shiny grey/white with no presence of scratches/fissures. Labral surface was in-tact and no damage was seen in connective tissues surrounding the labrum nor at the chondrolabral junction.
2	Loaded porcine hip joint (peak 900N, 4 hrs., 1Hz)	The articular surface was smooth and soft tissue was in-tact. Slight blushing (redness) found below the cartilage surface.
3	Loaded porcine hip joint (peak 1130N, 4 hrs., 1Hz)	A labral tear was found anterior-superiorly. Large Intra-substance labral tear. Increased blushing was found on the cartilage surface as some areas appeared darker than seen previously.
4	Loaded porcine hip joint (peak 1340N), 4 hrs., 1Hz	A labral tear was found anterior-superiorly. Chondrolabral separation. Increased blushing was found on the cartilage surface as some areas appeared darker than seen previously.

These samples were examined using multi-channel multiphoton microscopy. The multichannel set-up consisted of second harmonic generation (SHG) multiphoton imaging, two-photon fluorescence imaging (TPF) and spontaneous Raman spectroscopy (SRS) to visualise changes to collagen fibre alignment and orientation due to overloading.

6.3.3 Multi-channel multiphoton microscopy

Large area maps (sequence of square frame images capturing exposures) covering the entire chondrolabral junction of each sample were taken using multimodal multiphoton imaging. The map covered the essential structures on either side of the cartilaginous-fibrous interface. Two previously tested and deteriorated samples were also included to investigate damaged tissue with unique macroscopic features and intact overall tissue matrix structure (Table 6.1).

Image stacks containing multiple channel data representing SHG, TPF and SRS were processed in Image J (Figure 6.1). The initial tif file was converted into an RGB stack [Image>Type>RGB stack]. The image stack was separated into three channels [Image>Stacks>Stacks to Images]. This produced three different black-and-white images containing SHG (Channel 3), TPF (Channel 2) and SRS (Channel 1). If there was uneven exposure where important features such as collagen were over or under-exposed throughout the whole area strip, images were adjusted to preserve as much detail as possible and provide an even exposure. This was done by adjusting the image contrast [Image>Adjust>Brightness/Contrast]. Images were then assigned colours to represent each channel and then combined creating a composite image which was easier to visualise [Image>Colour>Merge Channels>C1(red) – assigned to SHG image, C2(green) – assigned to TPF, C3(blue) – assigned to SRS>Create composite]. The final composite (Figure 6.2) generated an auto-assigned colour balance between the three source images. If this was causing one channel to overexpose a certain colour, this was manually adjusted by correcting the colour balance [Image>Colour>Colour Balance].

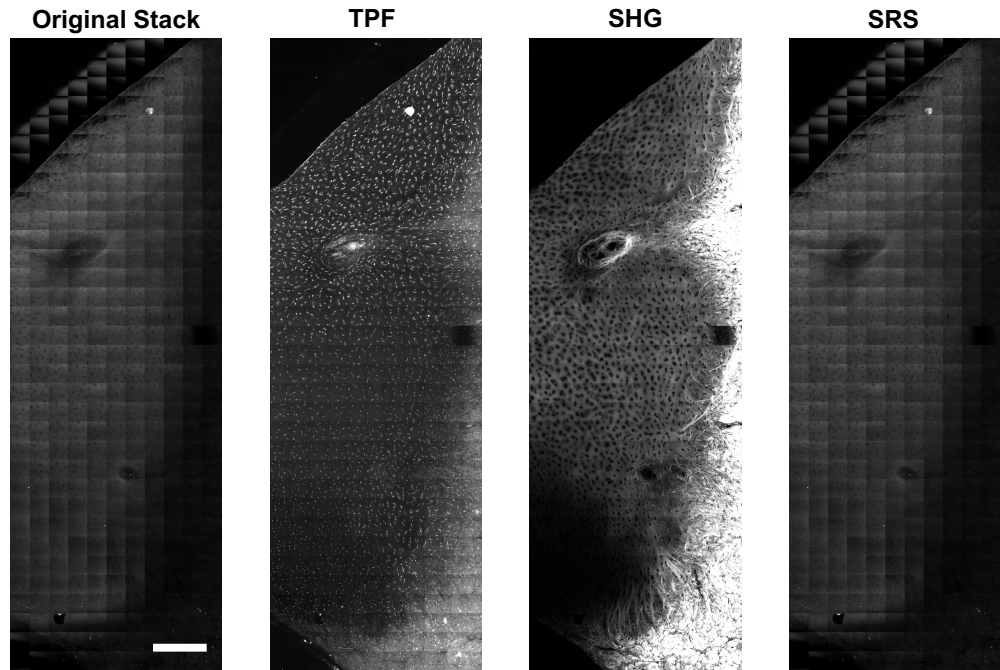


Figure 6.1 - The source file was a tif file containing a stack of TPF, SHG and SRS which were obtained from detectors from three separate channels of the microscopy system. Multichannel multiphoton image strip of anterior porcine labrum under scaled loading. Scale bar: 348.48 μm .

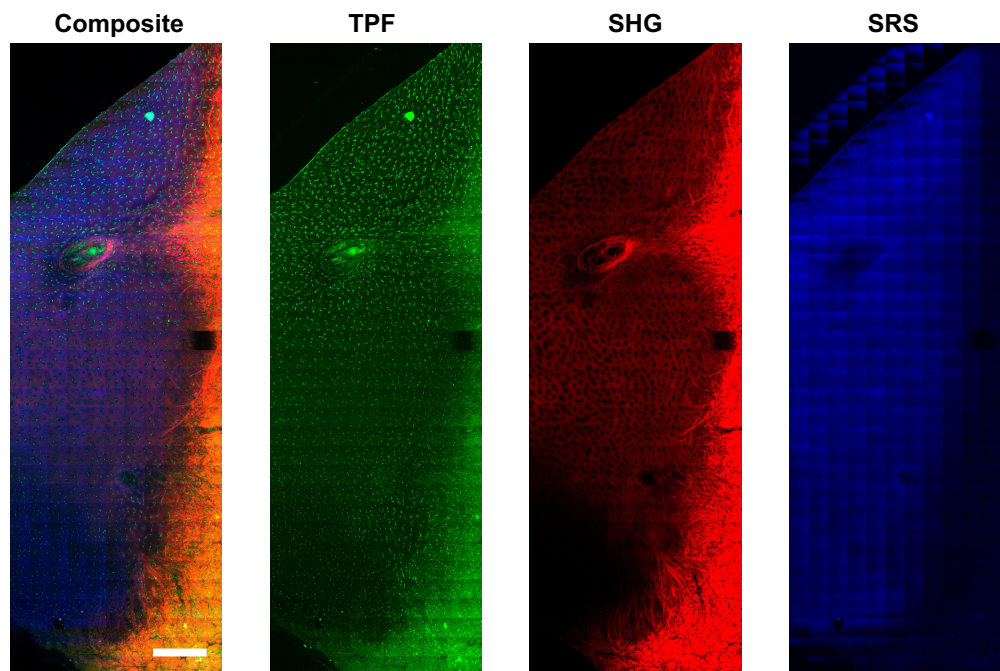


Figure 6.2 – Colour composite images which were created in Image J by combining the multiple channels from TPF, SHG and SRS into green, red, and blue channels respectively. Multichannel multiphoton image strip of anterior porcine labrum under scaled loading. Scale bar: 348.48 μm .

6.4 Results

The following sections contain composite images collected from the multi-channel multiphoton imaging for all samples. Each sample was investigated with a particular focus on the chondrolabral junction, the structure and distribution of extracellular matrix components - particularly to investigate the birefringence, fibre thickness, orientation, and collagen arrangement. The samples were investigated for microstructural changes to show chondrolabral tearing or damage features.

6.4.1 Untested Porcine labrum (Sample 1)

The untested porcine samples had intact chondrolabral margins in all three regions (anterior, posterior, and superior regions). There was an even exposure of the collagen matrix, with type II collagen from the SHG signals, presence of collagen (red) was seen throughout the specimen, with lower intensity detected in the cartilage portion and greater intensity in the labral portion. Collagen appears packed into more dense fibre bundles (linear patches of high signal intensity) in the labrum, while appearing more homogenous (lower intensity, evenly dispersed) in the cartilage. There is a phased transition at the chondrolabral junction where collagen signal gradually increases in intensity and the presence of fibre bundles becomes increasingly frequent as the hyaline cartilage transitions into labral tissue. (Figure 6.3, 6.4 and 6.5). Banding was caused because of the stitching of individual images. Minor channel imbalance and sliding with the SRS channel were generally reduced resulting in less banding, except for the superior region which was more fibrous and may have resulted in sliding during image capture. Overall, there was increased presence of cells detected in all regions through TPF. The autofluorescence could be from the nuclei or lipid droplets found near chondrocytes. SHG revealed that all chondrolabral margins had a distinct interface between the fibrous and cartilaginous regions. Type I collagen fibres were abundant in all three regions in the fibrous region of the labrum. Fine type II collagen fibres were dispersed in the cartilaginous region all throughout depicted by the pinkish-purple hue (Figure 6.3A, 6.4C and 6.4E). The

interface at the chondrolabral junction had varying amounts of large type II bundles integrated with the cellular region (Figure 6.3C). The arrangement and orientation of these fibres also varied with some perpendicular to the interface (posterior and anterior). In contrast, others were parallel (superior) or at acute angles (anterior and superior) to the interface (Figure 6.3D). Finally, there was the presence of high cellular clusters in small cavities within the immature cartilage which suggested the presence of blood vessels or areas where angiogenesis may have occurred, i.e., this has a similar appearance to perichondria papillae as described by (Gabner, Häusler and Böck, 2017) (Figure 6.3B).

6.4.1.1 Anterior labrum (Sample 1)

Chondrocytes were found in lacunae within a type II collagen matrix. The junction had several collagen type I fibre bundles integrating into the cartilaginous and fibrous regions (Figure 6.3C and 6.3D); the fibres generally ran perpendicular to the cartilage, with fewer fibres oriented at different angles aligned more parallel to the chondrolabral junction. The fibrous region (orange) was large with numerous visible cells (stained green). The type I fibres within the fibrous portion were non-homogeneous and ran in several orientations, where cross-sections of collagen fibre bundles and fibres were observed. There were no signs of degeneration to the tissue microstructure.

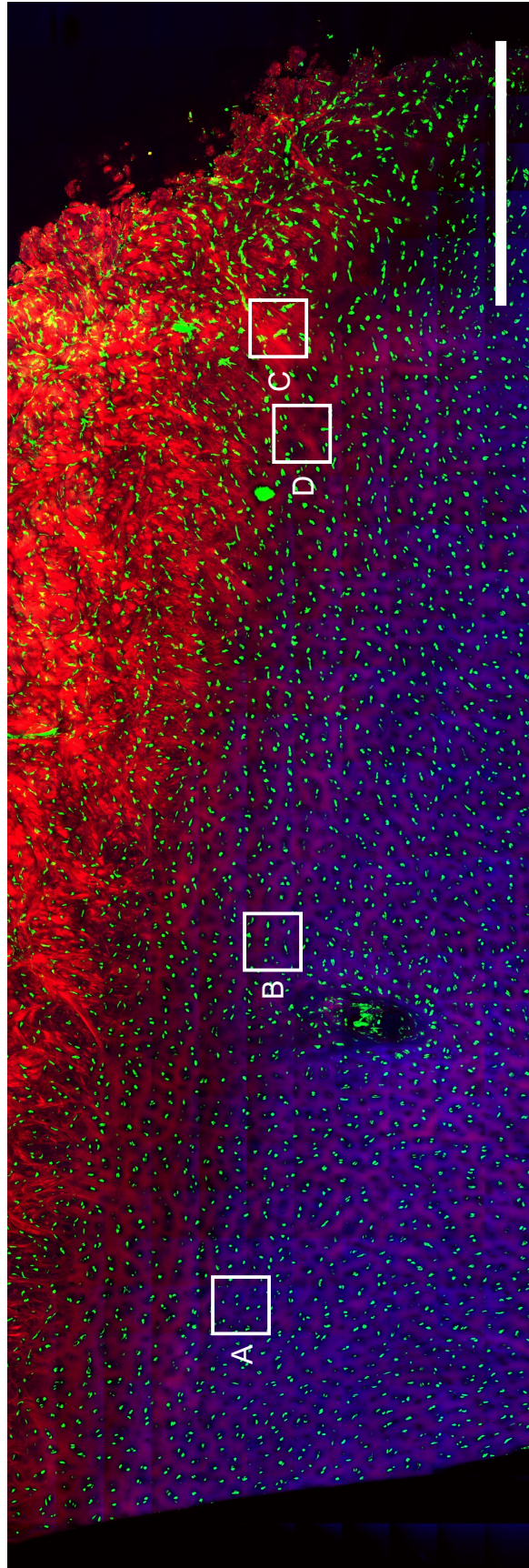


Figure 6.3 - Composite image of the anterior chondrolabral junction area strip from an unloaded, native porcine hip joint. Scale bar: 1042.22 μm (continued overleaf).

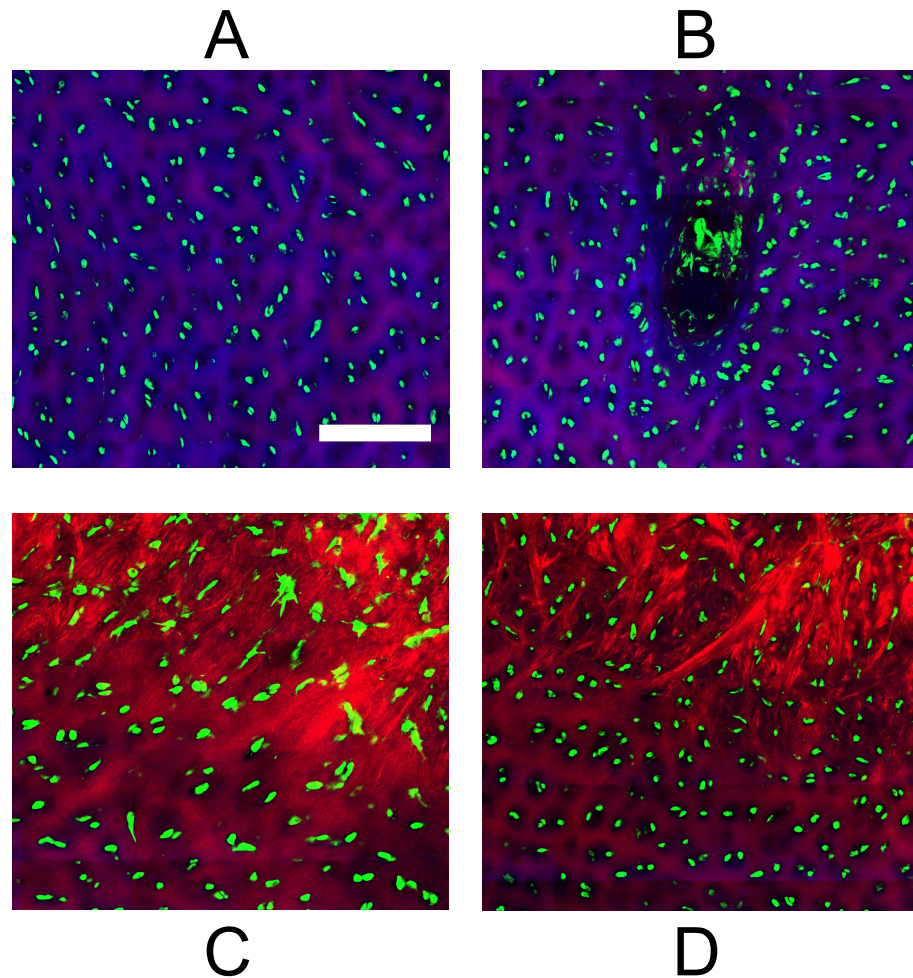


Figure 6.3 - **A** – Chondrocytes shown by a green TPF signal found in lacunae of the articular cartilage. Presence of type II collagen matrix is depicted by the red SHG signal found surrounding the cavities in the matrix. Scale bar: 143.29 μm . **B** – Developing vascular canal found within the articular cartilage, shown by the formation of cells in a large cavity where faint type I and type II collagen can be observed and elastin from thin green TPF signal. **C** – Chondrolabral junction with type II collagen fibres integrating into the fibrous region composed of larger type I collagen fibres and bundles with chondrocytes layered on top of the fibres. Cells had an irregular shape and appeared more elongated within the fibrous portion. Fibres were arranged regularly and almost perpendicular to the chondrolabral junction. **D** – Chondrolabral junction with type I collagen fibres integrating into the cartilage region at different orientations with cells found in layers above and below fibres. Fibres appear more distinct, and cells appear more rounded.

6.4.1.2 Posterior labrum (Sample 1)

The untested specimen had high number of visible cells with small structures resembling vascular canals found within certain areas the cartilage and the fibrous region of the labrum. Chondrocytes were found in lacunae within a type II collagen matrix. The chondrolabral junction had several collagen type I fibrils and large bundles integrating into the cartilaginous region, where fibres ran parallel with each other and perpendicularly to the junction, suggesting strong integration with the cartilaginous region. The fibrous region (orange) was more prominent with thicker type I fibres. Cross-sections of circumferential type I fibre bundles were observed towards the periphery with the cartilage, with fewer fibres integrating perpendicularly with the cartilage. A higher number of blood vessels were detected than in the anterior labrum. Developing blood vessels within this sample could be seen due to the higher green TPF signal with cell cluster formations. There were no signs of degeneration to the tissue microstructure.

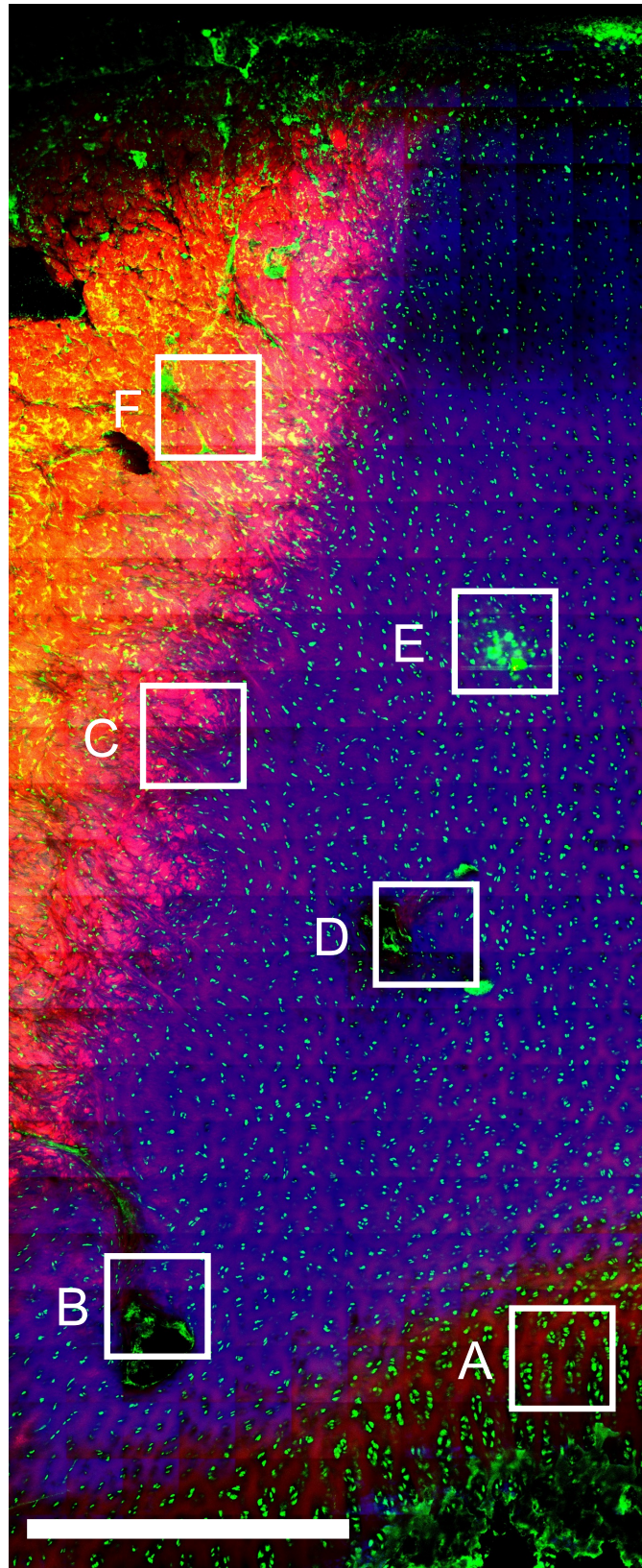


Figure 6.4 – Composite image of the posterior chondrolabral junction area strip from an unloaded, native porcine hip joint. Scale bar: 380 μm (continued overleaf).

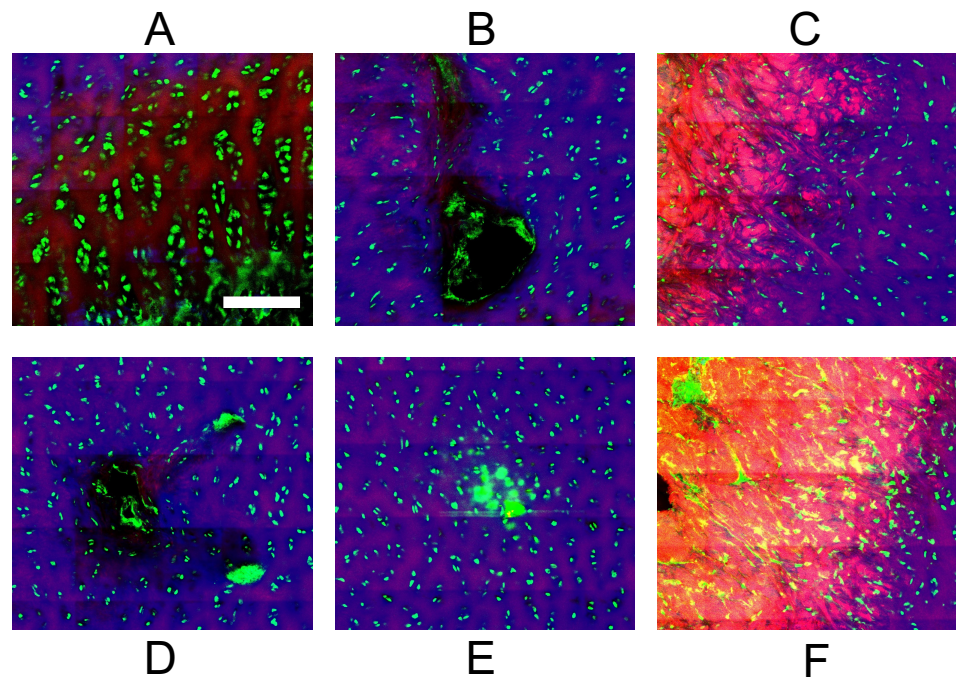


Figure 6.4 – A – deep zone of articular cartilage, with tidemark and calcified cartilage found towards the base. Scale bar: 129.44 μm . B – Vascular canal with extremely long type I fibres extended from the chondrolabral junction deep into the cartilage and surrounding the blood vessel. Type II fibres (red) and thin elastin fibres (green) were observed within the matrix. C – chondrolabral junction with thick type I fibre bundles aligned perpendicular to the fibrous-cartilaginous interface. The fibres appeared to overlap and weave deeper into the fibrous region. Cells were found embedded between collagen fibres and within the lacunae. D – blood vessels found within the cartilage. Type II fibres can be observed within the matrix. E – formation of a cell cluster where a blood vessel would develop in the immature cartilage. F – chondrolabral junction with type I fibres aligned perpendicular to the interface. Highly fluorescent, where the exact structure of collagen bundles cannot be observed in the matrix, suggests a highly dense fibrous matrix and high anisotropy, causing a higher SHG signal to be detected.

6.4.1.3 Superior labrum (Sample 1)

The specimen shows high cellularity with with small structures resembling vascular canals found within certain areas found within the cartilage and the fibrous region of the labrum. The number of cells interspersed with fibres was less than with other regions and was notably reduced near the interface. As with other regions, cells were found in lacunae within a type II collagen matrix. The cartilaginous region was much larger and thicker than the fibrous region within this sample. The junction has several collagen type I fibrils and large bundles integrating into the cartilaginous and fibrous regions, where fibres were interdigitated, and fibres frequently crossed each other but were generally perpendicular to the margin. There were no signs of degeneration to the tissue microstructure.

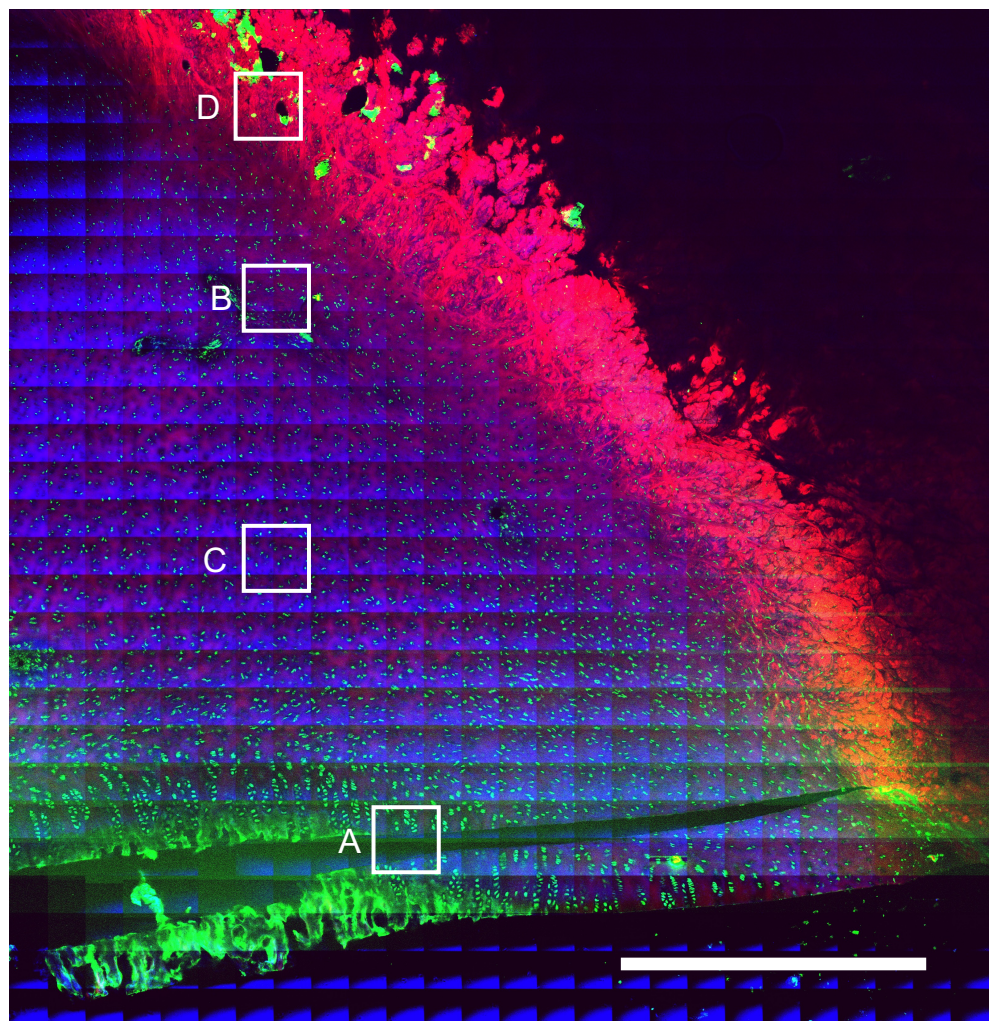


Figure 6.5 – Composite image of the superior chondrolabral junction area strip from an unloaded, native porcine hip joint. Scale bar: 426.28 μm (continued overleaf).

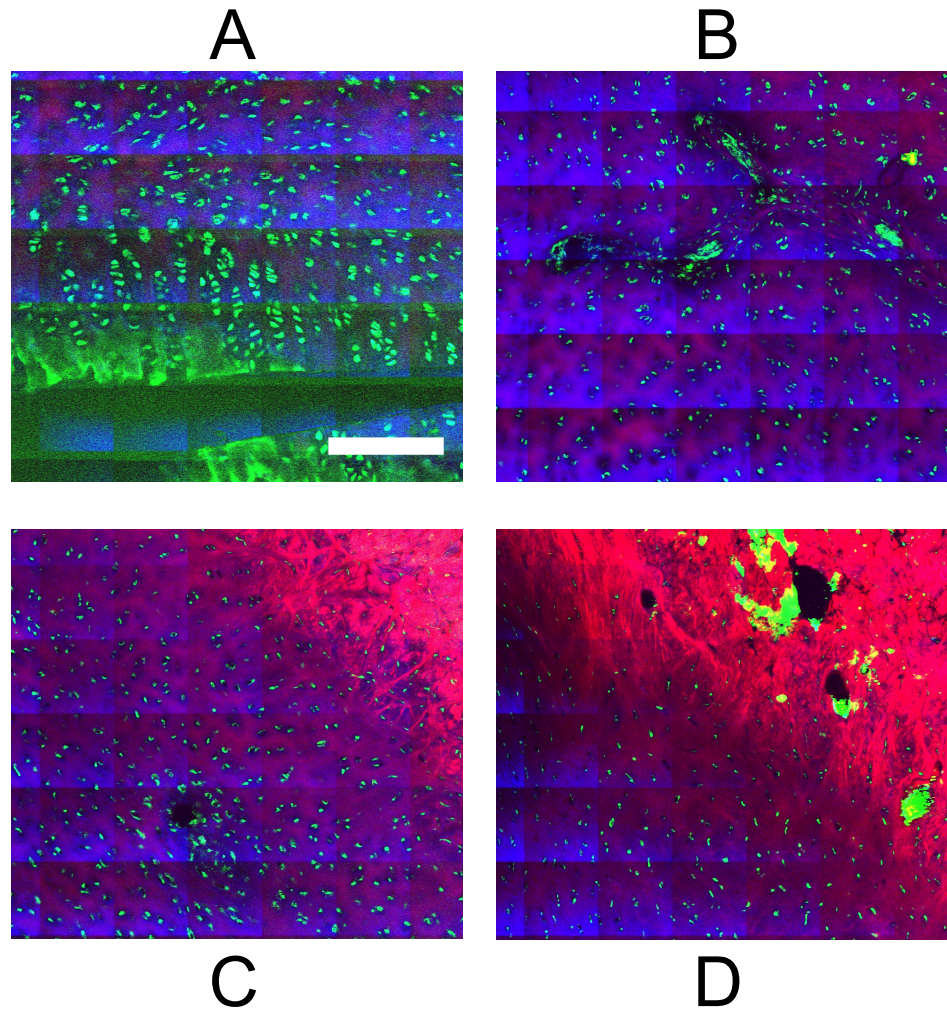


Figure 6.5 – A – Deep zone of articular cartilage, shows the regions of calcified cartilage and chondrocytes in columns and rows. The TPF (green) signal is very noisy in this region producing a grainy image. Scale bar: 192.83 μm . B – Several blood vessels like structures were found within the cartilage which appeared to be collapsing as the development would have ceased, which the presence of type I collagen within the cartilaginous region which was predominantly composed of type II fibres. C – Chondrolabral junction with type I fibres interdigitated with the cartilage. Chondrocytes in lacunae initially run parallel to the chondrolabral junction but

are more loosely packed and in a hollower larger matrix of type II fibres closer to the junction oriented perpendicular to the junction aligning with the type I fibres of the chondrolabral junction.

D – blood vessel like structure found in the fibrous region near the chondrolabral junction. High levels of fluorescence were found close to the blood vessels.

6.4.1.4 Transverse acetabular ligament (Inferior Acetabulum, (Sample 1)

The transverse acetabular ligament was included in the imaging to allow for comparisons with the labrum in the unloaded state. The specimen was composed of dense fibrous connective tissue. Most of the signal was from SHG, with most of the structure composed of type I collagen fibres. There was a considerable lack of cellularity compared with the labrum, with some fibroblasts and fibrocytes being found deep between fibres. The most fibrous regions contained a high order of crimping and waviness to the collagen structure suggesting the TAL is required in resisting tensile forces across the rim. The TAL had several vascular channels throughout the structure. Fine separations and holes also resembled small blood vessels like structures within the fibrous matrix. Some fine elastic fibres were present towards the articular region where the TAL would merge with the cartilage shown as blue due to the SRS signal. Overall, the exposure of the capture was dull in parts which may be due to the uneven surface when preparing the specimen for imaging.

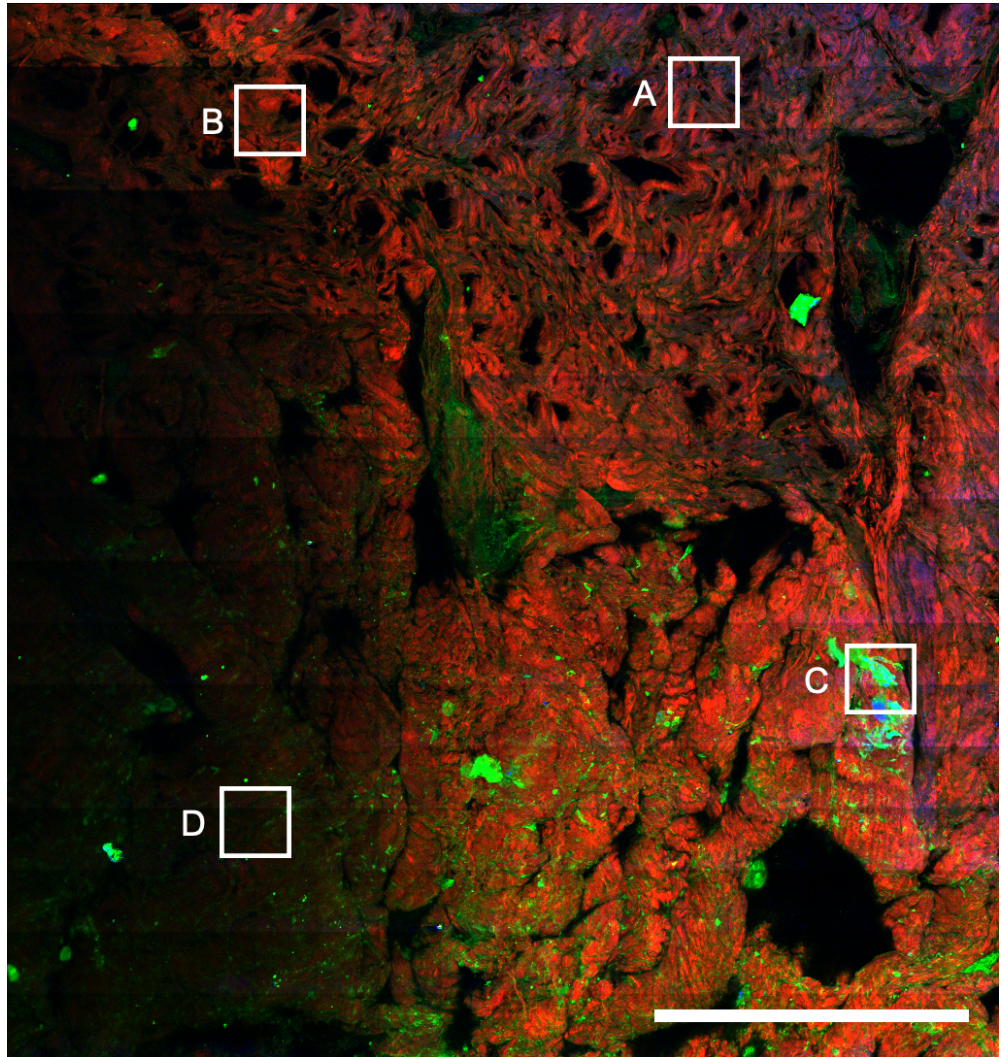


Figure 6.6 – Composite image of the unloaded inferior transverse acetabular ligament from a native porcine hip joint. Scale bar: 507.12 μm . (continued overleaf).

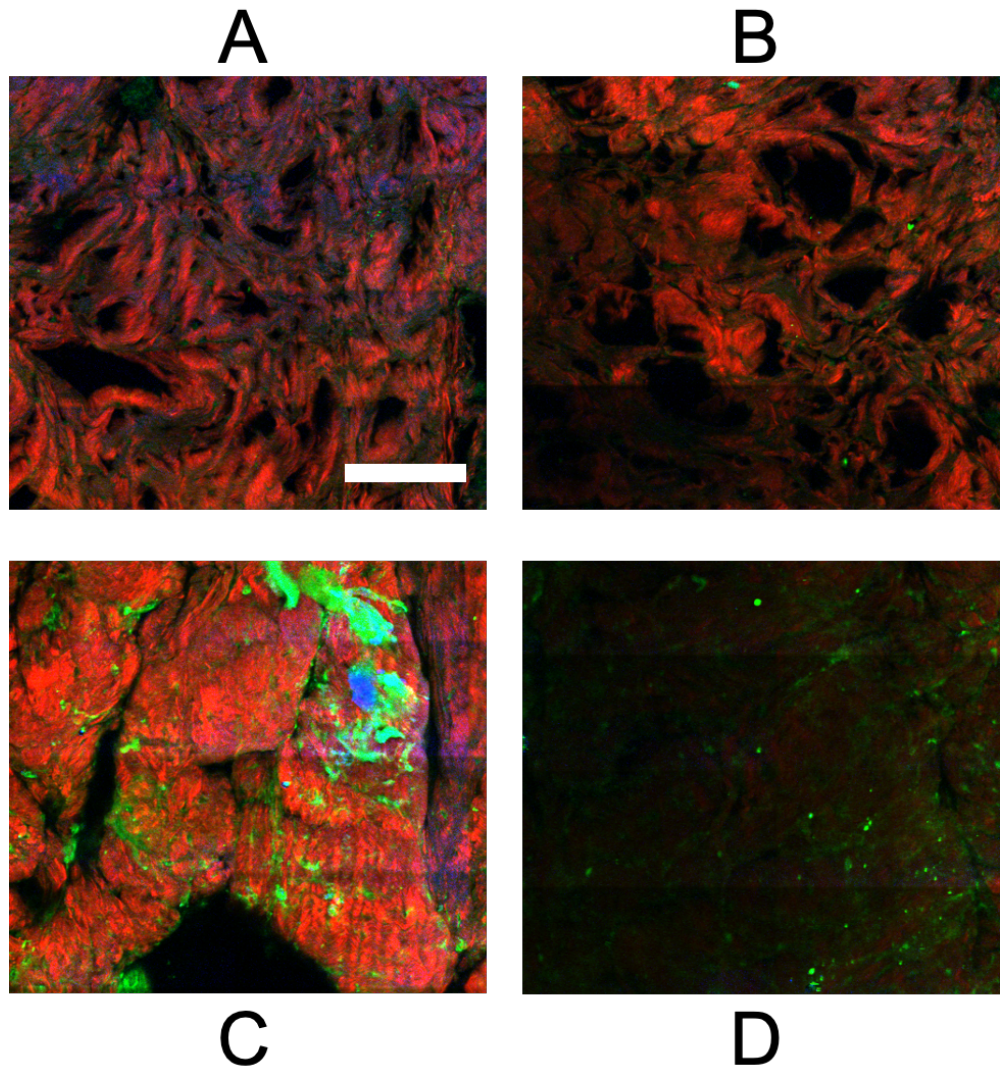


Figure 6.6 – A – A transitional zone where the structure has a fibrocartilaginous appearance due to the presence of type I and type II fibres and an increase in the TPF signal (blue). Type I collagen fibres are woven and have wavy appearance. Scale bar: 129.63 μm . B – Vascular canals pass with type I fibres arranged circumferentially over the circumference of these channels. C – Large type I fibre bundle with crimping visible towards the lower right. There was high fluorescence in the upper right corner, but it is unclear what these intensities were. Cells which emitted fluorescence were found between collagen fibres D – Dark signal from the SHG with fluorescent signals from cells; the darker red appearance suggests this layer of the TAL was lower than the objective resulting in the lack of signal.

6.4.2 Scaled 900N loading (Sample 2)

6.4.2.1 Anterior labrum (Sample 2)

The specimen had high a high number of visible cells, with cells found in lacunae within a type II collagen matrix. The development of a large cell cluster encircled by intense collagen signal. The margin between cartilaginous/fibrous region seems to deviate and associate with this feature, as seen by increased collagen intensity - it is hypothesised that this could represent a vascular canal based on observations by (Gabner, Häusler and Böck, 2017). Type I fibres extended from the chondrolabral junction towards the canal with fibres arranged parallel, which may be required to support the canal. The junction had several collagen type I fibres and bundles integrating into the cartilaginous region and these fibres are oriented at different angles to the interface. The higher SHG signal in the fibrous region (orange) shows fibres integrating with the cartilaginous portion and the cross-section of large type I collagen bundles. Fibroblasts or fibrocytes were be seen around the junction. There was a loss of red SHG signal towards the cartilaginous end near A, which could suggest there was a loss of type II collagen matrix, the junction remained in-tact as while there was a reduction in overall signal, the type I fibres extending from the fibrous region could still be observed.

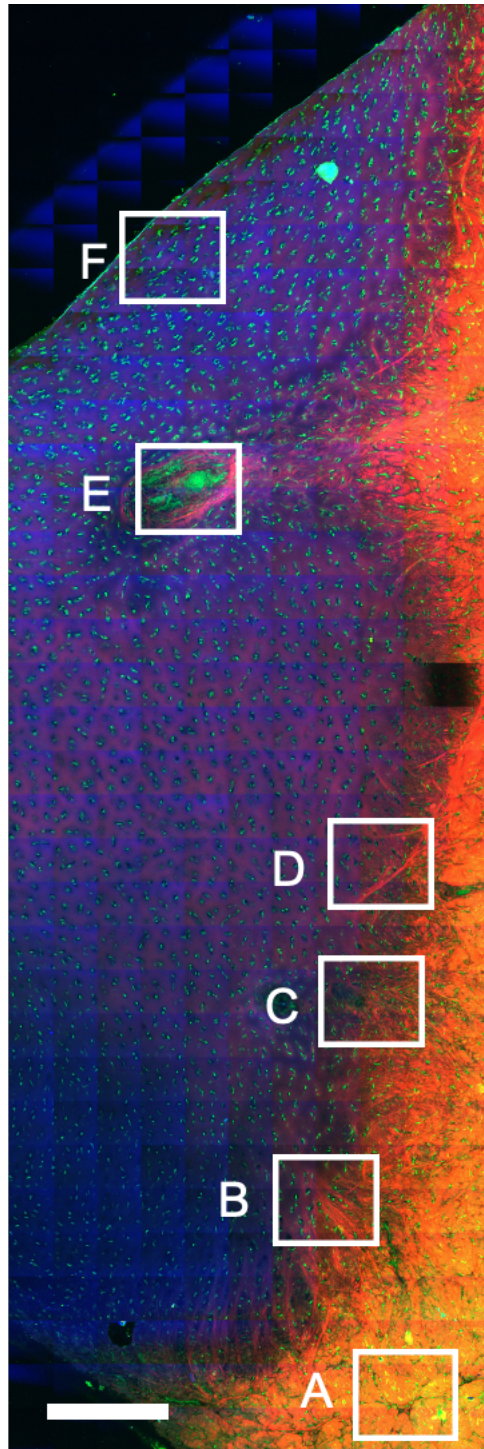


Figure 6.7 – Composite image of the anterior-superior chondrolabral junction area strip from a simulated scaled loaded (peak 900N) porcine hip joint. Scale bar: 348.48 μm . (continued overleaf).

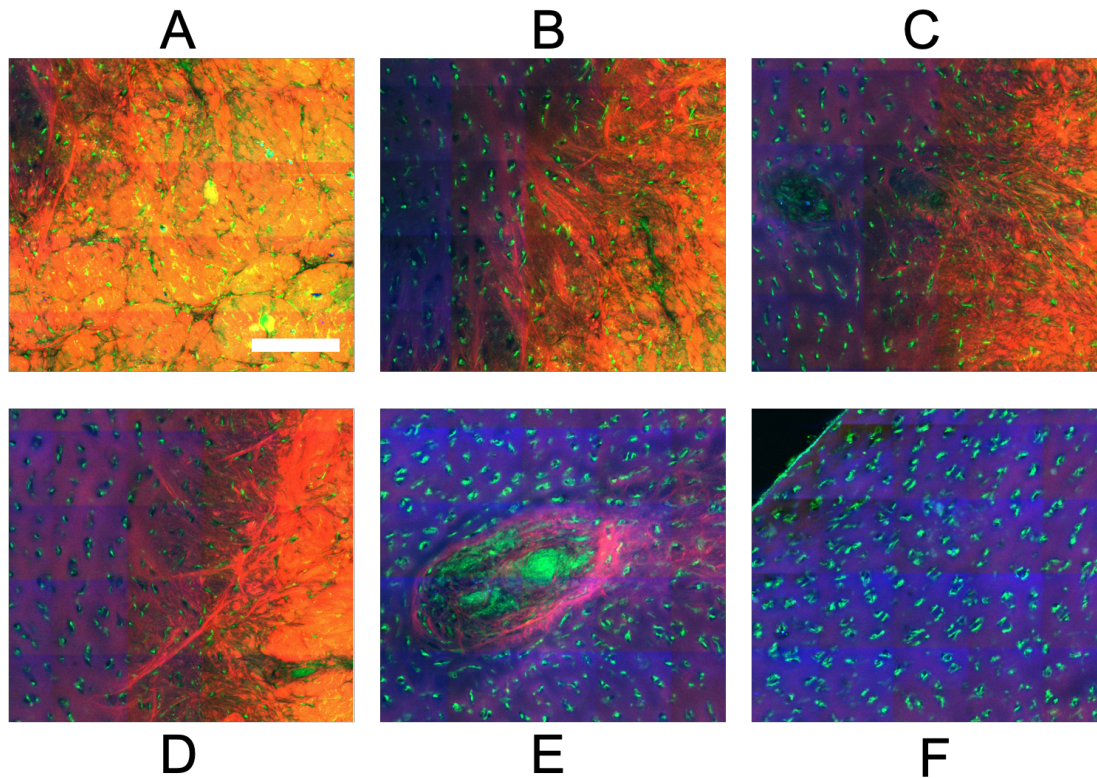


Figure 6.7 – A – Fibrous region towards the periphery of the labrum. Shows the cross-section of large collagen type I bundles interspersed with fibrochondrocytes (green) Scale bar: 145.69 μm . B – Type I collagen fibres merging with the cartilaginous matrix. Chondrocytes can be found interspersed with the collagen fibres. C – Smaller vascular canal like structure found near the chondrolabral junction. D – Long fibres extending beyond the chondrolabral junction into cartilage. E – Development of a large blood vessel found close to the chondrolabral junction. High fluorescent at the centre suggests high cellular activity. F – Chondrocytes found in lacunae of the articular cartilage. High cellularity with chondrocytes found in groups of two or three within the cartilaginous matrix.

6.4.2.2 Posterior labrum (Sample 2)

The specimen had high cellularity with chondrocytes found in lacunae within a type II collagen matrix. The junction has several large collagen type I fibrils and bundles integrating into a large cartilaginous region, with these fibres majorly oriented perpendicular to the interface. The fibrous region (orange) was highly fluorescent and showed fibres integrating with the cartilaginous portion and the cross-section of large type I collagen bundles which would run circumferentially through the labrum. There were no signs of degeneration to the microstructure in this region, although there was a loss in the intensity of the signal as the captured image was observed darker towards the periphery.

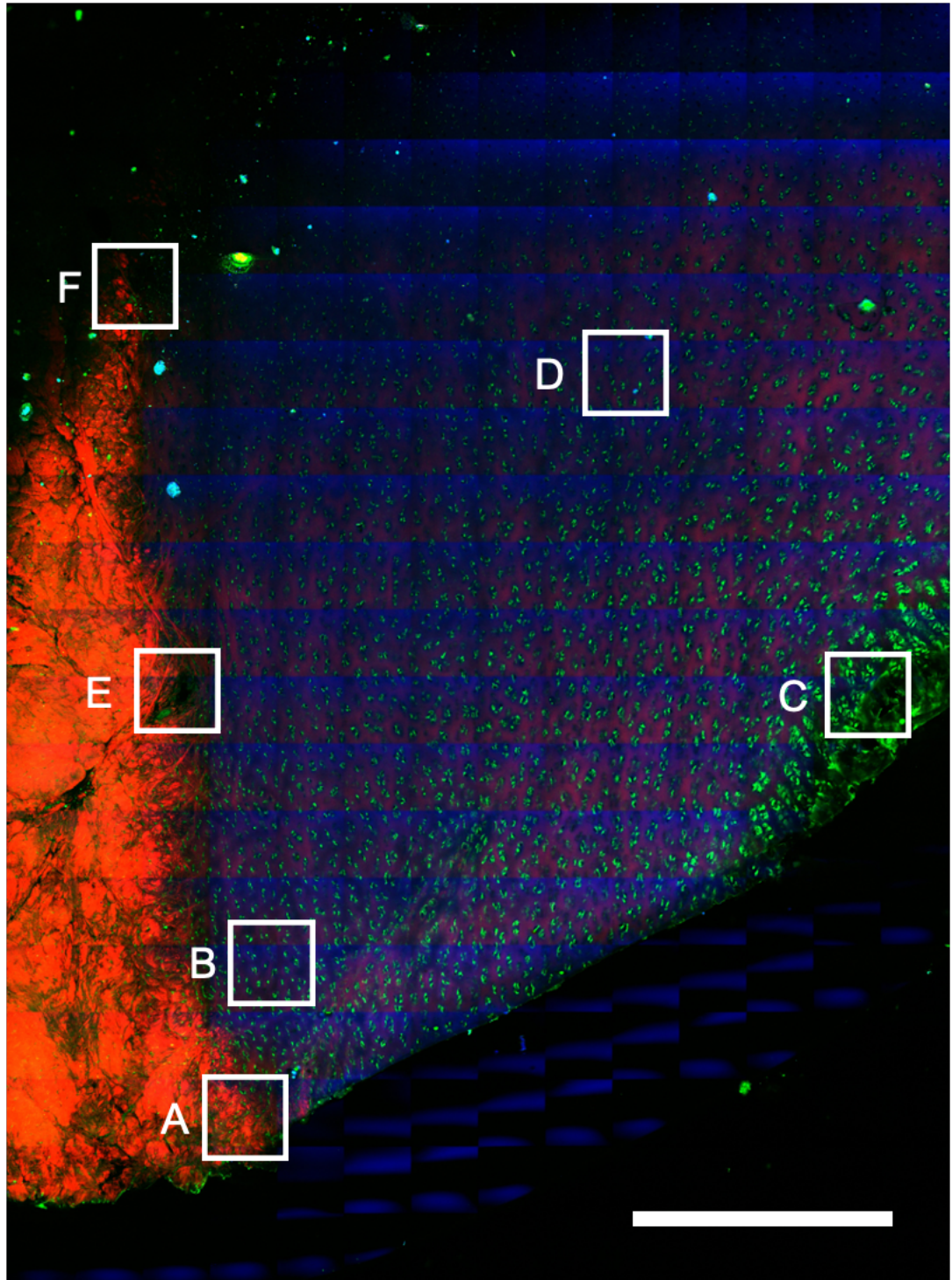


Figure 6.8 – Composite image of the posterior-superior chondrolabral junction area strip from a simulated scaled loaded (peak 900N) porcine hip joint. Scale bar: 293.42 μm . (continued overleaf).

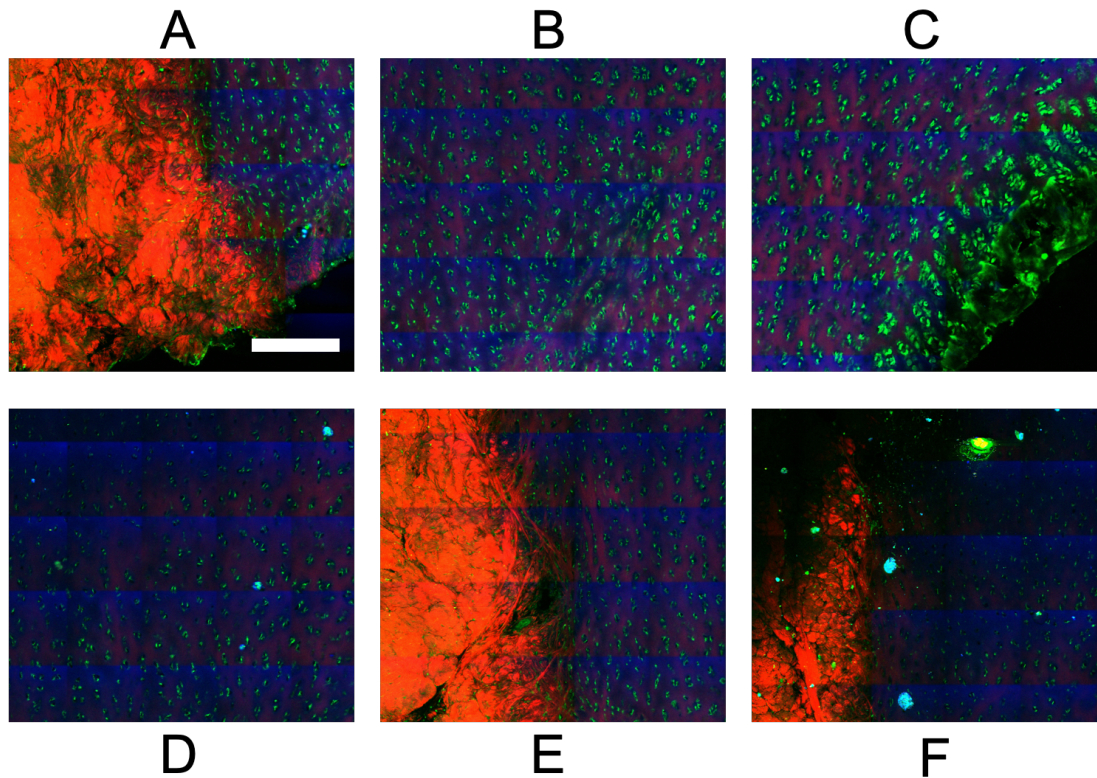


Figure 6.8 – **A** – Chondrolabral junction with transverse sections of large collagen type I bundles in the fibrous region. Chondrocytes were arranged parallel to the interface with some cells integrated into the fibres in the fibrous region Scale bar: 232.88 μm . **B** – Articular cartilage with some chondrocytes packed densely. Small regional clusters of chondrocytes could be arranged towards the base. Type II collagen was observed in the cartilage. **C** – Deep zone of articular cartilage with a tidemark and calcified cartilage and bone present towards the base shown by a bright green signal. Type II collagen was observed in the cartilage. **D** – Articular cartilage with type II collagen matrix and chondrocytes found in lacunae. There was a reduction in the SHG intensity in this region where Type II collagen was present. **E** – Development of a small blood vessel found at the chondrolabral junction where type I fibres are arranged around the vessel. **F** – Chondrocytes found in lacunae of the articular cartilage. Lots of small artefacts which emitted autofluorescence were observed with the TPF and SRS channels.

6.4.2.3 Superior labrum (Sample 2)

The specimen shows less cellularity compared with other regions; cells are found in lacunae within a type II collagen matrix. The cartilaginous region seems degenerated as there was no presence of red SHG signals where type II collagen matrix of fibres would have been expected. The cartilage was still intact however, which may have been as large type I collagen bundles extended from the fibrous region keeping the cartilage attached. These fibres were now running more parallel to the interface, which was different to the native state. The junction had several collagen type I fibrils and large bundles integrating into the cartilaginous region and into the fibrous region, the fibres run parallel and circumferentially with the cartilage with fewer fibres integrating perpendicularly with the cartilage. The fibrous region (orange) was much larger and thicker compared to the cartilage.

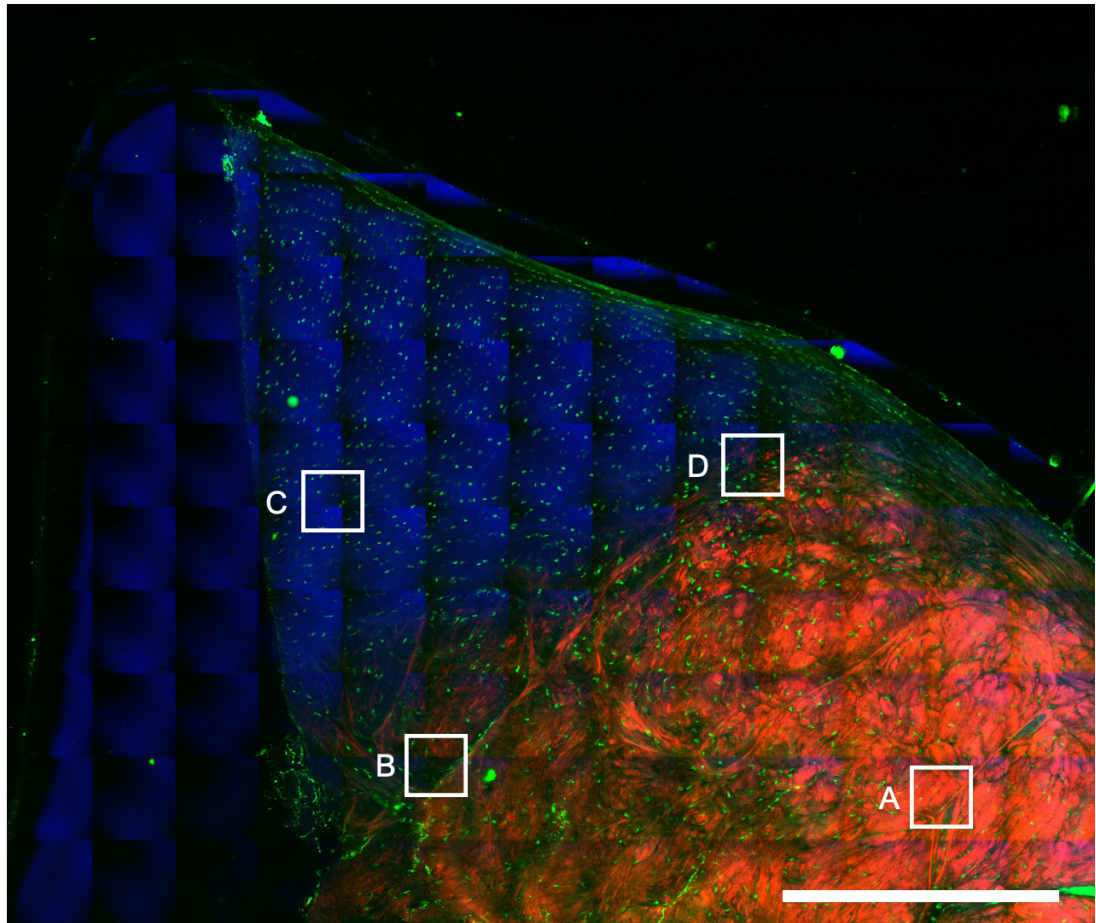


Figure 6.9 – Composite image of the superior chondrolabral junction area strip from a simulated scaled loaded (peak 900N) porcine hip joint. Scale bar: 272.56 μm . (continued overleaf).

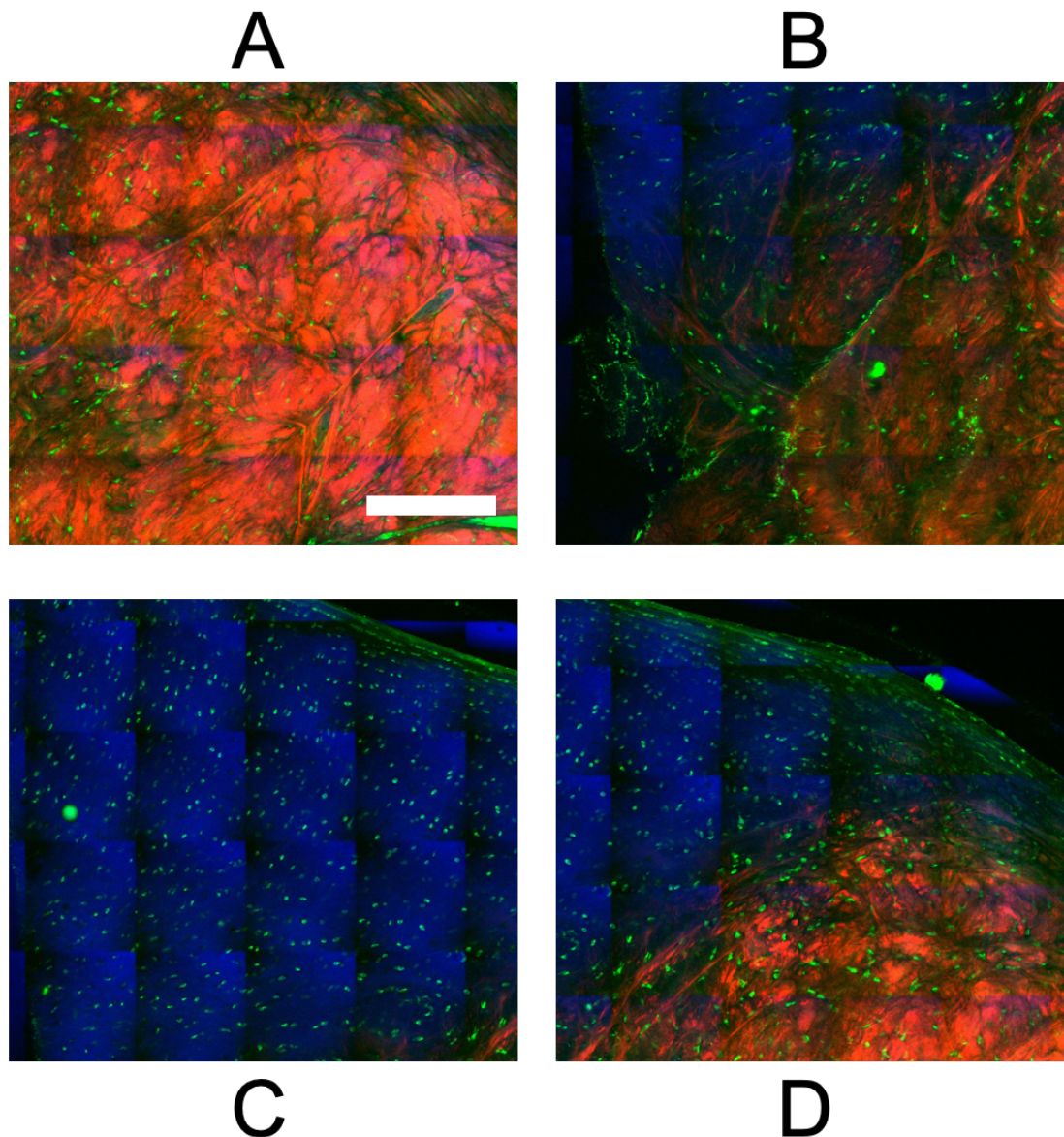


Figure 6.9 – A – Fibrous region of the external labrum. Large type I fibres can be observed with fibrochondrocytes found in the fibrous matrix. Transverse sections of collagen type I fibres were also observed. Fibroblasts were elongated and found interspersed within the fibrous matrix. Scale bar: 232.88 μm . B – Chondrolabral junction. Large collagen type I bundles form a wavy appearance with certain fibres intertwining throughout the fibrous region of the labrum. C – Articular cartilage. The cartilage appears degenerated as there was no SHG signal (red) where type II collagen was expected. D – Chondrolabral junction with type I fibres and bundles running parallel and circumferentially to the cartilage. The SHG signal resumed near the interface.

6.4.3 1300N loading (Sample 3)

6.4.3.1 Anterior labrum (sample 3)

The specimen had significantly fewer chondrocytes found in lacunae within the type II collagen matrix represented by a reduced green TPF signal. The junction had several collagen type I fibrils and bundles integrating into the cartilaginous region and these fibres are oriented at different angles. The fibrous region (orange) showed large bundles integrating with the cartilaginous portion and the cross-section of large type I collagen bundles running circumferentially through the fibrous region. The fibrous region had separations and fissures where the transverse sections of type I collagen fibres appeared broken.

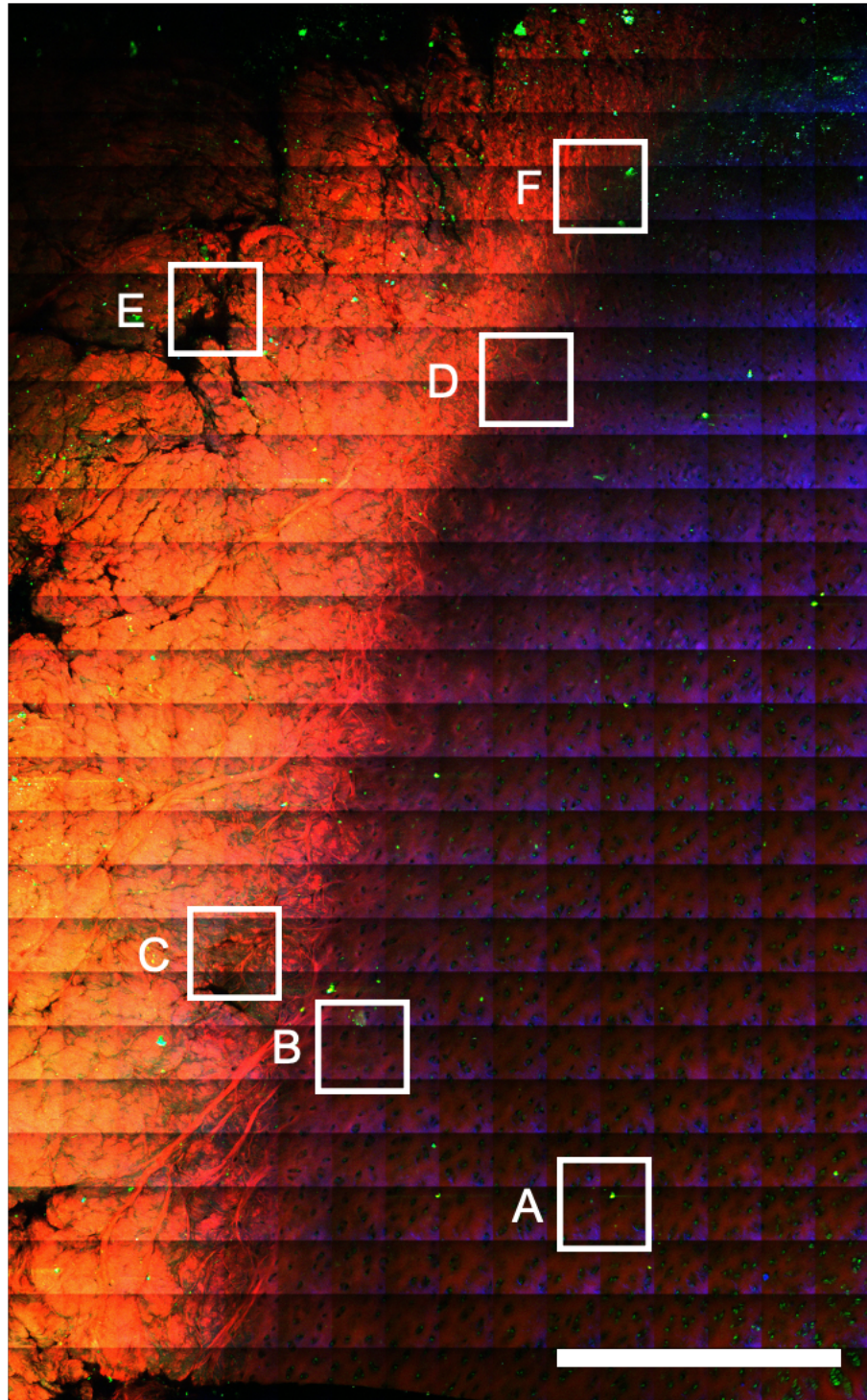


Figure 6.10 – Composite image of the anterior-superior chondrolabral junction area strip from a simulated overloaded (peak 1130N) porcine hip joint. Scale bar: 507.12 μ m. (continued overleaf).

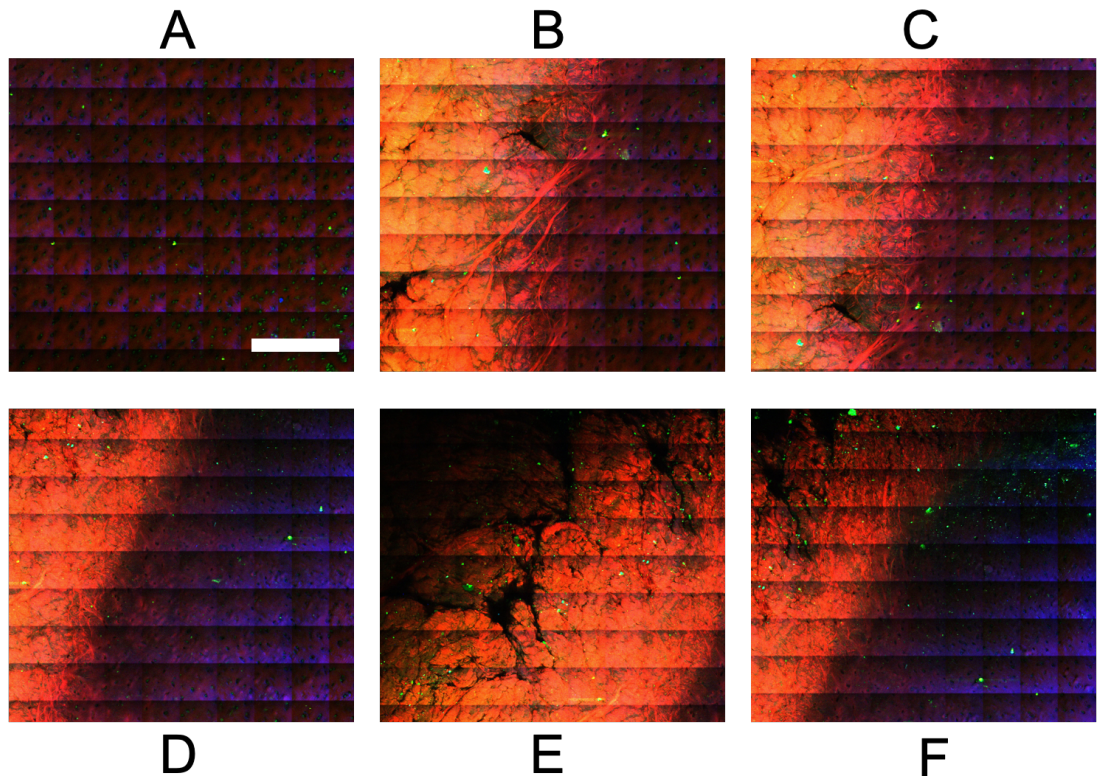


Figure 6.10 – A – Articular cartilage. Chondrocytes appear narrow and have reduced fluorescence with some cells found outside of the lacunae. The type II fibre intensity was higher suggesting the tissue may have lost the hydration indicating potential GAG loss. Scale bar: 291.38 μm . B – Chondrolabral junction. Large type I collagen fibres integrate into the cartilage. Small fissures and cracks are present close to the interface within the fibrous region suggesting labral tearing is present through the fibrous region. These fissures may also be small blood vessels which have been flattened, but it is difficult to conclude due to the lack of cells present. C – The collagen type I fibres appear elongated and interdigitated with random orientations throughout the interface between the fibrous and cellular margin. D – Chondrolabral junction. The margin appears intact. E – Fibrous region of the external labrum. Large tears are present in the fibrous region where transverse collagen type I fibres have been torn resulting in split fibres and fraying. F – Chondrocytes appeared out of the lacunae and spread around the periphery. Overall, the cartilage and chondrolabral junction appear degraded while the type II collagen matrix remained in-tact.

6.4.3.2 Posterior labrum (sample 3)

The specimen had an intraarticular-labral tear which extended from the articular cartilage, chondrolabral junction and through the fibrous region of the labrum. The articular cartilage appears degraded with a severe reduction in the fluorescent signal emitted from chondrocytes. The tear appeared to split fibres and the margin but not at the interface, this tear was able to rupture and split thick type I collagen fibre bundles present in the fibrous region. Additionally, the cartilage appeared flattened and degraded. The overall structure of the type I and type II collagen matrix was intact surrounding the tear.

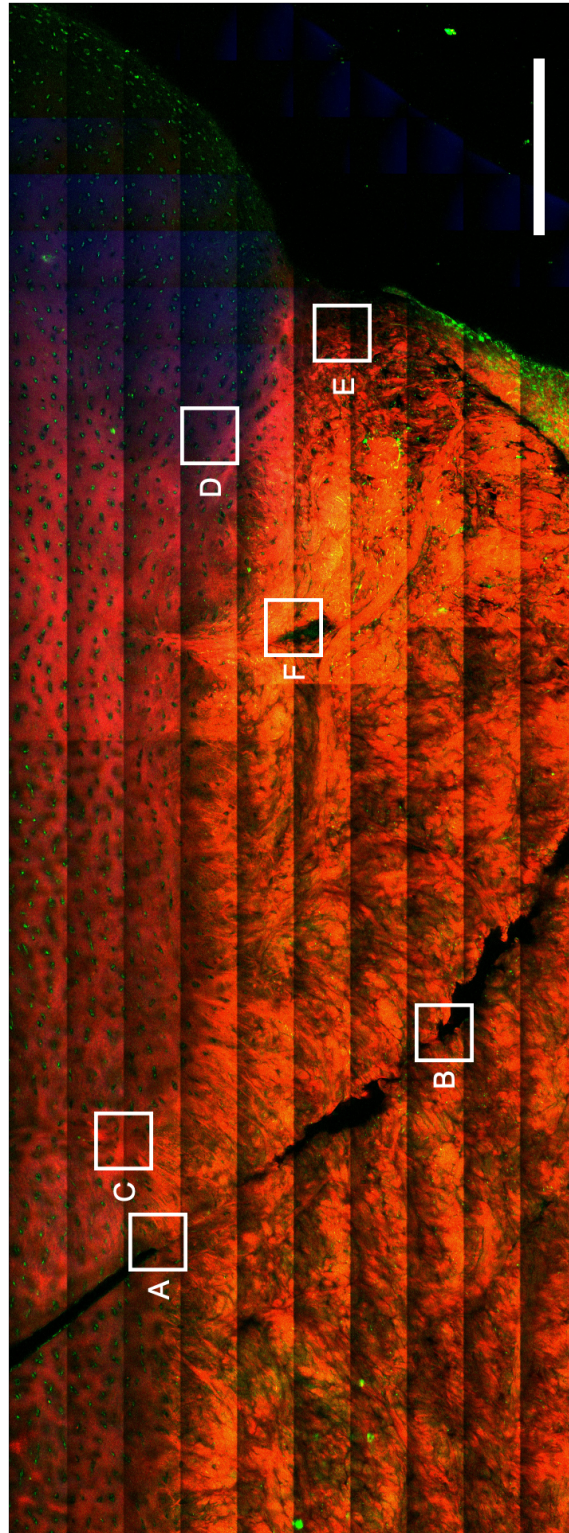


Figure 6.11 – Composite image of the posterior-superior chondrolabral junction area strip from an overloaded (peak 1130N) porcine hip joint. Scale bar: 854.70 μm .
(continued overleaf).

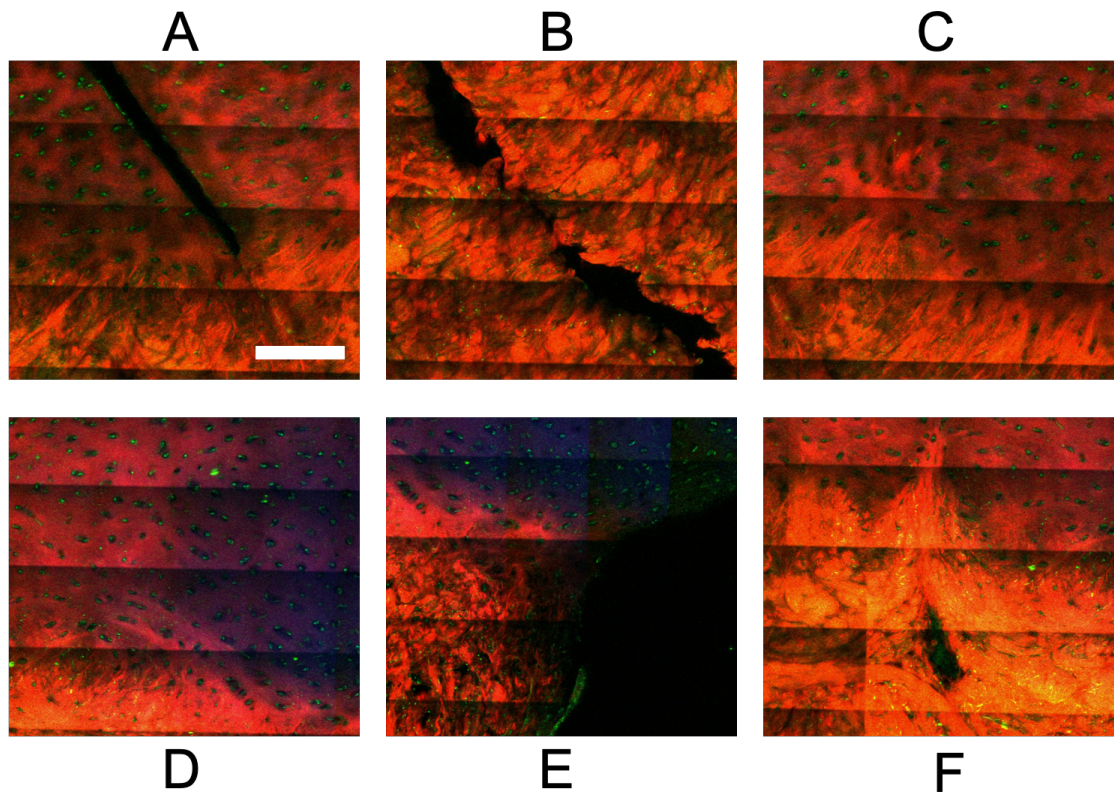


Figure 6.11 – A – A tear with separation had occurred through the cartilage and labrum where the interface was intact but split apart through the centre. Type II collagen fibres appeared to be oriented perpendicularly away from the tear. There was small fluorescence detected towards the margin at the edge of the tear. Scale bar: 138.57 μm . B – The tear extended into the fibrous region where type I collagen transverse circumferential fibres had split apart, producing blunt ends and fraying. C – The tissue structure remained intact on either side of the tear, albeit with reduced cell fluorescence. D – The tissue structure remained intact, but the cartilage appeared degenerated in some areas depicted by the reduction in red SHG signal, in addition, small fluorescent emissions were observed. E – The chondrolabral junction in this region appeared loosely intact, as type I collagen fibres were not integrated and attached with the cartilage. Collagen signal was reduced in this region, which could be attributed to disruption of collagen network caused by simulation damage. This may be representative of cartilage degeneration observed in cam impingement. Faint green lines from TPF signal showed the presence of elastin in this region. F – The remains of a vascular canal like structure or a cavity present in the fibrous region,

large type I collagen bundles appear to split on either side and merge with the type II collagen matrix in the cartilaginous region.

6.4.3.3 Superior labrum (sample 3)

The specimen showed several fluorescent signals dotted across the fibrous region, where chondrocytes were round and unevenly arranged. The fibrous region was dense with large type I fibres and bundles overlapping and were haphazardly arranged. The articular cartilage can be observed towards the top of the area strip. It is difficult to determine the extent of damage and degeneration as a larger area strip was not taken which could cover the whole chondrolabral junction due to processing.

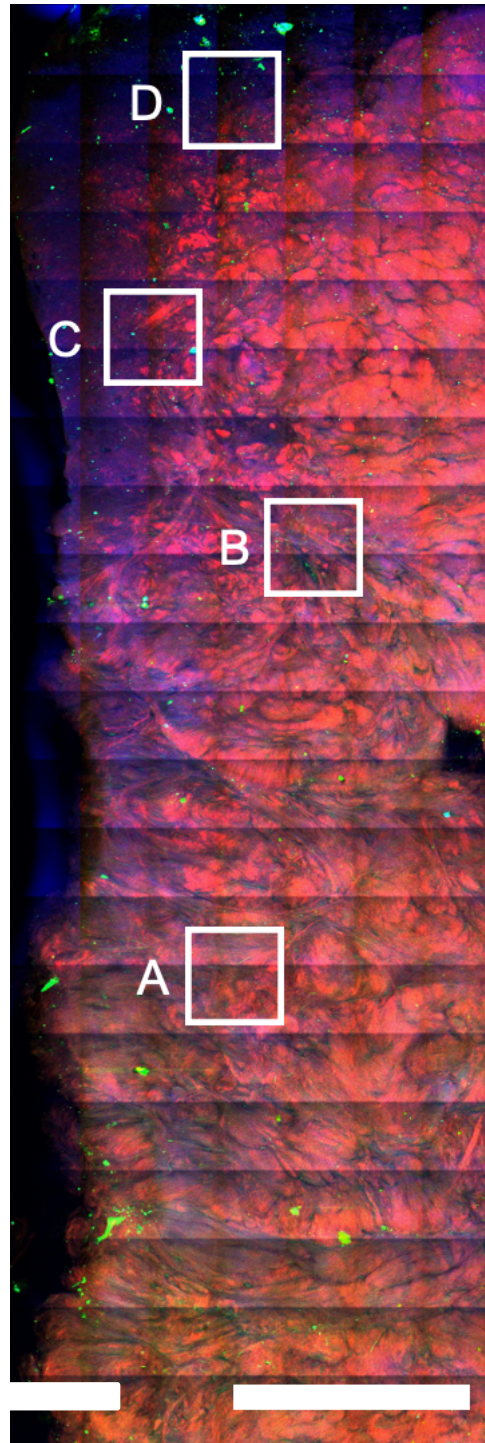


Figure 6.12 – Composite area strip of the superior fibrous region of the acetabular labrum from an overloaded (peak 1130N) porcine hip joint. Scale bar: 222.74 μm . (continued overleaf).

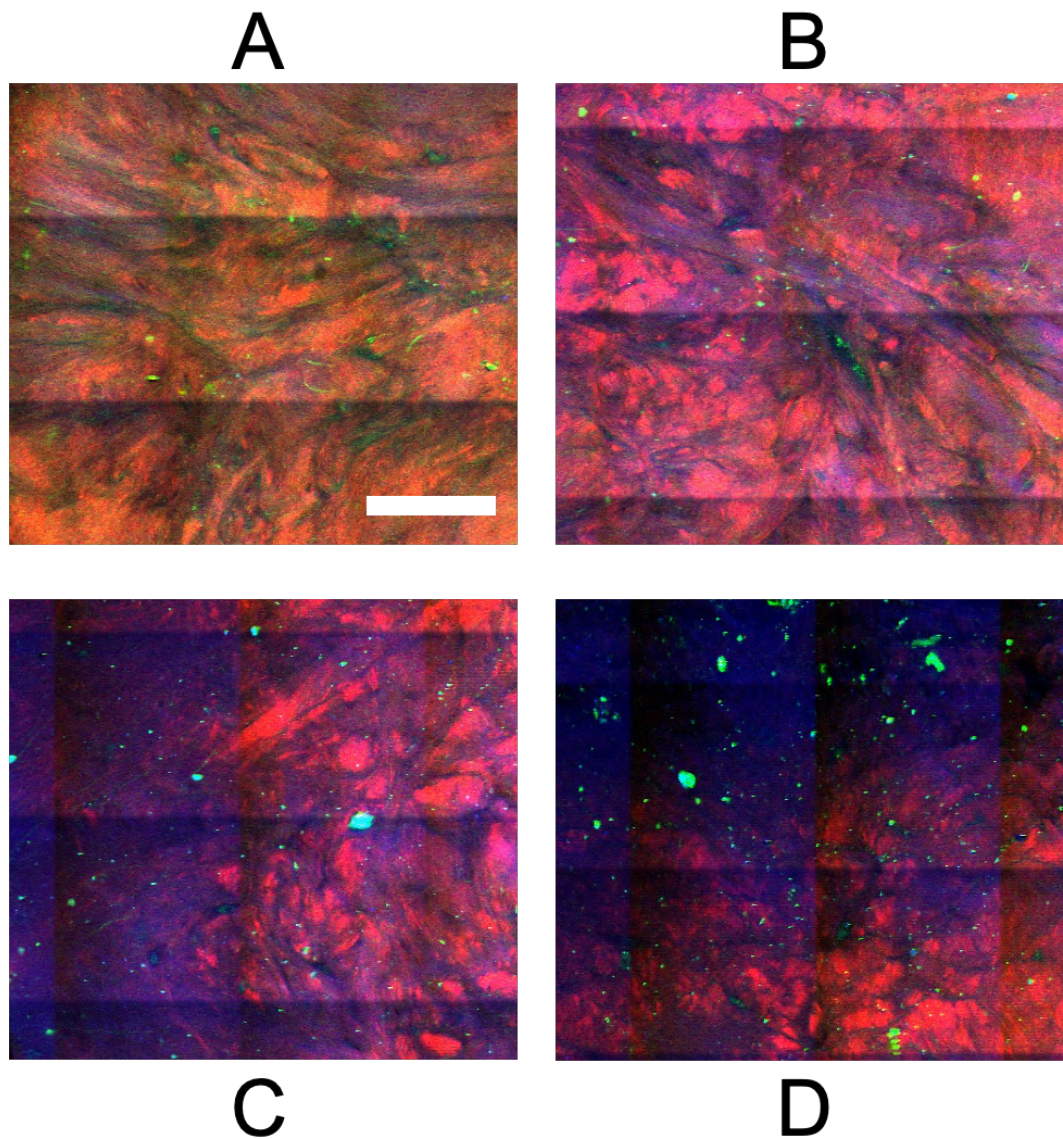


Figure 6.12 – A – Type I collagen fibres and elastin observed in the fibrous region. Scale bar: 86.77 μm . B – Type I collagen fibres. Thin green lines amongst larger type I collagen bundles suggest elastin is present in this region. C – Type I collagen fibres integrating into the cartilage. Artefacts and fluorescence from cells. D – circumferential type I collagen fibres. Artefacts and fluorescence from cells.

6.4.4 1340 N loading (Sample 4)

6.4.4.1 Anterior labrum (Sample 4)

The specimen showed reduced cellularity with fewer chondrocytes found in lacunae within the type II collagen matrix. Some deterioration occurred towards the articulating side or edge of the tissue as there was a reduction in signal intensities of SHG in both the fibrous and cartilaginous regions on either side of the interface. Additionally, there were unusually high levels of fluorescence toward the edge suggesting degradation.

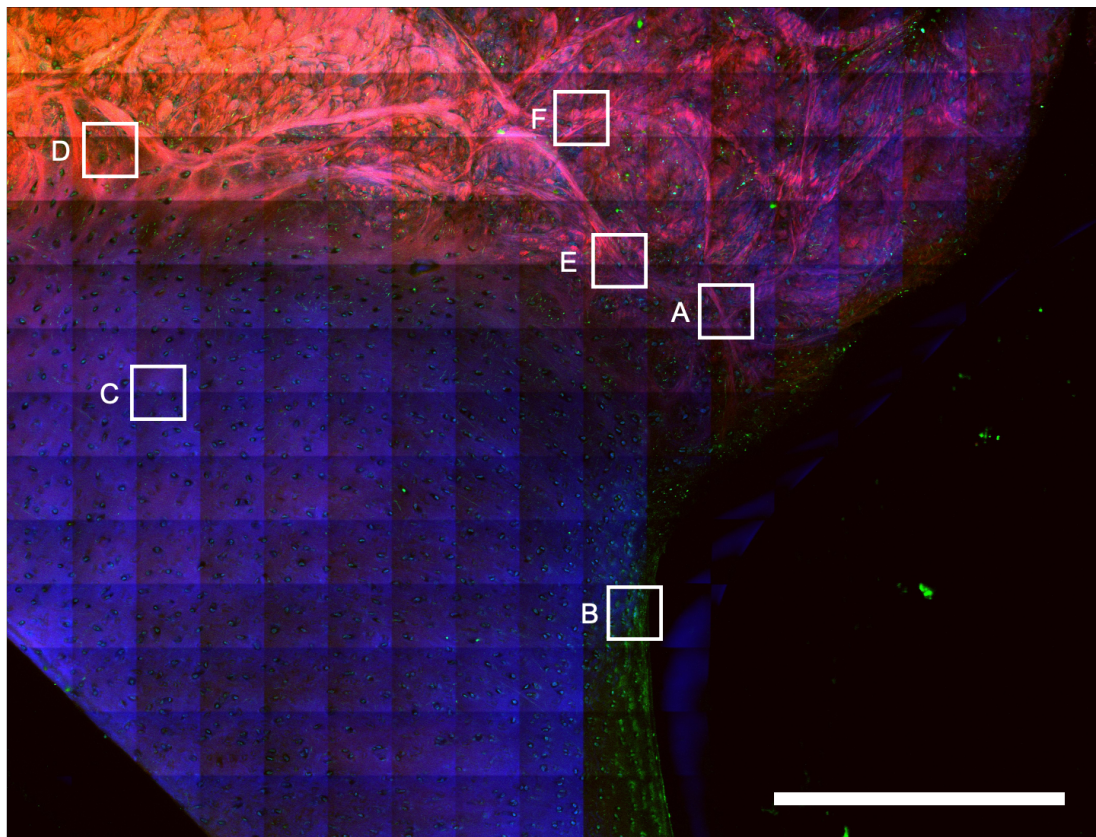


Figure 6.13 – Composite image of the anterior-superior chondrolabral junction area strip from a simulated (peak 1130N) loaded porcine hip joint. Scale bar: 538.72 μm . (continued overleaf).

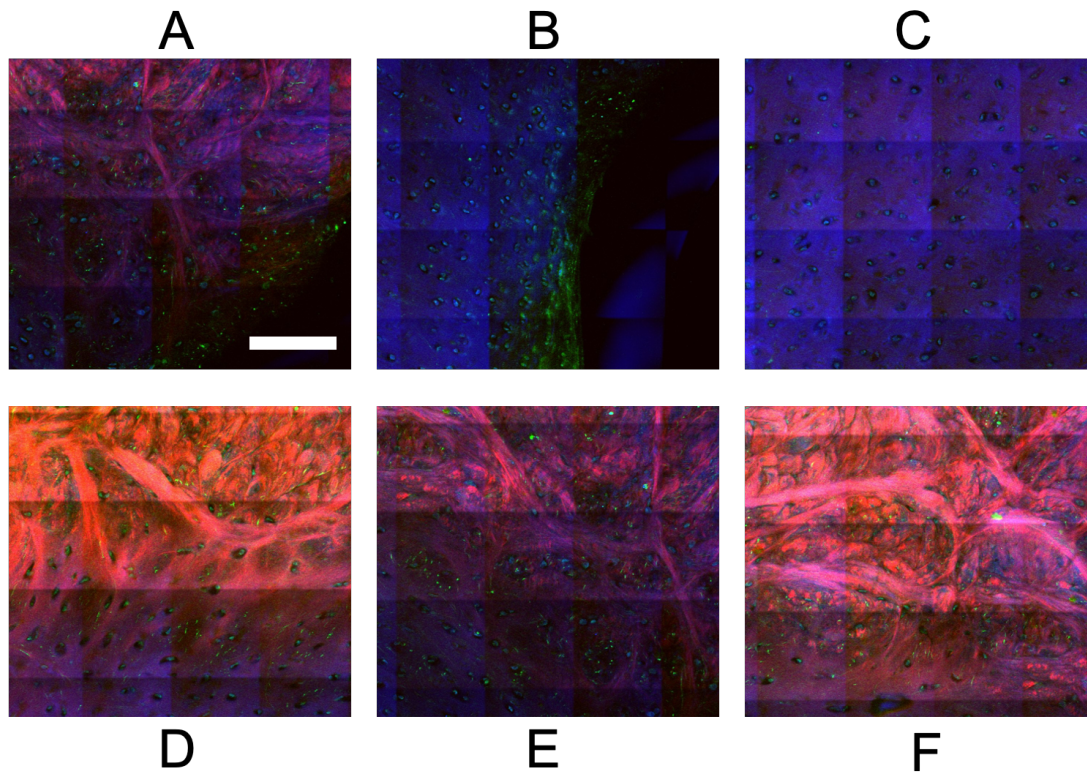


Figure 6.13 – A – Chondrolabral junction. Large type I collagen fibre bundles extend from the fibrous region into the cartilage. The signal is reduced compared with lesser loaded tissue. Scale bar: 122.12 μm . B – Superficial layer of articular cartilage. Chondrocytes had lost TPF intensity appearing less green and duller in appearance. C – Chondrocytes had lost TPF intensity appearing less green and duller in appearance. Only sparse chondrocytes were observed with many empty lacunae. There was a lack of type II collagen matrix which would have appeared as red fibres but were absent in this region. D – Large type I collagen fibre bundles extend from the fibrous region into the cartilage. The signal was more intense compared with other regions across the chondrolabral junction. E – Large type I collagen fibre bundles extend from the fibrous region into the cartilage. The signal was reduced compared with lesser loaded tissue. Dull clusters of cells were present among the branches of collagen bundles. F – Chondrolabral junction. Large type I collagen fibre bundles extend from the fibrous region into the cartilage. The signal was increased compared with other regions; the cartilage immediately proximal to the region had an increased reddish hue suggesting the type II collagen fibres were intact in this region.

6.4.4.2 Posterior labrum (Sample 4)

The specimen shows high number of visible cells found in lacunae within a type I collagen matrix. The junction had several collagen type I fibrils and bundles integrating into the cartilaginous region. Several blood vessel like structures were found dotted across the cartilage and fibrous regions. The yellow appearance of the fibrous region was caused by a pure red and green signal suggesting the fibrous region is extremely dense fibrous connective tissue and the large transverse cross sections of type I collagen bundles; There was external labral tearing towards the periphery at E. The gross appearance at the chondrolabral junction suggests the fibrous region is sheared away from the cartilage as most fibres are oriented at an angle when they were typically perpendicular to the cartilage. The darker blue signal in the cartilaginous region suggests type II collagen fibres were degraded.

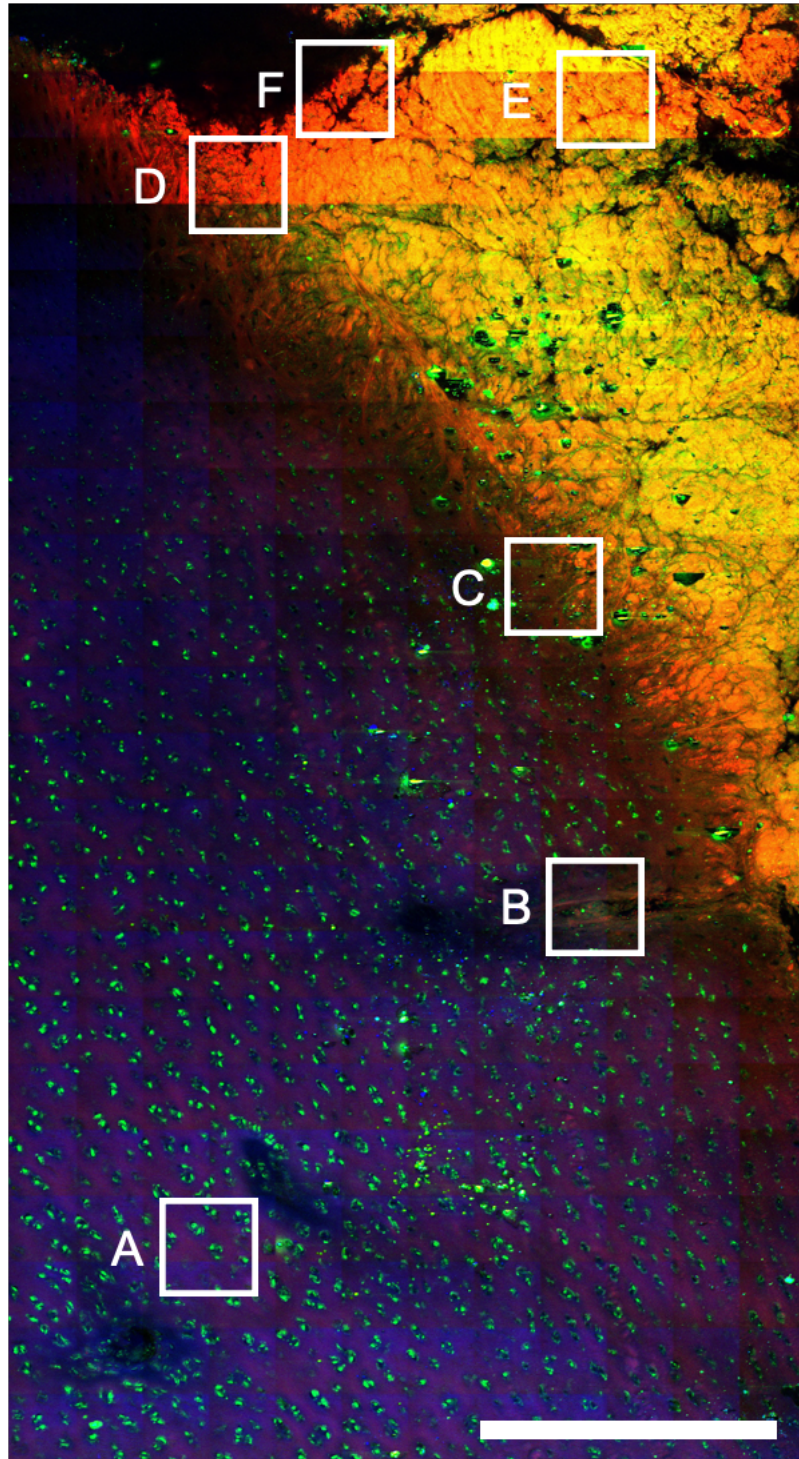


Figure 6.14 – Composite image of the posterior-superior chondrolabral junction area strip from an overloaded (peak 1340N) porcine hip joint. Scale bar: 380.73 μm . (continued overleaf).

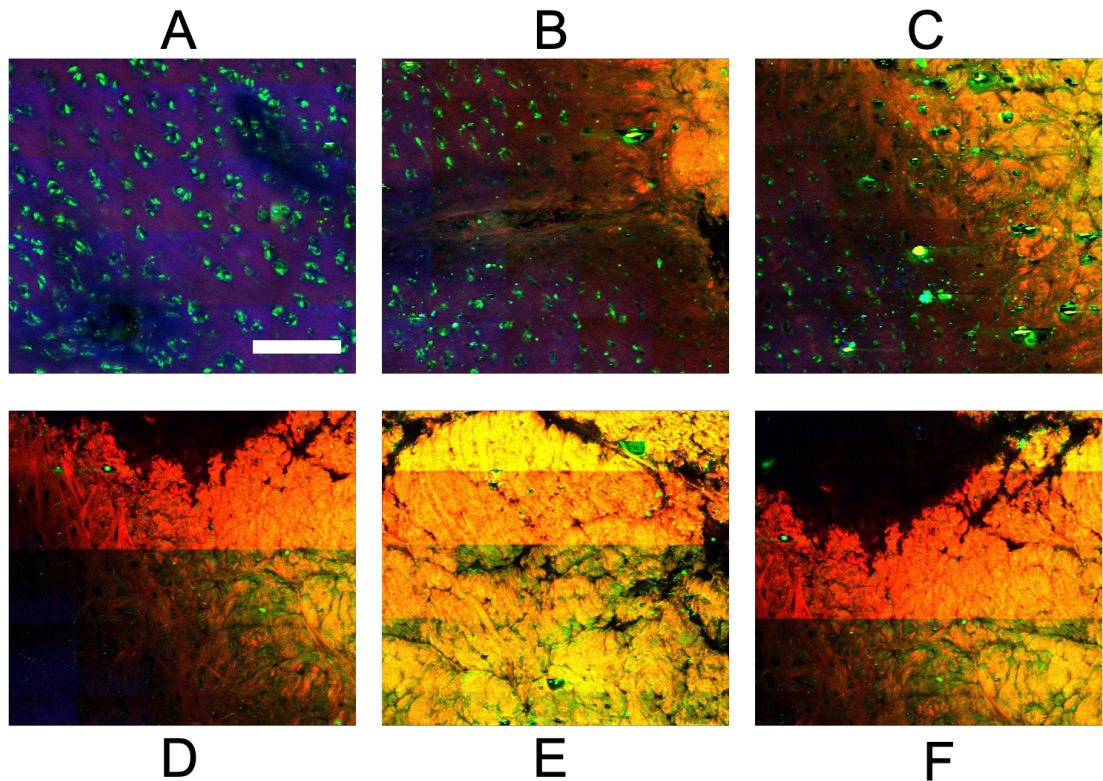


Figure 6.14 – A – Articular cartilage with chondrocytes found in lacunae in a type II matrix. Two blood vessel like structures were found in the cartilage where the cartilage appeared more hyaline and less fibrous in these regions Scale bar: 148.67 μm . B – Blood vessel at the chondrolabral junction, the cartilage and collagen fibres around this region appear degraded and cells appear damaged with many lacunae lacking chondrocytes C – Chondrolabral junction and fibrous region the interface appeared to be abrupt with fewer type I collagen fibres integrated into the cartilage matrix. D – Severe degeneration occurred to type I collagen fibres with fissures, broken fibres from the periphery and damage reaching the interface at the chondrolabral junction. The dark signal from the cartilaginous region suggested loss of type II collagen matrix. E – bright SHG and TPF signals from the fibrous region, with degeneration to type I collagen fibres with fissures and broken fibres. Fibres in this region maintained more of their structure and arrangement. F – bright SHG and TPF signals from the fibrous region, with degeneration to type I collagen fibres with fissures and broken fibres at the periphery.

6.4.4.3 Superior labrum (Sample 4)

The specimen showed significantly reduced cellularity, with sparse cells found in lacunae within a type I collagen matrix. The fibrous region was broken and torn with fragments of type I fibres. Additionally, the chondrolabral junction was torn with type I fibres elongated at the interface. There was a considerable increase in the TPF (green signal) in the fibrous region. There should have been a strong orange SHG signal suggesting that there was severe reduction of type I collagen fibres and bundles which appeared broken and frayed. Interestingly, compared to lesser-loaded samples, the type II collagen matrix remained in-tact which was undetected in similar regions in the superior sample.

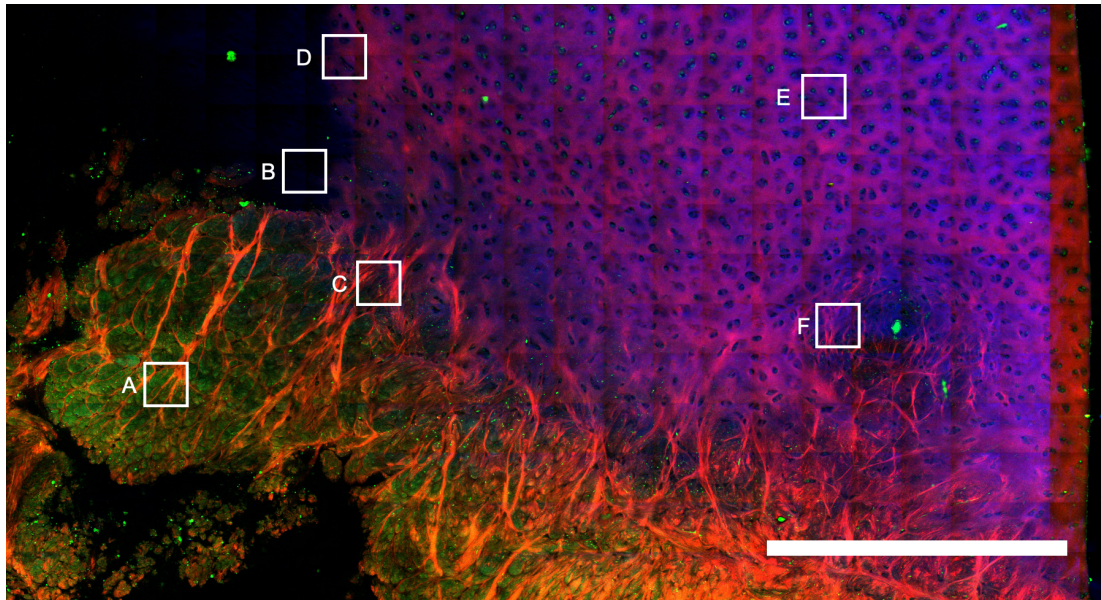


Figure 6.15 – Composite image of the superior chondrolabral junction area strip from a simulated overloaded (peak 1340N) porcine hip joint. Scale bar: 696.71 μm . (continued overleaf).

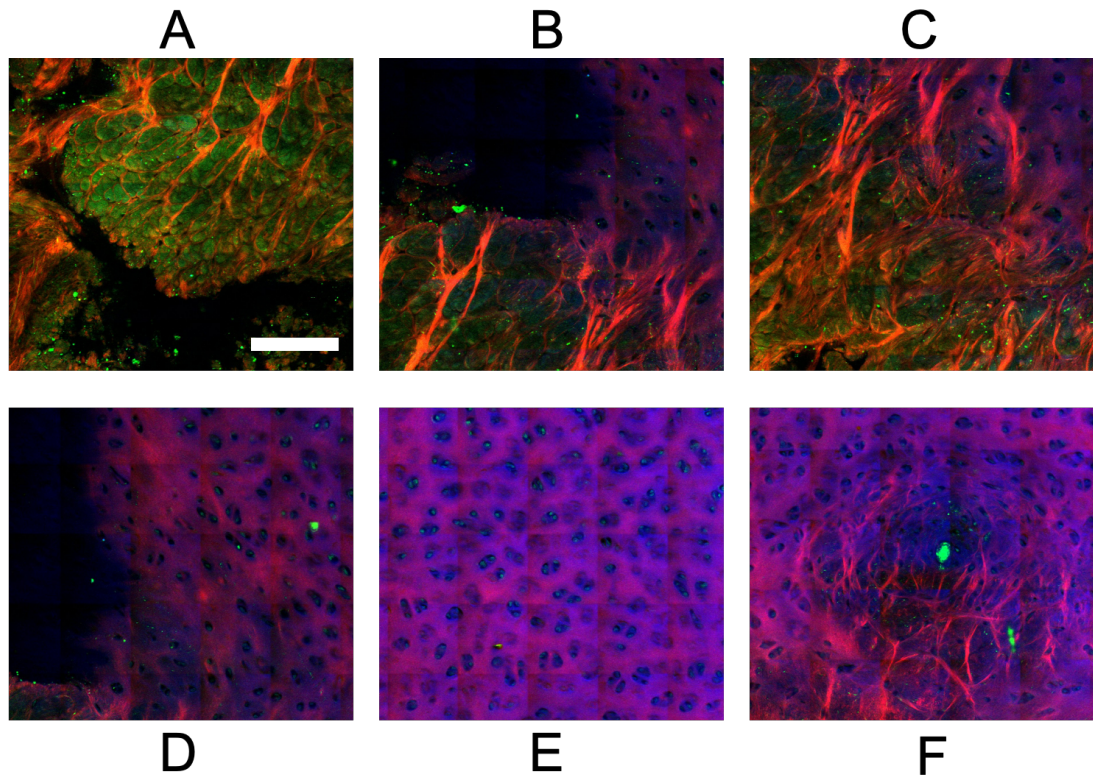


Figure 6.15 – A – Torn and fragmented fibrous region of the external labrum toward the joint capsule. Severe reduction in SRS signal. Type I fibres and branches were visible with high fluorescence (green picked up from the TPF). Scale bar: 155.40 μm . B – Damaged and fragmented chondrolabral junction where the cartilage had torn away from large perpendicular type I collagen bundles. C – Type I collagen bundles were well aligned, perpendicular to the chondrolabral junction. Fibre bundles appeared flatter, compacted and sheared. D – The cartilage appeared compressed with fluctuations in SHG signal where collagen type II cartilage matrix is observed with few cells and broken off at the margin where it would have met with the fibrous region of the labrum. E – Few chondrocytes were present within lacunae. Remaining type II collagen matrix found in-tact. F – Remnants of a large vascular canal like structure found close to the chondrolabral junction within the cartilage. The structure was surrounded with threaded collagen-type I fibres arranged circumferentially.

6.4.5 Specific example of tearing (chondrolabral separation)

The specimen shows distinct chondrolabral separation where the fibrous region had torn away from the cartilaginous region. The cartilaginous region showed degeneration proximal to the tear as there was a reduction in the red SHG signal suggesting the collagen type II matrix had collapsed and was broken. Further away from the tear in the cartilage, the red SHG signal is intact. There was also an overall reduction in the red SHG signal from the fibrous region. The fibrous region was broken and torn with fragments of type I fibres bundles oriented away from the tear and running parallel to the direction of the tear. There was a significantly reduced cellularity in all regions, with sparse cells found in lacunae within the type II collagen matrix and some fine elongated cells found among the type I collagen bundles. **Note:** this was a representative sample included to show chondrolabral separation, however, this tissue was affected by tissue defrosting.

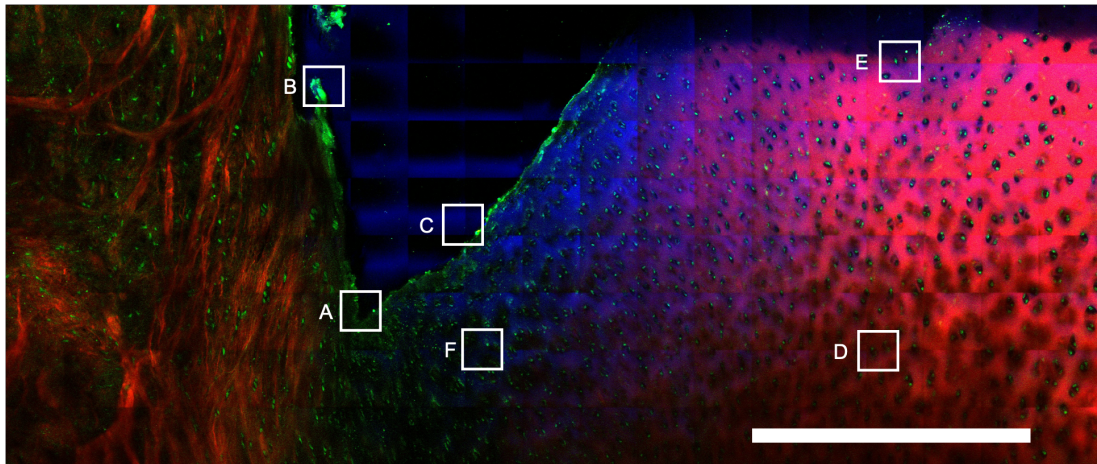


Figure 6.16 – Composite image of the anterior-superior chondrolabral junction area strip from a simulated overloaded (peak 1340N) porcine hip joint. Scale bar: 601.92 μm . (continued overleaf).

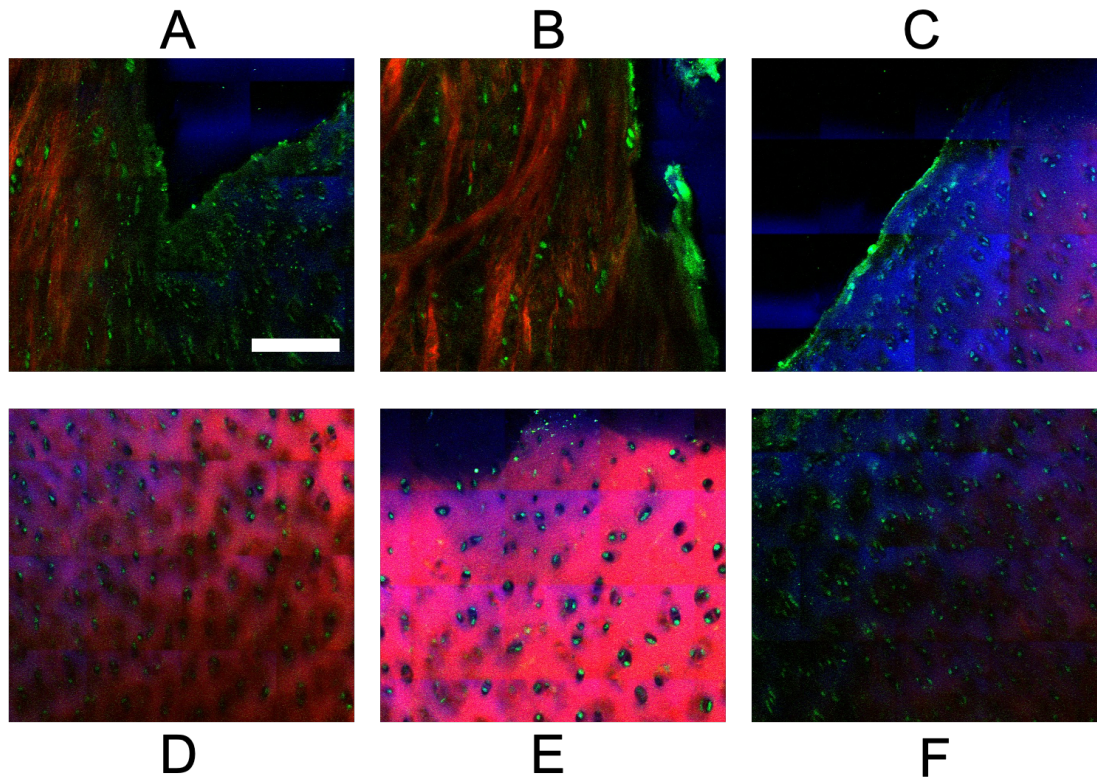


Figure 6.16– A – Point of tearing. Chondrolabral separation had occurred, with a loss of red SHG and blue SRS signals where the autofluorescence appeared as fragmented and compacted cells. Fine elastin fibres were also present with collagen fibre bundles. Type I fibre bundles appear aligned parallel to the direction of the tear. Scale bar: 115.26 μm . B – Damaged and fragmented chondrolabral junction where the cartilage had torn away from large perpendicular type I collagen bundles. C – green TPF autofluorescence at the margin of the cartilage which had split from the chondrolabral junction. D – Many chondrocytes present in lacunae in a type II collagen matrix. E – Few chondrocytes present within lacunae. Remaining type II collagen matrix found in-tact. F – Transition from deteriorated cartilage to more intact collagen, shown by an increase in a red SHG signal which suggests in-tact type II collagen matrix distal to the site of damage.

6.5 Discussion

This study addresses a major gap in the literature by providing some of the first sub-micron images of the porcine labrum under different loading conditions. Changes to the collagen structures around the chondrolabral margin of acetabular labrum samples were investigated and presented for the first time. This allowed the microscale effects on the collagen matrix microstructure to be studied, where changes to type I and II collagen fibres at the chondrolabral junction could be visualised. A summary of the main key observations are detailed in Table 6.2.

Table 6.2: Key findings and tissue observations after 14400 simulation cycles (four hours).

	Sample	Observation from mechanical simulation
1	Unloaded porcine hip joint (only dissected, control)	Chondrolabral junction with thick type I fibre bundles aligned perpendicular to the fibrous-cartilaginous interface. The fibres appeared to overlap and weave deeper into the fibrous region. Cells were found embedded between collagen fibres and within the lacunae
2	Loaded porcine hip joint (peak 900N, 4 hrs., 1Hz)	There was a loss of red SHG signal towards the cartilaginous end, which could suggest there was a reduction in the signal intensity of type II collagen matrix, the junction remained in-tact as while there was a reduction in overall signal, the type I fibres extending from the fibrous region could still be observed.
3	Loaded porcine hip joint (peak 1130N, 4 hrs., 1Hz)	The specimen had an intraarticular-labral tear which extended from the articular cartilage, chondrolabral junction and through the fibrous region of the labrum. The articular cartilage appears degraded with a severe reduction in the fluorescent signal emitted from chondrocytes. The tear appeared to split fibres and the margin but not at the interface, this tear was able to rupture and split thick type I collagen fibre bundles present in the fibrous region
4	Loaded porcine hip joint (peak 1340N), 4 hrs., 1Hz	Severe degeneration occurred to type I collagen fibres with fissures, broken fibres from the periphery and damage reaching the interface at the chondrolabral junction. The dark signal from the cartilaginous region suggested that there was loss of type II collagen matrix signal intensity

This preliminary study shows how multi-channel multiphoton imaging can characterise damaged tissue microstructure in the acetabular labrum and articular cartilage. Damage induced by mechanical loading appears in the form of structural differences and through changes in the signal intensities of the different channels in the microstructure of the chondrolabral junction.

The technique relied on unstained tissue sections which can be adapted to be used with other cartilaginous tissue provided certain conditions are met; explain about autofluorescence.

The combination of experimentation, non-invasiveness and resolution means we can understand the damage mechanism in a novel way not possible with conventional imaging. The main findings from using this imaging method in this overloading study were summarised and reported in Table 6.2.

TPF image shows auto-fluorescence from the peri-cellular matrix and a network of elastin fibres within the sample. An unexpected discovery was the high cellularity and presence of developing or fully formed structures resembling blood vessels (Kim and Azuma, 1995; Olstad *et al.*, 2013; T, Lecture and Taber, 2015; Shirshin *et al.*, 2017; Sato *et al.*, 2023). The margin between cartilaginous/fibrous region seems to deviate and associate with this feature, as seen by increased collagen intensity - it is hypothesised that this could represent a vascular canal based on observations by (Gabner, Häusler and Böck, 2017). Type I fibres extended from the chondrolabral junction towards the canal with fibres arranged parallel, which may be required to support the canal. Like the meniscus, the labrum does receive a vascular and nervous supply.(Fox, Bedi and Rodeo, 2012) However, it was not expected within the cartilage, which may be accounted for due to the age of the tissue being immature porcine tissue. The canals may have developed and eventually collapsed and closed off as the cartilage did not have a fully developed structure(Julkunen *et al.*, 2009).

This study has shown the immense potential of multiphoton imaging for use in biomedical applications for visualising the sub-micron structure of the acetabular labrum and cartilage.

Novel multiphoton imaging methods were successfully used to characterise microstructural changes to the collagen matrix and alignment of collagen fibres in unloaded and experimentally overloaded porcine labrum samples.

It was hypothesised that changes to the collagen orientation and arrangement would occur with damage and that these changes could be observed using nonlinear imaging methods and Raman spectroscopy.

The high number of chondrocytes, fibroblasts and chondrofibrocytes present in the entire labrum structure suggests they would have an essential role in mechanotransduction and respond to increased loading. This could not be tested in this study as it was done in vitro.

The disruption of the collagen matrix at the chondrolabral junction can improve our understanding of the damage to the anterior-superior rim of the acetabulum. The combination of generating damage through experimental simulation and evaluation with non-linear imaging techniques provides powerful insight into the damage due to mechanical failure at the anterior-superior labrum. This could improve our understanding of the abnormal mechanical environment that leads to microstructural chondrolabral damage and macroscopic labral tearing.

Multiphoton imaging can study damaged tissue microstructure in the acetabular labrum and articular cartilage. Of the three channels, it was SHG which is of most important use for determining how mechanical damage impacts the microstructural arrangement of collagen.

When comparing the anterior-superior junction to the posterior-superior junction, it was evident that the anterior labrum had a larger area of cartilage compared to the external labrum which had a higher abundance of collagen fibres. This matches the function of the anterior-superior region as it is the main load-bearing region (Moores *et al.*, 2007) which makes most contact with the femur during motion, which suggests it requires more elasticity and resistance to compression compared to the posterior regions which are more stable. This is further supported as there was the presence of a larger fibrous region posteriorly, with larger type I collagen bundles and more integrations which strongly attach the chondrolabral junction posteriorly compared with the anterior-superior regions. In all examples, the posterior region had the least

microstructural damage with the anterior region sustaining the most degradation followed by the superior region.

Under increased loading, there were notable changes to the microstructure, particularly areas surrounding the chondrolabral junction, which included type I fibre bundles were aligned parallel to the direction of the tear/damage and type II collagen fibres were deteriorated or a drop in the amount of detected signal for type II collagen was lost near the tear suggesting cartilage damage had also occurred. This was theorised to occur as the large type I fibre bundles extended from the fibrous region and connected and attached to the type II collagen matrix; they would typically be attached perpendicular to the junction keeping the chondrolabral junction intact. When damaged or torn, these fibres ruptured and split at the interface no longer in tension, as they separated from the cartilaginous matrix. This may have been because of initial cartilage deterioration and damage first to the type II collagen matrix which was shown by a reduced SHG signal where areas went from purple/red to blue suggesting the red SHG signal showing type II collagen in the cartilage was no longer detected in these areas. This was further supported by the increase in degraded collagen peaks when investigated with spontaneous Raman spectroscopy.

Some challenges in using non-linear imaging techniques in porcine labrum tissue for the first time was due to processing. While the use of SHG allowed high penetration into the tissue it was limited by diffraction. The samples had to be as flat as possible which was challenging to achieve due to the nature of damaged tissue as the processing tried to avoid introducing damage to the microstructure. Therefore, in some instances, it was difficult to determine if some drop in signal intensity was due to the processing and because the section was lower than the objective or if it was due to deterioration and damage within the tissue.

An overall limitation was the banding effect found on all images which was due to the stitching done by the software. There was consistent vignetting on each frame as the

centre of laser is where the focus is whereas the edges of each individual frame were darker causing the banding to be seen.

Due to the unique and complex architecture which makes up the labrum it was challenging to set the detectors to expose evenly for all tissue elements and to account for uneven surfaces due to the large variations in tissue components which make up the labrum. Lack of sufficient fluorescence where fluorescent signals would have been expected could be artefacts caused by processing where the tissue was not flat resulting in the laser depth not reaching the tissue.

more samples would be characterised with better processing to ensure even surfaces and thicknesses although this is quite challenging to achieve in practice.

Further testing on smaller labral sections could be conducted to observe how fibres respond to load with a small loading cell and live SHG imaging to observe how the type I and type II junction respond with applied compression or tension up to failure to understand the micromechanics further.

This would help elucidate whether damage first occurs through a weakened type II collagen matrix, followed by rupturing and detachment of the larger type I collagen fibres which hold the cartilage in place. Testing this hypothesis would help clinicians gauge the condition and quality of the labrum to determine the intervention or surgical technique to use.

Overall, multiphoton imaging has proven to be a useful tool for characterising the structure of

Chapter 7 Overall Discussion

7.1 General discussion

Femoroacetabular impingement frequently results in labral tearing and acetabular chondral delamination, making early identification and treatment crucial to preventing further damage to the hip (Neumann et al. 2022). The findings from the hip simulation were consistent with prior in vitro investigations of natural cartilage specimens (Katta et al., 2009; Lizhang, 2010; Pallan, 2016), which have revealed a correlation between increasing load and escalating damage. The majority of the observed damage was situated in the anterior-superior region of the acetabulae, a finding that is in line with clinically reported damage locations (Beaulé, O'Neill and Rakhra, 2009; Cho et al., 2022; Battistelli et al., 2023).

Increased loading resulted in labral tearing at the anterior-superior region of the labrum which was similar to peripheral tearing observed clinically. Increasing the load was expected to increase contact pressures and promote wear of the labrum/cartilage (Anwander et al., 2018; Bedi et al., 2011; Crawford et al., 2007; Diamond et al., 2016; MacLean et al., 2016) as studies have highlighted the effect of increased wear and damage with increases in a patient's body mass index (BMI) with higher possibility of developing early onset of osteoarthritis and tears when patients were overweight or obese (Chee et al., 2010; Recnik et al., 2009; Reyes et al., 2016). Most experimental studies investigating contact stresses in the hip were static (Ferguson et al., 2003; Konrath et al., 1998; Macirowski, 1994; Y. Song et al., 2012) and limited to lower axial loads (Koh & Gupta, 2017; Lertwanich et al., 2016). In addition, they were concerned with the fluid pressurisation and seal of the labrum. This was to determine the best surgical approach for labral repairs and to assess the impact of removal of the labrum. Due to the lack of electromechanical hip simulators the rigs were limited mechanically in how many degrees of freedom and motion they would allow

Natural hip simulation with use of mechanical hip simulators shows promise for in vitro investigations of abnormal environments experienced in the hip, which would be otherwise extremely difficult to study in vivo. The mechanical hip simulator was able to apply a repeatable and programmable abnormal mechanical loading environment with simplified and localized loading scenarios for understanding how damage can occur at the chondro-labral junction and articulating surfaces. This opens possibilities for creating different abnormal mechanical testing environments for the purpose of generating the types of damage observed in the natural hip.

Chondral damage was generated using a dynamic torsion profile where compression and rotation were applied to cause shearing on the surface of the cartilage to generate delamination-type damage. With increased loading and torsion, the tissue was prone to OARSI grade I and II type damage with the appearance of an uneven surface texture resembling blisters on the cartilage surface, causing fissures and chondral flaps in more severe cases. In addition, at severe loads, the torsion loading profile also resulted in labral tearing at the anterior-superior junction in the presence of the blistered surface. This suggests that chondral damage may be due to shearing-type damage and the labral tearing may be due to overloading and impingement.

200N load increase over time may result in tearing, this is concerning to patients who are overweight or obese and can help in our understanding of how overloading related to labral tearing or articular cartilage damage and how conditions like FAI may exacerbate damage and compromise health of the joint.

To investigate changes to the collagen microstructure and understand how tearing is seen at the microscale, a suitable imaging method which complemented the natural hip simulation was required. Multiphoton imaging was possible on porcine labrum samples without the use of exogenous staining. This resulted in reduced processing-related damage on samples and the resolution allowed individual collagen bundles and fibres to be traced allowing further capabilities to allow polarised light

investigation and Raman spectroscopy to determine the detailed arrangement of collagen in the labrum samples. Initial tests on native samples revealed similarities with observations from histological examination, this suggested that anteriorly, the labrum was more prone to damage as it had a reduced fibrous region. The resolution provided by multiphoton also allowed investigation of the interface between the labrum and articular cartilage allowing novel visualisation into the transition zone and how there is interface where cartilage cells and collagen fibres spindle into thicker, larger collagen bundles into the more fibrocartilaginous structure. This suggested that changes to the collagen matrix could be observed on damaged samples which could aid in our understanding of how damage is occurring and what factors surgeons should consider when choosing repair techniques.

The orientation and dominant direction of collagen fibres appeared different between untested and loaded specimen, where fibres were aligned with the principal direction of the tear as it progresses through the chondrolabral junction. The fibres appeared to be held in tension and a force perpendicular can result in the splitting of these collagen fibre bundles. It is the cross-links which are most likely broken. In some instances, the collagen fibres appeared to change from a non-homogenous structure to a homogenous structure in response to overloading.

Chondrolabral tearing at the anterior-superior region caused by overloading was consistent with the clinical presentation of labral tears (Gdalevitch, Smith and Tanzer, 2009; Waldstein *et al.*, 2016; Brittberg, 2022; G. Gao *et al.*, 2022). Chondrolabral separation was characterised by a degraded type II collagen matrix and reorientation of type I collagen fibres from perpendicular to the junction to parallel to the direction of the tear. Other types of chondrolabral damage such as delamination, blushing, indentations, scratches, and catastrophic damage such as chondrolabral flaps were observed from the simulations. The appearance of blistering on the surface resembled delamination damage at the articular cartilage (Gdalevitch, Smith and Tanzer, 2009; Waldstein *et al.*, 2016; Brittberg, 2022; G. Gao *et al.*, 2022). However,

processing issues resulted in uneven surfaces and could not be characterised microscopically.

Studying the microstructural changes to the collagen fibre arrangement, associated with damaged or degenerated hip tissue, can help predict the underlying mechanisms involved with chondrolabral tearing and degeneration. The microscale disruption can help inform the macroscopic state which in turn can be used to develop or select the best repair techniques to promote repair and preservation of the labrum. To the author's knowledge, this was the first study to generate and characterise clinically relevant damage experimentally in vitro on porcine samples, through natural hip simulation.

The findings show chondrolabral separation anterior-superiorly caused by overloading, where the type I collagen fibre bundles were oriented parallel to the direction of the tear. The type II collagen matrix cartilage deteriorated around the tear with the collagen matrix shifting away from the tear. This may have caused the chondrolabral separation.

Increasing the load was expected to increase contact pressures and promote wear of the labrum/cartilage (Anwander et al., 2018; Bedi et al., 2011; Crawford et al., 2007; Diamond et al., 2016; MacLean et al., 2016) as studies have highlighted the effect of increased wear and damage with increases in a patient's body mass index (BMI) with higher possibility of developing early onset of osteoarthritis and tears when patients were overweight or obese (Chee et al., 2010; Recnik et al., 2009; Reyes et al., 2016).

Through histological examination and multiphoton imaging, the structure of labrum was found to vary from microstructure and composition of collagen between the fibrous, transition and cartilaginous regions of the acetabular labrum. This was also reported in detailed SEM images by Petersen et al (2014), however their study was limited due to processing methods which may have introduced damage during

biopsy, additional artefacts may have been introduced due to processing and fixation required for SEM.

Findings from mechanical simulation and non-linear microscopy suggest that cartilage delamination may precede labral tearing at the anterior-superior rim. Torsional loading revealed important information on how abnormal loading could influence and lead to labral tears. The increased loading, compressive and shear forces in the natural hip joint over time can result in medial-lateral translation and sliding of the femoral head and Femoroacetabular impingement, resulting in chondral damage and abnormal contact at the anterior superior rim resulting in labral tearing. The findings from multiphoton imaging suggest that there is initial damage to the type II collagen fibres present in the cartilage followed by rupturing of the thick type I collagen fibres which connect the cartilage to the external fibrous labrum at the chondrolabral junction. Combining non-linear techniques with experimental simulation can serve as the basis for further investigation into chondrolabral damage and femoroacetabular impingement. These findings may be important in understanding labral tearing and promoting better repair strategies in the ongoing effort to prevent the early onset of osteoarthritis.

To create damage to the labrum and at the chondrolabral junction and cartilage, it was necessary to use the natural asphericity of the femoral head of the porcine hip to create an impingement like scenario. Because of natural variance in samples, there was a small degree of microinstability as well, which may have contributed where tearing was observed. Finally, by applying increased loading continuously over a long period of time caused irreversible damage to the collagen architecture as confirmed by the imaging and histology. Overloading degraded the type II collagen network weakening the area surrounding the anterior-superior region which may have appeared as blushing on the surface, while the thicker type I fibres remained in-tact. The multiphoton imaging revealed that type I fibres were held perpendicular to the junction and therefore shear forces would be needed to in a direction of the weak

axis to tear and rupture these fibres. Once torn, the fibres would lose their tension and were observed to run parallel to the direction of the tear, separating the chondrolabral junction. In the isolated testing where, only torsional motion with overloading was tested, delamination may have occurred and the breaking of the middle region of cartilage while the superficial layer remained intact. This may have caused the layers to slide resulting in the shear forces across the anterior-superior rim where an aspherical porcine head may have impinged, resulting in tearing across the junction. This was shown in some samples but not the others and would need further repeats to confirm. Surgeons should not completely base their assessment on visual characterisation using MR arthrography as while the tissue surface may appear in-tact and un-torn, the wavy pattern or blistering on the surface could indicate subchondral separation and delamination of cartilage. A labral tear could precede cartilage bruising or delamination or vice versa.

The main limitation of the study was a lack of large sample size during the characterisation studies which limited the extent of analysis using histology and non-linear imaging techniques. The immature porcine tissue affects the structure and makes it hard to compare with mature human or clinically relevant damage presentations but can compare with Pallan (2016) and experimental in vivo studies on animal labrum. Intraspecific variation of porcine samples also affected the characterisation, which was dependent on age of sacrifice, varies at time of year, can introduce irregularities in the concavity of the acetabulum, injuries, underdeveloped tissue with excess growth plate. It was difficult to compare non-linear imaging techniques as they were limited to articular cartilage, lack of studies into porcine labrum. SEM, histology and immunohistochemistry were most common methods used. Difficulties in processing may have resulted in uneven surfaces which means some tissue structures would be compacted or missed during data acquisition.

In the simulator studies, there may have been user errors in terms of processing, orientation, or matching centre of rotation – which could result in microinstability. The

study and parameter design were limited by the simulator used, reduced working space, capabilities of mounting larger joints, and slow and user-dependent process for cementing. Reduction in loads of gait profile ISO-14242 was based on a single gait study done on porcine tissue. Loads used represent worst-case and extreme conditions not found physiologically. There was some natural sample variance regarding the asphericity of the femoral head, mismatched head and cup sizes (diameters). Difficulties in processing may have resulted in uneven surfaces which means some tissue structures would be compacted or missed during data acquisition.

Since disarticulation and removal of greater trochanter were unavoidable due to the constraints of the simulator used, and the cut bone was not fully submerged in bone cement, it is possible that bony debris may have been generated as the testing progressed. This is a limitation of the testing setup. A hip simulator with a larger working space which can maintain the anatomical features of the native femur would provide more representative data. This could be the cause of some fine scratches and indentations observed from the simulation.

The current understanding regarding the progression of extraarticular and labral damage remains ambiguous, labral tears are theorised to destabilise the hip resulting in articular damage, while some have reported cartilage damage may precede the appearance of labral tearing. Vitucci et al (2023), suggests that changes in intraarticular pressure result in tearing, where tears result in intra-articular fluid leaving the contact area, promoting further wear. High pressures could cause cartilage damage and that an initially deteriorated articular surface could result in higher cavity pressures resulting in cartilage damage and tearing Vitucci et al (2023) In the future, the study could also incorporate and compare different activities of daily motion where an increased loading or torsion is experienced, and what effect that would have on the acetabular labrum. For example, in running where the frequency is increased and leads to higher peak axial forces (Bergmann et al., 1993), jumping

(D.J. et al., 2013) and sports related activities. These differences could be incorporated by changing the axial force or frequency or duration. Additionally for sports related activities, gait data could help design profiles specific to overloading scenarios linked with specific activities such as in ballet(Tepla et al., 2015) or a golf swing (Way et al., 2013).

An alternative approach would be to gather a depth map of the labrum during testing using a 3D scanner to detect fine surface profiles before and after the simulation. Additionally, post processing algorithms could be applied to precisely detect edges and identify defects in the tissue when taken top-down from a fixed height from the tissue.

Furthermore, the photogrammetry method for qualitatively assessing damage using the macroscopic lens, was able to show small and fine macroscopic details and surface level damage. When combined with further imaging analysis or microscopic examination it would provide a holistic view of the damage progression and help in understanding the mechanical causes for the types of damage observed clinically.

Conclusion

Labral tearing and chondral damage were generated experimentally using *In vitro* hip simulation in porcine hips. By utilising an electromechanical hip simulator, it was possible to generate clinically relevant chondrolabral damage suggesting the potential for use in preclinical testing for assessing early interventions for labral repair. Novel nonlinear imaging techniques using multimodal multiphoton microscopy allowed high-resolution imaging of collagen fibre orientation and arrangement in response to an altered mechanical environment. Second harmonic generation imaging of collagen provided novel insight into how chondrolabral separation presents at the microscale. As such further development in this area would help improve interventions for labral and cartilage damage linked with early onset of osteoarthritis.

Appendix

Details of the hip simulator

Prosim 1-Station Deep Flexion Hip Simulator

Serial Number: SSEMH-001

Year of Manufacture: 2013

Mass: 0.6 tonnes

Power: 3 \emptyset , 415V ac, 16 A/ \emptyset

Simulation Solutions Ltd. Unit 10, Rugby Park, Bletchley Road, Heaton Mersey,
Stockport SK5 7DL, UK.

Details of Photogrammetry

Equipment

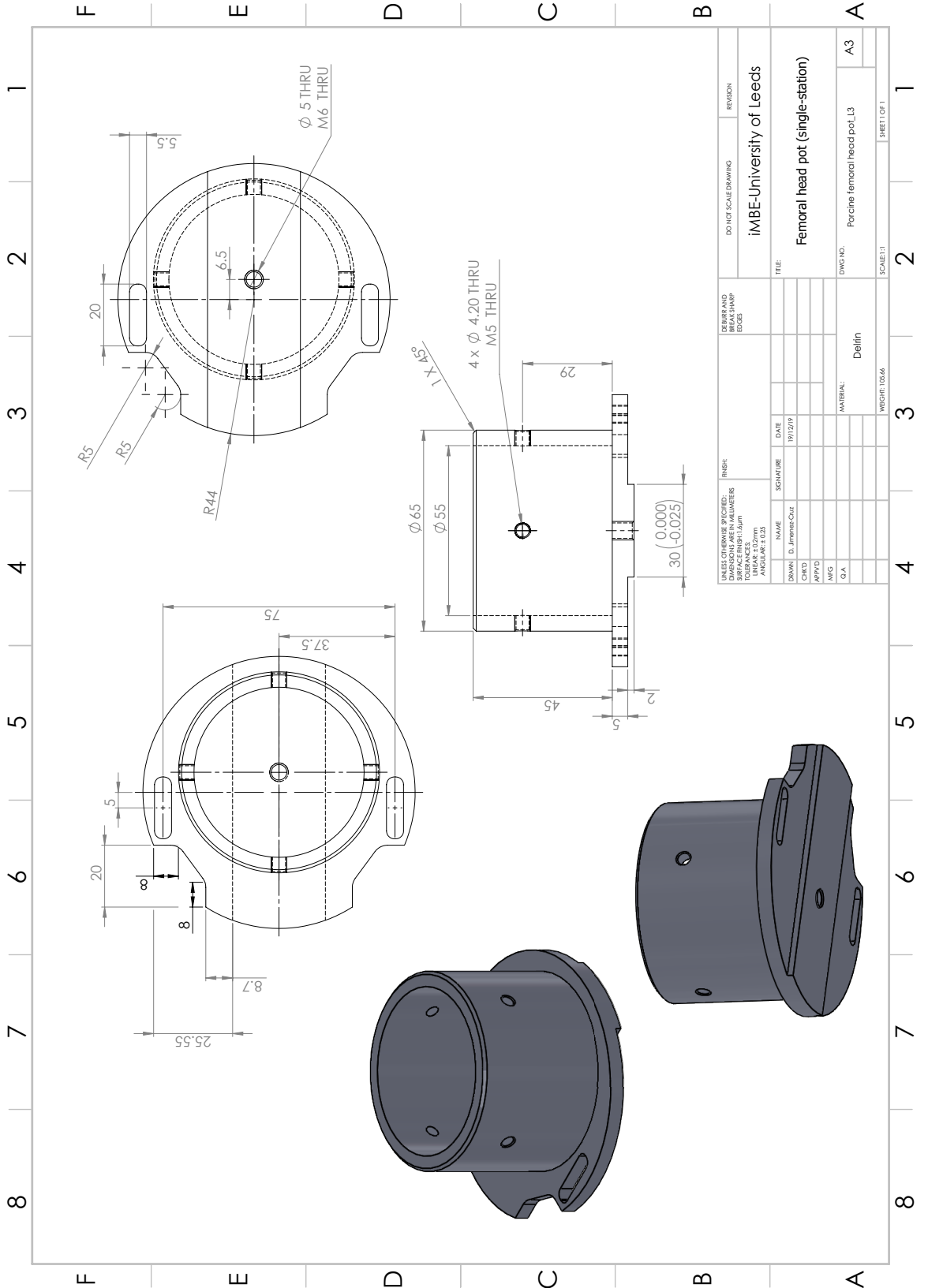
Canon 750D – flip screen to see sample while focusing

Canon EF 100mm f2.8 USM Macro lens @ 1:3 ISO 400 f5.6 1/60

28-70 mm Wide angle lens @ ISO 200 f5.6 1/60

Fine details at 1:1 @ ISO 200 f8 1/60





DESIGN APPROVALS:		DATE	
DESIGNED BY:	NAME	SIGNATURE	DATE
DRAWN BY:	D. Jimenez-Cruz		19/12/19
CHECKED BY:			
APPROVED BY:			
MATERIAL:	Delfin		
SCALE:	1:1		
WEIGHT:	103.66g		
REVISIONS:		REVISION	
iMBE-University of Leeds			
Femoral head pot (single-station)			
DWG NO.:	Parcine femoral head pot_L3		A3
SCALE: 1:1			SHEET 1 OF 1

References

- A.L, K. *et al.* (2016) 'Location, type and severity of chondrolabral damage in FAI patients', *Journal of Orthopaedic Research*, 34(Supplement 1), p. 2016. Available at: <http://dx.doi.org/10.1002/jor.23247>.
- Alashkham, A. *et al.* (2018) 'Histology, vascularity and innervation of the glenoid labrum', *Journal of Orthopaedic Surgery*, 26(2), pp. 1–8. Available at: <https://doi.org/10.1177/2309499018770900>.
- Alcaide-Ruggiero, L., Cugat, R. and Domínguez, J.M. (2023) 'Proteoglycans in Articular Cartilage and Their Contribution to Chondral Injury and Repair Mechanisms', *International Journal of Molecular Sciences*, 24(13), p. 10824. Available at: <https://doi.org/10.3390/ijms241310824>.
- Alhadtaq, H.A. *et al.* (2004) 'Detecting structural changes in early experimental osteoarthritis of tibial cartilage by microscopic magnetic resonance imaging and polarised light microscopy', *Annals of the Rheumatic Diseases*, 63(6), pp. 709–717. Available at: <https://doi.org/10.1136/ard.2003.011783>.
- Al-Talalwah, W. (2015) 'The Vascular Supply of Hip Joint and its Clinical Significant Suministro Vascular de la Articulación de la Cadera y su Significado Clínico', *Int. J. Morphol*, 33(1), pp. 62–67. Available at: <https://doi.org/10.4067/S0717-95022015000100010>.
- Alzaharani, A. *et al.* (2014) 'The innervation of the human acetabular labrum and hip joint: an anatomic study'. Available at: <https://doi.org/10.1186/1471-2474-15-41>.
- Amanatullah, D.F. *et al.* (2015) 'Femoroacetabular Impingement: Current Concepts in Diagnosis and Treatment', *Orthopedics*, 38(3), pp. 185–199. Available at: <https://doi.org/10.3928/01477447-20150305-07>.
- Anderson, K., Strickland, S.M. and Warren, R. (2001) 'Hip and groin injuries in athletes', *American Journal of Sports Medicine*. Available at: <https://doi.org/10.1177/03635465010290042501>.
- Angsutanasombat, C. *et al.* (2018) 'Design of hip simulation machine for hip labrum testing', *Engineering Journal*, 22(2), pp. 117–130. Available at: <https://doi.org/10.4186/ej.2018.22.2.117>.
- Anwander, H., Beck, M. and Büchler, L. (2018) 'Influence of evolution on cam deformity and its impact on biomechanics of the human hip joint', *Journal of Orthopaedic Research*, pp. 1–5. Available at: <https://doi.org/10.1002/jor.23863>.
- van Arkel, R.J., Amis, A.A. and Jeffers, J.R.T. (2015) 'The envelope of passive motion allowed by the capsular ligaments of the hip', *Journal of Biomechanics*, 48(14), pp. 3803–3809. Available at: <https://doi.org/10.1016/j.jbiomech.2015.09.002>.
- Arndt, C. *et al.* (2017) 'Shear stress and von Mises stress distributions in the periphery of an embedded acetabular cup implant during impingement', *Biomedizinische Technik*, 62(3), pp. 279–288. Available at: <https://doi.org/10.1515/bmt-2016-0107>.

Aspden, R.M. and Hukins, D.W.L. (1979) 'The lamina splendens of articular cartilage is an artefact of phase contrast microscopy', *Proc R Soc Lond B Biol Sci*, 206(1162), pp. 109–113. Available at: <https://doi.org/10.1098/rspb.1979.0094>.

Audenaert, E.A. *et al.* (2012) 'Histologic assessment of acetabular labrum healing', *Arthroscopy - Journal of Arthroscopic and Related Surgery*, 28(12), pp. 1784–1789. Available at: <https://doi.org/10.1016/j.arthro.2012.06.012>.

Austin, A.B. *et al.* (2008) 'Identification of Abnormal Hip Motion Associated With Acetabular Labral Pathology', *Journal of Orthopaedic & Sports Physical Therapy*, 38(9), pp. 558–565. Available at: <https://doi.org/10.2519/jospt.2008.2790>.

Aydingöz, U. and Öztürk, M.H. (2001) 'MR imaging of the acetabular labrum: A comparative study of both hips in 180 asymptomatic volunteers', *European Radiology*, 11(4), pp. 567–574. Available at: <https://doi.org/10.1007/s003300000597>.

Banerjee, P. and Mclean, C.R. (2011) 'Femoroacetabular impingement: a review of diagnosis and management', *Current Reviews in Musculoskeletal Medicine*, 4(1), pp. 23–32. Available at: <https://doi.org/10.1007/s12178-011-9073-z>.

Barros, A.A.G. *et al.* (2019) 'Determining Reliability of Arthroscopic Classifications for Hip Labral Tears', *Clinical Journal of Sport Medicine*, p. 1. Available at: <https://doi.org/10.1097/jsm.0000000000000717>.

Battistelli, M. *et al.* (2023) 'Hip Labral Morphological Changes in Patients with Femoroacetabular Impingement Speed Up the Onset of Early Osteoarthritis', *Calcified Tissue International*, 112(6), pp. 666–674. Available at: <https://doi.org/10.1007/s00223-023-01076-1>.

Beaulé, P.E., O'Neill, M. and Rakhra, K. (2009) 'Acetabular Labral Tears', *The Journal of Bone and Joint Surgery-American Volume*, 91(3), pp. 701–710. Available at: <https://doi.org/10.2106/JBJS.H.00802>.

Beck, M. (2005) 'Hip morphology influences the pattern of damage to the acetabular cartilage: FEMOROACETABULAR IMPINGEMENT AS A CAUSE OF EARLY OSTEOARTHRITIS OF THE HIP', *Journal of Bone and Joint Surgery - British Volume*, 87-B(7), pp. 1012–1018. Available at: <https://doi.org/10.1302/0301-620X.87B7.15203>.

Beck, M. *et al.* (2012) 'Mechanism of Femoroacetabular Impingement', in Ó. Marín-Peña (ed.) *Femoroacetabular Impingement*. Springer Berlin Heidelberg, pp. 9–22. Available at: https://doi.org/10.1007/978-3-642-22769-1_2.

Beck, M. and Universitätsspital, B. (2015) 'Femoroacetabular impingement: A cause for osteoarthritis of the hip', (JANUARY 2003), pp. 112–120. Available at: <https://doi.org/10.1097/01.blo.0000096804.78689.c2>.

Bedi, A. *et al.* (2011) 'Static and Dynamic Mechanical Causes of Hip Pain', *Arthroscopy: The Journal of Arthroscopic & Related Surgery*, 27(2), pp. 235–251. Available at: <https://doi.org/10.1016/j.arthro.2010.07.022>.

Benjamin, M. and Ralphs, J.R. (2004) 'Biology of Fibrocartilage Cells', in *International Review of Cytology*. Elsevier, pp. 1–45. Available at: [https://doi.org/10.1016/S0074-7696\(04\)33001-9](https://doi.org/10.1016/S0074-7696(04)33001-9).

- Bergmann, G. *et al.* (2001) 'Hip contact and gait patterns from routine activities.PDF', 34, pp. 859–871.
- Bergmann, G. *et al.* (2016) 'Standardized Loads Acting in Hip Implants', *PLOS ONE*. Edited by M.A. Pérez, 11(5), p. e0155612. Available at: <https://doi.org/10.1371/journal.pone.0155612>.
- Bergmann, G., Graichen, F. and Rohlmann, A. (1993) 'Hip joint loading during walking and running, measured in two patients', *Journal of Biomechanics*, 26(8), pp. 969–990. Available at: [https://doi.org/10.1016/0021-9290\(93\)90058-M](https://doi.org/10.1016/0021-9290(93)90058-M).
- Bergmann, G., Graichen, F. and Rohlmann, A. (1999) 'Hip joint forces in sheep', *Journal of Biomechanics*, 32(8), pp. 769–777. Available at: [https://doi.org/10.1016/S0021-9290\(99\)00068-8](https://doi.org/10.1016/S0021-9290(99)00068-8).
- Bliddal, H., Leeds, A.R. and Christensen, R. (2014) 'Osteoarthritis, obesity and weight loss: Evidence, hypotheses and horizons - a scoping review', *Obesity Reviews*, 15(7), pp. 578–586. Available at: <https://doi.org/10.1111/obr.12173>.
- Borile, G. *et al.* (2021) 'Label-Free Multiphoton Microscopy: Much More Than Fancy Images', *International Journal of Molecular Sciences*, 22(5), p. 2657. Available at: <https://doi.org/10.3390/ijms22052657>.
- Bortel, E.L., Charbonnier, B. and Heuberger, R. (2015) 'Development of a synthetic synovial fluid for tribological testing', *Lubricants*, 3(4), pp. 664–686. Available at: <https://doi.org/10.3390/lubricants3040664>.
- Bouma, H.W. *et al.* (2015) 'Can Combining Femoral and Acetabular Morphology Parameters Improve the Characterization of Femoroacetabular Impingement?', *Clinical Orthopaedics and Related Research®*, 473(4), pp. 1396–1403. Available at: <https://doi.org/10.1007/s11999-014-4037-4>.
- Bowland, P. *et al.* (2018) 'Development of a preclinical natural porcine knee simulation model for the tribological assessment of osteochondral grafts in vitro', *Journal of Biomechanics*, 77, pp. 91–98. Available at: <https://doi.org/10.1016/j.jbiomech.2018.06.014>.
- Bowman, K.F., Fox, J. and Sekiya, J.K. (2010) 'A clinically relevant review of hip biomechanics', *Arthroscopy - Journal of Arthroscopic and Related Surgery*, 26(8), pp. 1118–1129. Available at: <https://doi.org/10.1016/j.arthro.2010.01.027>.
- Boykin, R.E. *et al.* (2011) 'Hip Instability', *JAAOS - Journal of the American Academy of Orthopaedic Surgeons*, 19(6), p. 340.
- Brinckmann, P., Frobin, W. and Hierholzer, E. (1981) 'Stress on the articular surface of the hip joint in healthy adults and persons with idiopathic osteoarthritis of the hip joint', *Journal of Biomechanics* [Preprint]. Available at: [https://doi.org/10.1016/0021-9290\(81\)90021-X](https://doi.org/10.1016/0021-9290(81)90021-X).
- Brittberg, M. (2022) 'Knee chondral delaminations and blisters', *Journal of Cartilage & Joint Preservation*, 2(3), p. 100056. Available at: <https://doi.org/10.1016/j.jcjp.2022.100056>.
- Bryan, J.H.D. (1955) 'Differential Staining with a Mixture of Safranin and Fast Green FCF', *Stain Technology*, 30(4), pp. 153–157. Available at: <https://doi.org/10.3109/10520295509114456>.

BURNETT, R.S.J. *et al.* (2006) 'CLINICAL PRESENTATION OF PATIENTS WITH TEARS OF THE ACETABULAR LABRUM', *The Journal of Bone and Joint Surgery-American Volume*, 88(7), pp. 1448–1457. Available at: <https://doi.org/10.2106/00004623-200607000-00004>.

Burstein, A.H. (2001) 'Basic Biomechanics of the Musculoskeletal System. 3rd ed.', *The Journal of Bone and Joint Surgery-American Volume* [Preprint]. Available at: <https://doi.org/10.2106/00004623-200109000-00046>.

Byrd, J.W.T. (2005) 'Gross anatomy', *Operative Hip Arthroscopy*, pp. 100–109. Available at: https://doi.org/10.1007/0-387-27047-7_6.

Byrd, J.W.T. (2014) 'Femoroacetabular impingement in athletes: Current concepts', *American Journal of Sports Medicine*, 42(3), pp. 737–751. Available at: <https://doi.org/10.1177/0363546513499136>.

Byrne, D.P., Mulhall, K.J. and Baker, J.F. (2014) 'Anatomy & Biomechanics of the Hip', *The Open Sports Medicine Journal*, 4(1), pp. 51–57. Available at: <https://doi.org/10.2174/1874387001004010051>.

Cadet, E.R. *et al.* (2012) 'Investigation of the preservation of the fluid seal effect in the repaired, partially resected, and reconstructed acetabular labrum in a cadaveric hip model', *American Journal of Sports Medicine*, 40(10), pp. 2218–2223. Available at: <https://doi.org/10.1177/0363546512457645>.

Camplejohn, K.L. and Allard, S.A. (1988) 'Limitations of safranin "O" staining in proteoglycan-depleted cartilage demonstrated with monoclonal antibodies', *Histochemistry*, 89(2), pp. 185–188. Available at: <https://doi.org/10.1007/BF00489922>.

Carton, P.F. and Filan, D. (2017) 'Labral cuff refixation in the hip: rationale and operative technique for preserving the chondrolabral interface for labral repair: a case series', *Journal of Hip Preservation Surgery*, 5(1), pp. 78–87. Available at: <https://doi.org/10.1093/jhps/hnx038>.

Cashin, M. *et al.* (2008) 'Embryology of the acetabular labral-chondral complex', *Journal of Bone and Joint Surgery - Series B*, 90(8), pp. 1019–1024. Available at: <https://doi.org/10.1302/0301-620X.90B8.20161>.

Cassar-Gheiti, A.J. *et al.* (2017) 'Chondral Lesion in the Hip Joint and Current Chondral Repair Techniques', in *Cartilage Repair and Regeneration*. IntechOpen. Available at: <https://doi.org/10.5772/intechopen.70261>.

Cevallos, N. *et al.* (2021) 'Hip Arthroscopy Volume and Reoperations in a Large Cross-Sectional Population: High Rate of Subsequent Revision Hip Arthroscopy in Young Patients and Total Hip Arthroplasty in Older Patients', *Arthroscopy: The Journal of Arthroscopic & Related Surgery*, 37(12), pp. 3445-3454.e1. Available at: <https://doi.org/10.1016/j.arthro.2021.04.017>.

Charbonnier, C. *et al.* (2009) 'Motion study of the hip joint in extreme postures', *Visual Computer*, 25(9), pp. 873–882. Available at: <https://doi.org/10.1007/s00371-009-0317-5>.

Chegini, S., Beck, M. and Ferguson, S.J. (2009) 'The effects of impingement and dysplasia on stress distributions in the hip joint during sitting and walking: A finite

element analysis', *Journal of Orthopaedic Research*, 27(2), pp. 195–201. Available at: <https://doi.org/10.1002/jor.20747>.

Chen, X. *et al.* (2012) 'Second harmonic generation microscopy for quantitative analysis of collagen fibrillar structure', *Nature Protocols*, 7(4), pp. 654–669. Available at: <https://doi.org/10.1038/nprot.2012.009>.

Cho, Y.-J. *et al.* (2022) 'Patterns of labral tears and cartilage injury are different in femoroacetabular impingement and dysplasia', *Journal of Hip Preservation Surgery*, 9, pp. 151–157. Available at: <https://doi.org/10.1093/jhps/hnac026>.

Clohisy, J.C. *et al.* (2011) 'Radiographic structural abnormalities associated with premature, natural hip-joint failure', *Journal of Bone and Joint Surgery - Series A*, 93(SUPPL. 2), pp. 3–9. Available at: <https://doi.org/10.2106/JBJS.J.01734>.

Clohisy, J.C., John, L.C.S. and Schutz, A.L. (2010) 'Surgical treatment of femoroacetabular impingement: A systematic review of the literature', in *Clinical Orthopaedics and Related Research*, pp. 555–564. Available at: <https://doi.org/10.1007/s11999-009-1138-6>.

Cohen, N.P., Foster, R.J. and Mow, V.C. (1998) 'Composition and dynamics of articular cartilage: structure, function, and maintaining healthy state.', *The Journal of orthopaedic and sports physical therapy*, 28(4), pp. 203–15. Available at: <https://doi.org/10.2519/jospt.1998.28.4.203>.

Como, C.J. *et al.* (2021) 'Common animal models lack a distinct glenoid labrum: a comparative anatomy study', *Journal of Experimental Orthopaedics*, 8(1), p. 63. Available at: <https://doi.org/10.1186/s40634-021-00383-6>.

Cone, S.G., Warren, P.B. and Fisher, M.B. (2017) 'Rise of the Pigs: Utilization of the Porcine Model to Study Musculoskeletal Biomechanics and Tissue Engineering During Skeletal Growth', *Tissue Engineering Part C: Methods*, 23(11), pp. 763–780. Available at: <https://doi.org/10.1089/ten.tec.2017.0227>.

Copes, F. *et al.* (2019) 'Collagen-based tissue engineering strategies for vascular medicine', *Frontiers in Bioengineering and Biotechnology*. Frontiers Media S.A. Available at: <https://doi.org/10.3389/fbioe.2019.00166>.

Cramer, G.D. and Bakkum, B.W. (2014) 'Microscopic Anatomy of the Zygapophysial Joints, Intervertebral Discs, and Other Major Tissues of the Back', in *Clinical Anatomy of the Spine, Spinal Cord, and Ans.* Elsevier, pp. 586–637. Available at: <https://doi.org/10.1016/B978-0-323-07954-9.00014-1>.

Crawford, M.J. *et al.* (2007) 'The biomechanics of the hip labrum and the stability of the hip', *Clinical Orthopaedics and Related Research*, (465), pp. 16–22. Available at: <https://doi.org/10.1097/BLO.0b013e31815b181f>.

Cruveilhier, J. (1847) *The anatomy of the human body*. Available at: https://books.google.co.uk/books?id=7_LtAgAAQBAJ.

Czerny, C. *et al.* (1996) 'Lesions of the acetabular labrum: accuracy of MR imaging and MR arthrography in detection and staging.', *Radiology*, 200(1), pp. 225–230. Available at: <https://doi.org/10.1148/radiology.200.1.8657916>.

Degen, R.M. *et al.* (2022) 'Hip arthroscopy utilization and reoperation rates in Ontario: a population-based analysis comparing different age cohorts', *Canadian*

Journal of Surgery, 65(2), pp. E228–E235. Available at: <https://doi.org/10.1503/cjs.025020>.

D'lima, D.D. *et al.* (2000) 'The Effect of the Orientation of the Acetabular and Femoral Components on the Range of Motion of the Hip at Different Head-Neck Ratios *'.

Dowson, D. and Jobbins, B. (1988) 'Design and development of a versatile hip joint simulator and a preliminary assessment of wear and creep in Charnley total replacement hip joints.', *Engineering in medicine*, 17(3), pp. 111–7. Available at: <https://doi.org/10.1016/B978-0-08-102269-6.50002-1>.

Eleswarapu, S.V., Responde, D.J. and Athanasiou, K.A. (2011) 'Tensile properties, collagen content, and crosslinks in connective tissues of the immature knee joint', *PLoS ONE*, 6(10), pp. 1–7. Available at: <https://doi.org/10.1371/journal.pone.0026178>.

El-Radi, M.A. *et al.* (2018) 'Basics in hip chondrolabral lesions and state of the art', *Sicot-J*, 3, p. 73. Available at: <https://doi.org/10.1051/sicotj/2017040>.

Eschweiler, J. *et al.* (2021) 'The Biomechanics of Cartilage—An Overview', *Life*, 11(4), p. 302. Available at: <https://doi.org/10.3390/life11040302>.

Exposito, J.Y. *et al.* (2010) 'The fibrillar collagen family', *International Journal of Molecular Sciences*. Available at: <https://doi.org/10.3390/ijms11020407>.

Fairley, J. *et al.* (2016) 'Management options for femoroacetabular impingement: a systematic review of symptom and structural outcomes', *Osteoarthritis and Cartilage*. W.B. Saunders Ltd. Available at: <https://doi.org/10.1016/j.joca.2016.04.014>.

Felson, D.T. and Zhang, Y. (1998) 'AN UPDATE ON THE EPIDEMIOLOGY OF KNEE AND HIP OSTEOARTHRITIS WITH A VIEW TO PREVENTION', 41(8), pp. 1343–1355. Available at: [https://doi.org/10.1002/1529-0131\(199808\)41:8<1343::AID-ART3>3.0.CO;2-9](https://doi.org/10.1002/1529-0131(199808)41:8<1343::AID-ART3>3.0.CO;2-9).

Ferguson, S.J. *et al.* (2003) 'An in vitro investigation of the acetabular labral seal in hip joint mechanics', *Journal of Biomechanics*, 36(2), pp. 171–178. Available at: [https://doi.org/10.1016/S0021-9290\(02\)00365-2](https://doi.org/10.1016/S0021-9290(02)00365-2).

Fermor, H.L. *et al.* (2015) 'Biological, biochemical and biomechanical characterisation of articular cartilage from the porcine, bovine and ovine hip and knee', *Bio-Medical Materials and Engineering*, 25(4), pp. 381–395. Available at: <https://doi.org/10.3233/BME-151533>.

Forster, H. and Fisher, J. (1996) 'The influence of loading time and lubricant on the friction of articular cartilage', *Proceedings of the Institution of Mechanical Engineers. Part H, Journal of Engineering in Medicine*, 210(2), pp. 109–119. Available at: https://doi.org/10.1243/PIME_PROC_1996_210_399_02.

Fox, A.J.S., Bedi, A. and Rodeo, S.A. (2012) 'The Basic Science of Human Knee Menisci', *Sports Health: A Multidisciplinary Approach*, 4(4), pp. 340–351. Available at: <https://doi.org/10.1177/1941738111429419>.

Fransen, M. *et al.* (2011) 'Hip and knee pain: Role of occupational factors', *Best Practice and Research: Clinical Rheumatology*, 25(1), pp. 81–101. Available at: <https://doi.org/10.1016/j.berh.2011.01.012>.

Gabner, S., Häusler, G. and Böck, P. (2017) 'Vascular Canals in Permanent Hyaline Cartilage: Development, Corrosion of Nonmineralized Cartilage Matrix, and Removal of Matrix Degradation Products', *The Anatomical Record*, 300(6), pp. 1067–1082. Available at: <https://doi.org/10.1002/AR.23537>.

Gahunia, H.K. *et al.* (2020) 'Articular cartilage of the knee: Health, disease and therapy', *Articular Cartilage of the Knee: Health, Disease and Therapy*, pp. 1–498. Available at: <https://doi.org/10.1007/978-1-4939-7587-7/COVER>.

Gahunia, H.K. and Pritzker, K.P.H. (2020) 'Structure and function of articular cartilage', *Articular Cartilage of the Knee: Health, Disease and Therapy*, pp. 3–70. Available at: https://doi.org/10.1007/978-1-4939-7587-7_1.

Ganz, R. *et al.* (2008) 'The etiology of osteoarthritis of the hip: An integrated mechanical concept', *Clinical Orthopaedics and Related Research*, 466(2), pp. 264–272. Available at: <https://doi.org/10.1007/s11999-007-0060-z>.

Gao, G. *et al.* (2022) 'Accuracy of Magnetic Resonance Imaging in the Diagnosis of Acetabular Chondral Delamination in Femoroacetabular Impingement', *Orthopaedic Journal of Sports Medicine*, 10(8), p. 23259671221119225. Available at: <https://doi.org/10.1177/23259671221119225>.

Gao, L. *et al.* (2022) 'Lubrication Modelling of Artificial Joint Replacements: Current Status and Future Challenges'. Available at: <https://doi.org/10.3390/lubricants10100238>.

Gardner, D.L. (2008) 'An Introduction to the Biomechanics of Joints and Joint Replacement', *Annals of the Rheumatic Diseases* [Preprint]. Available at: <https://doi.org/10.1136/ard.41.4.439-c>.

Gdalevitch, M., Cra, K.S. and Tanzer, M. (no date) 'Delamination Cysts A Predictor of Acetabular Cartilage Delamination in Hips with a Labral Tear'. Available at: <https://doi.org/10.1007/s11999-008-0564-1>.

Gdalevitch, M., Smith, K. and Tanzer, M. (2009) 'Delamination Cysts: A Predictor of Acetabular Cartilage Delamination in Hips with a Labral Tear', *Clinical Orthopaedics and Related Research*, 467(4), pp. 985–991. Available at: <https://doi.org/10.1007/s11999-008-0564-1>.

Gerhardt, M. *et al.* (2012) 'Characterisation and classification of the neural anatomy in the human hip joint', *HIP International* [Preprint]. Available at: <https://doi.org/10.5301/HIP.2012.9042>.

Goodfellow, J., Hungerford, D.S. and Zindel, M. (1976) 'Patello-femoral joint mechanics and pathology. 1. Functional anatomy of the patello-femoral joint', *The Journal of Bone and Joint Surgery. British Volume*, 58(3), pp. 287–290. Available at: <https://doi.org/10.1302/0301-620X.58B3.956243>.

Gopinathan, P.A. *et al.* (2020) 'Reexploring picosirius red: A review', *Indian Journal of Pathology and Oncology*, 7(2), pp. 196–203. Available at: <https://doi.org/10.18231/j.ijpo.2020.038>.

Greaves, L.L. (2008) 'Effect of Acetabular Labral Tears, Repair and Resection on Hip Cartilage Strains: A 7T MR Study', p. 183.

Greenwald, a S. and Haynes, D.W. (1972) 'Weight-bearing areas in the human hip joint.', *The Journal of bone and joint surgery. British volume*, 54(1), pp. 157–163. Available at: <https://doi.org/10.1038/2171290a0>.

Greenwald, A.S. and Nelson, C.L. (1973) 'Biomechanics of the reconstructed hip', *Orthopedic Clinics of North America*, 4(2).

Greenwald, A.S. and O'Connor, J.J. (1971) 'The transmission of load through the human hip joint', *Journal of Biomechanics*, 4(6), pp. 507–528. Available at: [https://doi.org/10.1016/0021-9290\(71\)90041-8](https://doi.org/10.1016/0021-9290(71)90041-8).

Groh, M.M. and Herrera, J. (2009) 'A comprehensive review of hip labral tears', *Current Reviews in Musculoskeletal Medicine*, 2(2), pp. 105–117. Available at: <https://doi.org/10.1007/s12178-009-9052-9>.

Groves, D. (2016) 'Geometric variances in hip oseoarthritis ad tribology of the natural hip', (June).

Groves, D., Fisher, J. and Williams, S. (2017) 'An in vitro simulation method for the tribological assessment of complete natural hip joints', *PLoS ONE*, 12(9), pp. 1–15. Available at: <https://doi.org/10.1371/journal.pone.0184226>.

Gruber, H.E., Massry, S.G. and Brautbar, N. (1994) 'Effect of relatively long-term hypomagnesemia on the chondro-osseous features of the rat vertebrae', *Miner Electrolyte Metab*, 20.

Haas, S.S., Brauer, G.M. and Dickson, G. (1975) 'A characterization of polymethylmethacrylate bone cement', *The Journal of Bone and Joint Surgery. American Volume*, 57(3), pp. 380–391.

Han, E. *et al.* (2011) 'Contribution of Proteoglycan Osmotic Swelling Pressure to the Compressive Properties of Articular Cartilage', *Biophysical Journal*, 101(4), pp. 916–924. Available at: <https://doi.org/10.1016/j.bpj.2011.07.006>.

Harris, J.D. (2016) 'Hip labral repair: options and outcomes', *Current Reviews in Musculoskeletal Medicine*, 9(4), pp. 361–367. Available at: <https://doi.org/10.1007/s12178-016-9360-9>.

Harris, J.D. *et al.* (2016) 'Microinstability of the Hip and the Splits Radiograph', *Orthopedics*, 39(1), pp. e169–e175. Available at: <https://doi.org/10.3928/01477447-20151228-08>.

Helmchen, F. and Denk, W. (2005) 'Deep tissue two-photon microscopy', *Nature Methods*, 2(12), pp. 932–940. Available at: <https://doi.org/10.1038/nmeth818>.

Henak, C.R. *et al.* (2011) 'Role of the acetabular labrum in load support across the hip joint', *Journal of Biomechanics*, 44(12), pp. 2201–2206. Available at: <https://doi.org/10.1016/j.jbiomech.2011.06.011>.

Hill, A.M. *et al.* (2008) 'Collagenous microstructure of the glenoid labrum and biceps anchor', *Journal of Anatomy*, 212(6), pp. 853–862. Available at: <https://doi.org/10.1111/j.1469-7580.2008.00904.x>.

Hodaei, M., Farhang, K. and Maani, N. (2014) 'A Contact Model for Establishment of Hip Joint Implant Wear Metrics', *Journal of Biomedical Science and Engineering*, 07(04), pp. 228–242. Available at: <https://doi.org/10.4236/jbise.2014.74026>.

Holleyman, R. *et al.* (2018) 'NAHR 3rd Annual report 2018', *Non-Arthroplasty Hip Registry*. Available at: <https://doi.org/1.1>.

Holleyman, R. *et al.* (2023) 'Hip arthroscopy for femoroacetabular impingement is associated with significant improvement in early patient reported outcomes: analysis of 4963 cases from the UK non-arthroplasty registry (NAHR) dataset', *Knee Surgery, Sports Traumatology, Arthroscopy*, 31(1), pp. 58–69. Available at: <https://doi.org/10.1007/s00167-022-07042-y>.

Horner, W.E. (1846) *Special Anatomy and Histology*. Lea & Blanchard. Available at: <https://books.google.co.uk/books?id=j1Y5AQAAMAAJ>.

Horvai, A. (2011) 'Anatomy and Histology of Cartilage', in *Cartilage Imaging*. Springer New York, pp. 1–10. Available at: https://doi.org/10.1007/978-1-4419-8438-8_1.

Hosseini, S.M. *et al.* (2013) 'Is collagen fiber damage the cause of early softening in articular cartilage?', *Osteoarthritis and Cartilage*, 21(1), pp. 136–143. Available at: <https://doi.org/10.1016/j.joca.2012.09.002>.

Hoy, R.C. *et al.* (2020) 'Advanced glycation end products cause RAGE-dependent annulus fibrosus collagen disruption and loss identified using in situ second harmonic generation imaging in mice intervertebral disk in vivo and in organ culture models', *JOR SPINE*, 3(4), p. e1126. Available at: <https://doi.org/10.1002/jsp2.1126>.

Hu, M.Y. and Nukavarapu, S. (2019) 'Scaffolds for cartilage tissue engineering', *Handbook of Tissue Engineering Scaffolds: Volume One*, pp. 211–244. Available at: <https://doi.org/10.1016/B978-0-08-102563-5.00011-3>.

Hunt, D., Clohisy, J. and Prather, H. (2007) 'Acetabular Labral Tears of the Hip in Women', *Physical Medicine and Rehabilitation Clinics of North America*. Available at: <https://doi.org/10.1016/j.pmr.2007.05.007>.

Hunt, M.A., Gunther, J.R. and Gilbert, M.K. (2013) 'Kinematic and kinetic differences during walking in patients with and without symptomatic femoroacetabular impingement', *Clinical Biomechanics*, 28(5), pp. 519–523. Available at: <https://doi.org/10.1016/j.clinbiomech.2013.05.002>.

Huyse, W.C.J. and Verstraete, K.L. (2021) 'Cartilage Trauma', *Medical Radiology*, pp. 69–97. Available at: https://doi.org/10.1007/174_2020_248/COVER.

Ipavec, M. *et al.* (1999) 'Mathematical modelling of stress in the hip during gait', in *Journal of Biomechanics*. Available at: [https://doi.org/10.1016/S0021-9290\(99\)00119-0](https://doi.org/10.1016/S0021-9290(99)00119-0).

Jackson, K.A. *et al.* (2015) 'Assessing risk factors for early hip osteoarthritis in activity-related hip pain: A Delphi study', *BMJ Open*, 5(9), pp. 1–10. Available at: <https://doi.org/10.1136/bmjopen-2015-007609>.

Julkunen, P. *et al.* (2009) 'Biomechanical, biochemical and structural correlations in immature and mature rabbit articular cartilage', *Osteoarthritis and Cartilage*, 17(12), pp. 1628–1638. Available at: <https://doi.org/10.1016/j.joca.2009.07.002>.

Julkunen, P. *et al.* (2013) 'A review of the combination of experimental measurements and fibril-reinforced modeling for investigation of articular cartilage and chondrocyte response to loading', *Computational and Mathematical Methods in Medicine*, 2013(May 2014). Available at: <https://doi.org/10.1155/2013/326150>.

Junqueira, L.C.U., Bignolas, G. and Brentani, R.R. (1979) 'Picrosirius staining plus polarization microscopy, a specific method for collagen detection in tissue sections', *The Histochemical Journal*, 11(4), pp. 447–455. Available at: <https://doi.org/10.1007/BF01002772>.

Katta, J. *et al.* (2007) 'Effect of load variation on the friction properties of articular cartilage', *Proceedings of the Institution of Mechanical Engineers, Part J: Journal of Engineering Tribology*, 221(3), pp. 175–181. Available at: <https://doi.org/10.1243/13506501JET240>.

Katta, J. *et al.* (2009) 'Chondroitin sulphate: an effective joint lubricant?', *Osteoarthritis and Cartilage*, 17(8), pp. 1001–1008. Available at: <https://doi.org/10.1016/j.joca.2009.02.010>.

Kaya, M. *et al.* (2016) 'Hip morphology influences the pattern of articular cartilage damage', *Knee Surgery, Sports Traumatology, Arthroscopy*, 24(6), pp. 2016–2023. Available at: <https://doi.org/10.1007/s00167-014-3297-6>.

Kaya, T. (2014) 'Evaluation of Labral Pathology and Hip Articular Cartilage in Patients with Femoroacetabular Impingement (FAI): Comparison of Multidetector CT Arthrography and MR Arthrography', *Polish Journal of Radiology*, 79, pp. 374–380. Available at: <https://doi.org/10.12659/PJR.890910>.

Keene, G.S. and Villar, R.N. (1994) 'Arthroscopic anatomy of the hip: An in vivo study', *Arthroscopy*, 10(4), pp. 392–399. Available at: [https://doi.org/10.1016/S0749-8063\(05\)80189-6](https://doi.org/10.1016/S0749-8063(05)80189-6).

Kim, Y.H. (1984) 'Acetabular dysplasia and osteoarthritis developed by an eversion of the acetabular labrum.', *Yonsei medical journal*, 25(2), pp. 97–104. Available at: <https://doi.org/10.3349/ymj.1984.25.2.97>.

Kim, Y.T. and Azuma, H. (1995) 'The Nerve Endings of the Acetabular Labrum', *CLINICAL ORTHOPAEDICS AND RELATED RESEARCH Number* [Preprint]. Available at: <https://doi.org/10.1097/00003086-199511000-00029>.

King, L.K., March, L. and Anandacoomarasamy, A. (2013) 'Obesity & osteoarthritis', *The Indian Journal of Medical Research*, 138(2), p. 185.

King, R.G. (1966) 'A rheological measurement of three synovial fluids', *Rheologica Acta* [Preprint]. Available at: <https://doi.org/10.1007/BF01973577>.

Kistenev, Y.V. *et al.* (2019) 'Analysis of Collagen Spatial Structure Using Multiphoton Microscopy and Machine Learning Methods', *Biochemistry (Moscow)*, 84(S1), pp. 108–123. Available at: <https://doi.org/10.1134/S0006297919140074>.

Koh, J.L. and Gupta, K. (2017) 'Evaluation of repair of the hip labrum under simulated full weight-bearing', *HIP International*, 27(1), pp. 104–109. Available at: <https://doi.org/10.5301/hipint.5000472>.

Kohl, S. *et al.* (2011) 'Histology of damaged acetabular cartilage in symptomatic femoroacetabular impingement: An observational analysis', *HIP International*, 21(2), pp. 154–162. Available at: <https://doi.org/10.5301/HIP.2011.6515>.

Konrath, G.A. *et al.* (1998) 'The Role of the Acetabular Labrum and the Transverse Acetabular Ligament in Load Transmission in the Hip*', *JBJS*, 80(12), p. 1781.

Kotzar, G.M. *et al.* (1991) 'Telemeterized in vivo hip joint force data: A report on two patients after total hip surgery', *Journal of Orthopaedic Research*, 9(5), pp. 621–633. Available at: <https://doi.org/10.1002/jor.1100090502>.

Kraeutler, M.J. *et al.* (2016) 'Hip instability: A review of hip dysplasia and other contributing factors', *Muscles, Ligaments and Tendons Journal*, 6(3), pp. 343–353. Available at: <https://doi.org/10.11138/mltj/2016.6.3.343>.

Kumar, R. *et al.* (2017) 'Multiphoton microscopy of osteoarthritic articular cartilage', in *Optics in the Life Sciences Congress*. OSA, p. NW4C.4. Available at: <https://doi.org/10.1364/NTM.2017.NW4C.4>.

Kumar, R. and Kumar, A. (2019) 'Assessment of Articular Cartilage by Second Harmonic Microscopy: Challenges and Opportunities', *Frontiers in Physics*, 7. Available at: <https://www.frontiersin.org/articles/10.3389/fphy.2019.00137> (Accessed: 17 September 2023).

Laumonerie, P. *et al.* (2021) 'Sensory Innervation of the Hip Joint and Referred Pain: A Systematic Review of the Literature', *Pain Medicine*, 22(5), pp. 1149–1157. Available at: <https://doi.org/10.1093/pm/pnab061>.

Lee, A.J.J. *et al.* (2015) 'The prevalence of acetabular labral tears and associated pathology in a young asymptomatic population', *Bone and Joint Journal* [Preprint]. Available at: <https://doi.org/10.1302/0301-620X.97B5.35166>.

Lertwanich, P. *et al.* (2016) 'Biomechanical evaluation contribution of the acetabular labrum to hip stability', *Knee Surgery, Sports Traumatology, Arthroscopy*, 24(7), pp. 2338–2345. Available at: <https://doi.org/10.1007/s00167-015-3555-2>.

Lewis, C.R. and Sahrmann, S.A. (2006) 'Acetabular labral tears', *Phys. Ther.*, 86(1), pp. 110–121.

Li, A.E. *et al.* (2016) 'MRI for the preoperative evaluation of femoroacetabular impingement', *Insights into Imaging*, 7(2), pp. 187–198. Available at: <https://doi.org/10.1007/s13244-015-0459-0>.

Li, J. *et al.* (2016) 'The influence of the representation of collagen fibre organisation on the cartilage contact mechanics of the hip joint', *Journal of Biomechanics*, 49(9), pp. 1679–1685. Available at: <https://doi.org/10.1016/j.jbiomech.2016.03.050>.

Lievensse, A.M. *et al.* (2002) 'Influence of obesity on the development of osteoarthritis of the hip: a systematic review', *Rheumatology*, 41(10), pp. 1155–1162. Available at: <https://doi.org/10.1093/RHEUMATOLOGY/41.10.1155>.

Liu, A. *et al.* (2015) 'Tribology studies of the natural knee using an animal model in a new whole joint natural knee simulator', *Journal of Biomechanics*, 48(12), pp. 3004–3011. Available at: <https://doi.org/10.1016/j.jbiomech.2015.07.043>.

Liu, J. *et al.* (2021) 'Picosirius-Polarization Method for Collagen Fiber Detection in Tendons: A Mini-Review', *Orthopaedic Surgery*, 13(3), pp. 701–707. Available at: <https://doi.org/10.1111/os.12627>.

Lizhang, J. (2010) 'Tribology of hemiarthroplasty - OpenGrey'. Available at: <http://www.opengrey.eu/item/display/10068/1004232>.

Lizhang, J. *et al.* (2013) 'Effect of clearance on cartilage tribology in hip hemiarthroplasty', *Proceedings of the Institution of Mechanical Engineers, Part H: Journal of Engineering in Medicine*, 227(12), pp. 1284–1291. Available at: <https://doi.org/10.1177/0954411913502156>.

Löhe, F. *et al.* (1996) 'Structure, strain and function of the transverse acetabular ligament', *Acta anatomica*, 157(4), pp. 315–323. Available at: <https://doi.org/10.1159/000147894>.

Macirowski, T. (1994) 'Cartilage Stresses in the Human Hip Joint', *Journal of Biomechanical Engineering*, 116(1), p. 10. Available at: <https://doi.org/10.1115/1.2895693>.

MacLean, K.F.E., Callaghan, J.P. and Maly, M.R. (2016) 'Effect of obesity on knee joint biomechanics during gait in young adults', *Cogent Medicine*, 3(1). Available at: <https://doi.org/10.1080/2331205x.2016.1173778>.

Mak, M. *et al.* (2011) 'Influence of Acetabular Cup Rim Design on the Contact Stress During Edge Loading in Ceramic-on-Ceramic Hip Prostheses', *Journal of Arthroplasty*, 26(1), pp. 131–136. Available at: <https://doi.org/10.1016/j.arth.2009.10.019>.

Makovitch, S.A., Mills, C.A. and Eng, C. (2020) 'Update on Evidence-Based Diagnosis and Treatment of Acetabular Labral Tears', *Current Physical Medicine and Rehabilitation Reports*, 8(4), pp. 342–353. Available at: <https://doi.org/10.1007/s40141-020-00295-z>.

Malviya, A. *et al.* (2023) *NAHR Annual Report 2023*. Non-Arthroplasty Hip Registry. Available at: https://www.nahr.co.uk/wp-content/uploads/2023/03/NAHR-2023-Final_compressed.pdf (Accessed: 15 September 2023).

Mansfield, J. (2008) 'Multi-photon microscopy of cartilage', (September). Available at: <http://hdl.handle.net/10036/42345%5Cnhttp://ethos.bl.uk/OrderDetails.do?uin=uk.bl.ethos.489238>.

Mansfield, J. *et al.* (2009) 'The elastin network: Its relationship with collagen and cells in articular cartilage as visualized by multiphoton microscopy', *Journal of Anatomy*, 215(6), pp. 682–691. Available at: <https://doi.org/10.1111/j.1469-7580.2009.01149.x>.

Mansfield, J.C. *et al.* (2019) 'Collagen reorganization in cartilage under strain probed by polarization sensitive second harmonic generation microscopy', *Journal of The Royal Society Interface*, 16(150), p. 20180611. Available at: <https://doi.org/10.1098/rsif.2018.0611>.

- Mansfield, J.C., Bell, J.S. and Winlove, C.P. (2015) 'The micromechanics of the superficial zone of articular cartilage', *Osteoarthritis and Cartilage*, 23(10), pp. 1806–1816. Available at: <https://doi.org/10.1016/j.joca.2015.05.030>.
- Maquer, G. *et al.* (2016) 'Head-Neck Osteoplasty has Minor Effect on the Strength of an Ovine Cam-FAI Model: In Vitro and Finite Element Analyses', *Clinical Orthopaedics and Related Research*, 474(12), pp. 2633–2640. Available at: <https://doi.org/10.1007/S11999-016-5024-8>.
- Martin, R.B. *et al.* (2015) 'Skeletal Tissue Mechanics', *Skeletal Tissue Mechanics* [Preprint]. Available at: <https://doi.org/10.1007/978-1-4939-3002-9>.
- Martin, R.L. *et al.* (2006) 'Acetabular Labral Tears of the Hip: Examination and Diagnostic Challenges', *Journal of Orthopaedic & Sports Physical Therapy*, 36(7), pp. 503–515. Available at: <https://doi.org/10.2519/jospt.2006.2135>.
- Masłoń, A. *et al.* (2011) 'Vascularity of the hip labrum during the foetal period', *Annals of Anatomy*, 193(1), pp. 37–42. Available at: <https://doi.org/10.1016/j.aanat.2010.08.007>.
- Matsuda, D., Hurst, J. and Biomet, Z. (2016) 'Hip Acetabular Labral Repair with the Juggernaut Long Soft Anchor'. Zimmer Biomet.
- Maynard, R.L. and Downes, N. (2019) 'Chapter 3 - Introduction to the Skeleton: Bone, Cartilage and Joints', in R.L. Maynard and N. Downes (eds) *Anatomy and Histology of the Laboratory Rat in Toxicology and Biomedical Research*. Academic Press, pp. 11–22. Available at: <https://doi.org/10.1016/B978-0-12-811837-5.00003-4>.
- McCarthy, J.C. *et al.* (2001) 'The watershed labral lesion: Its relationship to early arthritis of the hip', *Journal of Arthroplasty*, 16(8 SUPPL. 1), pp. 81–87. Available at: <https://doi.org/10.1054/arth.2001.28370>.
- McCarthy, J.C. *et al.* (2003) 'Acetabular and Labral Pathology', in *Early Hip Disorders*. New York: Springer-Verlag, pp. 113–133. Available at: https://doi.org/10.1007/0-387-21795-9_12.
- Melluso, G. and Mansi, L. (2017) 'Atlas of Anatomy - Third Edition. Anne M. Gilroy and Brian R. MacPherson (Eds) On the basis of the work of Michael Schuenke, Erik Schulte and Udo Schumaker', *European Journal of Nuclear Medicine and Molecular Imaging* [Preprint]. Available at: <https://doi.org/10.1007/s00259-017-3628-1>.
- Mikula, J.D. *et al.* (2017) 'Quantitative Anatomic Analysis of the Native Ligamentum Teres', *Orthopaedic Journal of Sports Medicine*, 5(2), p. 232596711769148. Available at: <https://doi.org/10.1177/2325967117691480>.
- Miozzari, H.H. *et al.* (2004) 'Effects of removal of the acetabular labrum in a sheep hip model', *Osteoarthritis and Cartilage*, 12(5), pp. 419–430. Available at: <https://doi.org/10.1016/j.joca.2004.02.008>.
- Miozzari, H.H. *et al.* (2015) 'No Regeneration of the Human Acetabular Labrum After Excision to Bone', *Clinical Orthopaedics and Related Research*, 473(4), pp. 1349–1357. Available at: <https://doi.org/10.1007/s11999-014-4021-z>.

Mirkiani, S. *et al.* (2022) 'Overground gait kinematics and muscle activation patterns in the Yucatan mini pig', *Journal of Neural Engineering*, 19(2), p. 026009. Available at: <https://doi.org/10.1088/1741-2552/AC55AC>.

Moore, A.L. *et al.* (2007) 'Regional load bearing of the canine acetabulum', *Journal of Biomechanics*, 40(16), pp. 3732–3737. Available at: <https://doi.org/10.1016/j.jbiomech.2007.06.026>.

Musumeci, G. (2016) 'The Effect of Mechanical Loading on Articular Cartilage', *Journal of Functional Morphology and Kinesiology*, 1(2), pp. 154–161. Available at: <https://doi.org/10.3390/jfmk1020154>.

Nepple, J.J. *et al.* (2014) 'The hip fluid seal-Part II: The effect of an acetabular labral tear, repair, resection, and reconstruction on hip stability to distraction', *Knee Surgery, Sports Traumatology, Arthroscopy*, 22(4), pp. 730–736. Available at: <https://doi.org/10.1007/s00167-014-2875-y>.

Netter, F.H. (2006) *Atlas of human anatomy*. 18th edn. Saunders/Elsevier.

Neumann, G. *et al.* (2007) 'Prevalence of labral tears and cartilage loss in patients with mechanical symptoms of the hip: evaluation using MR arthrography', *Osteoarthritis and Cartilage*, 15(8), pp. 909–917. Available at: <https://doi.org/10.1016/j.joca.2007.02.002>.

Ng, K.C.G. *et al.* (2016) 'Hip joint stresses due to cam-type femoroacetabular impingement: A systematic review of finite element simulations', *PLoS ONE*, 11(1), pp. 1–18. Available at: <https://doi.org/10.1371/journal.pone.0147813>.

Ng, K.C.G. *et al.* (2019) 'Hip Joint Torsional Loading Before and After Cam Femoroacetabular Impingement Surgery', *American Journal of Sports Medicine*, 47(2), pp. 420–430. Available at: <https://doi.org/10.1177/0363546518815159>.

Novakofski, K.D. *et al.* (2016) 'High-Resolution Methods for Diagnosing Cartilage Damage In Vivo', *Cartilage*, 7(1), pp. 39–51. Available at: <https://doi.org/10.1177/1947603515602307>.

Novoa-Parra, C.D. *et al.* (2023) '[Translated article] Past and projected temporal trends in arthroscopic hip surgery in Spain between 1998 and 2018', *Revista Española de Cirugía Ortopédica y Traumatología*, 67(1), pp. T35–T42. Available at: <https://doi.org/10.1016/j.recot.2022.10.007>.

Ockert, B. *et al.* (2012) 'Fibrocartilage in various regions of the human glenoid labrum. An immunohistochemical study on human cadavers', *Knee Surgery, Sports Traumatology, Arthroscopy*, 20(6), pp. 1036–1041. Available at: <https://doi.org/10.1007/s00167-011-1686-7>.

Olstad, K. *et al.* (2013) 'Transection of vessels in epiphyseal cartilage canals leads to osteochondrosis and osteochondrosis dissecans in the femoro-patellar joint of foals; a potential model of juvenile osteochondritis dissecans', *Osteoarthritis and Cartilage*, 21(5), pp. 730–738. Available at: <https://doi.org/10.1016/j.joca.2013.02.005>.

Pallan, R.L. (2016) 'Characterisation and in vitro simulation of the natural hip', (September).

Palmer, A.J.R. *et al.* (2016) 'Past and projected temporal trends in arthroscopic hip surgery in England between 2002 and 2013', *BMJ Open Sport & Exercise Medicine*, 2(1), p. e000082. Available at: <https://doi.org/10.1136/bmjsem-2015-000082>.

Pascual-Garrido, C. *et al.* (2018) 'Canine hip dysplasia: A natural animal model for human developmental dysplasia of the hip', *Journal of Orthopaedic Research*, 36(7), pp. 1807–1817. Available at: <https://doi.org/10.1002/jor.23828>.

Paul, J.P. (1967) 'Forces at the human hip joint', *Glasgow Theses Services - University of Glasgow*, p. 305.

Petersen, W., Petersen, F. and Tillmann, B. (2003) 'Structure and vascularization of the acetabular labrum with regard to the pathogenesis and healing of labral lesions', *Archives of Orthopaedic and Trauma Surgery*, 123(6), pp. 283–288. Available at: <https://doi.org/10.1007/s00402-003-0527-7>.

Philippon, M.J. (2010) 'Acetabular Labral Tears : Resection vs . Repair', *University of Pennsylvania Orthopaedic Journal*, 20, pp. 83–87.

Philippon, M.J. *et al.* (2014) 'The hip fluid seal-Part I: The effect of an acetabular labral tear, repair, resection, and reconstruction on hip fluid pressurization', *Knee Surgery, Sports Traumatology, Arthroscopy* [Preprint]. Available at: <https://doi.org/10.1007/s00167-014-2874-z>.

Philippon, M.J., Arnoczky, S.P. and Torrie, A. (2007) 'Arthroscopic Repair of the Acetabular Labrum: A Histologic Assessment of Healing in an Ovine Model', *Arthroscopy - Journal of Arthroscopic and Related Surgery*, 23(4), pp. 376–380. Available at: <https://doi.org/10.1016/j.arthro.2007.01.017>.

Pieri, E.D. *et al.* (2019) 'Patient characteristics affect hip contact forces during gait', *Osteoarthritis and Cartilage* [Preprint], (xxxx). Available at: <https://doi.org/10.1016/j.joca.2019.01.016>.

Poole, A.R. *et al.* (2002) 'Type II collagen degradation and its regulation in articular cartilage in osteoarthritis.', *Annals of the rheumatic diseases*, 61 Suppl 2(fig 1), pp. ii78-81.

Pritzker, K.P.H. *et al.* (2006) 'Osteoarthritis cartilage histopathology: Grading and staging', *Osteoarthritis and Cartilage*, 14(1), pp. 13–29. Available at: <https://doi.org/10.1016/j.joca.2005.07.014>.

Prokopi, N. *et al.* (123AD) 'Collagen orientation probed by polarized Raman spectra can serve as differential diagnosis indicator between different grades of meniscus degeneration', *Scientific Reports* |, 11, p. 20299. Available at: <https://doi.org/10.1038/s41598-021-99569-2>.

Ramage, J.L. and Varacallo, M. (2022) 'Anatomy, Bony Pelvis and Lower Limb, Medial Thigh Muscles', *StatPearls* [Preprint]. Available at: <https://www.ncbi.nlm.nih.gov/books/NBK534775/>.

Rathnayake, M.S.B. *et al.* (2021) 'Macromolecular Interactions in Cartilage Extracellular Matrix Vary According to the Cartilage Type and Location', *Cartilage*, 13(2 Suppl), pp. 476S-485S. Available at: <https://doi.org/10.1177/19476035211000811>.

- Raud, B. *et al.* (2020) 'Level of obesity is directly associated with the clinical and functional consequences of knee osteoarthritis', *Scientific Reports*, 10(1), p. 3601. Available at: <https://doi.org/10.1038/s41598-020-60587-1>.
- Ravanfar, M. *et al.* (2017) 'Parametric imaging of collagen structural changes in human osteoarthritic cartilage using optical polarization tractography', *Journal of Biomedical Optics*, 22(12), p. 1. Available at: <https://doi.org/10.1117/1.jbo.22.12.121708>.
- Recnik, G. *et al.* (2009) 'The role of obesity, biomechanical constitution of the pelvis and contact joint stress in progression of hip osteoarthritis', *Osteoarthritis and Cartilage*, 17(7), pp. 879–882. Available at: <https://doi.org/10.1016/j.joca.2008.12.006>.
- Reiman, M.P. *et al.* (2014) 'Examination of acetabular labral tear: A continued diagnostic challenge', *British Journal of Sports Medicine*, 48(4), pp. 311–319. Available at: <https://doi.org/10.1136/bjsports-2012-091994>.
- Rexwinkle, J.T., Hunt, H.K. and Pfeiffer, F.M. (2017) 'Characterization of the surface and interfacial properties of the lamina splendens', *Frontiers of Mechanical Engineering*, 12(2), pp. 234–252. Available at: <https://doi.org/10.1007/s11465-017-0409-2>.
- Reyes, C. *et al.* (2016) 'Association between overweight and obesity and risk of clinically diagnosed knee, hip, and hand osteoarthritis: a population-based cohort study', *Arthritis & rheumatology (Hoboken, N.J.)*, 68(8), p. 1869. Available at: <https://doi.org/10.1002/ART.39707>.
- Ricard-Blum, S. (2011) 'The Collagen Family', *Cold Spring Harbor Perspectives in Biology*, 3(1), pp. 1–19. Available at: <https://doi.org/10.1101/CSHPERSPECT.A004978>.
- Ricciardi, A. (2015) 'Thieme Atlas of Anatomy: General Anatomy and Musculoskeletal System', *The Yale Journal of Biology and Medicine*, 88(1), p. 100.
- Rieppo, J. *et al.* (2009) 'Changes in spatial collagen content and collagen network architecture in porcine articular cartilage during growth and maturation', *Osteoarthritis and Cartilage*, 17(4), pp. 448–455. Available at: <https://doi.org/10.1016/j.joca.2008.09.004>.
- Rosenberg, L. (1971) 'Chemical Basis for the Histological Use of Safranin O in the Study of Articular Cartilage', *JBJS*, 53(1), p. 69.
- Ross, K.A. *et al.* (2013) 'Comparison of Three Methods to Quantify Repair Cartilage Collagen Orientation', *Cartilage*, 4(2), pp. 111–120. Available at: <https://doi.org/10.1177/1947603512461440>.
- Rydell, N.W. (2014) 'Acta Orthopaedica Scandinavica Forces Acting on the Femoral Head-Prosthesis: A Study on Strain Gauge Supplied Prostheses in Living Persons'. Available at: <https://doi.org/10.3109/ort.1966.37.suppl-88.01>.
- Safran, M.R. *et al.* (2011) 'Strains Across the Acetabular Labrum during Hip Motion: A Cadaveric Model', *American Journal of Sports Medicine*, 39(1_suppl), pp. 92S–102S. Available at: <https://doi.org/10.1177/0363546511414017>.

Samaan, M.A. *et al.* (2017) 'Joint Loading in the Sagittal Plane during Gait Is Associated with Hip Joint Abnormalities in Patients with Femoroacetabular Impingement', *American Journal of Sports Medicine*, 45(4), pp. 810–818. Available at: <https://doi.org/10.1177/0363546516677727>.

Sato, Y. *et al.* (2023) 'Expression of Acetabular Labral Vascular Endothelial Growth Factor and Nerve Growth Factor Is Directly Associated with Hip Osteoarthritis Pain: Investigation by Immunohistochemical Staining', *International Journal of Molecular Sciences*, 24(3), p. 2926. Available at: <https://doi.org/10.3390/ijms24032926>.

Schmerl, M., Pollard, H. and Hoskins, W. (2005) 'Labral injuries of the hip: A review of diagnosis and management', *Journal of Manipulative and Physiological Therapeutics*, 28(8), pp. 1–8. Available at: <https://doi.org/10.1016/j.jmpt.2005.08.018>.

Schon, J. *et al.* (2020) 'Expression profile of matrix metalloproteinases in the labrum of femoroacetabular impingement', *Bone & Joint Research*, 9(4), pp. 173–181. Available at: <https://doi.org/10.1302/2046-3758.94.BJR-2019-0083.R1>.

Schuck, M., Noble, P.C. and McCarthy, J.C. (2000) 'The healing potential of lesions of the acetabular labrum', in *46th Annual Meeting, Orthopaedic Research Society*, p. 77030.

Seldes, R.M. *et al.* (2001a) 'Anatomy, Histologic Features, and Vascularity of the Adult Acetabular Labrum', *Clinical Orthopaedics and Related Research*, 382, pp. 232–240. Available at: <https://doi.org/10.1097/00003086-200101000-00031>.

Seldes, R.M. *et al.* (2001b) 'Clin Orthop Relat Res. 2001 Jan;(382) 232-40', (382), pp. 232–240.

Shi, Y. *et al.* (2019) 'Acetabular labral reconstruction using autografts reduces osteoarthritis development compared with labral resection in a porcine model', *Am J Transl Res*. Available at: www.ajtr.org.

Shindle, M.K. *et al.* (2008) 'Arthroscopic management of labral tears in the hip', *Journal of Bone and Joint Surgery - Series A*, 90(SUPPL. 4), pp. 2–19. Available at: <https://doi.org/10.2106/JBJS.H.00686>.

Shirshin, E.A. *et al.* (2017) 'Two-photon autofluorescence lifetime imaging of human skin papillary dermis in vivo: assessment of blood capillaries and structural proteins localization', *Scientific Reports*, 7(1), p. 1171. Available at: <https://doi.org/10.1038/s41598-017-01238-w>.

Sienko, A., Ekhtiari, S. and Khanduja, V. (2023) 'The growth of hip preservation as a speciality', *Knee Surgery, Sports Traumatology, Arthroscopy*, 31(7), pp. 2540–2543. Available at: <https://doi.org/10.1007/s00167-023-07409-9>.

Singleton, M.C. and Leveau, B.F. (no date) 'The Hip Joint: Structure, Stability, and Stress A Review'. Available at: <https://academic.oup.com/ptj/article-abstract/55/9/957/4567800>.

Slattery, C. and Kweon, C.Y. (2018) 'Classifications in Brief: Outerbridge Classification of Chondral Lesions', *Clinical Orthopaedics and Related Research*, 476(10), pp. 2101–2104. Available at: <https://doi.org/10.1007/s11999-0000000000000255>.

Smith, C.D. *et al.* (2009) 'A biomechanical basis for tears of the human acetabular labrum', *British Journal of Sports Medicine*, 43(8), pp. 574–578. Available at: <https://doi.org/10.1136/bjism.2008.053645>.

Smith, M.V. *et al.* (2011) 'Effect of Acetabular Labrum Tears on Hip Stability and Labral Strain in a Joint Compression Model', *American Journal of Sports Medicine*, 39(1_suppl), pp. 103S-110S. Available at: <https://doi.org/10.1177/0363546511400981>.

Song, K. *et al.* (2021) 'Acetabular Edge Loading During Gait Is Elevated by the Anatomical Deformities of Hip Dysplasia', *Frontiers in Sports and Active Living*, 3, p. 187. Available at: <https://doi.org/10.3389/FSPOR.2021.687419/BIBTEX>.

Song, Y. *et al.* (2012) 'Articular cartilage friction increases in hip joints after the removal of acetabular labrum', *Journal of Biomechanics*, 45(3), pp. 524–530. Available at: <https://doi.org/10.1016/j.jbiomech.2011.11.044>.

Sophia Fox, A.J., Bedi, A. and Rodeo, S.A. (2009) 'The Basic Science of Articular Cartilage', *Sports Health*, 1(6), pp. 461–468. Available at: <https://doi.org/10.1177/1941738109350438>.

Stelzeneder, D. *et al.* (2012) 'Patterns of joint damage seen on MRI in early hip osteoarthritis due to structural hip deformities', *Osteoarthritis and Cartilage*, 20(7), pp. 661–669. Available at: <https://doi.org/10.1016/j.joca.2012.03.014>.

Su, T. *et al.* (2023) 'Tissue Regrowth and Its Vascularization Through Bone Marrow Stimulation: Microfracture at the Acetabular Rim for Irreparable Labral Tear in a Porcine Model', *The American Journal of Sports Medicine*, 51(4), pp. 1024–1032. Available at: <https://doi.org/10.1177/03635465231151226>.

Su, T., Chen, G.-X. and Yang, L. (2019) 'Diagnosis and treatment of labral tear', *Chinese Medical Journal*, 132(2), pp. 211–219. Available at: <https://doi.org/10.1097/CM9.000000000000020>.

Suarez, J.C. *et al.* (2013) 'Comprehensive approach to the evaluation of groin pain', *The Journal of the American Academy of Orthopaedic Surgeons*, 21(9), pp. 558–570. Available at: <https://doi.org/10.5435/JAAOS-21-09-558>.

Swanson, K.A. (2017) *FINITE ELEMENT ANALYSIS OF GLENOHUMERAL LABRAL TEARS IN THE SHOULDER JOINT*. Worcester Polytechnic Institute.

T, A.E., Lecture, S.O. and Taber, C.D. (2015) 'Arthroscopic Labral Anatomy and Management Anatomy of the Labrum Function of Labrum Relative Stability • Motion of the Cartilage Compression • Contact stresses in removed Anatomy-Blood supply', pp. 1–16.

T Otsuka, K.Y.R.T., N. Takasu, N. Yamada (1995) 'Structure of the most superficial layer of articular cartilage', *J Bone and Joint Surg [Br]*, 77(B), pp. 460–464.

Tallitsch, R.B. (2009) *Histology: An Identification Manual*. Illustrate. Edited by R.S. Gaustaferrri. Mosby/Elsevier.

Tannast, M. *et al.* (2008) 'Hip Damage Occurs at the Zone of Femoroacetabular Impingement', *Clinical Orthopaedics and Related Research*, 466(2), pp. 273–280. Available at: <https://doi.org/10.1007/s11999-007-0061-y>.

- Tauviquirrahman, M. *et al.* (2023) 'Analysis of contact pressure in a 3D model of dual-mobility hip joint prosthesis under a gait cycle', *Scientific Reports*, 13(1), p. 3564. Available at: <https://doi.org/10.1038/s41598-023-30725-6>.
- Taylor, S.D. (2012) 'An In-vitro Medium Term Simulation of Hip Hemiarthroplasty', (April).
- Thorup, V.M., Laursen, B. and Jensen, B.R. (2008) 'Net joint kinetics in the limbs of pigs walking on concrete floor in dry and contaminated conditions', *Journal of Animal Science*, 86(4), pp. 992–998. Available at: <https://doi.org/10.2527/jas.2007-0581>.
- Toricelli, D. *et al.* (2016) 'Human-like compliant locomotion: state of the art of robotic implementations', *Bioinspiration & Biomimetics*, 11(5), p. 051002. Available at: <https://doi.org/10.1088/1748-3190/11/5/051002>.
- Turley, G.A. *et al.* (2013) 'Evaluation of range of motion restriction within the hip joint', *Medical and Biological Engineering and Computing*, 51(4), pp. 467–477. Available at: <https://doi.org/10.1007/s11517-012-1016-3>.
- Urban, J.P. (1994) 'The chondrocyte: a cell under pressure', *British Journal of Rheumatology*, 33(10), pp. 901–908. Available at: <https://doi.org/10.1093/rheumatology/33.10.901>.
- Vera, A.M. *et al.* (2021) 'Hip Instability in Ballet Dancers: A Narrative Review', *Journal of dance medicine & science : official publication of the International Association for Dance Medicine & Science*, 25(3), pp. 176–190. Available at: <https://doi.org/10.12678/1089-313X.091521c>.
- Viitala, R. and Saikko, V. (2020) 'Effect of random variation of input and various daily activities on wear in a hip joint simulator', *Journal of Biomechanics*, 106. Available at: <https://doi.org/10.1016/j.jbiomech.2020.109831>.
- Wagner, F.V. *et al.* (2012) 'Capsular Ligaments of the Hip: Anatomic, Histologic, and Positional Study in Cadaveric Specimens with MR Arthrography', *Radiology*, 263(1), pp. 189–198. Available at: <https://doi.org/10.1148/radiol.12111320>.
- Waldstein, W. *et al.* (2016) 'OARSI osteoarthritis cartilage histopathology assessment system: A biomechanical evaluation in the human knee', *Journal of Orthopaedic Research*, 34(1), pp. 135–140. Available at: <https://doi.org/10.1002/jor.23010>.
- Weiss, J. *et al.* (2013) '* Cartilage and Labrum Mechanics in Normal and Pathomorphologic Hips', *Orthopaedic Proceedings*, 95-B(SUPP_34), pp. 202–202. Available at: https://doi.org/10.1302/1358-992X.95BSUPP_34.ISTA2013-202.
- Wenger, D.E. *et al.* (2004) 'Acetabular Labral Tears Rarely Occur in the Absence of Bony Abnormalities', *Clinical Orthopaedics and Related Research*, 426, pp. 145–150. Available at: <https://doi.org/10.1097/01.blo.0000136903.01368.20>.
- Wu, J.P., Kirk, T.B. and Zheng, M.H. (2008) 'Study of the collagen structure in the superficial zone and physiological state of articular cartilage using a 3D confocal imaging technique', *Journal of Orthopaedic Surgery and Research*, 3(1), pp. 1–11. Available at: <https://doi.org/10.1186/1749-799X-3-29/FIGURES/6>.

Yeh, A.T. *et al.* (2005) 'Nonlinear optical microscopy of articular cartilage', *Osteoarthritis and Cartilage*, 13(4), pp. 345–352. Available at: <https://doi.org/10.1016/j.joca.2004.12.007>.

Zaghloul, A. (2019) 'Hip Joint: Embryology, Anatomy and Biomechanics', *Biomedical Journal of Scientific & Technical Research*, 12(3), pp. 9304–9318. Available at: <https://doi.org/10.26717/bjstr.2018.12.002267>.

Zaltz, I. (2012) 'The biomechanical case for labral débridement', *Clinical Orthopaedics and Related Research*, 470(12), pp. 3398–3405. Available at: <https://doi.org/10.1007/s11999-012-2446-9>.

Zhang, C. *et al.* (2012) 'Lubricin Distribution in the Menisci and Labra of Human Osteoarthritic Joints', *Cartilage*, 3(2), pp. 165–172. Available at: <https://doi.org/10.1177/1947603511429699>.

Zusmanovich, M. *et al.* (2022) 'The Incidence of Hip Arthroscopy in Patients With Femoroacetabular Impingement Syndrome and Labral Pathology Increased by 85% Between 2011 and 2018 in the United States', *Arthroscopy: The Journal of Arthroscopic & Related Surgery*, 38(1), pp. 82–87. Available at: <https://doi.org/10.1016/j.arthro.2021.04.049>.